# EXPERIMENTAL AND NUMERICAL STUDIES OF UNDERWATER EXPLOSIONS

Suresh Menon
School of Aerospace Engineering
Georgia Institute of Technology
Atlanta, Georgia 30332-0150

Annual Report
for the period
June 1995 - September 1996
for Grant No. N00014-91-J-1993

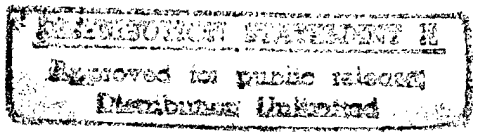


Submitted to
The Office of Naval Research
October 1996

SECURITY CLASSIFICATION OF THIS PAGE

# REPORT DOCUMENTATION PAGE

Form Approved
OMB No. 0704-0188

| | |
|---|---|
| 1a. REPORT SECURITY CLASSIFICATION<br>Unclassified | 1b. RESTRICTIVE MARKINGS |
| 2a. SECURITY CLASSIFICATION AUTHORITY | 3. DISTRIBUTION/AVAILABILITY OF REPORT<br>Approved for public release; distribution unlimited. |
| 2b. DECLASSIFICATION/DOWNGRADING SCHEDULE | |
| 4. PERFORMING ORGANIZATION REPORT NUMBER(S) | 5. MONITORING ORGANIZATION REPORT NUMBER(S) |
| 6a. NAME OF PERFORMING ORGANIZATION<br>Georgia Institute of Tech.<br>School of Aerospace Eng. | 6b. OFFICE SYMBOL (*If applicable*) |
| | 7a. NAME OF MONITORING ORGANIZATION<br>Office of Naval Research |
| 6c. ADDRESS (*City, State, and ZIP Code*)<br>Atlanta, Georgia 30332-0150 | 7b. ADDRESS (*City, State, and ZIP Code*)<br>BALLSTON CTR., TOWER ONE<br>800 N. QUINCY STREET<br>WASHINGTON, DC 22217-5000 |
| 8a. NAME OF FUNDING/SPONSORING ORGANIZATION | 8b. OFFICE SYMBOL (*If applicable*) |
| | 9 PROCUREMENT INSTRUMENT IDENTIFICATION NUMBER<br>N00014-91-J-1993 |
| 8c. ADDRESS (*City, State, and ZIP Code*) | 10. SOURCE OF FUNDING NUMBERS<br>PROGRAM ELEMENT NO. / PROJECT NO. / TASK NO / WORK UNIT ACCESSION NO. |

11. TITLE (*Include Security Classification*)
Experimental & Numerical Studies of Underwater Explosions

12. PERSONAL AUTHOR(S)
Dr. Suresh Menon

| 13a. TYPE OF REPORT | 13b. TIME COVERED | 14. DATE OF REPORT (*Year, Month, Day*) | 15. PAGE COUNT |
|---|---|---|---|
| Final Technical | FROM 6/1/95 TO 9/30/96 | 9/30/96 | |

16. SUPPLEMENTARY NOTATION

| 17. COSATI CODES | | | 18. SUBJECT TERMS (*Continue on reverse if necessary and identify by block number*) |
|---|---|---|---|
| FIELD | GROUP | SUB-GROUP | UNDERWATER EXPLOSIONS, BUBBLE OSCILLATIONS, BUBBLE COLLAPSE, SURFACE IMPACT |
| | | | |
| | | | |

19. ABSTRACT (*Continue on reverse if necessary and identify by block number*)

**See reverside**

| | |
|---|---|
| 20. DISTRIBUTION/AVAILABILITY OF ABSTRACT<br>☐ UNCLASSIFIED/UNLIMITED ☐ SAME AS RPT. ☐ DTIC USERS | 21. ABSTRACT SECURITY CLASSIFICATION |
| 22a NAME OF RESPONSIBLE INDIVIDUAL | 22b TELEPHONE (*include Area Code*) / 22c OFFICE SYMBOL |

DD Form 1473, JUN 86 *Previous editions are obsolete.*

# SIMULATIONS OF UNDERWATER EXPLOSIONS

**S. Menon and S. Pannala**
**School of Aerospace Engineering**
**Georgia Institute of Technology**
**Atlanta, Georgia 30332-0150**

## Abstract

The dynamics of bubbles formed during underwater explosions is numerically investigated using an Arbitrary Lagrangian-Eulerian three-dimensional finite-element code. The expansion and the collapse of a vapor bubble in a water tank is first simulated to compare the predictions with data from a parallel experimental study. Experimental and numerical results show good qualitative and quantitative agreement and suggest that the excitation of Rayleigh-Taylor instability is a major cause of bubble interface instability. This observation is consistent with earlier data and confirms that interface instability plays a significant role in the loss of energy from the explosion. Simulations have also been carried out to investigate bubble-bubble and bubble-wall interactions. Results from the bubble-bubble interaction studies show the formation of a water jet as one bubble collapses into the other, in agreement with recent experimental observation. The collapse of a bubble near a rigid wall and the formation of high velocity re-entrant jet onto the wall has also been successfully simulated. The peak impact pressure and the fluid flow velocity agrees well with the experiments. In addition, the well known vortex ring bubble during the collapse process has been numerically captured. Application of the computational methodology to realistic deep sea explosions and to detonation cords used for mine destruction has also been carried. Results of these studies are also discussed in this report.

# SIMULATIONS OF UNDERWATER EXPLOSIONS

**S. Menon and S. Pannala**
**School of Aerospace Engineering**
**Georgia Institute of Technology**
**Atlanta, Georgia 30332-0150**

## Abstract

The dynamics of bubbles formed during underwater explosions is numerically investigated using an Arbitrary Lagrangian-Eulerian three-dimensional finite-element code. The expansion and the collapse of a vapor bubble in a water tank is first simulated to compare the predictions with data from a parallel experimental study. Experimental and numerical results show good qualitative and quantitative agreement and suggest that the excitation of Rayleigh-Taylor instability is a major cause of bubble interface instability. This observation is consistent with earlier data and confirms that interface instability plays a significant role in the loss of energy from the explosion. Simulations have also been carried out to investigate bubble-bubble and bubble-wall interactions. Results from the bubble-bubble interaction studies show the formation of a water jet as one bubble collapses into the other, in agreement with recent experimental observation. The collapse of a bubble near a rigid wall and the formation of high velocity re-entrant jet onto the wall has also been successfully simulated. The peak impact pressure and the fluid flow velocity agrees well with the experiments. In addition, the well known vortex ring bubble during the collapse process has been numerically captured. Application of the computational methodology to realistic deep sea explosions and to detonation cords used for mine destruction has also been carried. Results of these studies are also discussed in this report.

## 1. Introduction

Vapor and gas bubble dynamics are of great practical interest in the prediction and prevention of cavitation erosion of marine propeller and turbine blades (e.g., Rood, 1991). In addition to this effect from collapse of cavitation (small) bubbles, the destructive nature of strong underwater explosions near walls is also well known. Both experimental and numerical studies have been carried out in the past to study the complex flow fields associated with such explosions. Detailed reviews (e.g., Plesset and Prosperetti, 1977; Blake and Gibson, 1987; Prosperetti, 1982; Rood, 1991) have summarized past experimental and numerical results. Experimental studies are too numerous to list completely; however, most studies in the past focused on the dynamics of cavitation (small) bubbles. Controlled experimental studies of large scale explosions have been limited due to difficulties in acquiring the data. Some limited number of studies of large-scale bubbles have been reported (Cole, 1948; Snay et al., 1952). Bubble-bubble interactions have also been studied in the past using experimental and numerical methods (e.g., Warren and Rice, 1964; Chahine et al., 1992; Chahine, 1994). However, in most experimental cases, due to difficulties in acquiring detailed data, only limited information (e.g., pressure outside the bubble and bubble radius variation in time from photographic images) has been obtained. More recently, a series of experiments were carried out to investigate relatively large-scale bubble explosions (Menon and Lal, 1996a, b; Lal and Menon, 1996a, b). These experiments were conducted in shallow water (1 atmosphere ambient pressure) to investigate the dynamics of bubble-bubble and bubble-wall interactions in such flows and to investigate feasibility of targeting buried mines for destruction in beaches. The data obtained from these experiments have been used to validate the numerical model discussed in this paper.

Various numerical studies have also been conducted in the past. These range from very simple 1-D analytic solutions (e.g., Lauterborn, 1976; Plesset, 1971; Prosperetti, 1982) to more complex 2D/3D studies. Many of the past studies employed the Boundary Element Method (BEM) or its variants (e.g., Chahine et al., 1992, Chahine and Duraiswami, 1992; Chahine and Perdue, 1988; Duncan and Zhang, 1991; Blake et al., 1986, Taib et al., 1984; Plesset and Chapman, 1970). The BEM method is computationally very efficient since only the flow outside the bubble surface is computed which allows the reduction of the dimensionality of the problem by one. Results have shown that this method has the ability to capture many aspects of the bubble oscillation and collapse process (e.g., Chahine et al., 1992; Chahine, 1994; Kalumuck et al., 1995). However, due to the simplifications

incorporated into the BEM formulation, this method also has some inherent limitations. For example, compressibility in the gas cannot be included, the gas motion inside the bubble is not computed and in the study of bubble collapse near a surface, BEM can be used only up to the point of jet formation. To model the flow beyond the point of bubble collapse, BEM has been modified by introducing vortex elements (e.g., Zhang and Duncan, 1994; Zhang et al., 1993; Best and Kucera, 1992; Best, 1993). Another limitation of this approach is that to set up the simulation problem, some basic assumptions are required (for example, the gas is assumed to satisfy the polytropic equation of state, see Chahine, 1994). Although for many bubble/flow interaction situations, the assumptions inherent in the BEM method are acceptable, in general, for complex strong explosions the validity of these simplifications become questionable (see further discussion below).

A numerical method that includes both compressibility and an ability to capture the entire bubble collapse in complex configuration is used in this study. This numerical scheme, called the ALE3D, is based on the Arbitrary Lagrangian-Eulerian (ALE) method and was originally developed at the Lawrence Livermore Laboratory to study structural dynamics. Past applications of this method include the 2D ALE (e.g., Tipton, et al., 1992) and the full 3D calculations (Milligan et al., 1995) of bubble collapse. However, it appears that so far, the full capabilities of the ALE3D have not yet been exploited to simulate and investigate the dynamics of underwater explosions. This paper reports some recent results of single and double bubble explosions both in free field and in the vicinity of a rigid wall.

The current numerical approach is also motivated by the observation that many of the assumptions used in past numerical studies are violated by the bubble behavior as observed in the experiments. For example, the bubble oscillation process occurs in a very short time (typically, in a few micro or milliseconds) with significant compressible effects in the collapse phase, especially when the pressures experienced are comparable to the bulk modulus of water, as is the case in deep sea strong explosions. Bubble shape is also known to quickly deviate from sphericity at bubble maximum, thereby, violating axisymmetric assumptions used (e.g., Szymczak et al., 1993; Zhang and Duncan, 1994) in the past. Non-spherical bubble evolution requires full 3D treatment. Thus, simple 1-D or 2-D/axisymmetric analysis or incompressible methods cannot accurately resolve the bubble dynamics. Furthermore, some of the past simplified studies also fail to provide sufficient details of the flow field inside and outside the bubble and cannot account for the interaction between the vapor and the liquid phases. Conventional numerical methods (even using full 3D) such as Lagrangian or Eulerian techniques are also not practical for

bubble oscillation studies, since the expansion and collapse of bubbles create severe fluid motion so that a Lagrangian approach (in which the grid points move with the fluid resulting in severe grid distortion) becomes inappropriate, while a Eulerian approach becomes computationally very expensive since very high (adaptive) grid resolution in the regions of interest (which is essential) is required to resolve the bubble's shape.

The ALE3D employed here combines the lagrangian and eulerian features into one code. This code has been extended to study bubble instability and collapse in this study. In the present paper, section 2 contains a brief description of this code, followed by a discussion of the equations of state in section 3. The results are discussed in section 4 and the conclusions are summarized in section 5.

## 2. The Numerical Method

ALE3D (Anderson et al., 1994) is an explicit, 3D finite element code that simulates the fluid motion and elastic-plastic response on an unstructured grid. The grid may consist of arbitrarily connected hexahedral shell and beam elements. The ALE algorithm is implemented by carrying out a complete Lagrangian calculation followed by an advection step. After each lagrangian step, a new mesh is created using a finite element based equipotential method to relax the distorted grid. In the eulerian advection step, the fluid variables such as mass, density, energy, momentum and pressure are reevaluated on the new mesh by allowing fluid motion (based on the solution of the euler equations of motion). Following DYNA3D (Hallquist, 1982), the stress gradients and strain rates for the lagrange step are evaluated by a lowest order finite-element method. The equation of state and constitutive models are described elsewhere (e.g., Woodruff, 1976; Steinberg, 1991) and, therefore, are only summarized here for brevity.

The advection step uses methods similar to those developed for 2D ALE code, CALE (Tipton, 1990), and the 3D Eulerian code, JOY (Couch et. al., 1983). For pure zones, a second order, monotonic advection algorithm is used (Van Leer, 1977). This advection step can create mixed material elements (i.e., liquid and vapor). Material interfaces are not explicitly tracked but for the purpose of carrying out mixed element advection, they are inferred from volume fractions. Separate state variables are kept for each component of a mixed element. Further details of this code is given in the above mentioned references and therefore, avoided here for brevity.

To use this code, proper inputs must be provided to first generate the appropriate grid and then to model the fluid and structure properties. Some of the relevant details for the bubble studies are summarized in the next section.

### 3. Equation of State

A key requirement in employing ALE3D is the proper choice of the equations of state for the various materials in the problem. Only a brief summary is given here primarily to highlight some of the inherent limitations of the original code.

The explosion bubble is assumed to be of noncondensible steam and its equation of state is assumed to be gamma law with a gamma of 1.3. The equation of state is represented as:

$$p = (\gamma - 1)(1 + \mu)E \tag{1}$$

where, p is the pressure, the relative volume is given as: $\mu = \rho / \rho_0 - 1$ and E is the internal energy per unit volume.

The water is modeled using a Gruneisen form given as:

$$p = \frac{\rho_0 C^2 \left(1 + (1 - \gamma_0 / 2)\mu - a/2\mu^2\right)}{\left(1 - (S_1 - 1)\mu - S_2 \frac{\mu^2}{\mu + 1} - S_3 \frac{\mu^3}{(\mu + 1)^2}\right)^2} + (\gamma_0 + a\mu)E \tag{2}$$

For expanded material the above expression is replaced by

$$p = \rho_0 C^2 \mu + (\gamma_0 + a\mu)E \tag{3}$$

Here, C is the intercept of the shock velocity-particle velocity curve (the Huguenot curve), $S_1, S_2$ and $S_3$ are the coefficients of the slope of the shock velocity-particle velocity curve and $\gamma_0$ is the Gruneisen gamma and $a$ is the first order volume correction to $\gamma$. The common values of these coefficients are tabulated in Table I. Our present interest is in underwater explosions in shallow water. Comparison of the pressure predicted by the above equation of state with the data obtained from NIST (1988) in the appropriate temperature and pressure range of interest showed significant discrepancies. In order to circumvent this problem, water regime data was modified to obtain new coefficients. It

was determined that with these coefficients, the equation of state very closely agreed with the experimental results.

However, the current limitation of the ALE3D input structure is that it requires that the equation of state in the form (3) must be used in the code. Thus, the behavior of a material like water which has a discontinuous transition from steam to water can not be adequately represented by this form. A more general approach would involve actually reading the data directly rather than fitting it to the above form. This has not yet been accomplished but is under investigation.

The high explosive materials in the deep sea explosives are modeled using the Jones-Wilkins-Lee High Explosive equation of state. The equation of state is represented as

$$p = A\left(1-\frac{\omega}{R_1 V}\right)e^{-R_1 V} + B\left(1-\frac{\omega}{R_2 V}\right)e^{-R_2 V} + \omega V E \qquad (4)$$

The coefficients used for the case of pentolite (a representative high explosive) are given in Table II. Again, the current format of the ALE3D input. does not allow inclusion of explosion material that do not conform to the state equation (4). Thus, modifications are required to allow study of more complex explosive material.

The results of the numerical studies are reported in this paper. In addition, the earlier experimental results have been included as Appendices to this report. Appendix A summarizes the results of the bubble-wall experiments, Appendix B and Appendix C are copies of papers presented/submitted on the bubble-bubble interaction experiments and Appendix D contains a draft paper submitted for presentation on the numerical studies.

## 4. Results and Discussion

In this section, the results obtained for the various test cases are summarized and discussed. The present study was first carried out to compare with data obtained in an ongoing experimental study (Menon and Lal, 1996a; 1996b; Lal and Menon, 1996a, 1996b). These studies serve to identify the capabilities and limitations of the ALE3D code and to identify areas for further study. The computations were then extended to realistic deep sea explosions and detonation cord (used for mine destruction) explosions to demonstrate the capability of the present methodology.

### 4.1 Free Field Single Bubble Oscillation

This simulation employed test and geometrical conditions similar to the experimental set-up of Menon and Lal (1996a). The experimental case is idealized as a freely oscillating bubble placed in the center of a 1.5 m x 1.5 m x 1.5 m tank filled with water. The computational domain is considered an approximation to the actual tank, since, in the experiments, the tank had similar dimensions but the top surface was a free water surface. A current limitation of the ALE3D is that it requires all far field boundaries to be modeled as a rigid reflecting wall. This limitation of the code can be modified by appropriate changes to the source code; again, this is an issue for future investigation.

The initial bubble diameter is 6.34 cm and the initial explosion pressure is 9.34 atmospheres (both identical to the experimental case). The water pressure is 1 atmosphere and hence, these studies are relevant for shallow water explosions.. The water and the steam are modeled as described earlier. The ALE mesh treatment is applied to all the elements in the bubble and in the vicinity of the bubble. But away from the bubble where the bubble explosion does not cause much grid distortion, lagrangian mesh treatment is used. The number of elements used to resolve the bubble and the surrounding water was varied to confirm that the results are not grid dependent. In addition, both full bubble and 1/8-th section (using symmetry boundary conditions) were compared to determine if the reduced domain (which is computationally more efficient) could be employed for scaleup studies. Results showed that for most of these cases studied here, the 1/8 size domain computations were in very good agreement with the full 3D bubble results. For a typical 3D simulation, 50,000 elements were used to discretize the domain, while for the 1/8th domain, 10,000 elements were used. Figure 1 shows a representative grid distribution used for the single bubble calculations. Grid independence studies were carried out by repeating

representative simulations using grids as large as 150,000 element. Typical calculation using the full 3D coarser grid required around 3 CPU hours on a single processor Silicon Graphics Power Challenge (MIPS R8000/90 MHz). Although, various cases have been simulated, only characteristic results are discussed below.

The bubble grows after the explosion due to the high vapor pressure inside the bubble. Because of inertia, this results in an over expansion and the pressure inside the bubble falls below the ambient (water) pressure. As a result, the bubble collapses and reaches a bubble minimum at which time the internal pressure again exceeds the external pressure. Thus, a bubble oscillation process is set up and continues as long as there is sufficient energy available. However, energy is continuously lost during the oscillation due to irreversible mechanical work done on water and vapor and due to the onset of various instabilities. In Menon and Lal (1996a), detailed analyses of the energy loss and the instability mechanisms were performed and results suggest that during the collapse process the Rayleigh-Taylor (R-T) instability occurs at the interface. This results in a distortion in of vapor-water interface and a consequent loss of energy. The R-T instability has been captured in the numerical study. For example, Figs. 2a-f show the time sequence of bubble shape during the first bubble oscillation. These figures clearly show the loss of sphericity after the first bubble maximum (figs 2d-e) and, by the bubble minimum, the bubble interface has become distorted with the formation of large-amplitude wave-like disturbance. The deviation from sphericity and the formation of waves on the bubble interface is characteristic of Rayleigh-Taylor instability.

To ensure that this wave-like undulation of the bubble interface is not due to the acoustic reflections from the wall, a series of calculations were carried out (a) by extending the dimensions of the tank by a factor of 4, and (b) by replacing the rectangular domain by a spherical domain. Results (not shown) showed that although, there are changes in the bubble oscillation period (discussed below), in all cases, however, the wave-like interface distortion appears near the bubble minimum. Thus, these results clearly show that the R-T instability does occur (as observed in experimental data, Menon and Lal, 1996a,b) and has been captured in these calculations.

Figures 3a-c and 4a-c show respectively, the pressure field in terms of contours and gray-scale representation inside and outside the bubble during the bubble oscillation. The pressure field around 12 ms (as the bubble is collapsing) clearly shows the lack of spherical symmetry; however, after the bubble minimum (Figs 3c, 4c), the pressure field

again becomes more symmetric except very near the bubble interface. This is consistent with the R-T instability, since interface deformation only occurs during the bubble collapse, however, as the bubble rebounds into the next oscillation, the interface again becomes more spherical since the conditions are such that the R-T stability condition is satisfied.

The 3D nature of the flow field inside and outside the bubble can be visualized more easily in the velocity vector fields, as shown in Figs. 5a-c. Figure 5a shows the outward motion of the bubble just before the bubble maximum, Fig. 5b shows the velocity vectors during the first compression cycle and Fig. 5c shows the outward motion of the bubble just after the first bubble minimum. The magnitude of the velocity vectors also indicates that the acceleration of the fluid is minimum at the beginning and end of compression or expansion phases. These features demonstrate the complex nature of the flow field set up during bubble oscillation (and as discussed later, the flow patterns are even more complex for the bubble-bubble and bubble-wall cases).

The R-T instability can also be inferred by analyzing the variation of the radius with time. For example, Fig. 6 shows that $d^2R/dt^2 > 0$ (which is a necessary condition for R-T instability) occurs as the bubble collapses and reaches its first minimum. During the second expansion process, this criterion is no longer satisfied (not shown), consistent with the earlier observation that the interface becomes more smooth.

Figures 7a and 7b show respectively, the variation of the pressure within the bubble and the bubble radius with time. The computed results are compared with the data obtained in the recent (Menon and Lal, 1996a). The comparison shows that the computed first period of oscillation (around 15 ms), the first peak pressure (at first bubble maximum) and the maximum radius (at bubble maximum) agrees quite well with the experimental data. The slight differences during the contraction phase may be due to differences between the experimental and numerical setups. For example, the experimental set-up (described in Menon and Lal, 1996a) employed a glass globe (which contained the stoichiometric fuel-air mixture) with an insert that contained the pressure transducer and the spark generator while these features were ignored in the numerical model. In addition, the presence of the free water surface on the top boundary and the presence of glass fragments (formed during the glass globe explosion) in the experimental study were also not included in the numerical model. Furthermore, it is also not clear how much of the measured pressure is being modified (or contaminated) due to the present of the transducer in the bubble.

In spite of these differences it is interesting to observe that the numerical and experimental results are in relatively close agreement. This suggests that the experimental artifacts (identified above) are not significantly modifying the dynamics of the bubble oscillation process. Therefore, the present numerical study serves to provide an independent validation of the results described earlier in Menon and Lal (1996a) and in Lal and Menon (1996a, b).

To ensure that the observed decrepancies were not due to any numerically introduced artifacts, a series of parametric studies were carried out to address various numerical issues. For example, to study the effect of grid resolution, simulations employing 50,000 elements and 150,000 elements were compared. The higher resolution grid was clustered in the vicinity of the bubble. Figure 8 compares the results of these simulations. Although, the higher resolution results show a slightly better peak pressure at the first bubble minimum, the overall agreement between both the simulations is quite good. This clearly demonstrates that the results obtained with the relatively coarser grid are not grid dependent.

As mentioned earlier, to reduce the computational expense, the tank and the bubble configuration was also idealized as an octant with three planes of symmetries. This reduces the computational expense by a factor of eight. The results are compared in Fig. 9 and as expected, since the observed loss of sphericity (in the full 3D case) is not allowed in the octant simulation, the octant case deviates slightly from the full tank case especially near the bubble minimum. However, the period of oscillation and pressure peak at the bubble minimum are very close to the full 3D prediction and therefore, it was determined that the octant domain could be used (with substantial savings in the computational time) for parametric studies.

An inherent limitation of laboratory experiments is that the facility set up (e.g., the water tank) can modify the bubble oscillation dynamics making the experimental result not fully representative of a free field underwater explosion. For example, it has been pointed out in the past, that the acoustic reflections from the tank wall may modify the bubble dynamics and also control the formation of the interface instability. Although, the acoustic pressure is significantly lower (by an order of magnitude) than the explosion pressure, the high speed of acoustic waves (e.g., 1500 m/s) makes the waves to bounce back and forth (from the side and bottom walls and also from the free surface) numerous times during a typical

bubble oscillation period of 15 msec. To determine how the walls play a role in the bubble dynamics, simulations were carried by (a) moving the walls considerably further out (by a factor of 5) so that the total time for the acoustic wave to bounce from the wall is increased from around 1 msec to around 5 msec, and, (b) by changing the far field boundary from a rectangular domain to a spherical domain (so that characteristics of the reflected acoustic waves becomes different).

Figures 10a and 10b show respectively, the pressure signature observed near the wall in the experimental study and at a similar location in the computational model. The strength of the pressure fluctuation near the wall is very similar in both studies and the high frequency content of the pressure signature is also similar (although not identical). Spectral analysis of the pressure trace did confirm the presence of a high frequency in both the data. This high frequency is not clearly visible in the numerical data since the very coarse grid used in the far field damps this frequency considerably. Simulation using much higher grid resolution in the far field showed the presence of the high frequency.

Comparison of the results of all these cases demonstrated that the wave-like instability of the bubble interface remains unaffected by the changes in the wall location and shape. Thus, it was determined that the walls were not causing the distortion of the bubble interface and that the formation of wave like distortion on the interface was due to the R-T instability. However, acoustic wall reflections do have some subtle effects on the bubble oscillation period and the peak pressure at the bubble minimum. When the tank dimensions were increased, the period of oscillation increased and the peak pressure at the bubble minimum was decreased. This is shown in Fig. 11. Replacing the rectangular walls by a spherical wall in the far field showed no change in the time period but did show a decrease in the peak bubble pressure at the first minimum (Fig. 11).

An estimate for the time period for a freely oscillating bubble can be made relative to the reference time period T which is given by the relation $T = R_{max}(\rho/p_{\infty})^{1/2}$, where $R_{max}$ is the maximum radius of the bubble, $\rho$ and $p_{\infty}$ are respectively, the density and ambient pressure. Based on our experimental data, $R_{max}$ is approximately 7.5 cm, which results in an estimate for the reference time period as around 7.5 msec. Thus, the ratio of the actual period of oscillation in our experiment (around 15 msec) to the reference time period T is approximately 2. This ratio is in agreement with the observations in deep sea studies (e.g., Cole, 1948) where it was reported that the scaled time period is also around 2. Other scaling analysis (reported in Menon and Lal, 1996a) also suggests that the present

experiments are a reasonable (although not exact, since both the effects of depth and Froude number are not fully captured) representation of field explosions.

The current results do suggest that the presence of walls is effecting the time period (i.e., it is decreased). In free field, an increase in T will occur since the bubble will be allowed to expand further than the maximum reached in the laboratory tank. However, the maximum radius achieved is also a function of the initial explosion energy and thus, there is an upper limit to $R_{max}$ for every explosion. This suggests that if the outer boundaries are removed far enough, the numerical results will asymptotically reach the free field case. Free field explosion can also be simulated by replacing the outer wall boundary conditions with outflow boundary conditions. However, as mentioned earlier, the present ALE3D code requires that the far field boundary be modeled as a solid reflecting wall. This limitation of the code can be removed only by modifying the source code. This is will be investigated in the future.

In any event, for the experimental configuration, it appears that the bubble dynamics in the water tank cannot be considered identical to a free field bubble behavior. However, there are no glaring differences in the bubble oscillation dynamics. The interface distortion appears to be independent of the wall location and shape and overall nature of the bubble dynamics is captured relatively accurately with only differences in the exact value of the time period and peak bubble pressure.

Another issue that was addressed was the effect of pressure variation with depth. In shallow water explosions of small bubbles it is commonly assumed that the variation of pressure with depth will have very negligible effect on the bubble dynamics. However, since the present study is focused on relatively large bubbles (the radius at the bubble maximum is around 7.5 cm), the effect of pressure variation with depth may play a role. Therefore, simulations were carried out with and without pressure variation with depth and the results are shown in Figure 12. It can be seen that an increase (although not very significant) in the pressure peak at the first bubble minimum occurs when the pressure-depth variation was included.

The above studies clearly demonstrate the general capability of the ALE3D code. Comparison with the experimental data also provides confidence on the accuracy of the numerical predictions. With the basic code validated against our current experiments, the ability of the code to simulate realistic deep sea explosions can be evaluated by simple

modifications to the input conditions. Although detailed calculations of the deep sea explosions have not yet been completed, a sample calculation using a pentolite explosive at depth of 1000 m was simulated using this code. Figure 13 shows the pressure trace of the deep sea explosion. It can be seen that the deep sea explosion dynamics is qualitatively similar to that observed in the shallow water studies. The peak pressure at the first bubble minimum (when normalized by the explosion pressure) is approximately 0.83 in the deep sea case while in the shallow water experiment it is 0.94. Furthermore, when the time period is scaled with $R_{max}\sqrt{\rho/p_{\infty}}$, both the deep sea and the laboratory study predict a ratio of around 2 which is in agreement with earlier deep sea data (e.g., Cole, 1948).

Further simulations are planned to investigate deep sea explosions using actual explosive materials and configurations. These studies will be reported in the future.

4.2 Bubble-Bubble Interactions

To investigate bubble-bubble interactions, a series of studies were carried out using bubbles of various sizes. A limitation of the ALE3D code current setup is that it does not allow the effect of phase difference (which was explored in the experiments, see Lal and Menon, 1996a, b) to be incorporated into the model. Thus, for all simulations, both bubbles explode simultaneously and are therefore, in phase. However, by using different bubble sizes the effective volumetric energy release from each bubble was varied. The explosion energy per unit volume in each bubble was also varied for the same bubble size to determine interaction between two equal size but disparate explosions. The effect of inter-bubble distance on the interaction process was also studied using the current ALE3D setup. Some characteristic results are discussed below.

As for the free bubble case, the mesh within and in the vicinity of the bubbles is treated using the ALE algorithm while the rest of the field is treated using Lagrangian approach. For a typical simulation, 25,000 elements are used to resolve the bubble regions with another 38,000 elements were used to resolve the surrounding and far field. Again, grid independence studies were carried out to ensure that the results are not grid dependent. The water and steam equations of state are modeled as described earlier.

Consider first the situation of two identical bubbles of radii 3.17 cm placed approximately 8 cm apart in the water tank (similar to an experimental case). The explosion energy in both bubbles were identical and hence, this scenario essentially models (by virtue of the

method of images) a single bubble explosion near a reflective wall. The bubbles expand and then collapse onto each other and a reentrant water jet with a high speed (30 m/s) is formed in both vertical and horizontal directions. Figures 14a-f shows a time sequence of the bubble-bubble interaction and also views from different angles. The corresponding pressure contours and the velocity vector field are shown in Figs. 15 and 16, respectively. The jet directed towards the adjacent bubble impinges on its counterpart as in a stagnation point flow. As the bubble-bubble process continues, two counter vortex rings are formed with the velocity between the bubble increasing to as high as 50 m/s (Fig. 16c). Formation of this type of vortex ring bubble has been observed in experimental studies of bubble collapse near a rigid wall.

For comparison, the images for a similar study carried out in our experimental facility is shown in Figs. 17a-c. Comparison between Figs. 14 and 17 show remarkable similarity in the bubble-bubble interaction and the collapse stage.

The pressure time trace for this bubble-bubble interaction is shown in Fig. 18. Since both bubbles are identical, their oscillation period and peak pressure at the first minimum are also identical. The pressure in-between the two bubbles (which can be considered the impact location) is higher than the pressure in the bubble itself at the bubble minimum. This increase in peak impact pressure is similar to that seen when a bubble collapses near a wall (described in the next section) and is due to the impingement of the water jet.

When same size bubbles were exploded at the same distance as before, but with one bubble containing four time more energy than the other, a similar result was obtained except that in this case, the weaker bubble is sucked into the other bubble with a velocity reaching a maximum of around 85 m/s. Figures 19a-h show this interaction process along with different views of the collapse of one bubble into the other. The reentrant water jet is first formed in the weaker bubble during the first oscillation (Fig. 19a) and the vortex ring thus formed merges into the (still coherent) stronger bubble (Fig. 19b). The shapes of the two bubbles (bubbles can be identified in the figures by the colors: the cyan bubble energy is less than the blue colored bubble) at the instant of jet formation in the weaker bubble (Figs. 19c and 19d) and at the merging of the two bubbles (Figs 19e-h) are shown in these figures. The jet formation in the stronger bubble is delayed till the second oscillation at which time the second bubble also collapses.

Figure 20 shows the pressure time trace for this case. The general behavior is similar to the earlier (identical explosion case) except that here, the peak pressure in the bubbles at the bubble minimum is different due to different energy content. The pressure in-between the bubbles is still somewhat higher than even the stronger bubble pressure peak due to the high reentrant water jet velocity (85 m/sec compared to 30 m/sec for the case described in Figs. 14-16).

When two bubble of different sizes, e.g., of radii 3.17 cm and 2.17 cm (and thus, with different total explosion energy) are exploded, the results are quite similar to the case discussed above. Figs. 21a-f shows the time sequence of this bubble-bubble interaction and Figs 22a-c shows the corresponding velocity vector field (the time index in the figures can be used to correlate these two figure sets. In Fig. 21a, the bubbles are expanding but because of the greater inertia and explosion strength of the bigger bubble, the smaller bubble is inhibited as seen at their first maximum, (Figs. 21b-c). During the collapse, the pressure drop in-between the bubbles is more than on the other sides and as result, this pressure differential causes the smaller bubble to be engulfed into the larger bubble. The center of motion of the water jet directed towards the bubbles does not immediately adjust to the motion of the bubbles and thus, the water motion is directed off center of the bubble. This creates a very high pressure on the side of the smaller bubble away from the larger bubble. This high pressure and the low pressure in-between the bubbles creates enough momentum to form a water jet through the bubbles which penetrates to the other side of the bubble as shown in Figs. 21d-f

The velocity vector field (Figs. 22a-c) shows very clearly the formation of the water jet. Experimental study also showed a similar behavior when two bubbles of unequal sizes were exploded simultaneously (Lal and Menon, 1996a,b). Figure 23 shows a characteristic image obtained from the experimental study. Formation of the water jet was also observed in the experiments when two identical bubbles were exploded out-of-phase. Out-of-phase explosion essentially changes the relative strength of the bubble explosion during interaction and is therefore, somewhat similar in the dynamics to the present case with two unequal bubbles exploding simultaneously. However, as mentioned earlier, since the current ALE3D code cannot simulate phase difference between the adjacent explosions, it is premature to correlate these different types of initial conditions. Once the ability to include phase difference in the simulation code is incorporated, more details investigation of the interaction can be carried out.

Finally, Fig. 24 compares the pressure between the two bubbles for the various test cases simulated so far. As can be seen, all cases demonstrate the same period of oscillation. However, the case with increased energy content shows the strongest water jet formation (around 85 m/s) and as a result, causes the largest impact pressure at the first bubble minimum.

4.3 Bubble-Wall Interactions

Bubble collapse near a rigid wall is of significant interest due to a variety of reasons related to its ability to cause serious damage to the structure. This is because when the bubble collapses near a rigid surface, a strong reentrant water jet is formed that is directed towards the wall. The peak impact pressure on the wall due to this water jet can be substantially higher that the explosion pressure especially when the initial explosion energy is very large. The dynamics of this collapse process has been under investigation for some time; however, experimental capability to record all the effects of the interaction process is limited due to the difficulty in accessing the interaction zone. Past numerical studies have been able to capture the collapse process, but as noted before, such calculations resorted to obtaining information from experiments to ensure that the simulation initial conditions agreed with experimental data. The ALE3D approach employed here allows for the entire process to be captured without making any adjustments. For a typical simulation, a total of 22,000 elements were used to resolve the bubble and the wall region and another 35,000 elements were used for the rest of the domain. Various simulations were performed by varying the explosion strength and distance of the bubble from the rigid plate. However, only characteristic results are discussed here to highlight the pertinent observations.

Two cases are discussed here with bubble placed 5 cm above (buoyancy inhibiting jet formation) and 5 cm below (buoyancy aiding the jet formation) the wall. Figures 25a-i show the time sequence of the expansion and collapse of a bubble near a rigid wall, for the first case. Different views of the bubble collapse process is also shown in this figure. Figures 26a-i and 27a-i show respectively, the corresponding pressure gray scale and contours and Figs. 28a-i show the velocity vector field. Figure 25a shows that the bubble is almost spherical at the first maximum. As observed earlier, the bubble begins to distort as it collapse (Figs. 25b-f). As the bubble collapses, the differential pressure forces a reentrant water jet to be formed as shown in figs. 25b-d (and also seen more clearly in Figs. 28b-d). As this jet impacts on the rigid plate, a ring bubble vortex is formed as

shown in Figs 28g-i. The physics of the re-entrant jet formation is quite similar to the bubble-bubble case. The bubble expands until it touches the wall. Since there is less volume of water between the wall and the bubble during the collapse, the pressure drop is quite large relative to the pressure on other sides of the bubble. This pressure differential further forces the bubble towards the wall as can be seen in Figs. 26-28. Since steam is lighter, the bubble tends to move further away from the wall (due to buoyancy) for the case where the gravitational force is inhibiting the jet formation (Figs 26-28) while for the second case, the bubble is further accelerated towards the wall (not shown since the general characteristics are qualitatively similar to the case described in Figs. 25-28).

The effect of buoyancy in the formation of jet is very evident in Fig. 29a where the impact pressure on the wall is plotted versus time. The buoyancy-aided case almost doubles the impact pressure when compared to the buoyancy-inhibited case. The impact pressure for even the low explosion bubbles is as much as two-and-half time that of the peak explosion pressure for the buoyancy aided case.

The current methodology is also able to capture the vortex ring bubble as shown in the above figures. This vortex ring bubbles after the jet impact has been also observed both in experiments (Tomita and Shima, 1986 and Vogel et al., 1989) and in recent numerical work (Best, 1993; Szymczak, et al., 1993; Zhang and Duncan 1994).

Finally, Fig. 29b compares the peak impact pressure measured at the flat plate in our experiments (see Appendix A) with the current numerical prediction. The experimental data suggested that there is an optimum distance $d/R_o$, d is the distance above the plate where the initial bubble is located. Data suggests that for $d/R_o = 2$, the impact pressure (normalized by the explosion pressure) is a maximum with the impact pressure more that 4 times the explosion pressure. The numerical study shows a similar trend, i.e., there is an optimum distance for peak impact pressure. However, the numerical data shows that this optimum distance is smaller that observed in the experiment but interestingly enough, the predicted peak pressure at the impact location is very similar to that observed in the experiment. The discrepancy between the optimum location measured and predicted may be related to the limitations of the experimental set up, as noted earlier,(such as, the presence of the transducer and spark igniter inside the bubble which are not included in the simulation model. More detailed analysis is currently underway to understand the physics of this interaction that leads to such an optimum location. This will be reported in the near future.

## 4.4 Detonation Cord Explosions

Currently, there is an ongoing study of underwater detonation using explosive cord at NSWC, Indian Head Division. Such explosives are long cylindrical cord made of explosive material that is place next to surfaces targeted for destruction and then ignited. Experiments have shown some contradictory results as related to the explosion bubble behavior. To demonstrate the capability of the ALE3D code to simulate realistic underwater detonation of currently employed munitions, a series of calculations were recently performed to study the behavior of detonation cord in shallow water. Three cases are discussed below: (a) a single 30 cm long cord of 0.5 cm diameter exploding in free field, (b) a 30 cm long cord of 0.5 cm diameter exploding 1 cm above a rigid wall and (c) a rectangular mesh of 20 cm x 20 cm square of cord of 0.5 cm diameter exploding 1 cm above a rigid wall. The last configuration is a very close idealization of the cord used for actual field studies. The explosive material was assumed to be pentolite which is strictly incorrect, however, the present study is more of demonstration nature. Realistic cord material properties can be easily included at a later stage. Some characteristic results are discussed below to demonstrate the ability of the ALE3D code to capture these types of realistic detonation.

Figures 30a-i show the bubble expansion and collapse process for the foot long (30 cm) cord exploding in free field. Figures 31a-i show the corresponding velocity vector field for the expansion and collapse process and Fig. 32a and 32b show two other perspective of the velocity field. As can be see, initially the bubble expands almost cylindrical, however, as it begins to collapse, the collapse process is faster along its major axis (from the ends) than along its minor axis. This is seen in Figs. 30b, c and 31b, c. This differential collapse results in the surrounding water rushing into the bubble at a higher velocity along the major axis when compared to the fluid motion along the minor axis. Thus, the bubble collapses along the major axis while it bulges along the major axis (in the central portion of the cord). The water jet formation due to this collapse process is shown in Figs. 30d-f, 31d and 32a, b. After the jet is formed, the bubble rebounds (Figs. 30g-i, 31e-f) and a double vortex ring bubble is formed (similar to the ring bubble seen earlier for the bubble-bubble case).

Figures 33a-i show the time sequence for the cord explosion near the rigid wall. Figures 33a-f shows the bubble shape during collapse, Fig. 33g shows the shape during jet

formation and Figs. 33h-i show the shape during the rebound stage. Figures 34a-f show the corresponding velocity vector field and Figs. 35a and 35b shows different perspective of the flow field during collapse process.. Additional visualization of the flow field are shown in Figs. 36a, b (velocity field at 6.8 ms - see Fig. 33), Figs. 37a-c (pressure contours) and Figs. 38a-c (bubble shape).

Figures 33a-i show the oscillation of the bubble formed during cord explosion near the wall and shows a picture quite different from the spherical bubble collapse studied earlier. It appears that unlike the spherical bubble case, where the differences between the pressure on the side of the wall and away from the wall drives the jet formation, in the cord case, the bubble experiences (in addition to this pressure differential) another pressure differential due to the asymmetric bubble expansion along the major and minor axis. As shown in Figs. 34a and 35a,b, this causes the water to rush into the bubble at an angle (while in the spherical bubble case the jet motion is perpendicular). As a result, the jet formation for the cord-wall case is much more complicated, as shown in Figs. 33g, 34d and 36a, b. Finally, the rebound of the bubble is also more complicated as shown in Figs. 33h, i and 34e, f.

Finally, a simulation was carried out for a cord mesh adjacent to the wall. As mentioned above, this is a close approximation to the actual field device. Figure 39 shows two images of the grid domain just after the initial explosion. The grid is clustered near the cord region and near the wall to resolve the bubble dynamics. The cord region and the surrounding water is treated as ALE materials while the far field water is treated as lagrangian. Figures 40a-i show the bubble shape at various stages of the expansion and collapse process and Figs. 41 and 42 show different views of the bubble shape at 5.8 ms and 6 ms (by which time the collapse process is almost completed). The fluid motion during this interaction process is shown in Figs. 43a-f and the pressure contours corresponding to Figs. 42b and 42e are shown in Figs. 44a and 44b, respectively.

The bubble expansion and collapse process is even more complex for this cord-mesh case. However, the general collapse process is similar to the cord-wall case with the major difference being related to the uneven expansion of the bubble. During the collapse process the diagonal regions travel at a different speed compared to the normal direction. As a result, the jet formation is also modified by this differential collapse and the jet is formed at an angle to the wall as can be seen in Figs. 43b and 43e.

## 5. Conclusions

These studies show that the present implementation of the ALE3D for underwater explosion studies has the potential for addressing fundamental issues related to the highly complex process of bubble oscillation and collapse under various conditions. The basic code has been validated using shallow water explosion data obtained in recent experiments. In addition to isolated bubbles exploding in (an approximate) free field, bubble-bubble and bubble-wall interaction studies were also performed. It has been shown that all the features observed in past experiments have been captured in these studies. The formation of reentrant water jet as the bubble collapses near a rigid surface and the formation of ring vortex bubble has been captured in the simulation. These features are in good qualitative agreement with experimental data. Furthermore, the ability of the ALE3D code to study realistic deep sea explosions or detonation of realistic explosives such as detonation cord (used for mine destruction) has been demonstrated in these studies.

Limitations of the current ALE3D code have also been identified during these studies. For example, the current code is unable to simulate bubble-bubble interaction with a phase difference between the explosions. The far field boundary conditions currently cannot be changed from reflecting wall. Time dependent spatially moving detonations are also not feasible using the present code. However, such limitations can be removed by proper modifications to the code. These issues are still under investigation.

## Acknowledgments

This work was supported by the Office of Naval Research under grant No. N00014-91-J-1993. The ALE3D code was provided by Lawrence Livermore Laboratory..

## References

Anderson, S., Dube, E., Futral, S., Otero , I., and Sharp, R., (1994) " Users Manual For ALE3D," Lawrence Livermore National Lab., CA.

Best, J. (1993) "The formation of toroidal bubbles upon the collapse of transient cavities,"J. Fluid Mech., 251, pp. 79-107.

Best, J. P., and Kucera, A., (1992) "A numerical investigation of non-spherical rebounding bubbles,"J. Fluid Mech., 245, pp. 137-154.

Blake, J. R., Taib, B. B., and Doherty, G., (1986) "Transient Cavities Near Boundaries. Part I. Rigid Boundary," J. Fluid Mech., 170, pp. 479-497.

Chahine, G. L., and Perdue, T. O., (1988) "Simulation of the Three-Dimensional Behavior of an Unsteady Large Bubble near a Structure," 3rd International Colloquium on Bubbles and Drops, Monterey, CA.

Chahine, G. L., and Duraiswami, R., (1992) "Dynamical Interactions in a Multi-Bubble Cloud," Trans. ASME, 114, pp. 680-686.

Chahine, G. L., Duraiswami, R., and Rebut, M. (1992) "Analytical and Numerical Studies of Large Bubble/Bubble and Bubble/Flow Interactions," 19th ONR Symposium on Naval Hydrodynamics, Seoul, S. Korea.

Chahine, G. L. (1994) "Bubble Dynamics and Cavitation Inception in Non-Uniform Flow Fields," 20th ONR Symposium on Naval Hydrodynamics, Santa Barbara, CA.

Chahine, G. L. (1994) "Strong Interactions Bubble/Bubble and Bubble/Flow," in Bubble Dynamics and Interface Phenomena, Blake, J. R et al. (eds.), Kluwer Academic Publishers, The Netherlands, pp. 195-206.

Cole, R. H. (1948) "Underwater Explosions," Princeton University Press, Princeton.

Couch, R., Albright, E., and Alexander, N., (1983) "JOY Computer Code", Lawrence Livermore National Lab., CA, UCID-19688.

Duncan, J. H., and Zhang, S., (1991) " On the Interaction of a Collapsing Cavity and a Compliant Wall," J. of Fluid Mech., 226, pp. 401-423.

Fujikawa, S., Takahira, H., and Akamatsu, T., (1985) "Underwater Explosion of Two Spherical or Non spherical Bubbles and Their Interaction With Radiated Pressure Waves," Shock Waves and Shock Tubes, Proc. of the Fifteenth International Symp., Berkeley, CA, pp. 737-744.

Hallquist, J. O., (1982) "Theoretical Manual for DYNA3D, Lawrence Livermore National Laboratory, Livermore, CA, UCID-19401.

Kalumuck, K. M., Duraiswami, R., and Chahine, G. L. (1995) "Bubble Dynamics Fluid-Structure Interaction Simulation by Coupled Fluid BEM and Structural FEM codes," Journal of Fluids and Structures, Vol., 9, pp. 861-883.

Lal, M. K., and Menon, S., (1996a) "Interaction of Two Underwater Explosion Bubbles", ASME, Fluids Engg. Div. Conf., Vol. 1, pp. 595-600.

Lal, M. K., and Menon, S., (1996b) "Dynamics of Interaction between Two Underwater Explosion Bubbles," submitted to Journal of Fluids Engineering.

Lauterborn, W., (1976) "Numerical Investigation of Nonlinear Oscillations of Gas Bubbles in Liquids," J. Acoust. Soc. Am., 59, pp. 283-293.

Menon, S., and Lal, M. K., (1996a) "On the Dynamics and Instability of Bubbles Formed During Underwater Explosions," submitted to Fluids and Thermal Science Journal.

Menon, S. and Lal, M. K., (1996b) "Collapse of Underwater Explosion Bubbles near Exposed and Submerged Rigid Surfaces," under preparation.

Menon, S. and Pannala, S., (1997) "Simulations of Underwater Explosion Bubble Dynamics using an Arbitrarily Lagrangian-Eulerian Formulation," to be presented at the 1997 ASME Fluid Engineering Summer Meeting, Vancouver BC.

Milligan, C. D., Duncan, J. H, and Stillman, D. J., (1995) "A Numerical Study of Underwater Explosion Bubble Phenomena," preprint.

NIST (1988) "Thermophysical Properties of Water (Steam)," NIST Standard Reference Database 10, U. S. Department of Commerce.

Plesset, M. S., (1971) "The Dynamics of Cavitation Bubbles," Trans. ASME, J. Appl. Mech., 16, pp. 277-282.

Plesset, M. S. and Prosperetti, A. (1977) "Bubble Dynamics and Cavitation," Annual Review of Fluid Mechanics, Vol. 9, pp. 145-185.

Prosperetti, A., (1982) "A Generalization of the Rayleigh-Plesset Equation of Bubble Dynamics," Phys. Fluids, 25, pp. 409-410.

Rood, E. P. (1991) "Review - Mechanism of Cavitation Inception," Journal of Fluid Engineering, Vol. 113, pp. 163-175.

Snay, H. G., Goertner, J. F. and Price, R. S. (1952) "Small Scale Experiments to Determine Migration of Explosion Gas Globes Towards Submarines," NAVORD Report No. 2280, U. S. Naval Ordnance Lab., White Oak, MD.

Steinberg, D., (1991) "Equation of State and Strength Properties of Selected Materials," Lawrence Livermore Natn. Lab., Livermore, CA, UCRL-MA-106439.

Szymczak, W. G., Rogers, J. C. W., Solomon, J. M. and Berger A. E., (1993) "A numerical algorithm for hydrodynamic free boundary problems," J. Comput. Phys., 106, pp. 319-336.

Tomita. Y., and Shima. A., (1986) "Mechanisms of Impulsive Pressure Generation and Damage Pit Formation by Bubble Collapse," J. Fluid Mech., 169, pp. 535-564.

Tipton, R., (1990) "CALE User's Manual," Lawrence Livermore Natn. Lab., B-Division Internal Document, Livermore, CA.

Tipton, R. E., Steinberg, D. J., and Tomita, Y., (1992) "Bubble Expansion and Collapse Near a Rigid Wall," Japan Soc. of Mech. Engg., 35, pp. 67-75.

Van Leer, B., (1977) "Towards the Ultimate Conservative Difference Scheme. IV. A New Approach to Numerical Convection," J. Comp. Phys., Vol. 23, pp. 276-299.

Vogel, A., Lauterborn, W. and Timm, R., (1989) "Optical and acoustic investigations of the dynamics of laser-produced cavitation bubbles near a solid boundary," J. Fluid Mech., 206, pp. 299-338.

Warren, G. R. and Rice, T. W., (1964) "The Interaction of the Gas Bubbles from Two Adjacent Underwater Explosions," Foulness Division Note 9-64, Atomic Weapons Research Establishment, United Kingdom Atomic Energy Authority.

Woodruff, J. P., (1976) "KOVEC User's Manual," Lawrence Livermore National Laboratory, Livermore, CA, UCID-17306.

Zhang, S., Duncan, J. H. and Chahine, G. L., (1993) "The final stage of the collapse of a cavitation bubble near a rigid wall," J. Fluid Mech., 257, pp. 147-181.

Zhang, S. and Duncan, J. H., (1994) "On the non spherical collapse and rebound of a cavitation bubble," Phys. Fluids, 6, pp. 2352-2362.

**TABLE I**

| Coefficients | Present EOS | Original EOS |
|---|---|---|
| C | 0.02769 | 0.148 |
| S0 | 2.56 | 2.56 |
| S1 | -1.986 | -1.986 |
| S2 | .2268 | .2268 |
| $\gamma 0$ | .007288 | .5 |
| a | -0.05469 | 0.0 |

*Coefficients of the Grunesein Form used for equation of state ofwater.*

**TABLE II**

| | |
|---|---|
| A | 5.4094 |
| B | 0.0973 |
| R1 | 4.5 |
| R2 | 1.1 |
| $\omega$ | .35 |

*Coefficients used to model EOS of Pentolite using JWL High Explosive form.*

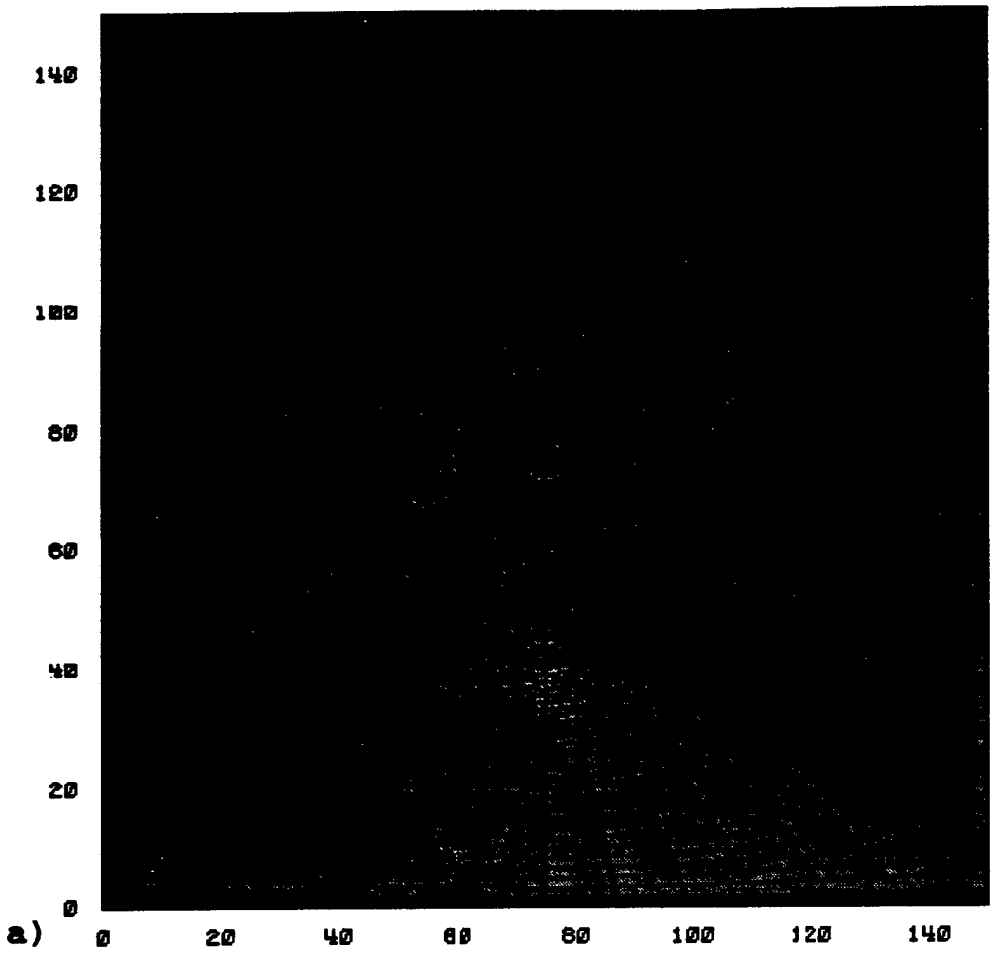


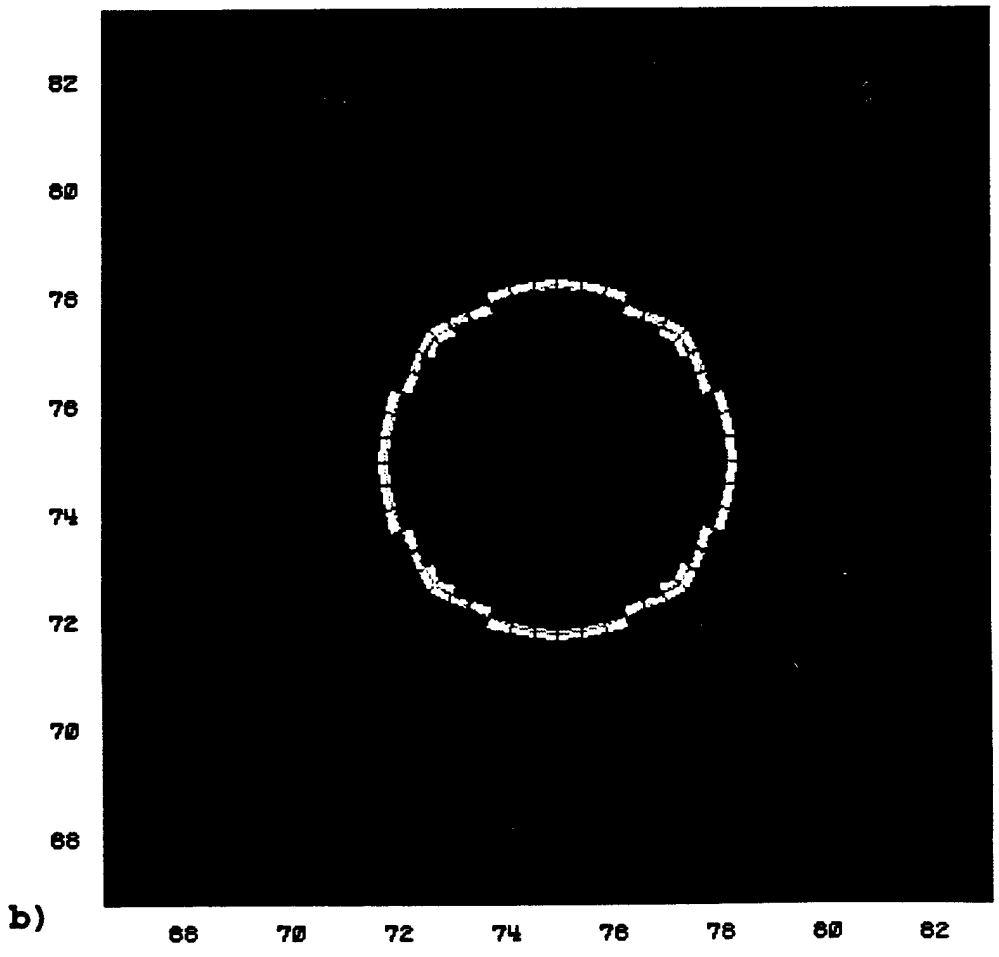


**Fig. 1: Figure showing the grid used in ALE3D freely oscillating runs. a) The View of the whole domain & b) View of the domain in the proximity of the bubble.**

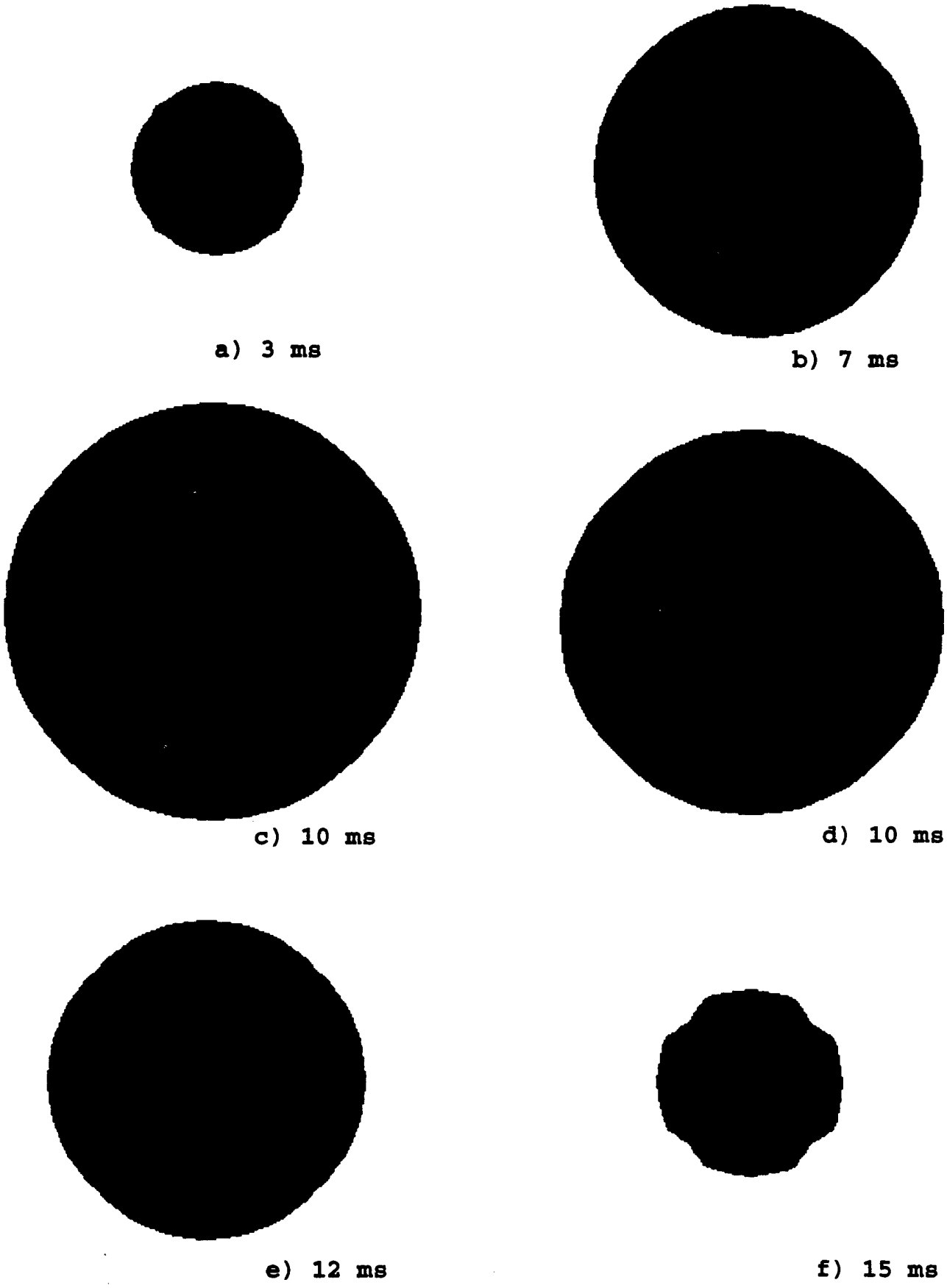


Fig. 2 Time Sequence of the collapse and rebound of a freely oscillating bubble for a complete cycle.

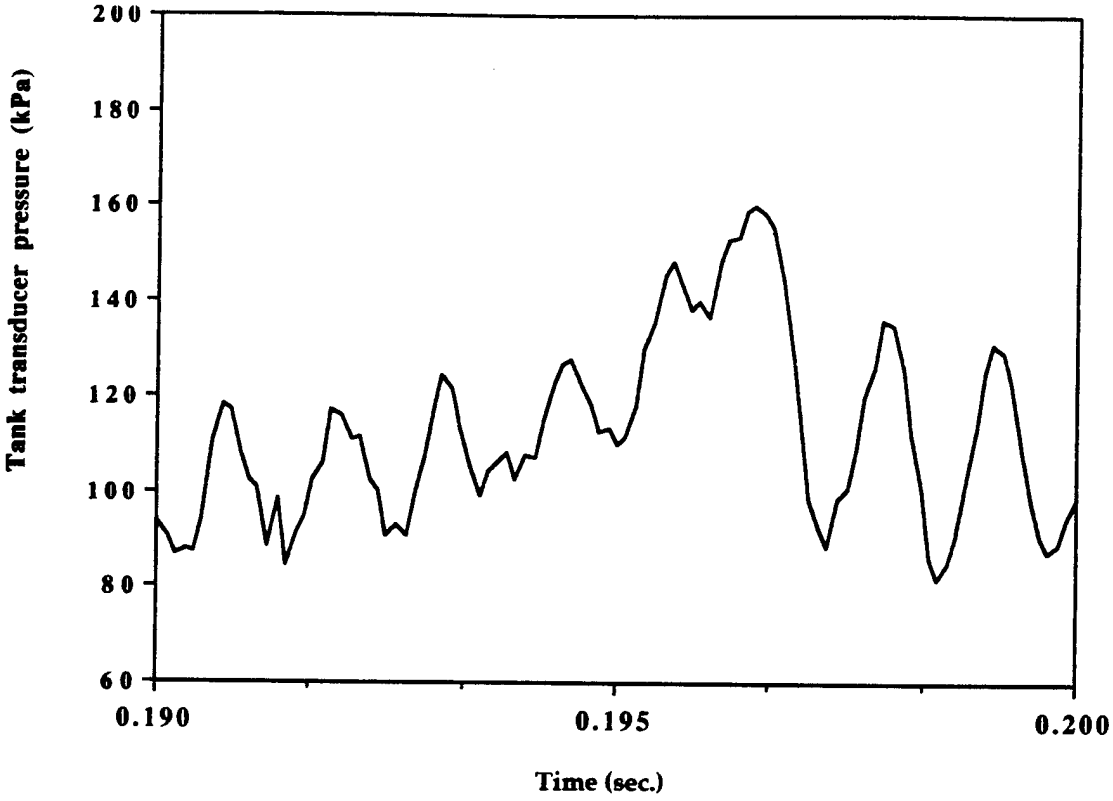


Fig. 10a) : Pressure fluctuation measured near the side wall of the experimental facility(Menon and Lal 1996a)

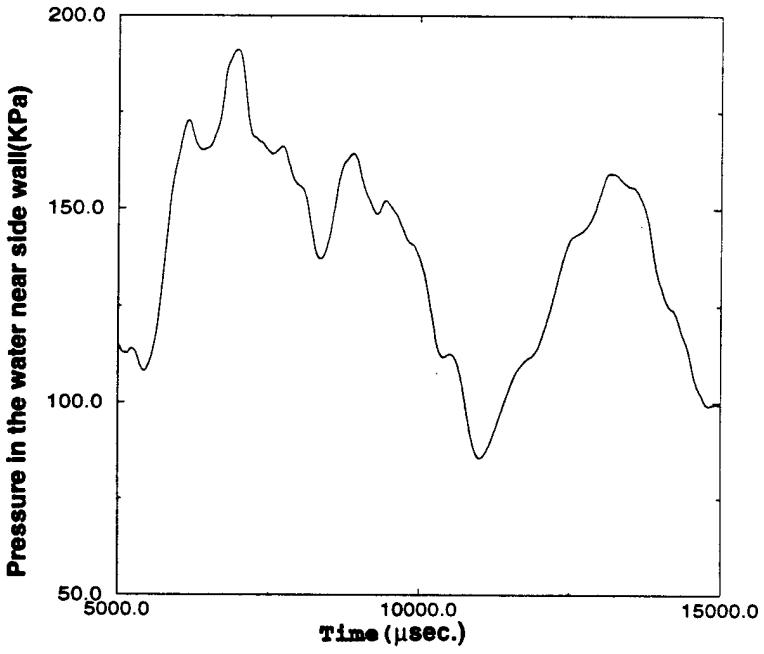


**Figure 10b) : Computed pressure near the side wall in the computational domain.**

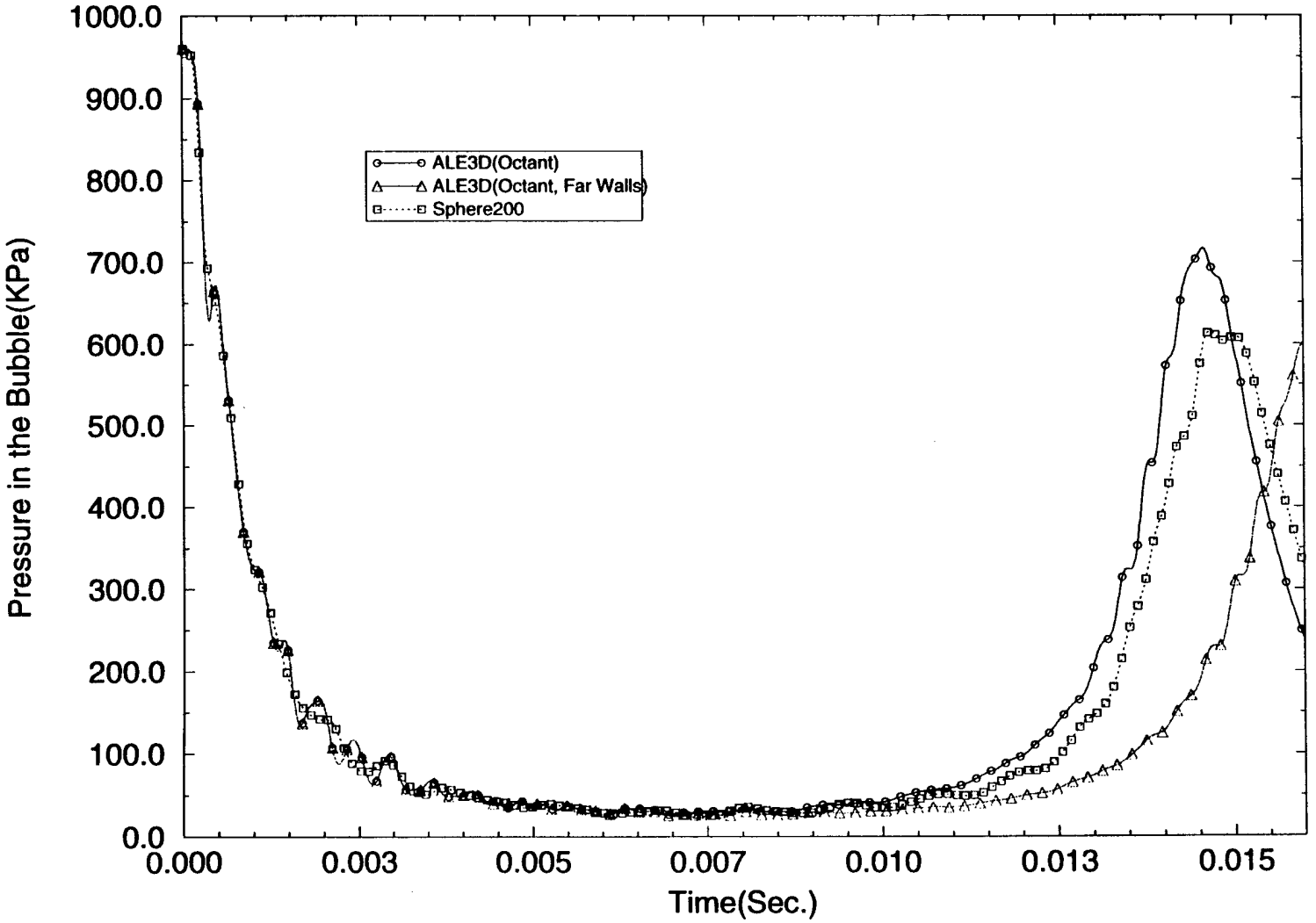


**Figure 11: Effect of wall location and shape on the bubble oscillation.**

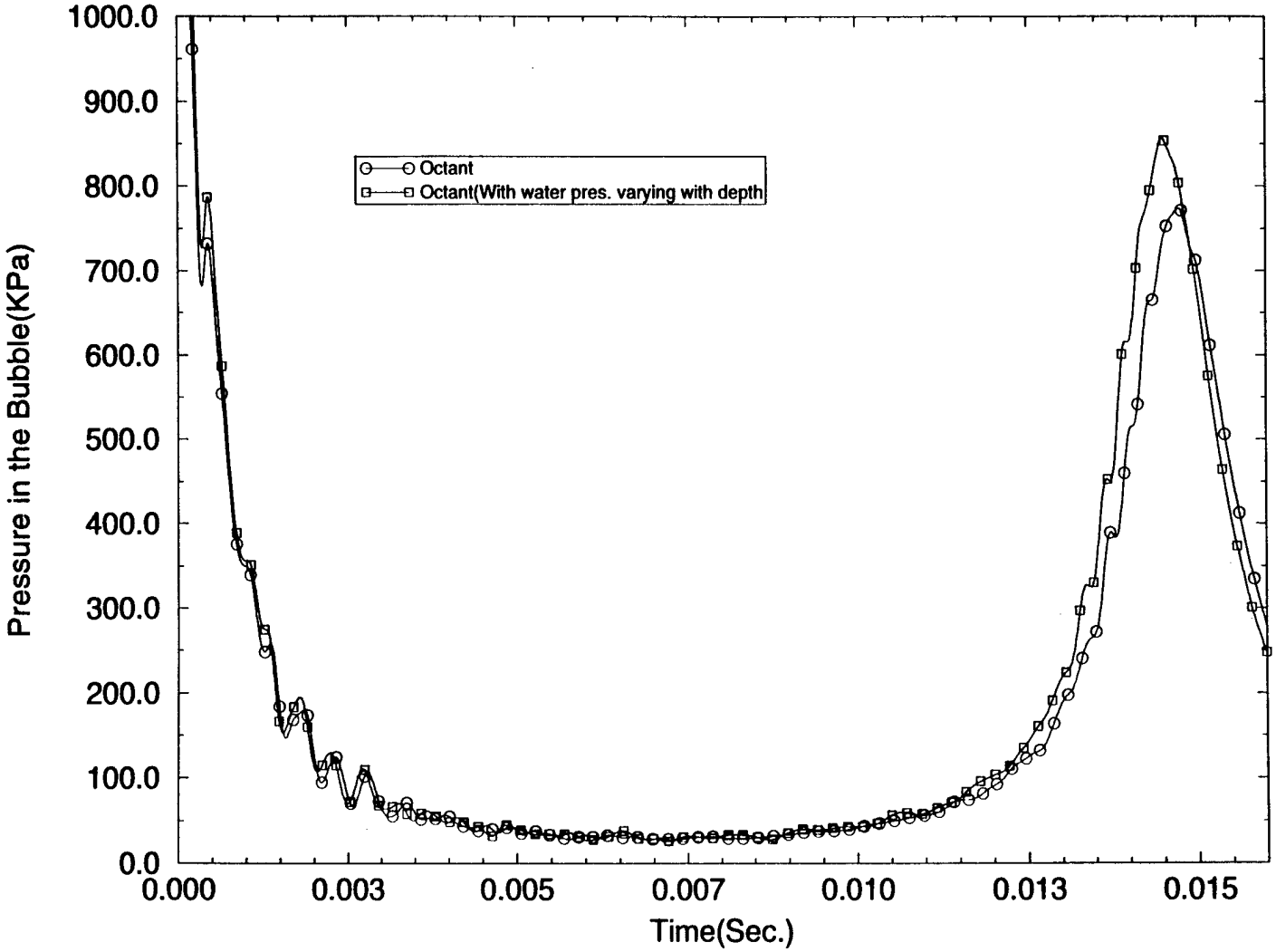


**Figure 12: Effect of pressure variation with depth on the bubble oscillation.**

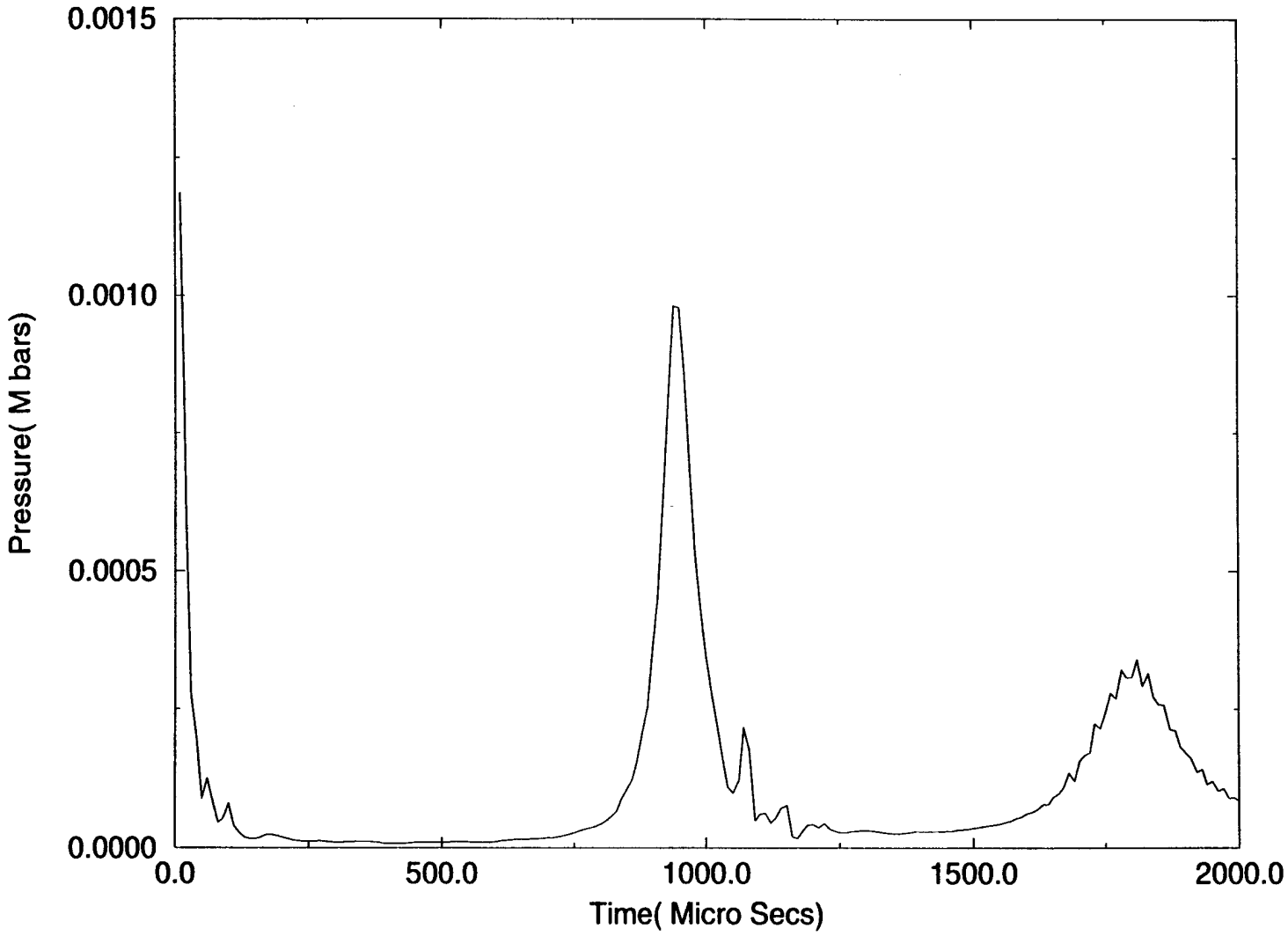


**Figure 13: Pentolite explosion at a depth of 1000 meters.**
**(The init. bubble radius was .8cm and the maximum radius at bubble max. was around 5cm)**

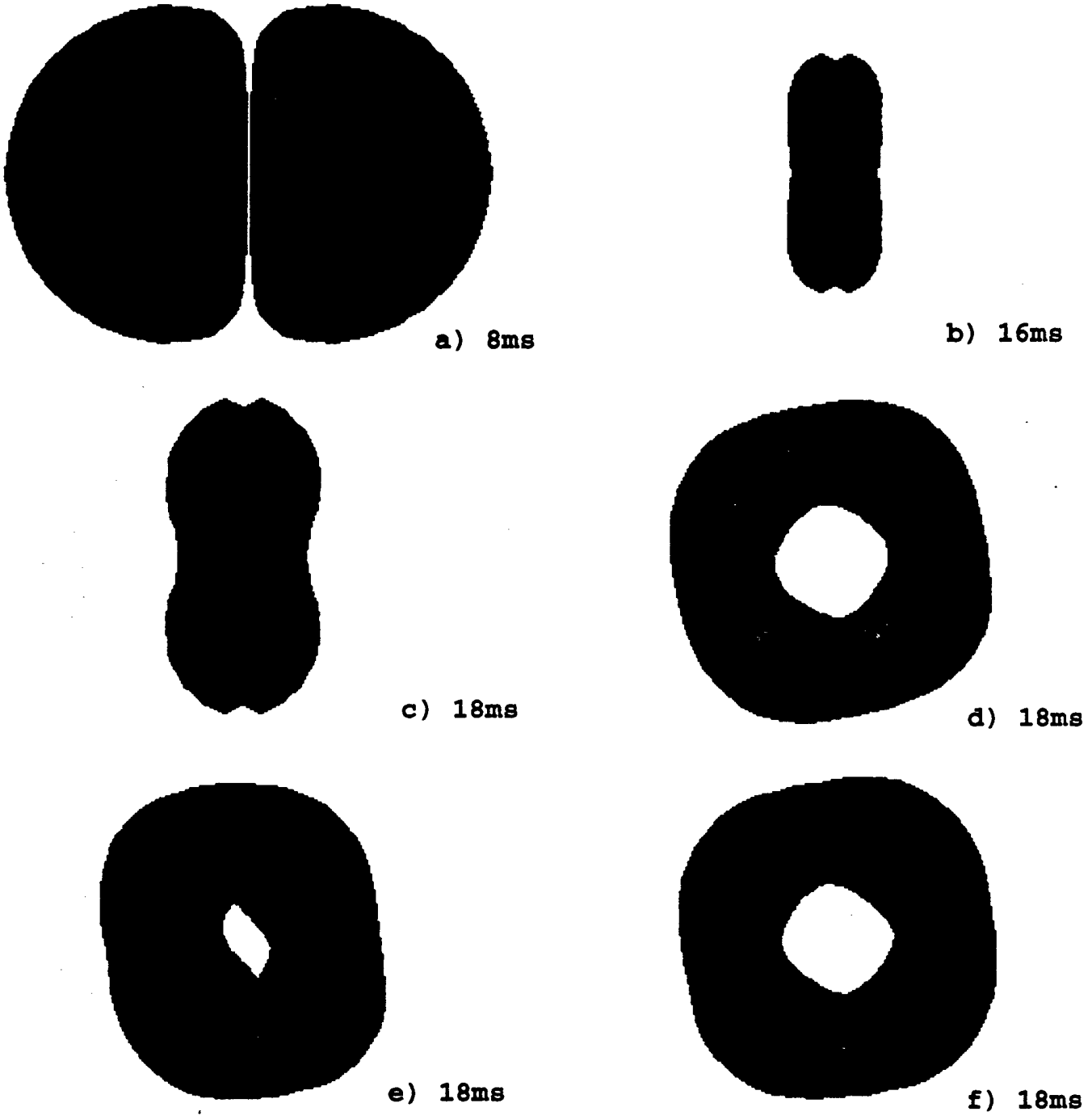


Fig. 14 The time sequence of interaction between bubbles of same size. a) Side view at Bubble Max. b) Side View just before the jet formation. c) Side view just after the jet formation. d), e) and f) are different angles of the bubbles after the jet is formed.

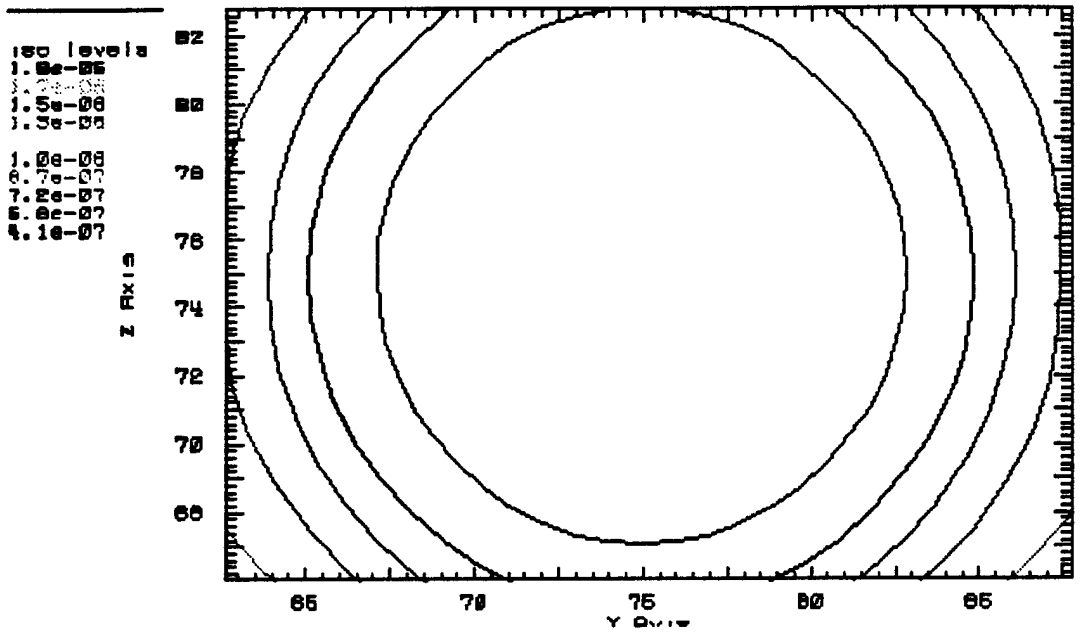


a) 7 ms

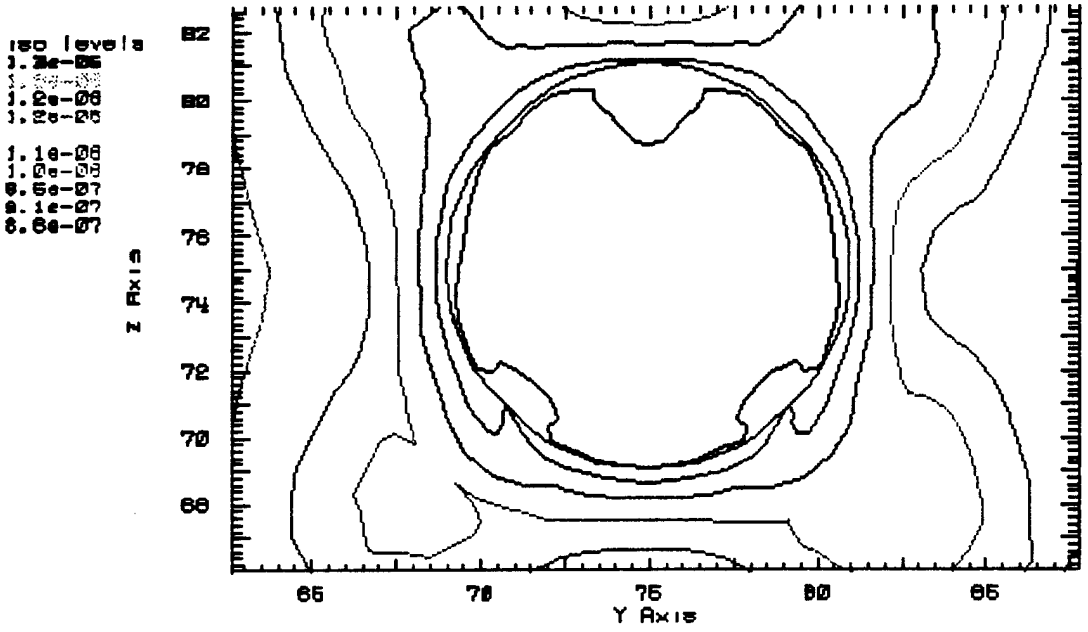


Fig. 3 Time Sequence of the smooth pressure contours around a freely oscillating bubble.

b) 12 ms

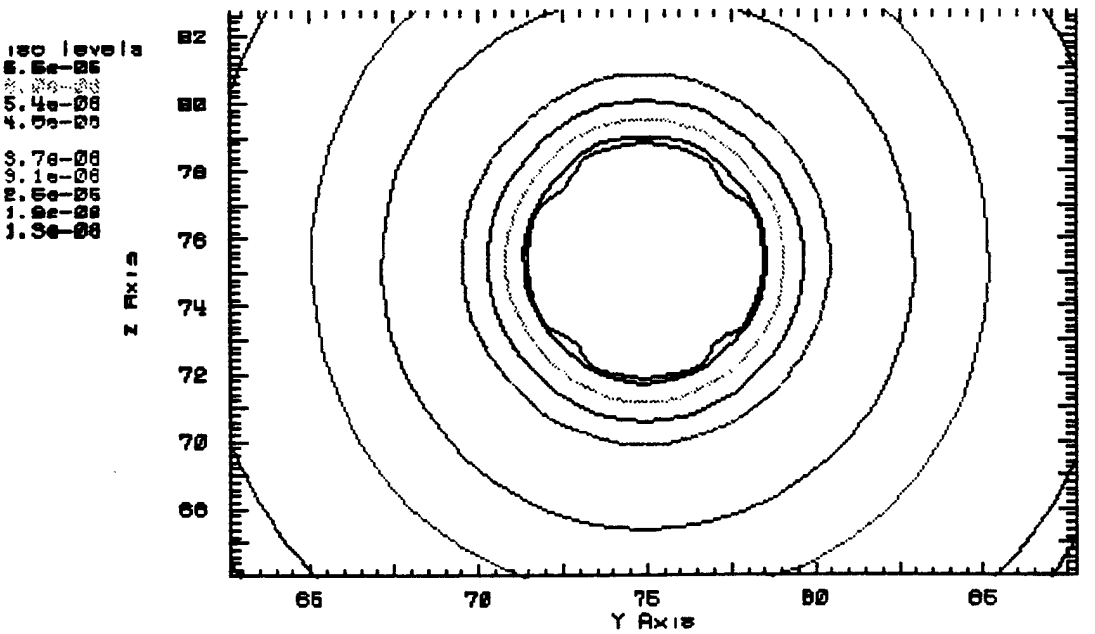


c) 15 ms

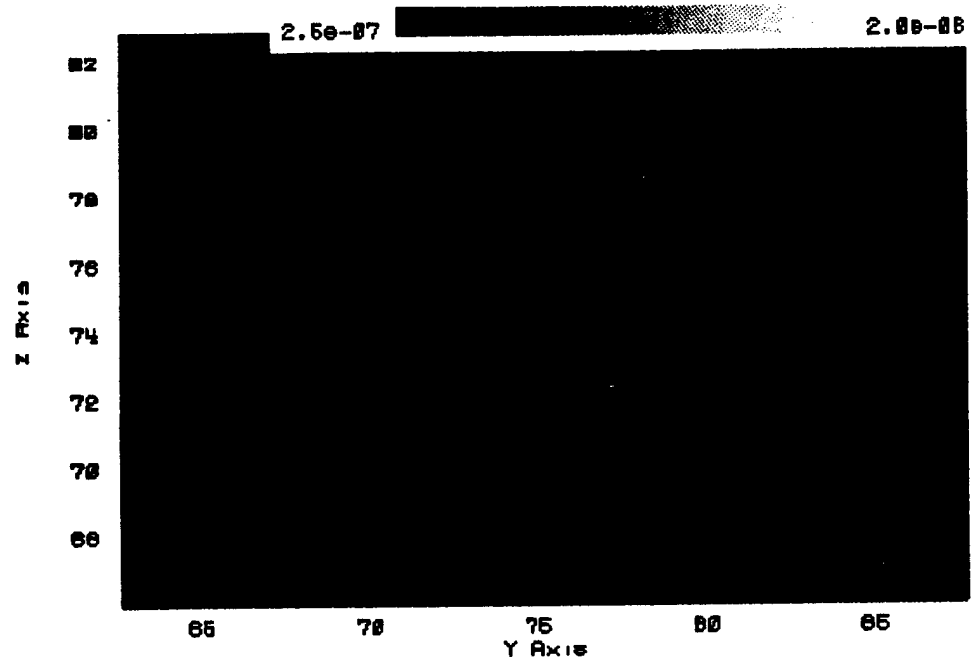


a) 7 ms

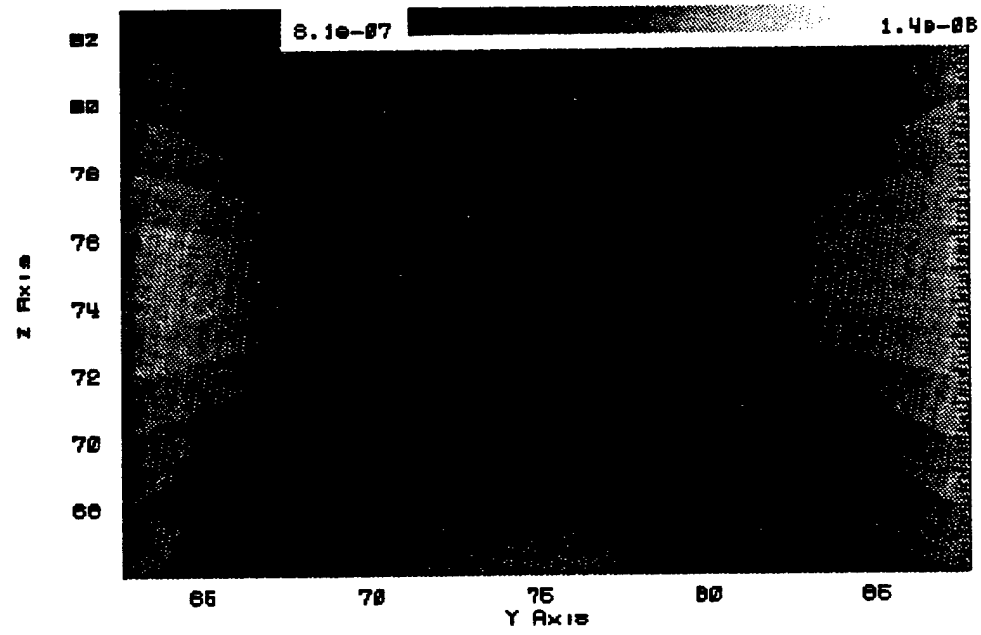


b) 12 ms

Fig. 4 Time Sequence of the smooth pressure contours around a freely oscillating bubble.

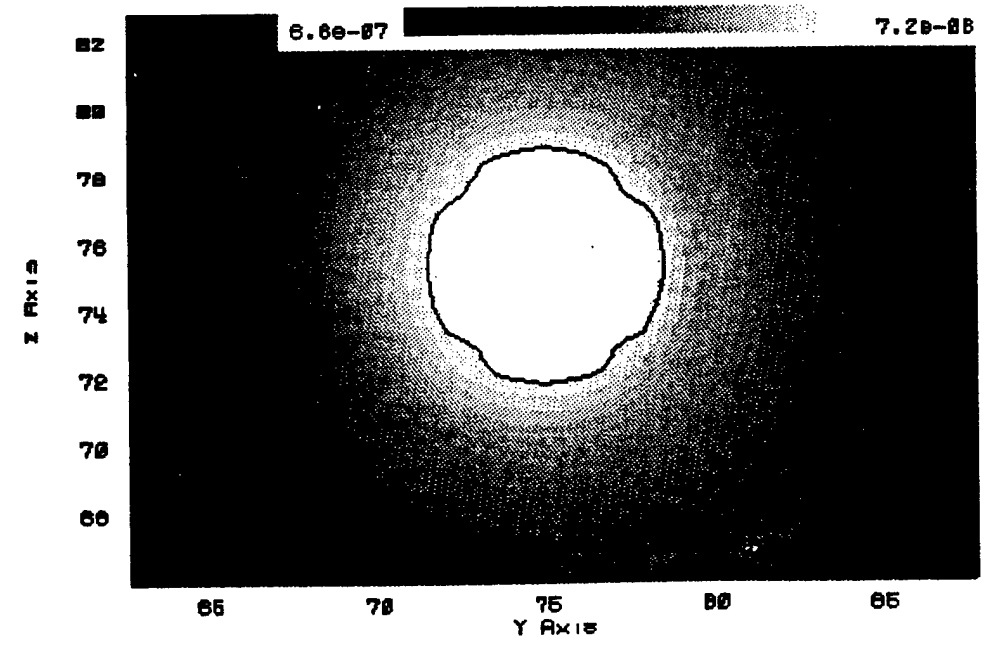


c) 15 ms

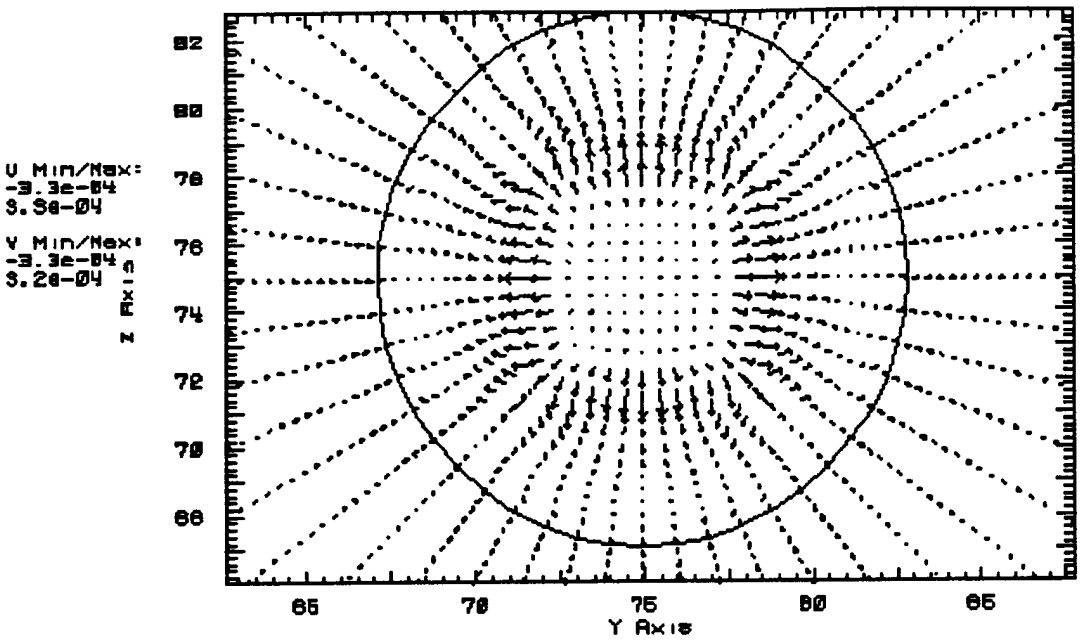


a) 7 ms

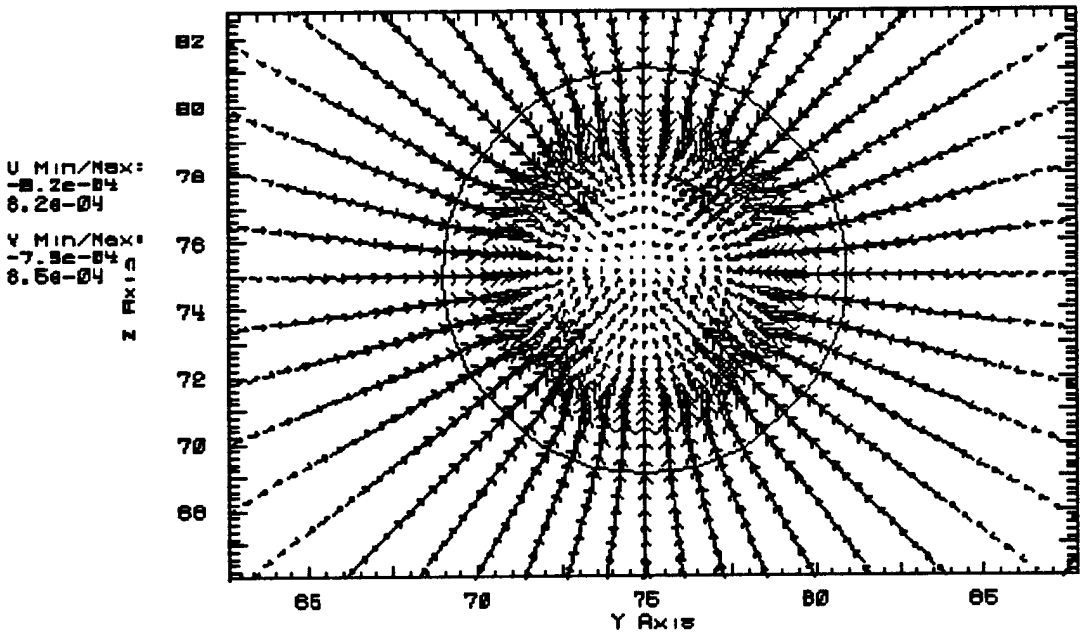


b) 12 ms

Fig. 5 Time Sequence of the velocity contours around a freely oscillating bubble.

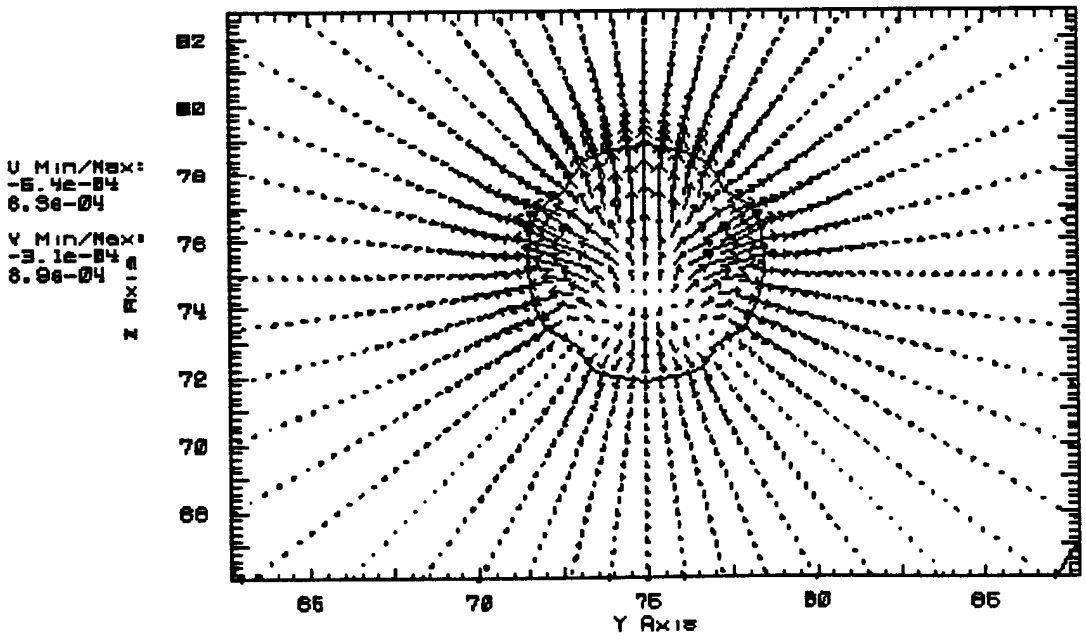


c) 15 ms

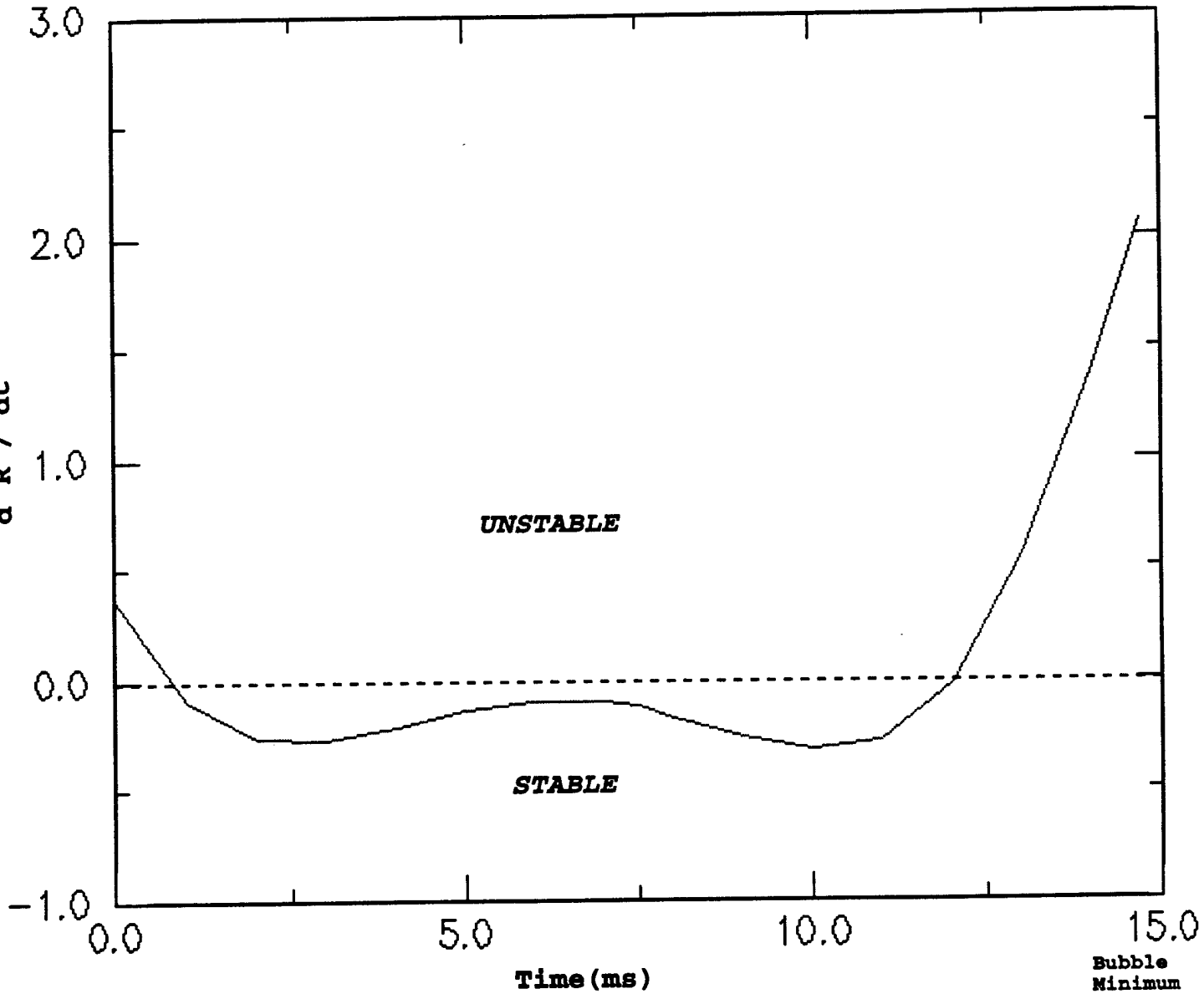


**Fig. 6: Variation of $d^2R / dt^2$ with time showing that R-T instability criteria is satisfied near bubble minimum.**

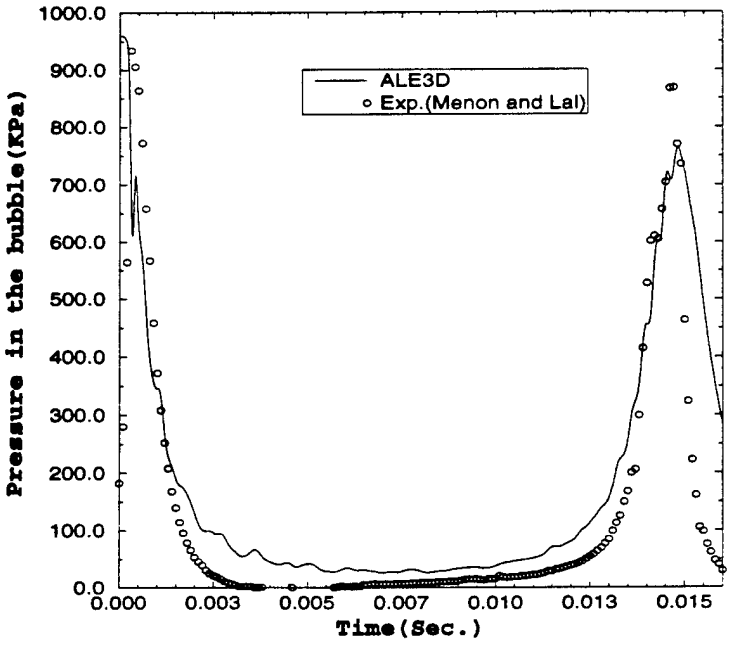


**Figure 7a: Variation of bubble pressure with time.**

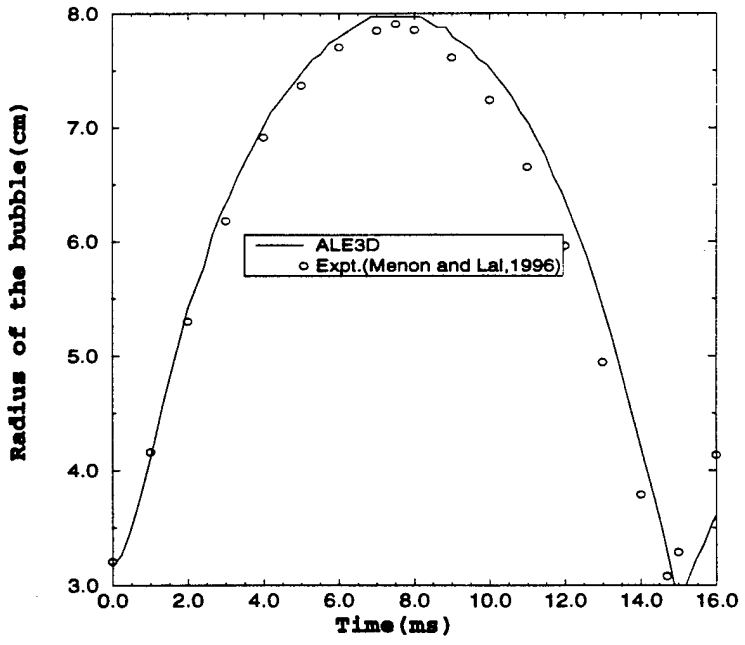


**Figure 7b: Variation of bubble radius with time.**

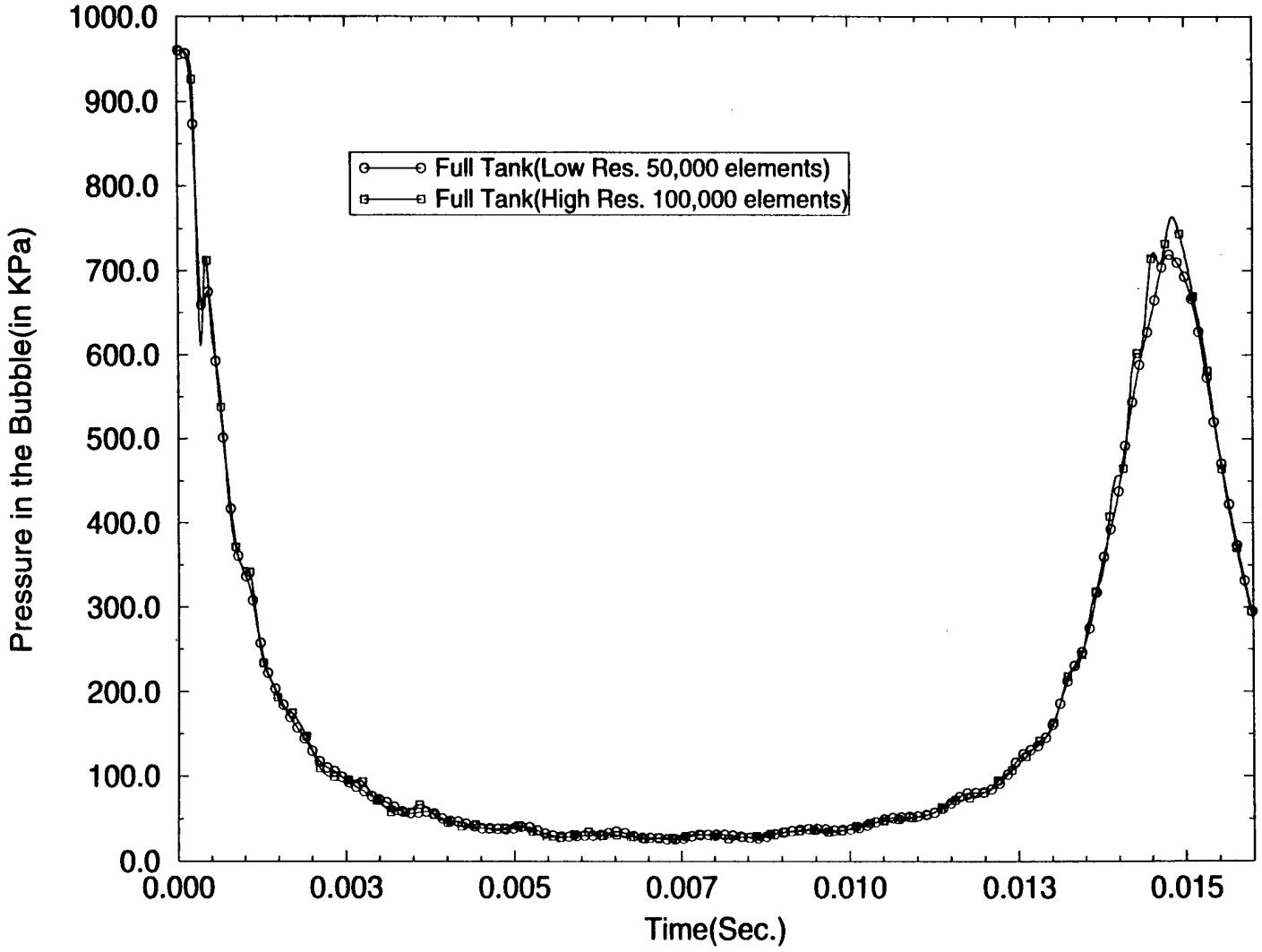


**Figure 8. Effect of grid resolution on the pressure in the bubble.**

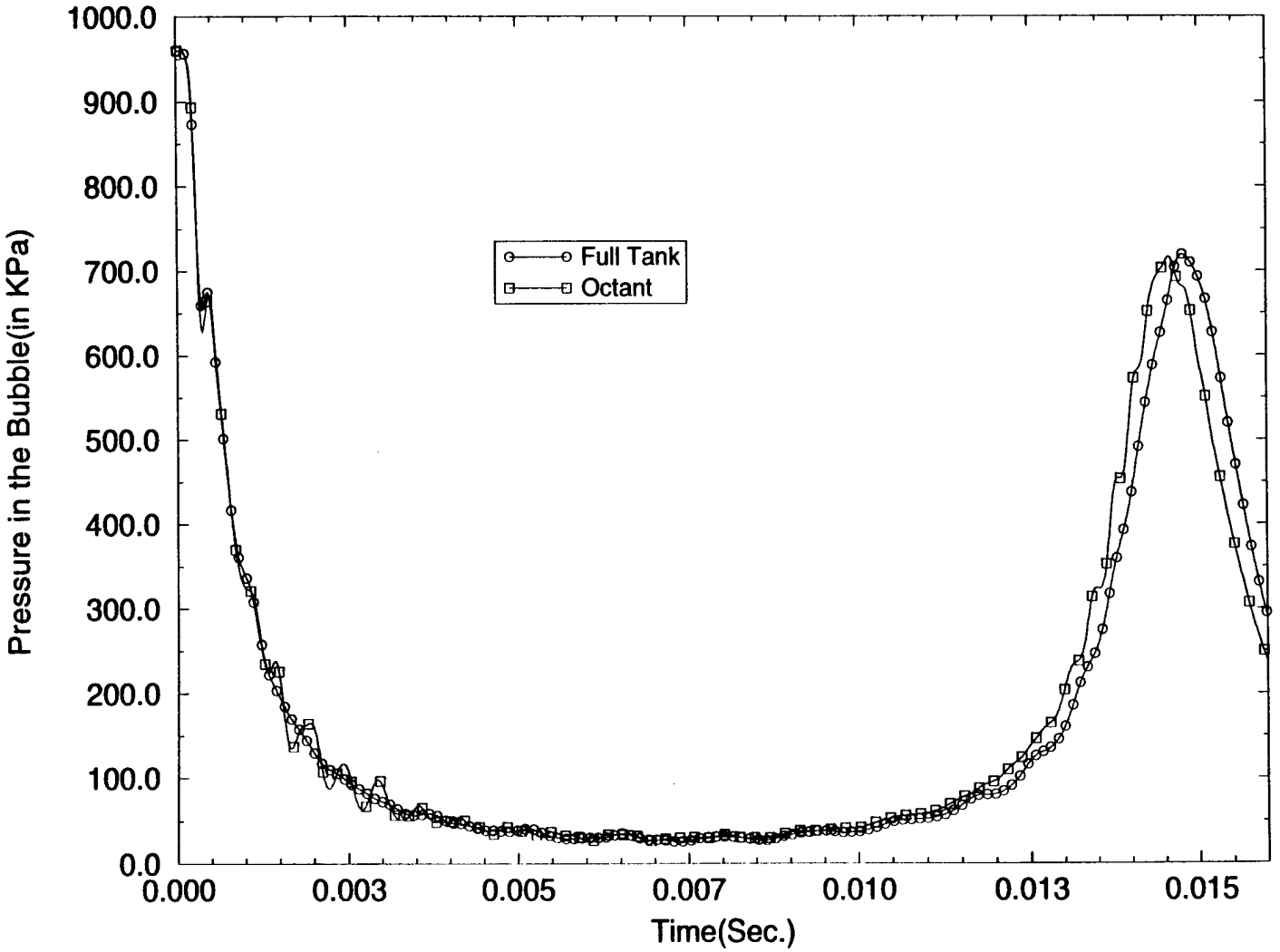


**Figure 9: Comparision of pressure in the bubble for full 3D domain and Octant(1/8th) domain.**

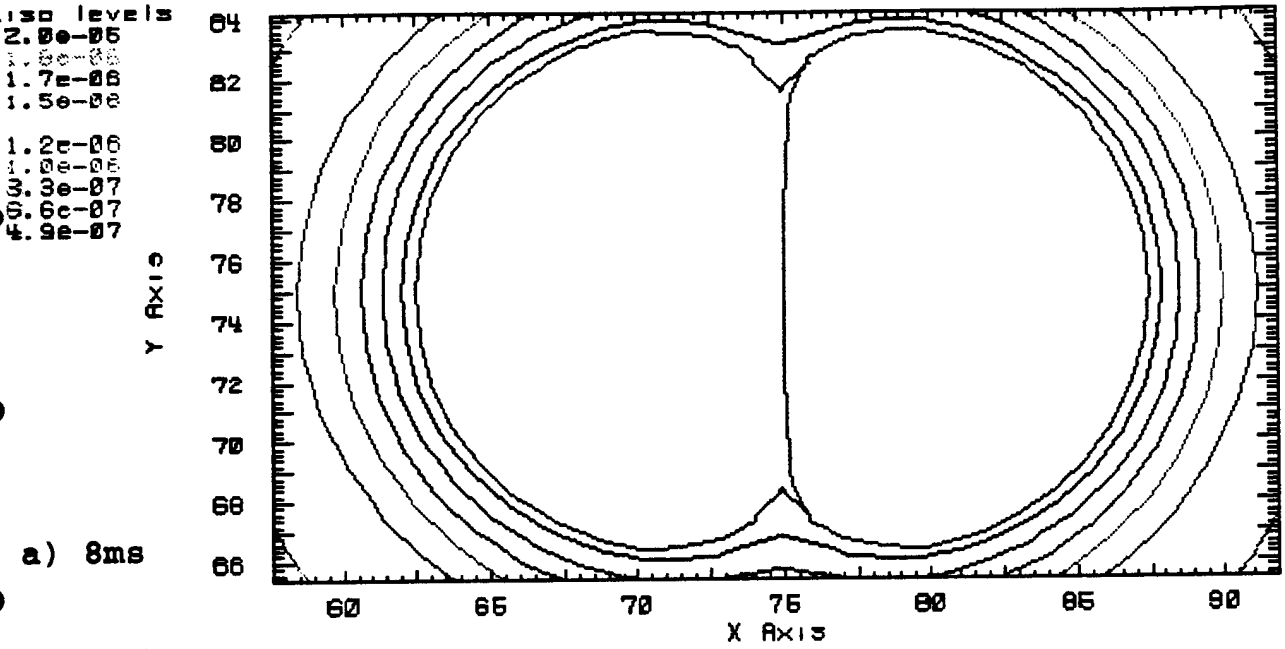


a) 8ms

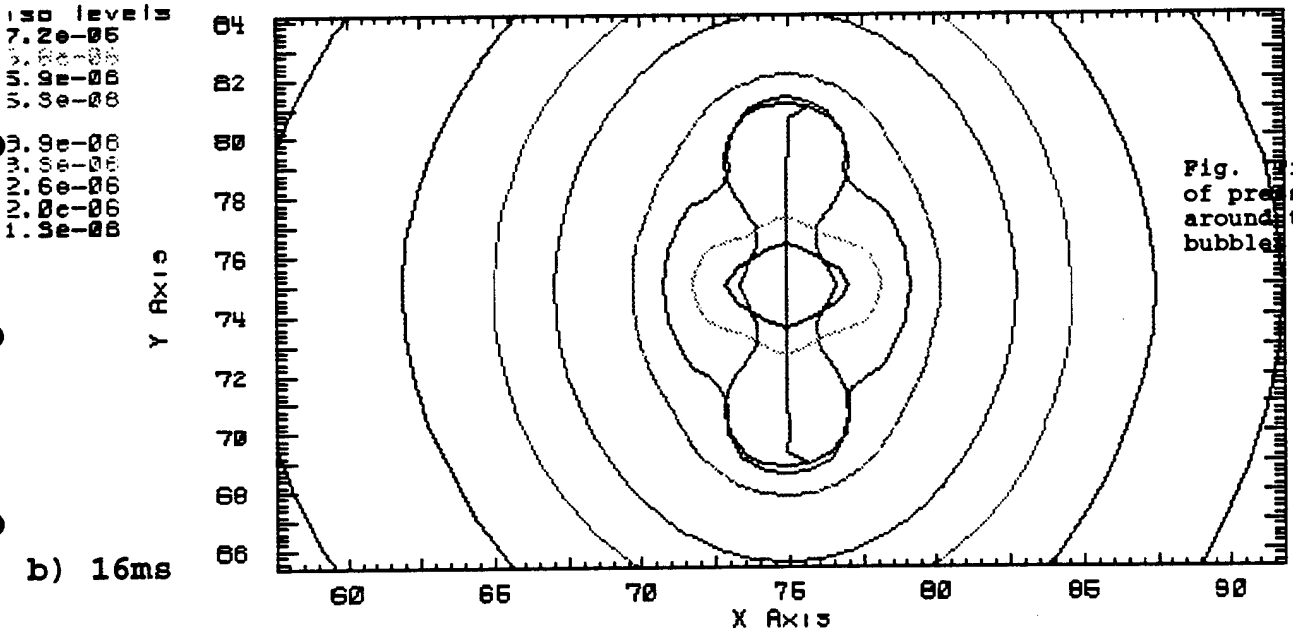


b) 16ms

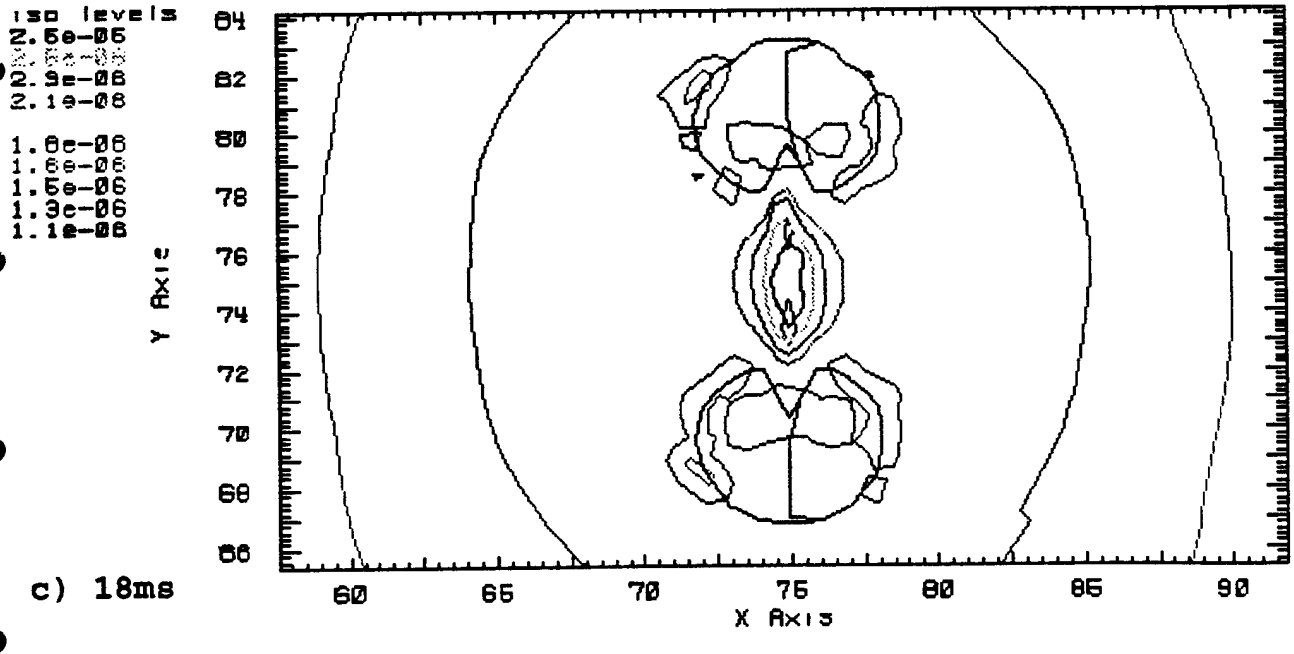


c) 18ms

Figure 15

Fig. Time Sequence of pressure contours around two interacting bubbles of same size.

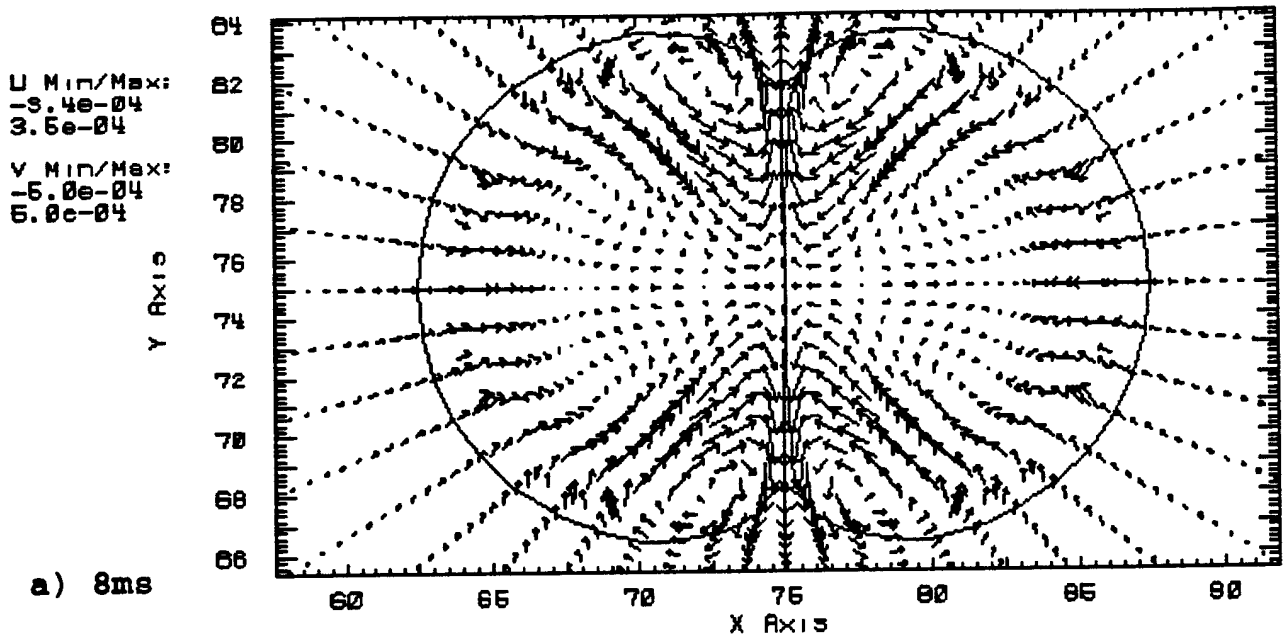


a) 8ms

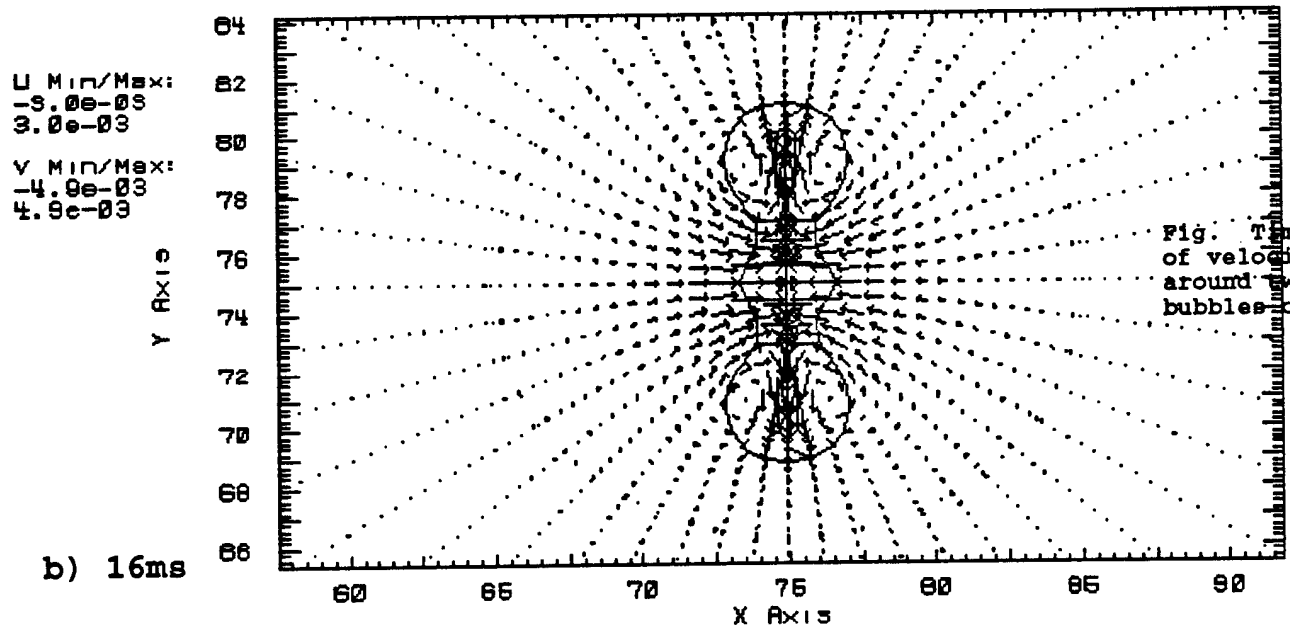


b) 16ms

Figure 16

Fig. Time Sequence of velocity vectors around two interacting bubbles of same size.

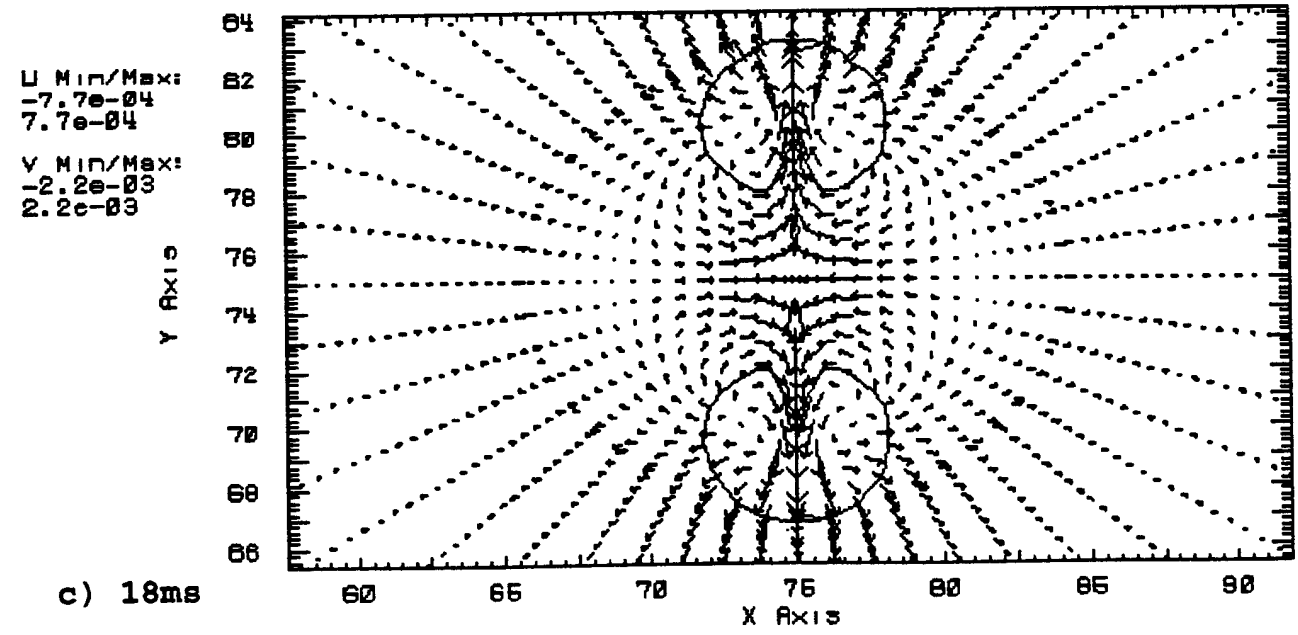


c) 18ms

a) At respective bubble Max.

b) During Collapse

c) During Jet Formation.

Figure 17: Experimental(Lal and Menon,1996) pictures of two bubbles of same size interacting after they are exploded simulataneously.

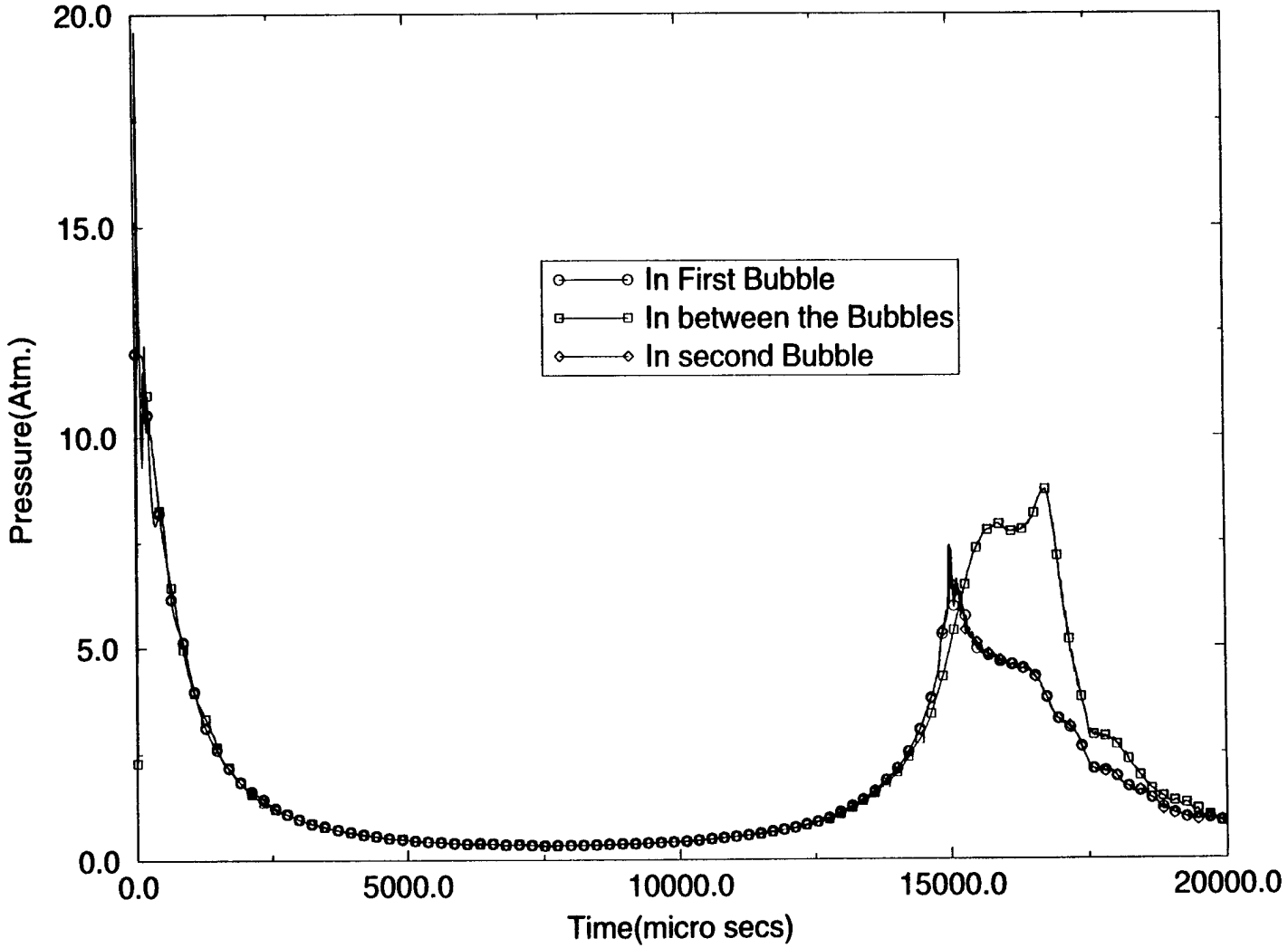


**Figure 18: Pressure variation when two identically sized bubbles with identical energy are exploded near each other.**

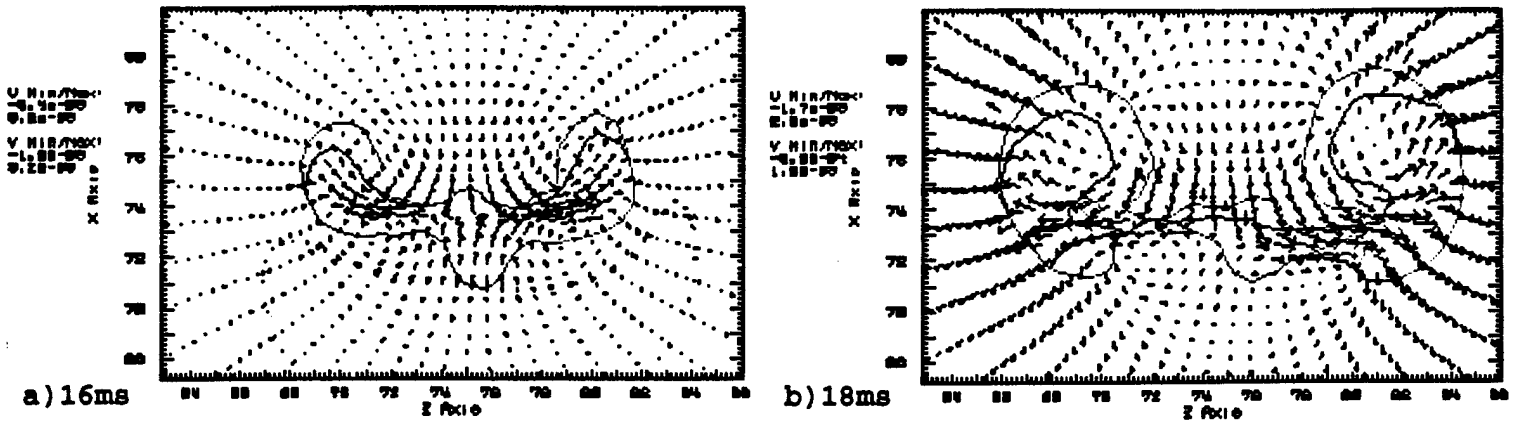


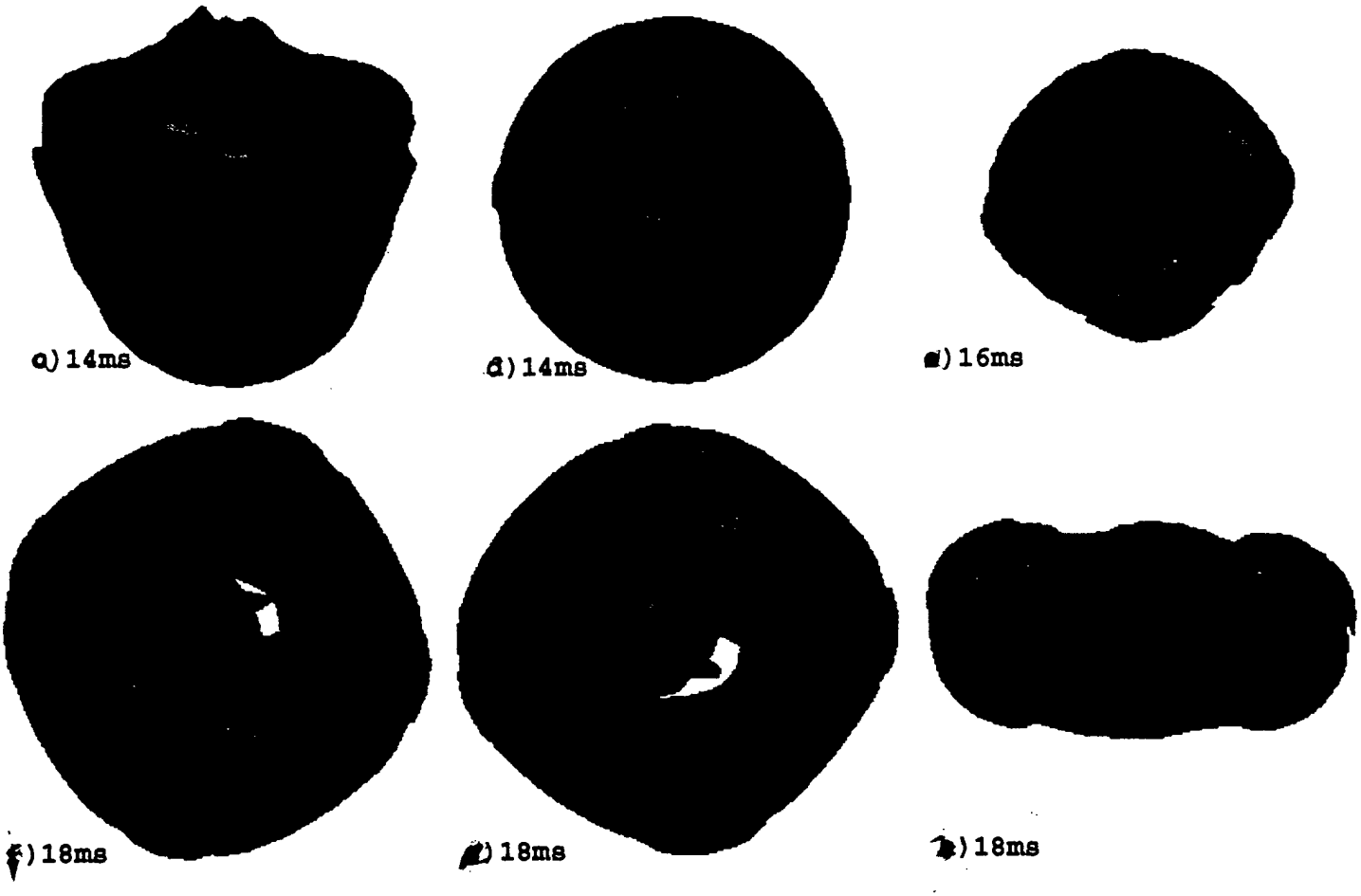


Fig.19 Interaction of bubbles of different energy but of same volume. a) Velocity vectors after the jet impinges the smaller bubble, b) Velocity vectors during the rebound at the time the jet pierces the second bubble, c)&d) are two different views when the jet pierces the smaller bubble, e) during rebound & f),g) & h) are three different views after the jet pierces the bigger bubble.

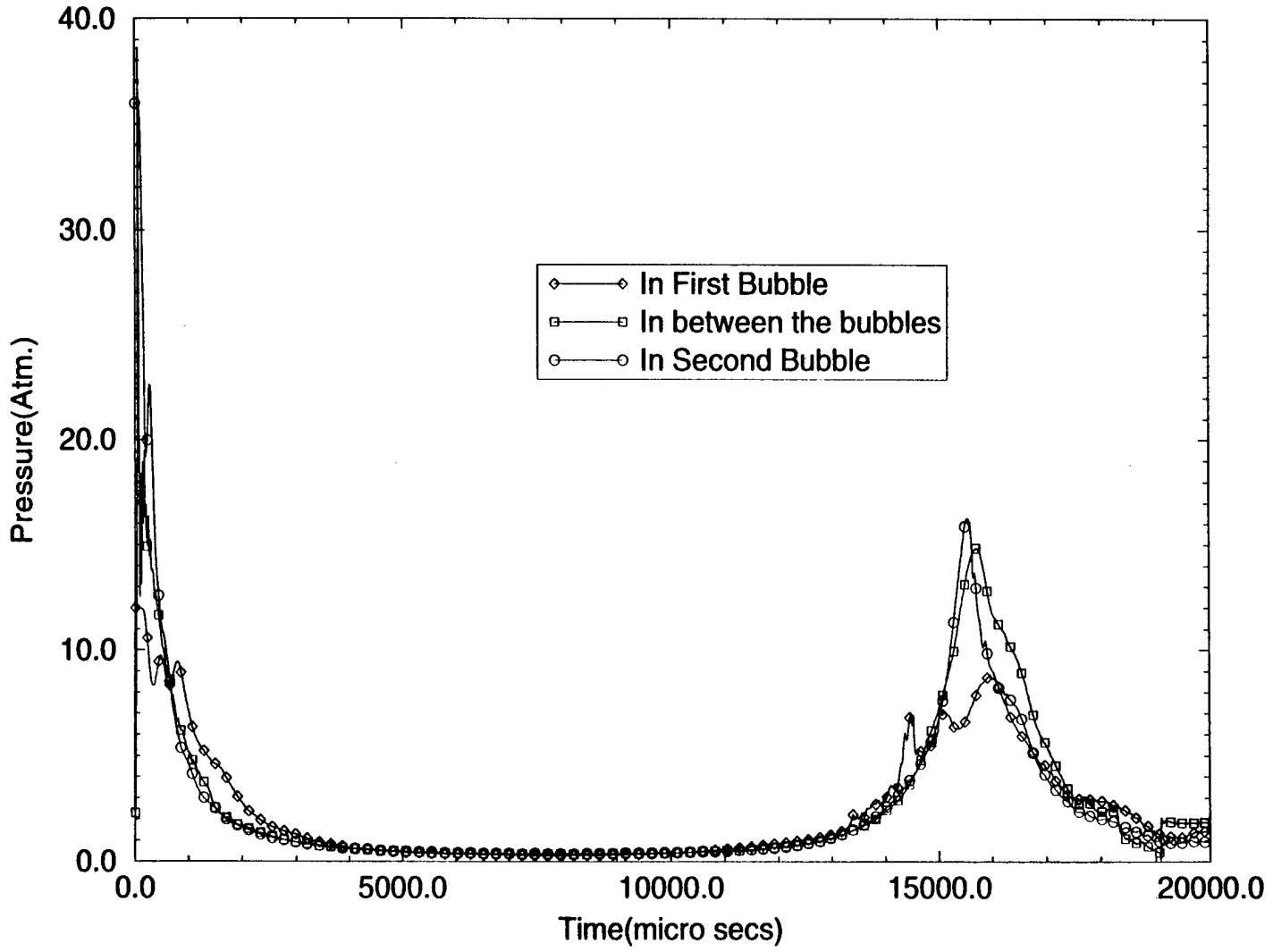


**Figure 20: Pressure variation when two bubbles of identical size but of different energies( One four times the other) are exploded.**

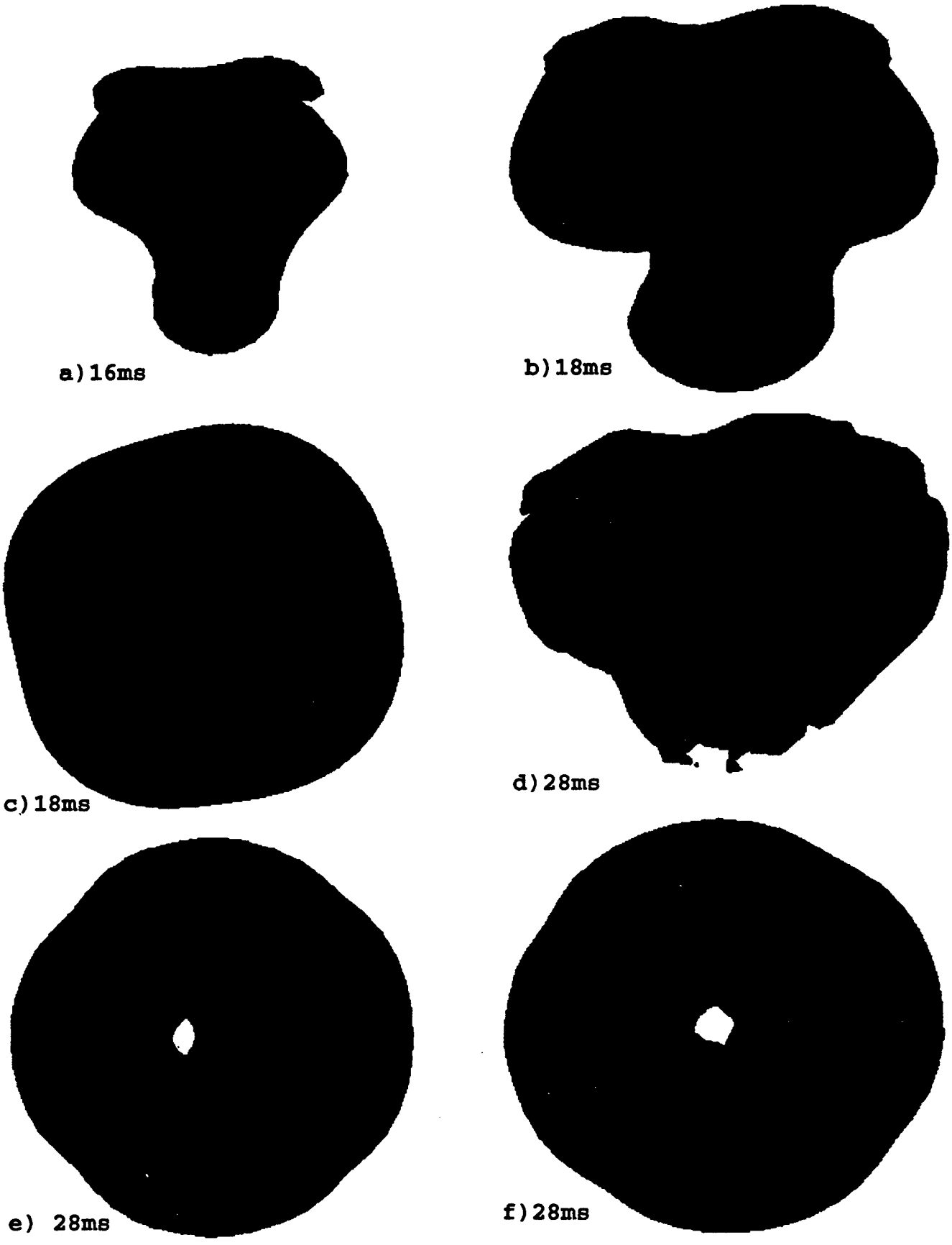


Fig.2 Time sequence of the interaction of a bubble with a bubble of 30% its volume but with the same energy density. a) Just before the jet formation, b)&c) Two different views after the jet passed through the small bubble, d),e)&f) are three different views at the time of jet formation through the bigger bubble.

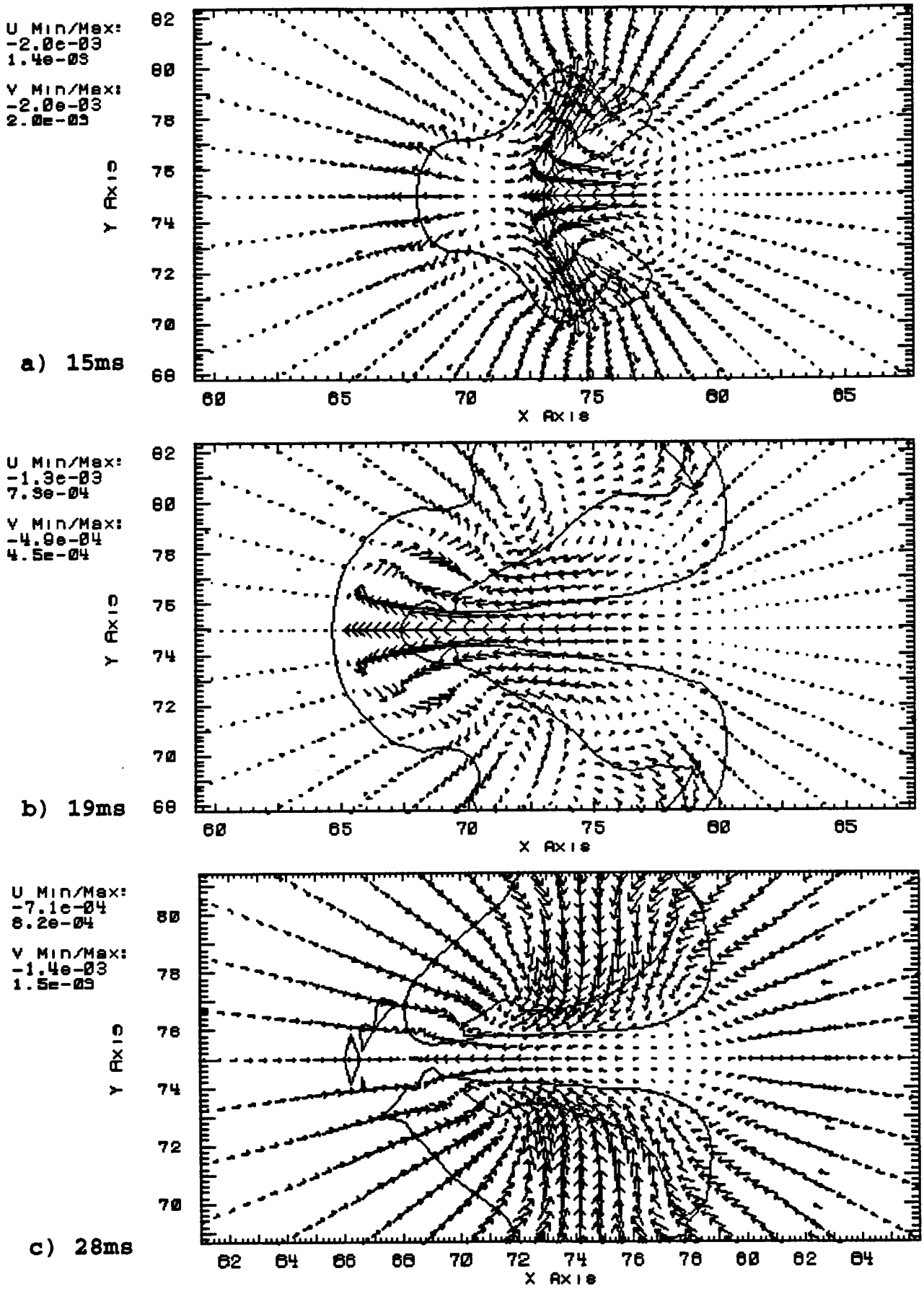


Fig.22Velocity vectors around the interacting bubbles of different volumes.a) At the time of jet formation through smaller bubble b) During rebound & c) At the time of jet formation throught the bigger bubble.

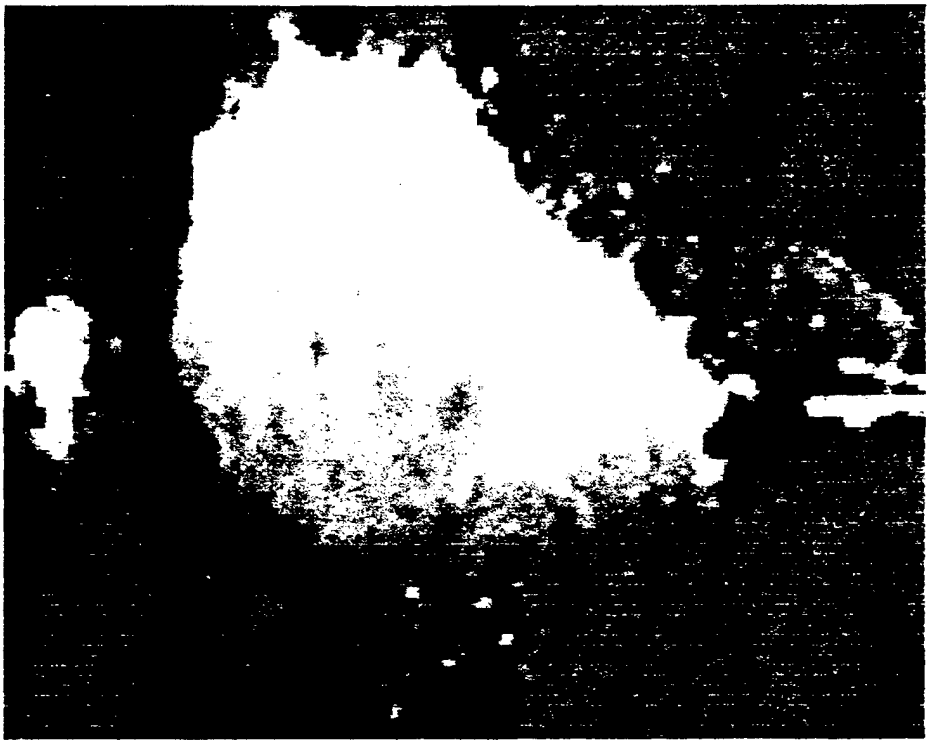

Figure 23: Experimental( Lal and Menon,1996) picture showing the merging of two out of phase exploded bubbles.

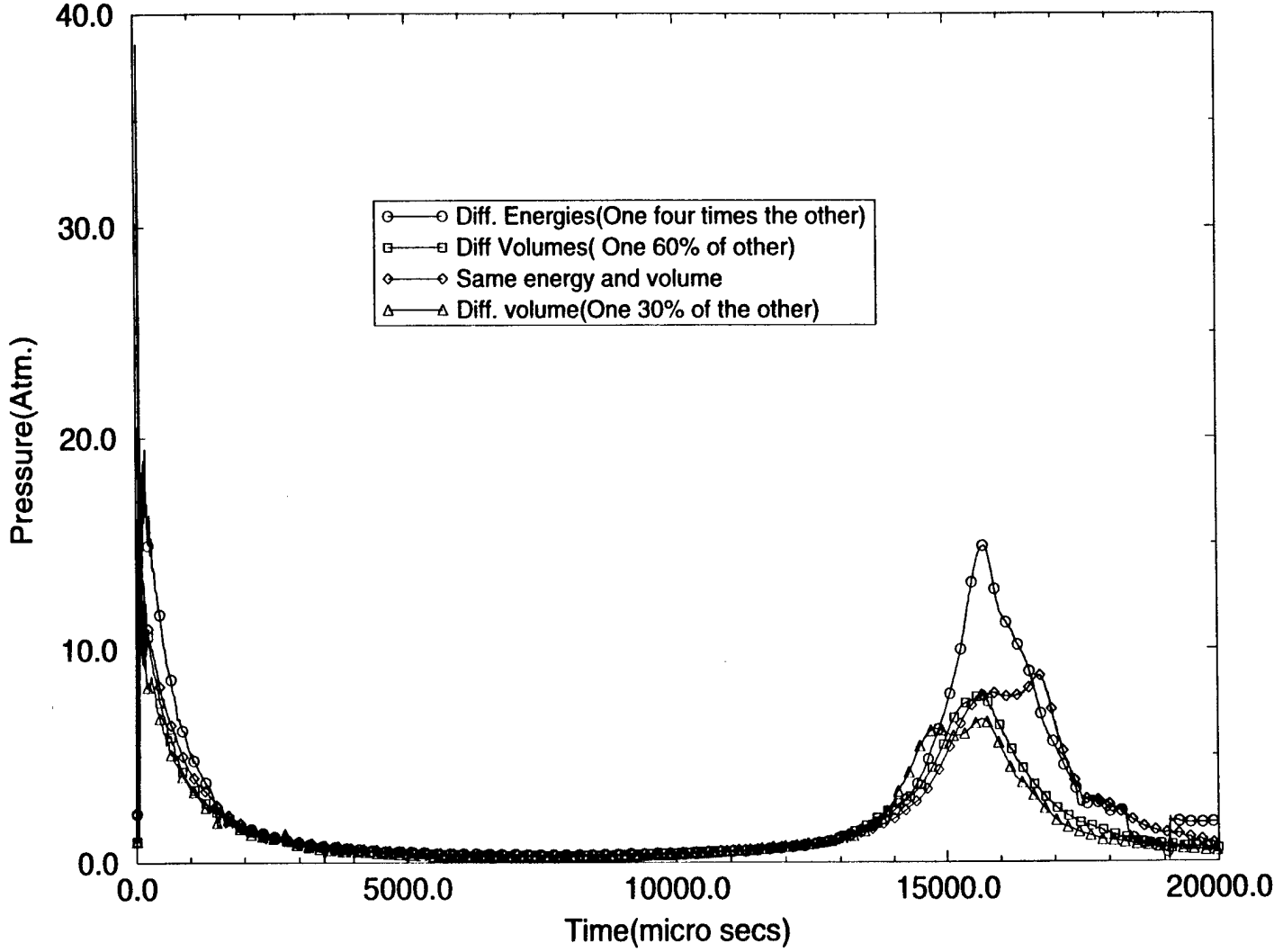


**Figure 24: Pressure in between the interacting bubbles for four different cases.**

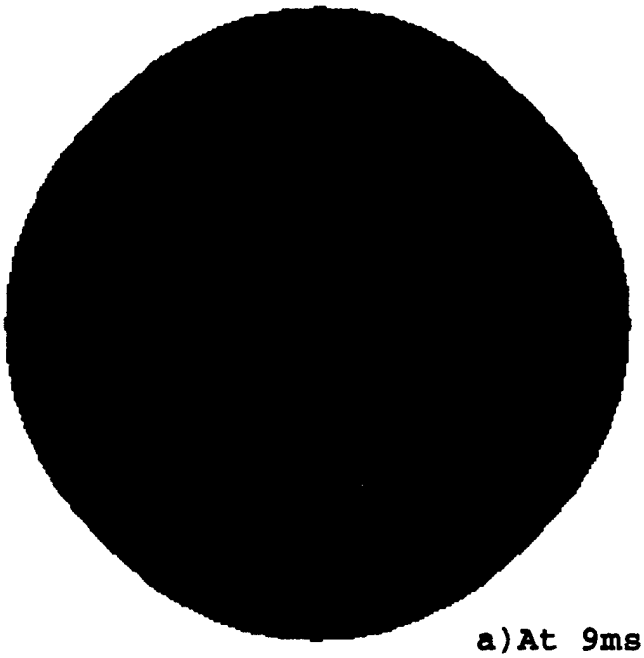

a)At 9ms

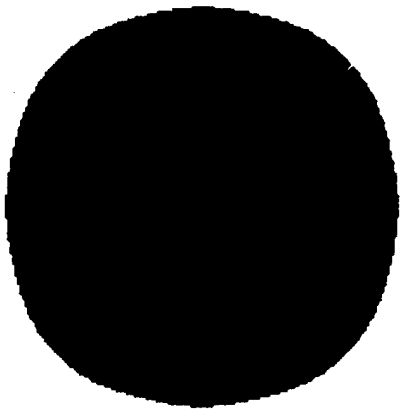

b) At 15ms

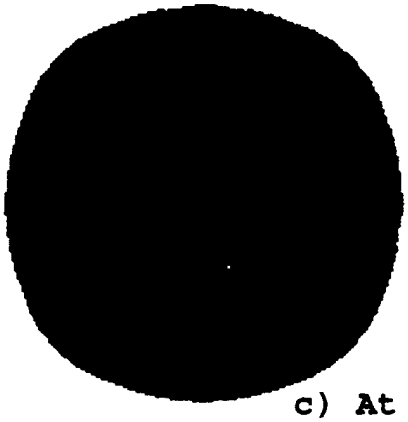

c) At 15.6ms

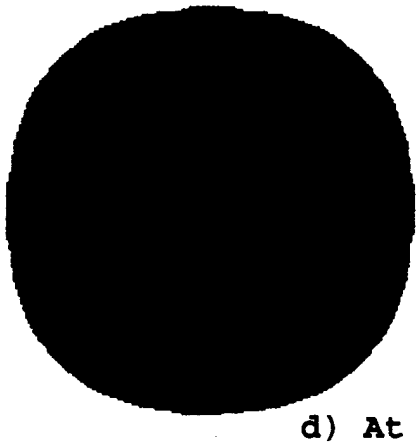

d) At 15.9ms

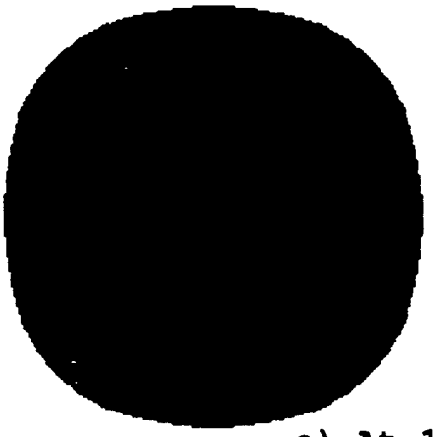

e) At 16.1ms

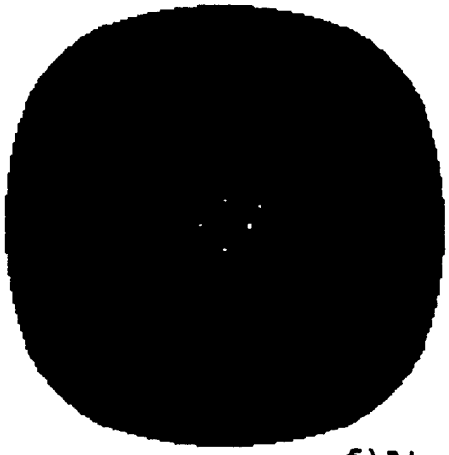

f)At 16.4ms

View From the Wall Side

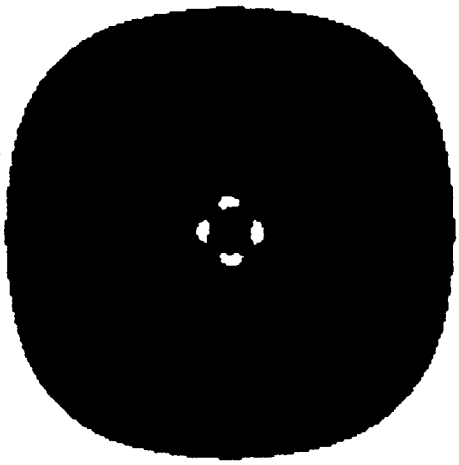

g) At 16.5ms

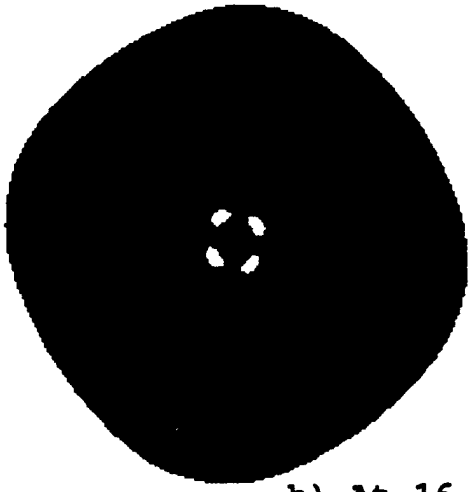

h) At 16.5ms

Side View

i) At 16.5ms

View from an Angle

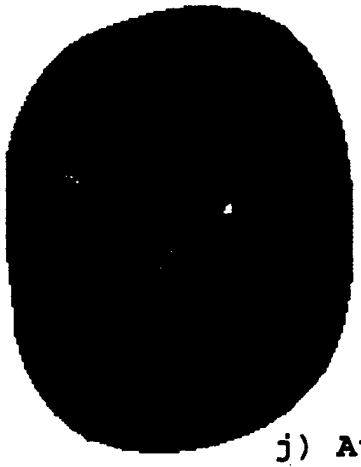

j) At 16.5ms

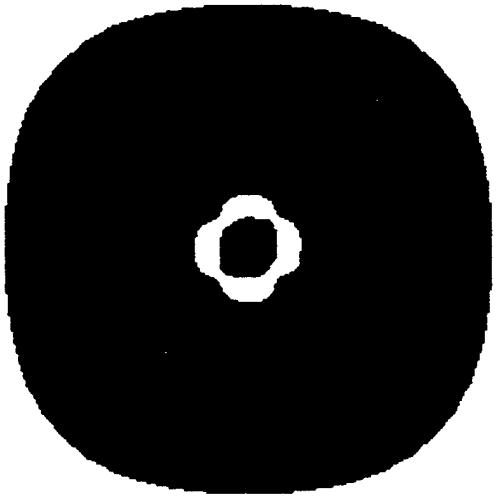

k) At 16.5ms

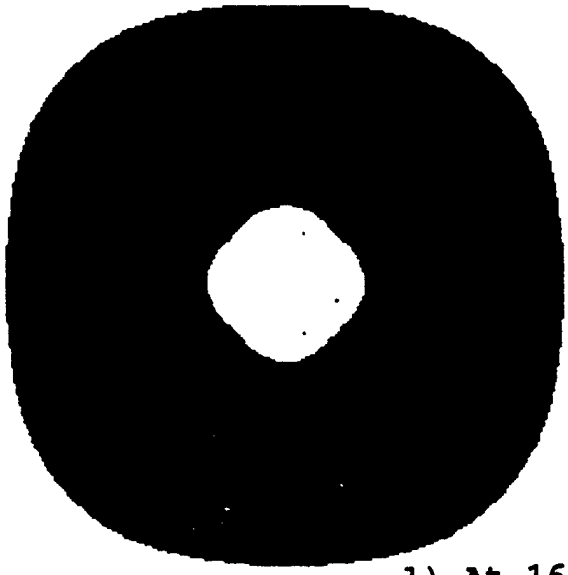

l) At 16.5ms

Fig.25 Time sequence of the bubble expansion and collapse near a wall( View from the side away from the wall, unless specified)

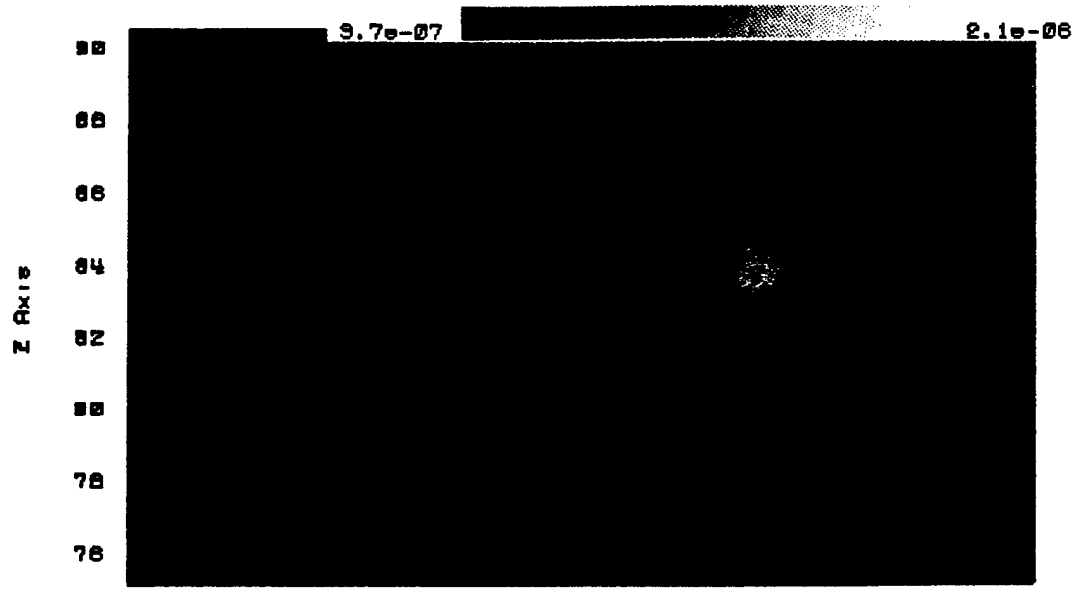


a) 9 ms

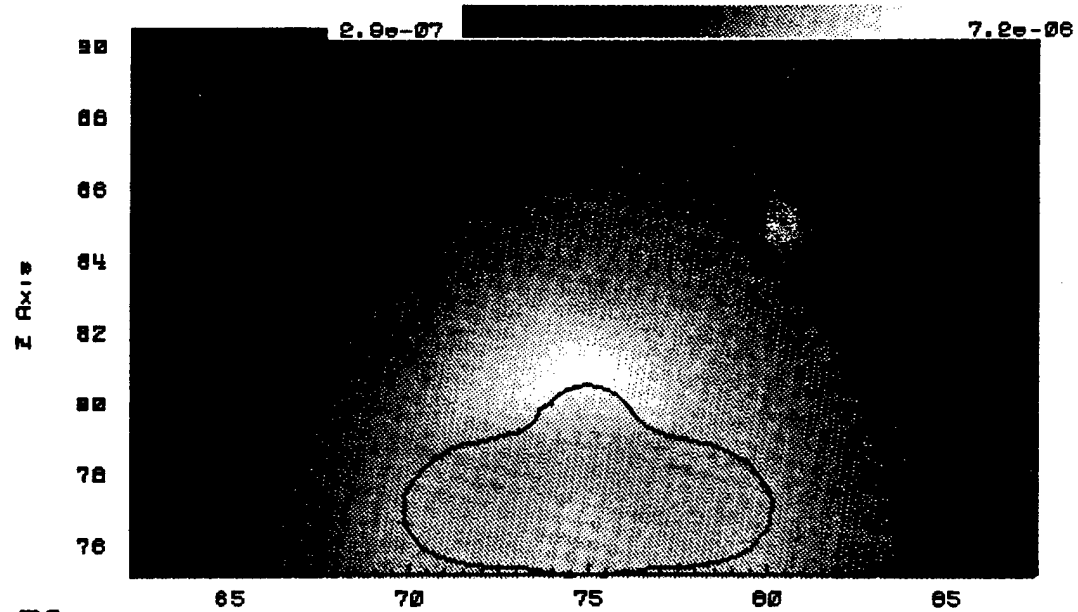


b) 15 ms

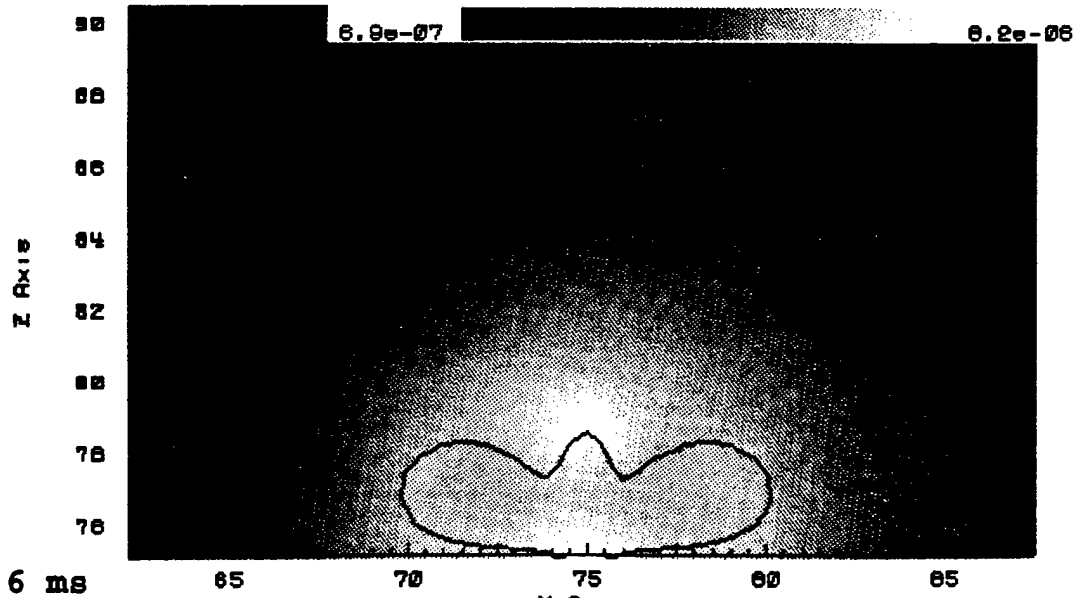


c) 15.6 ms

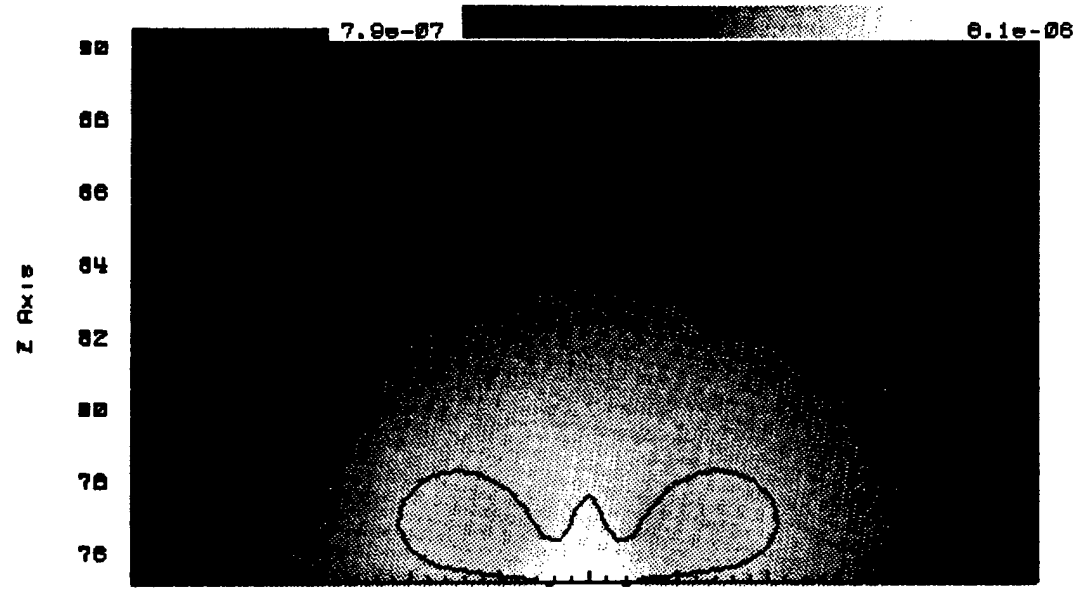


d) 15.9 ms

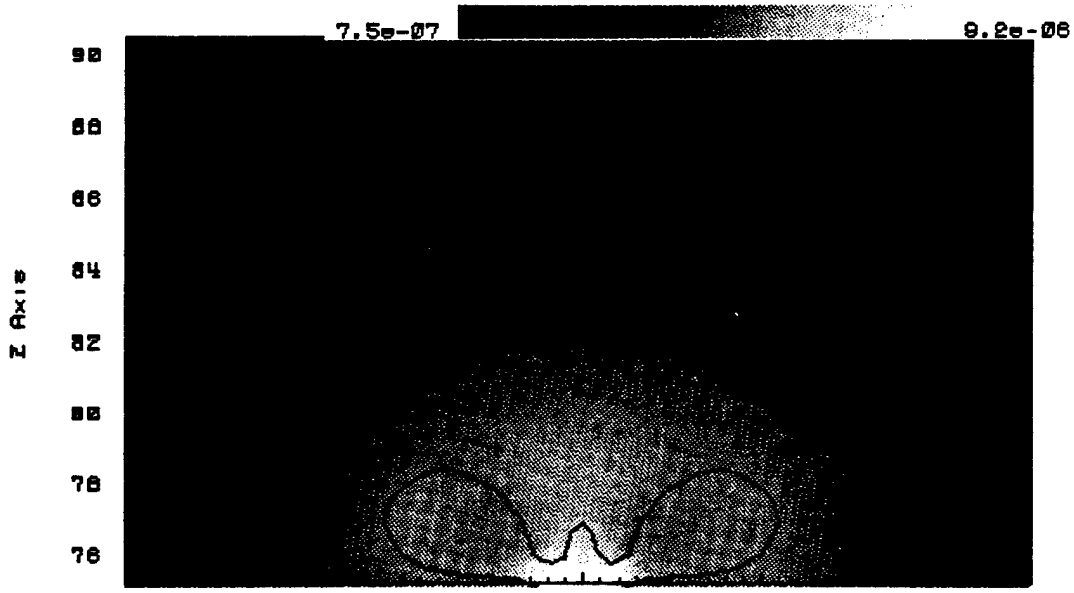


f) 16.1 ms

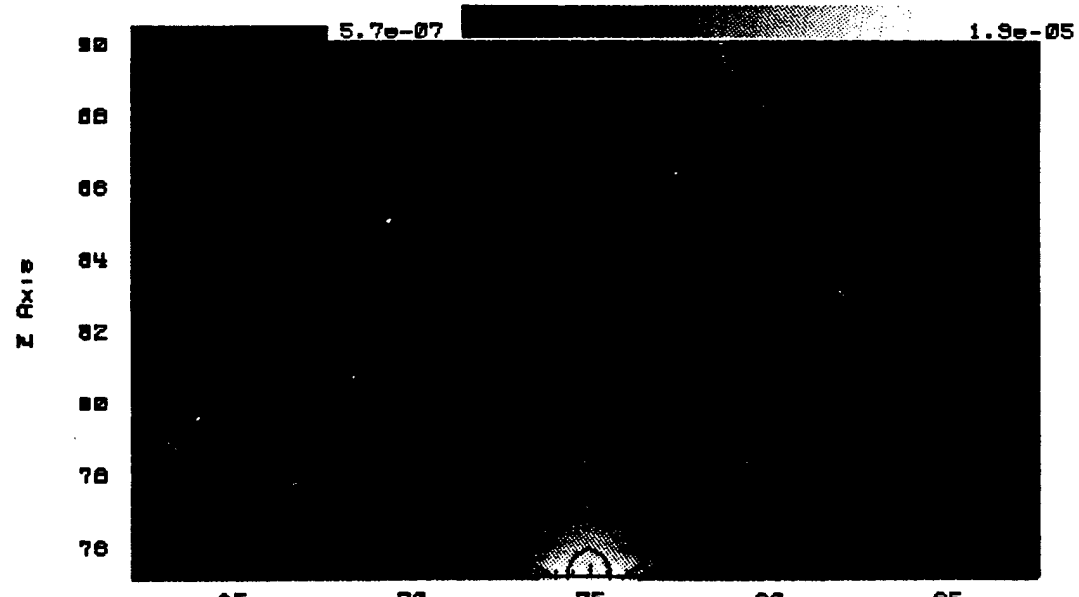


g) 16.4 ms

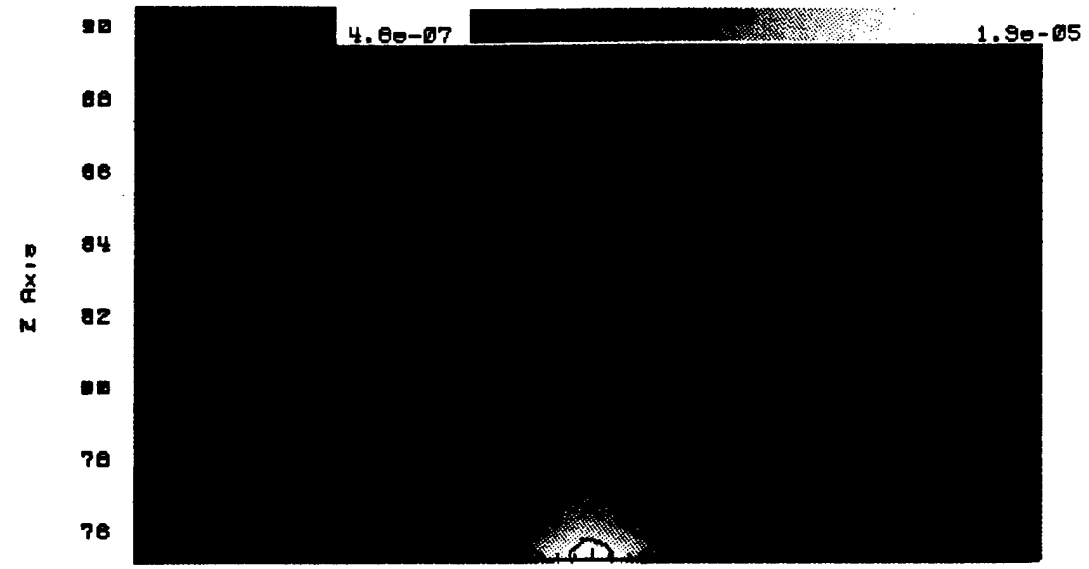


g) 16.5 ms

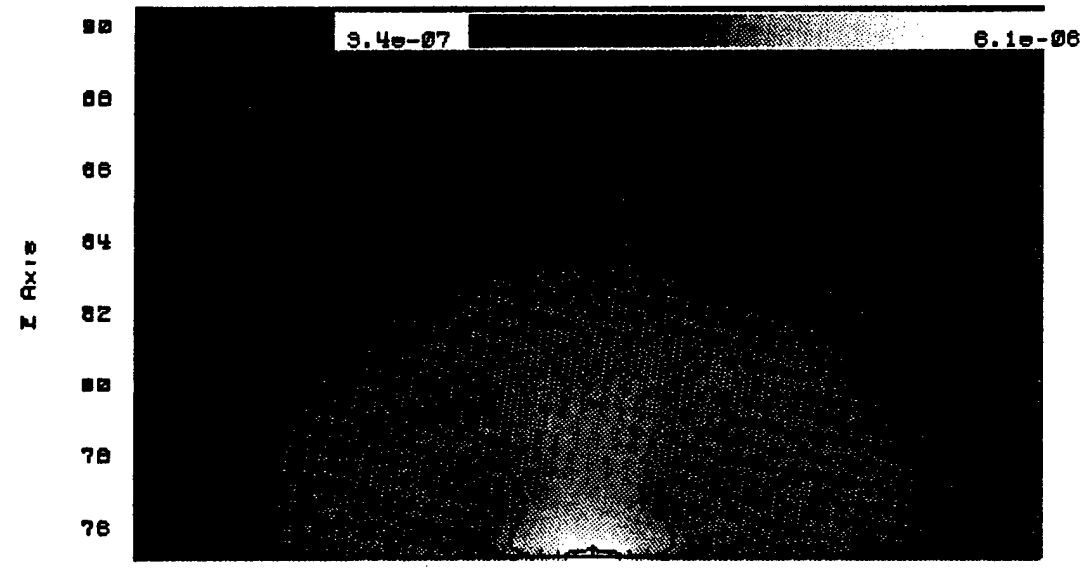


h) 17 ms

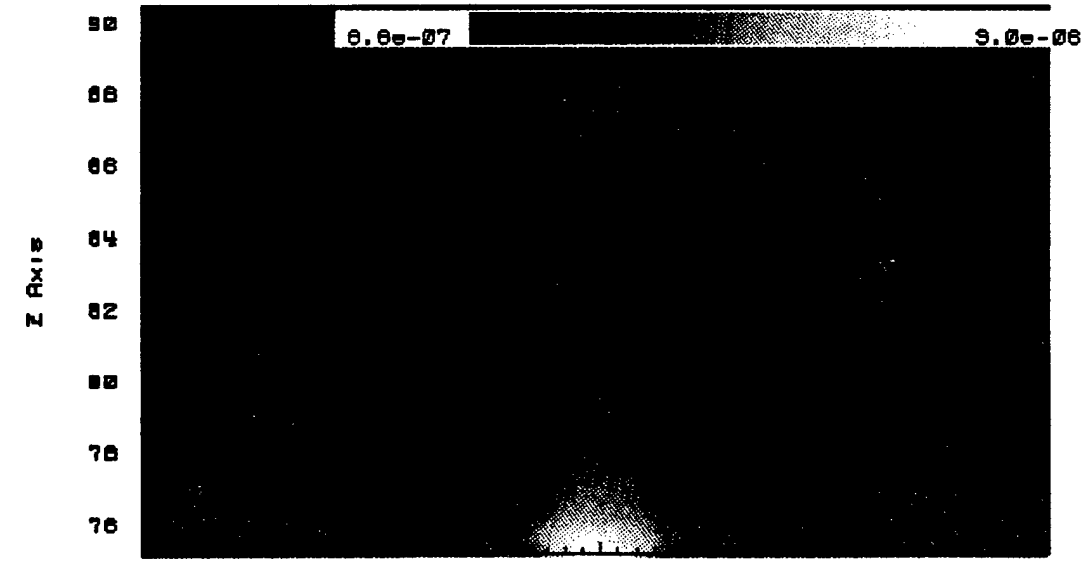


i) 18 ms

Fig.25 Smooth pressure contours of bubble collapsing near a wall

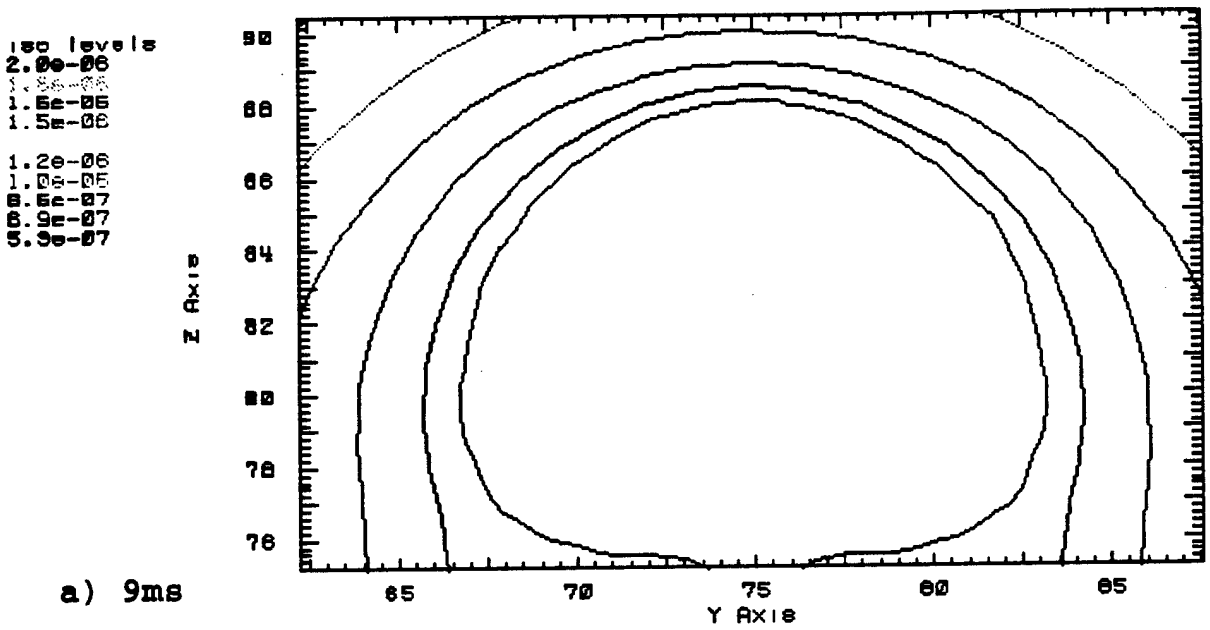


a) 9ms

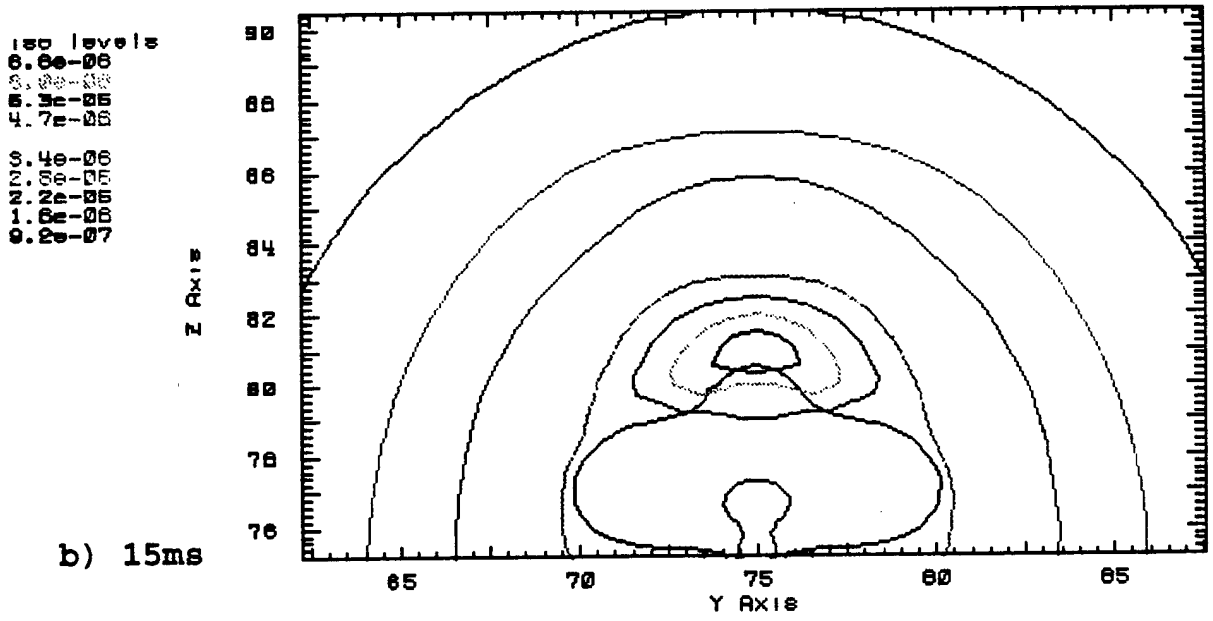


b) 15ms

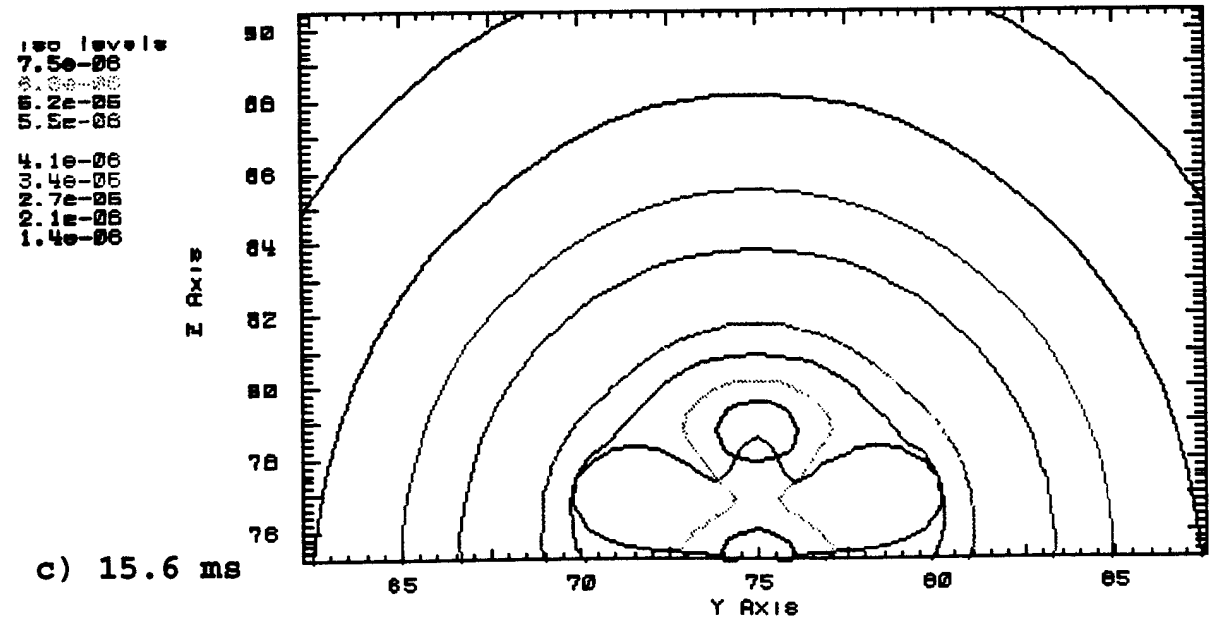


c) 15.6 ms

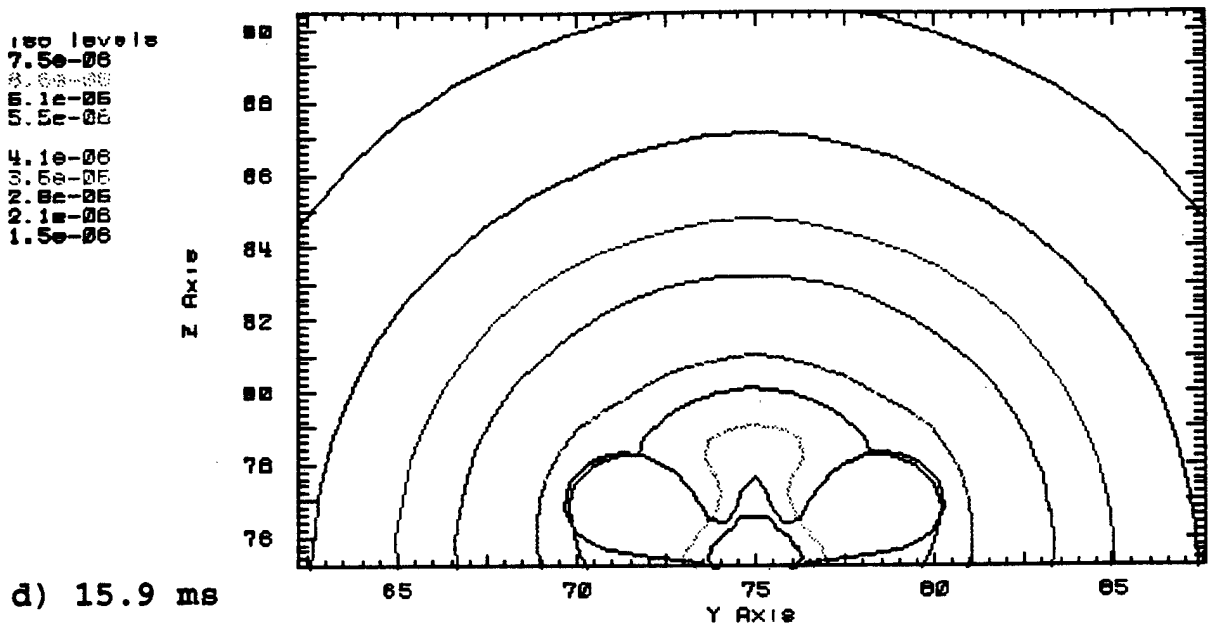


d) 15.9 ms

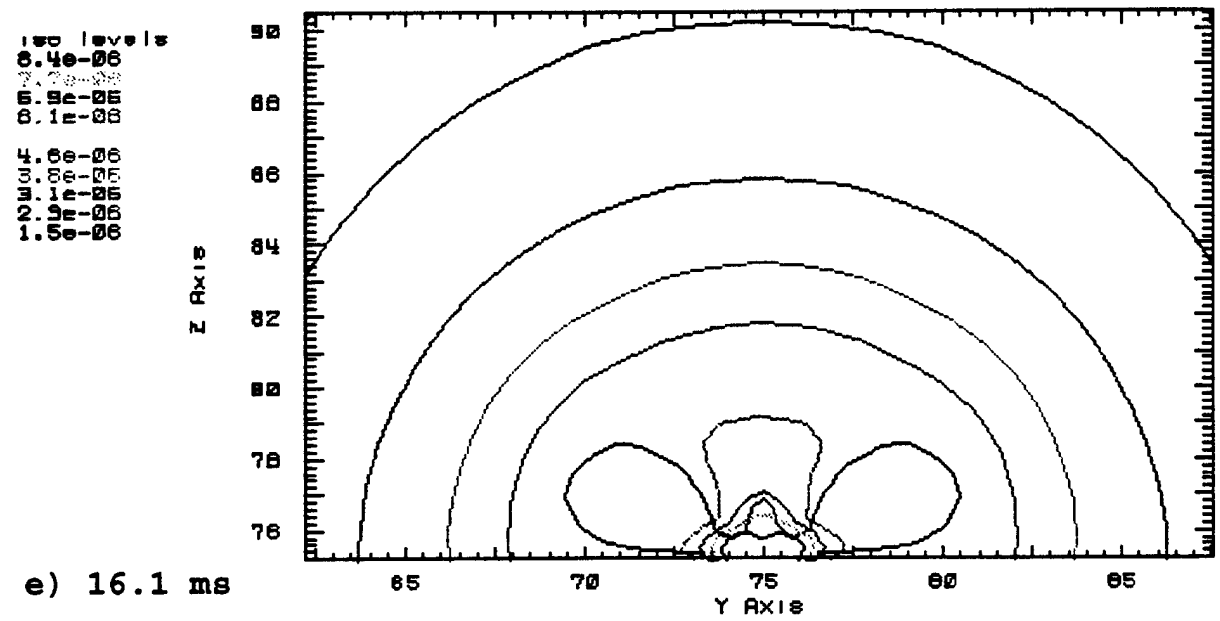


e) 16.1 ms

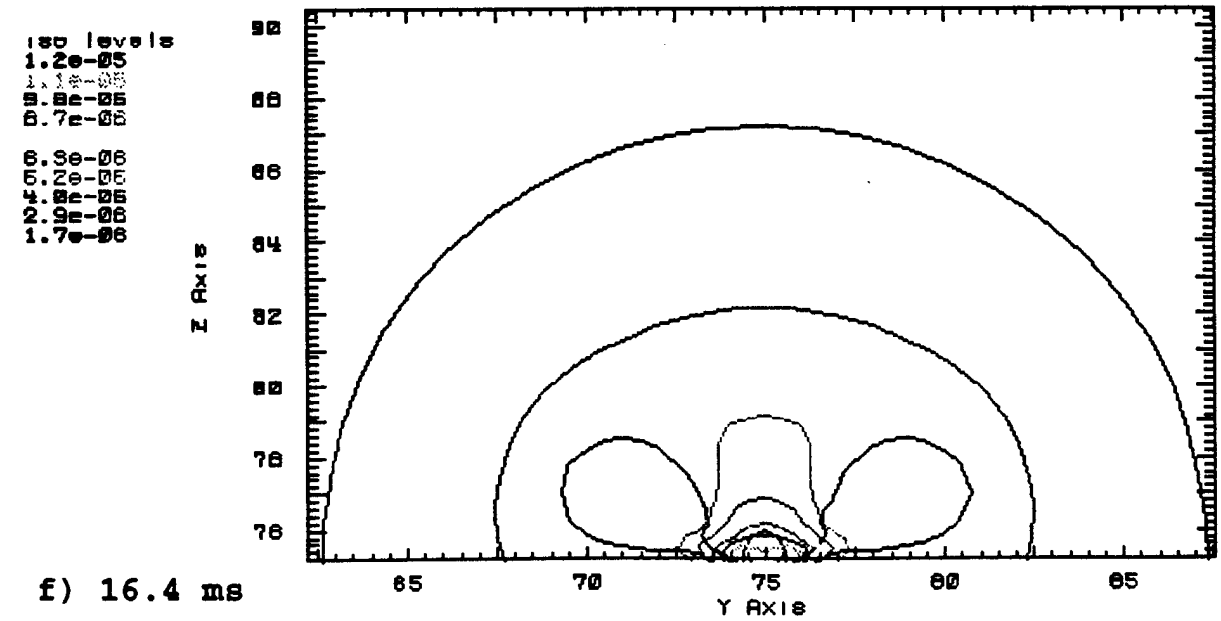


f) 16.4 ms

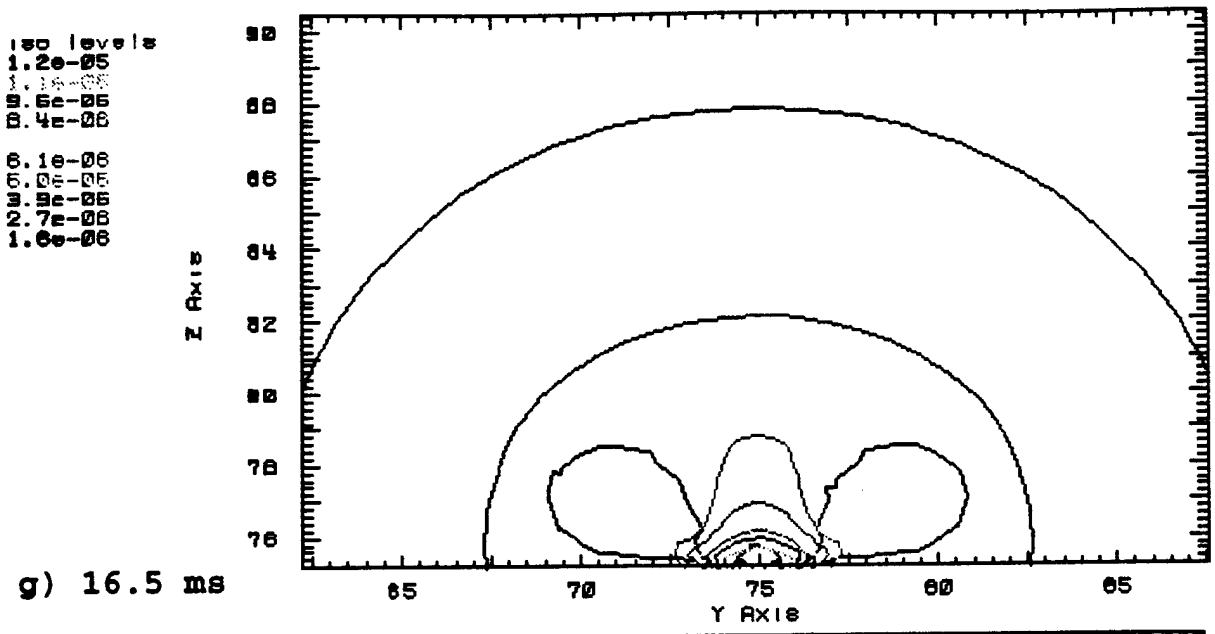


g) 16.5 ms

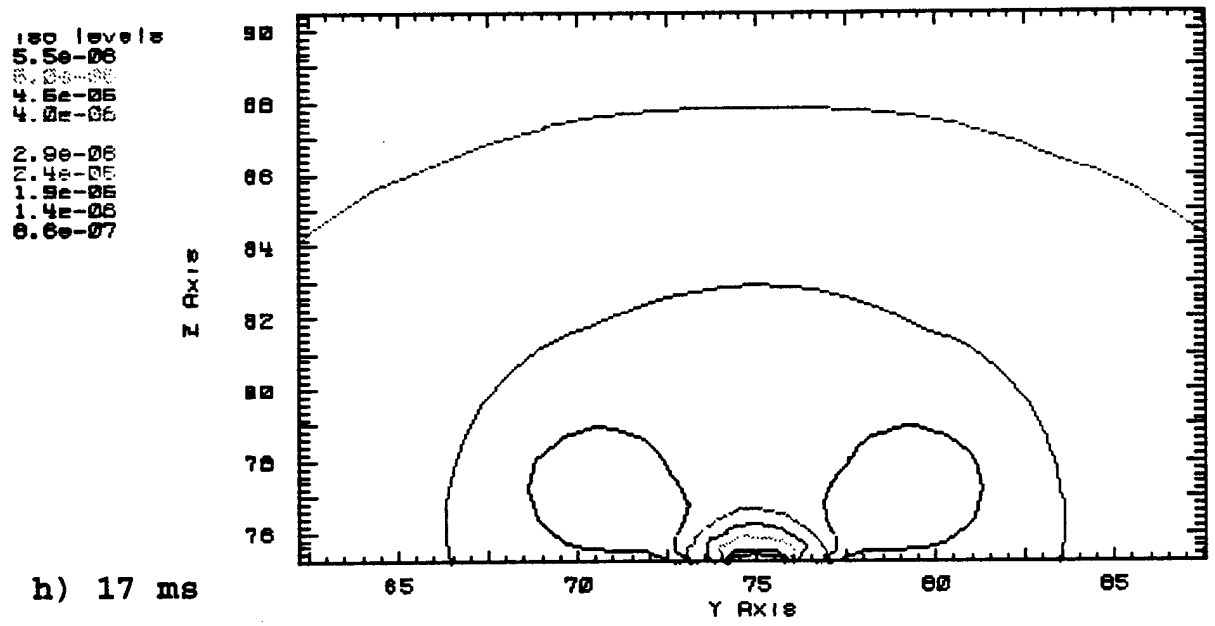


h) 17 ms

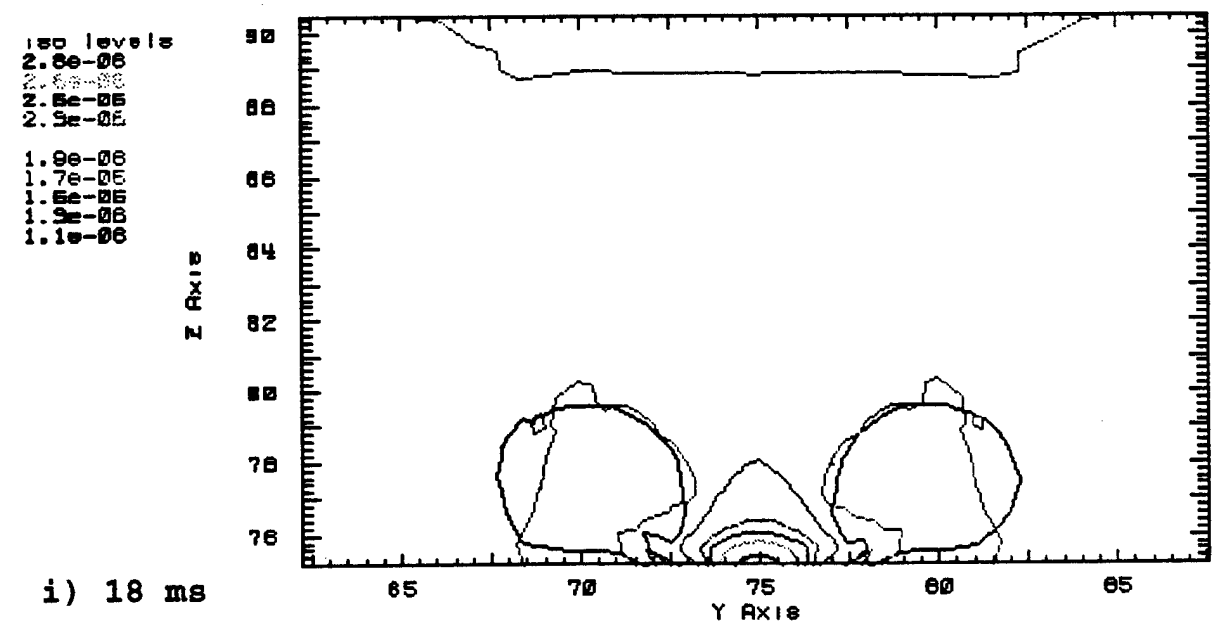


i) 18 ms

Fig.27 Pressure Contours for the collapse of bubble near a wall.

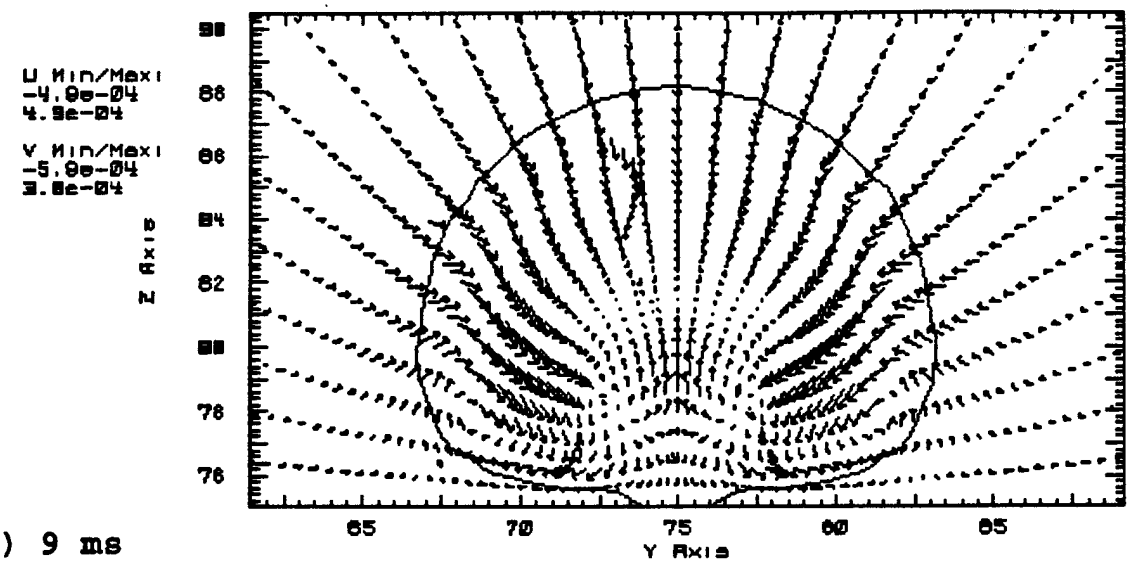


a) 9 ms

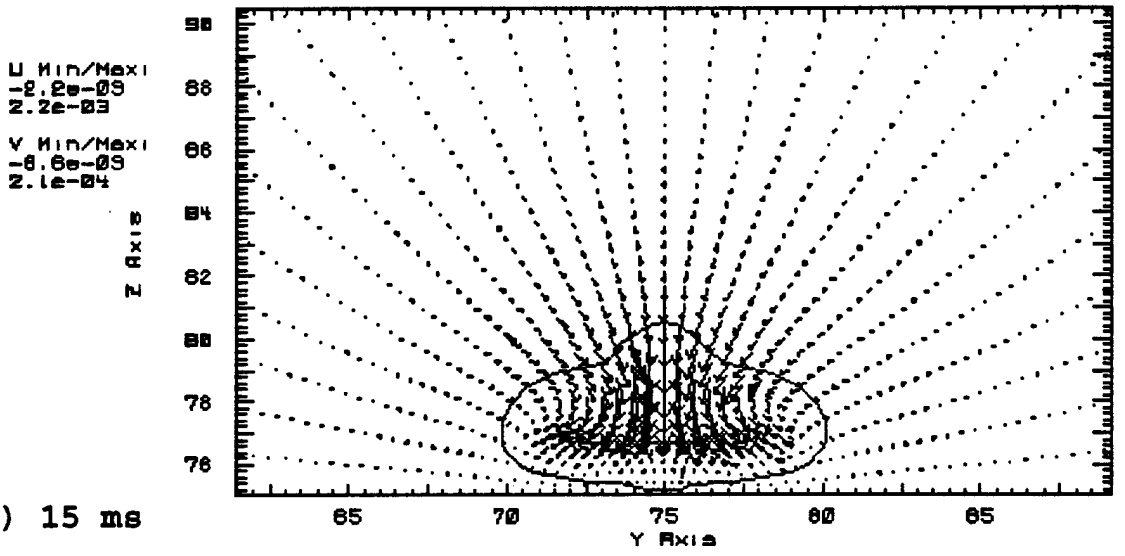


b) 15 ms

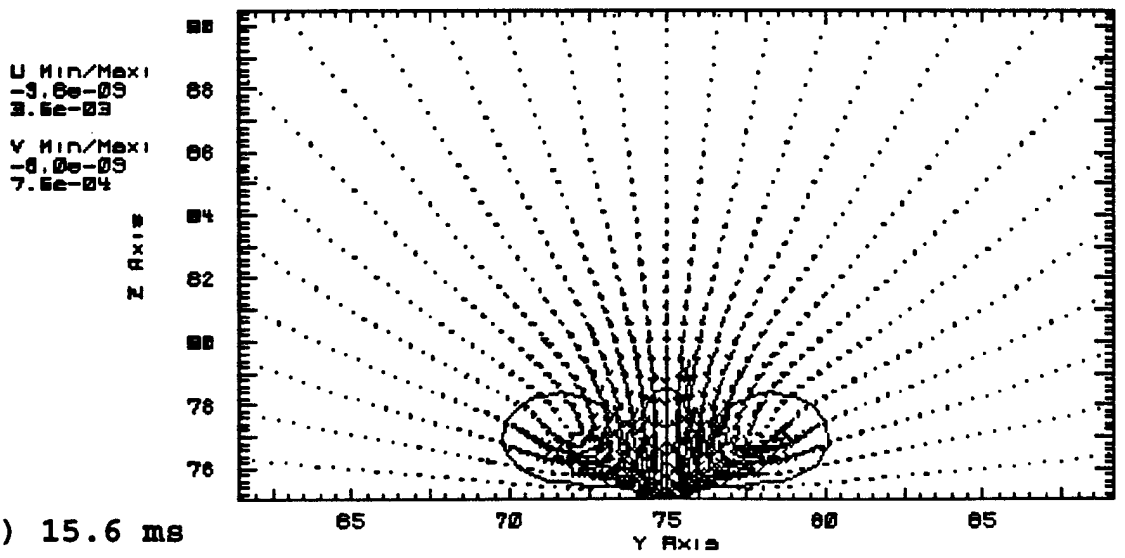


c) 15.6 ms

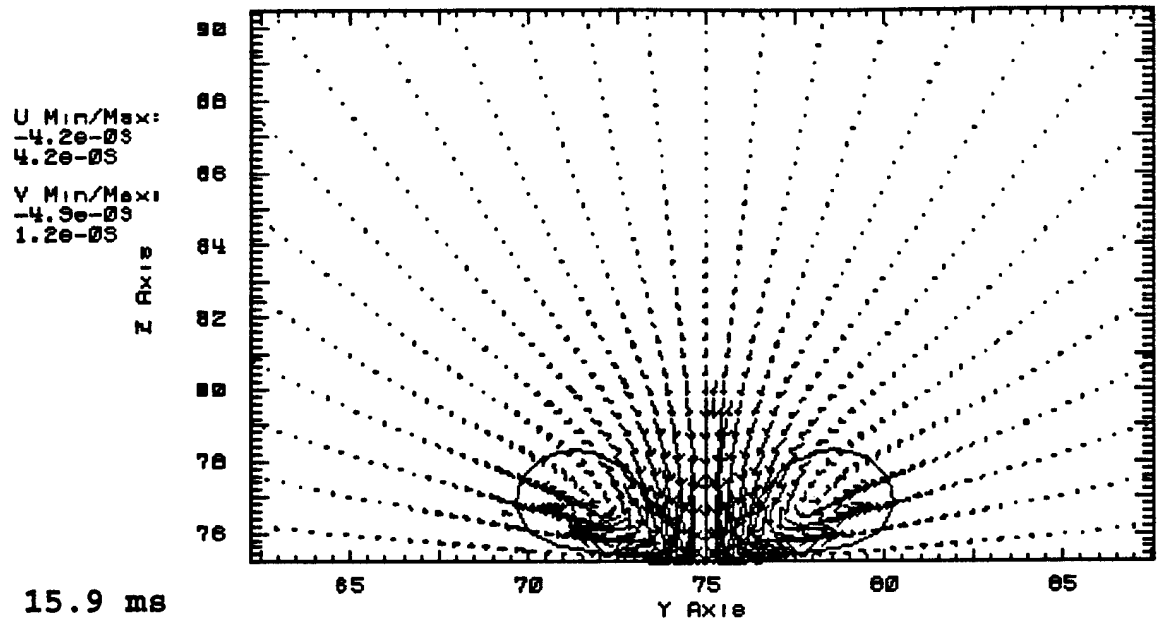


d) 15.9 ms

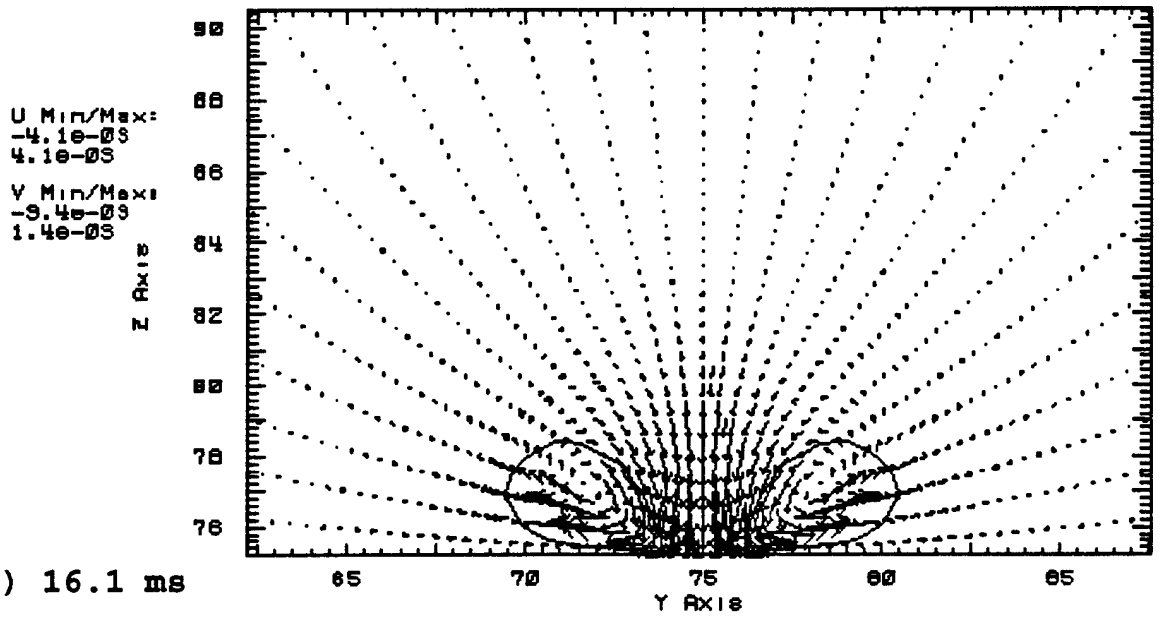


e) 16.1 ms

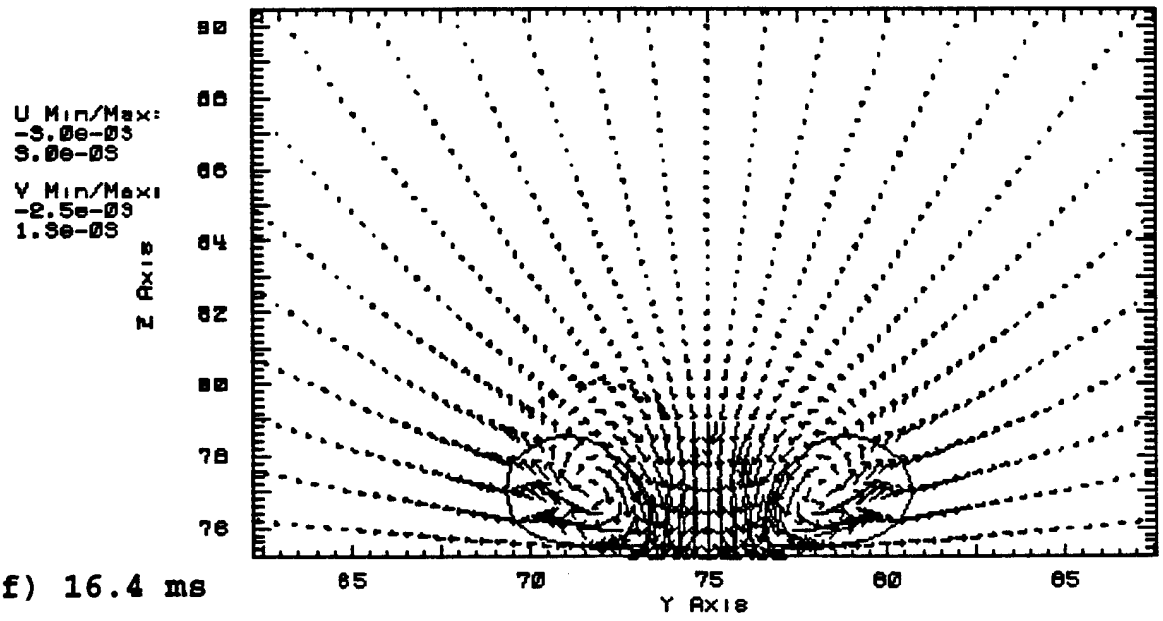


f) 16.4 ms

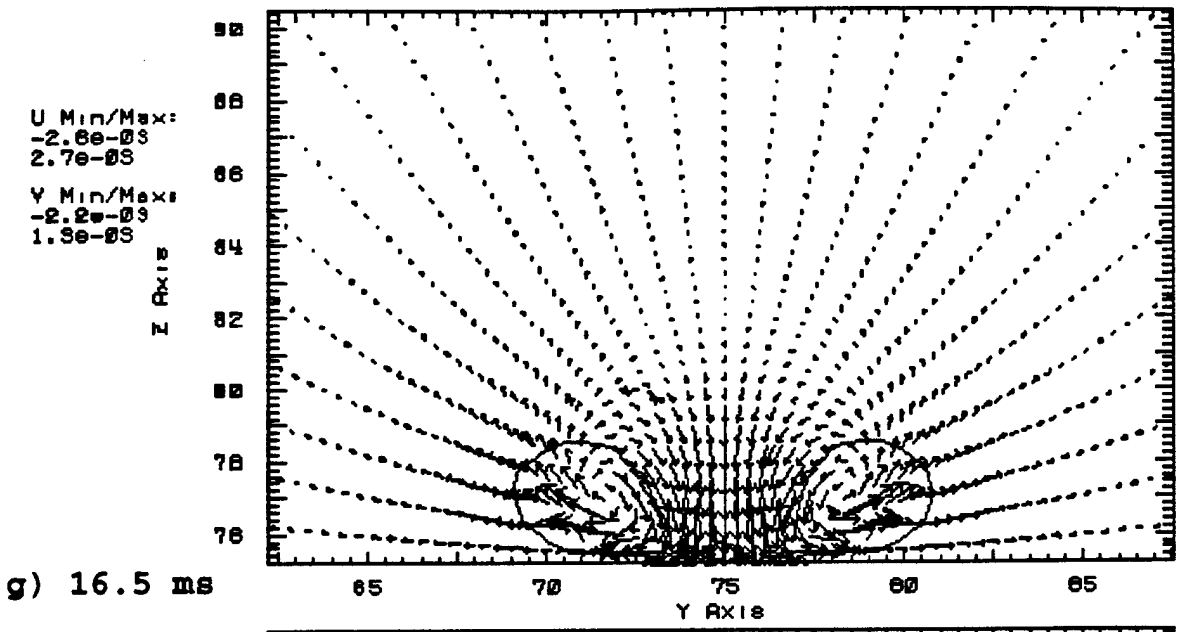


g) 16.5 ms

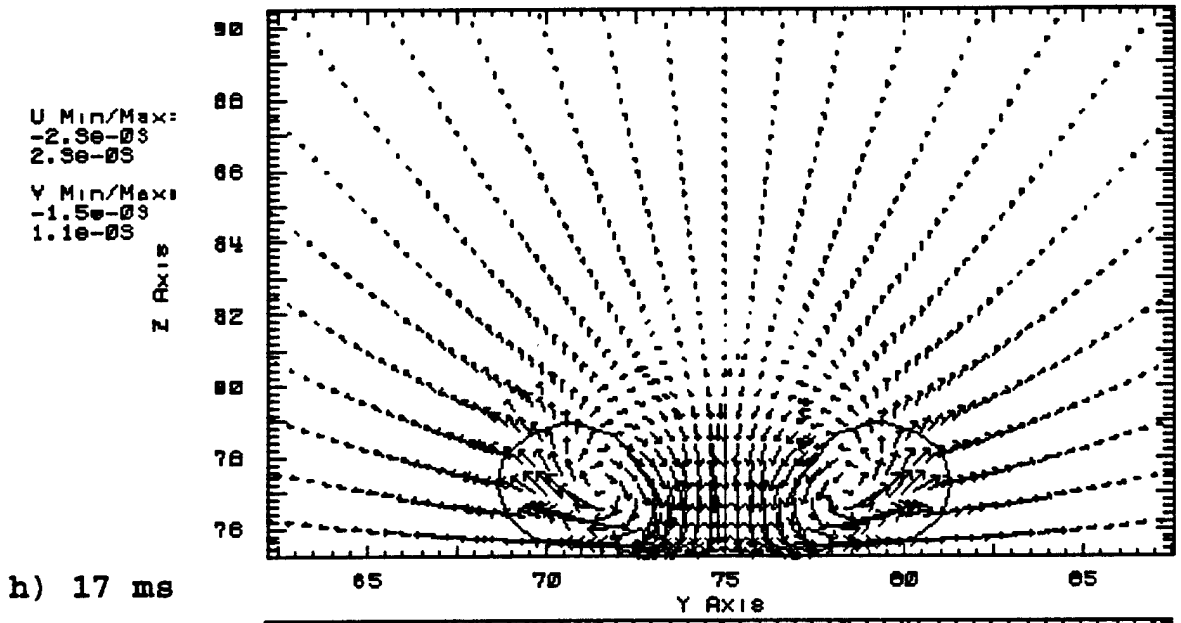


h) 17 ms

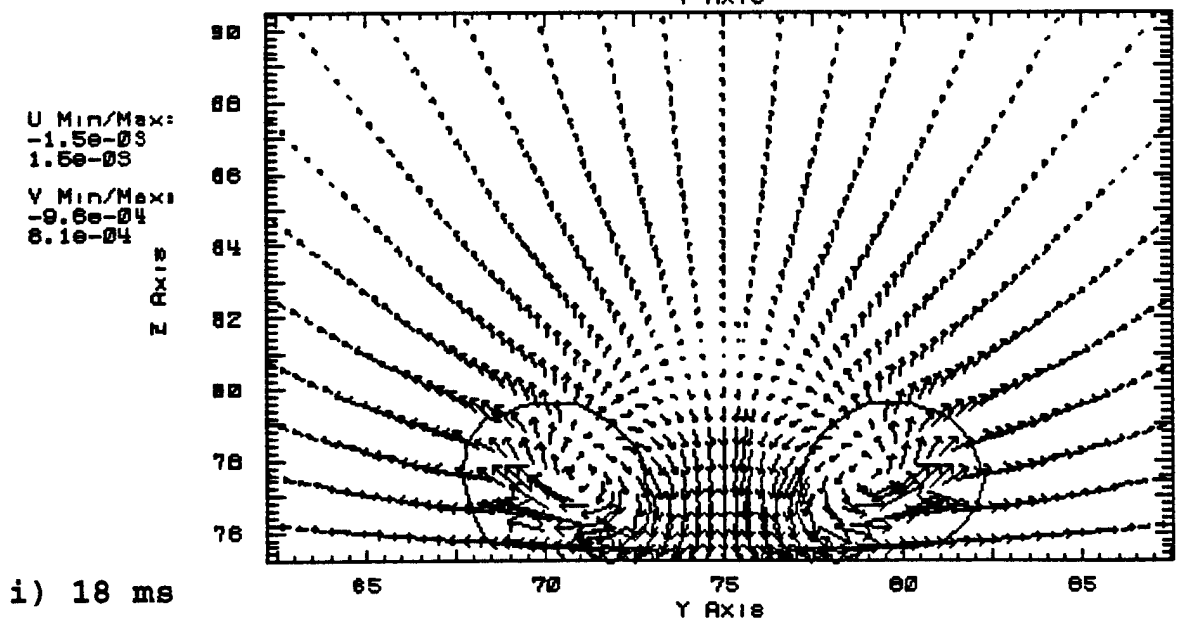


i) 18 ms

Figure 28

**Fig. Velocity Vectors Showing the development of jet during the collapse and rebound of a bubble near a wall.**

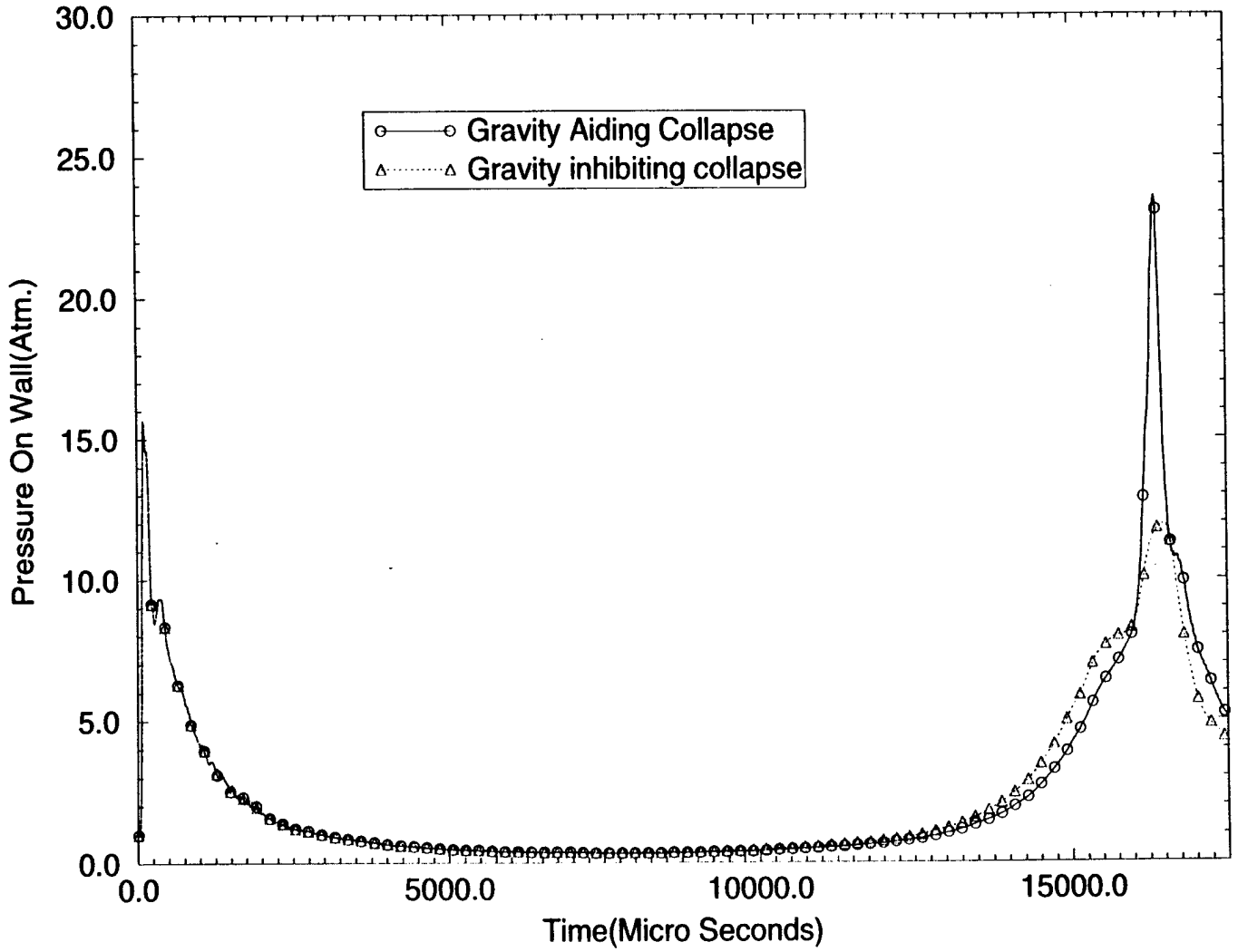


**Figure 29α: Impact pressure computed on the wall for the gravity aided and inhibited cases.**

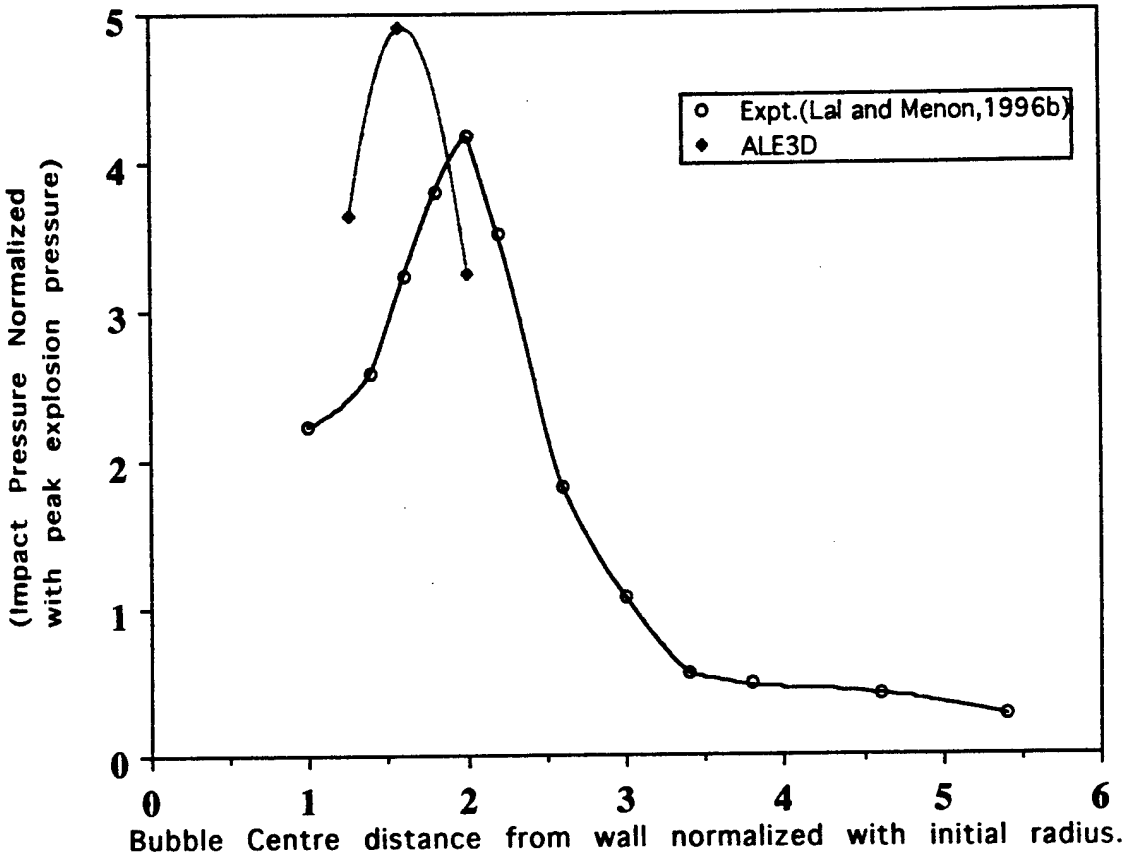


Fig. 29b Variation of impact pressure on the wall with distance of the bubble from wall.

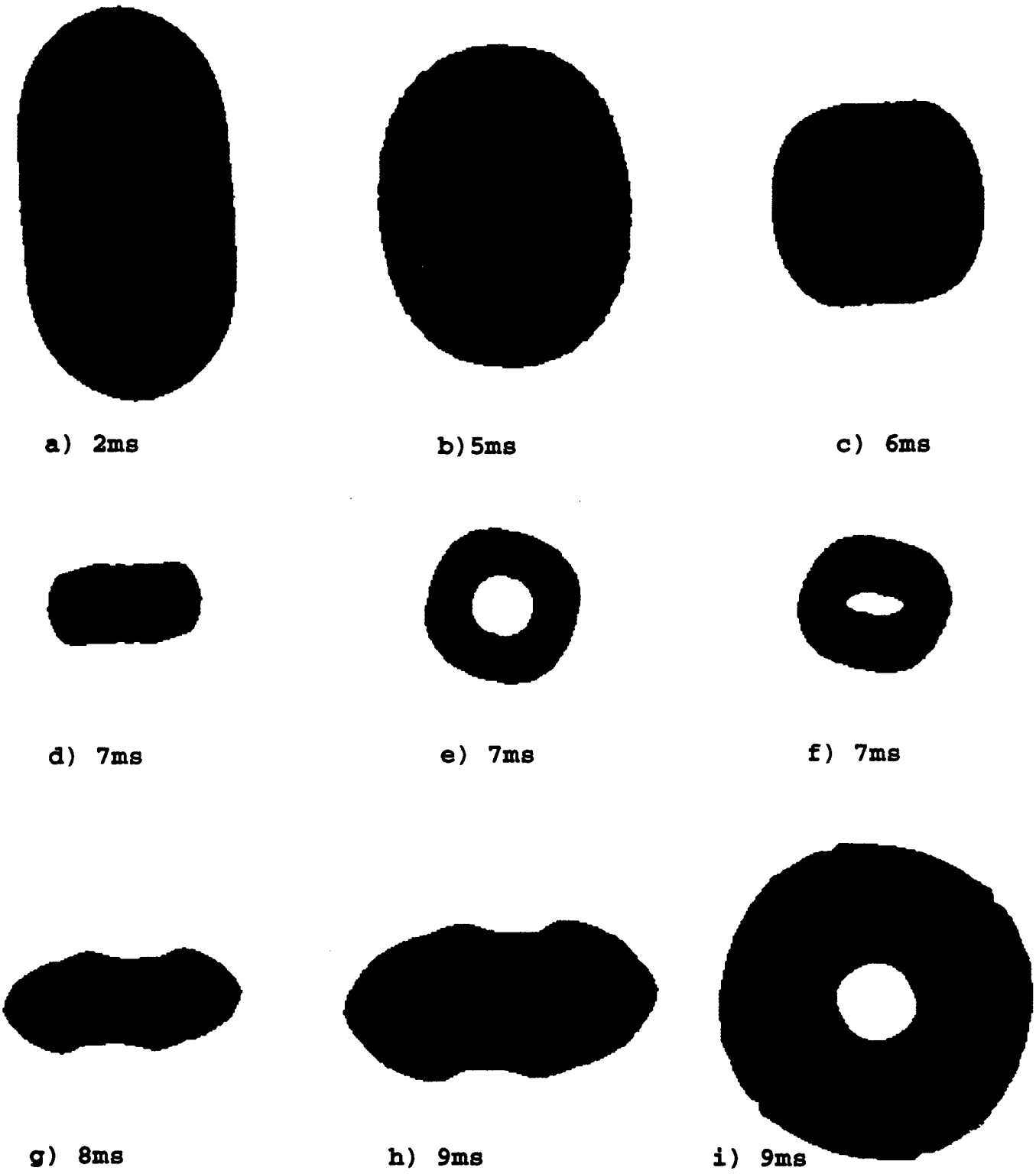


Fig.30 Bubble formed by a explosive cord in a free field. a) At bubble max when it is almost cylindrical, b)&c) the collpase along the axis of the cylinder and expansion in the horizontal direction, d),e) and f) show the different views of the bubble after the jet is formed, g) during rebound and h)&i) show the different views at the maximum of the second oscillation.

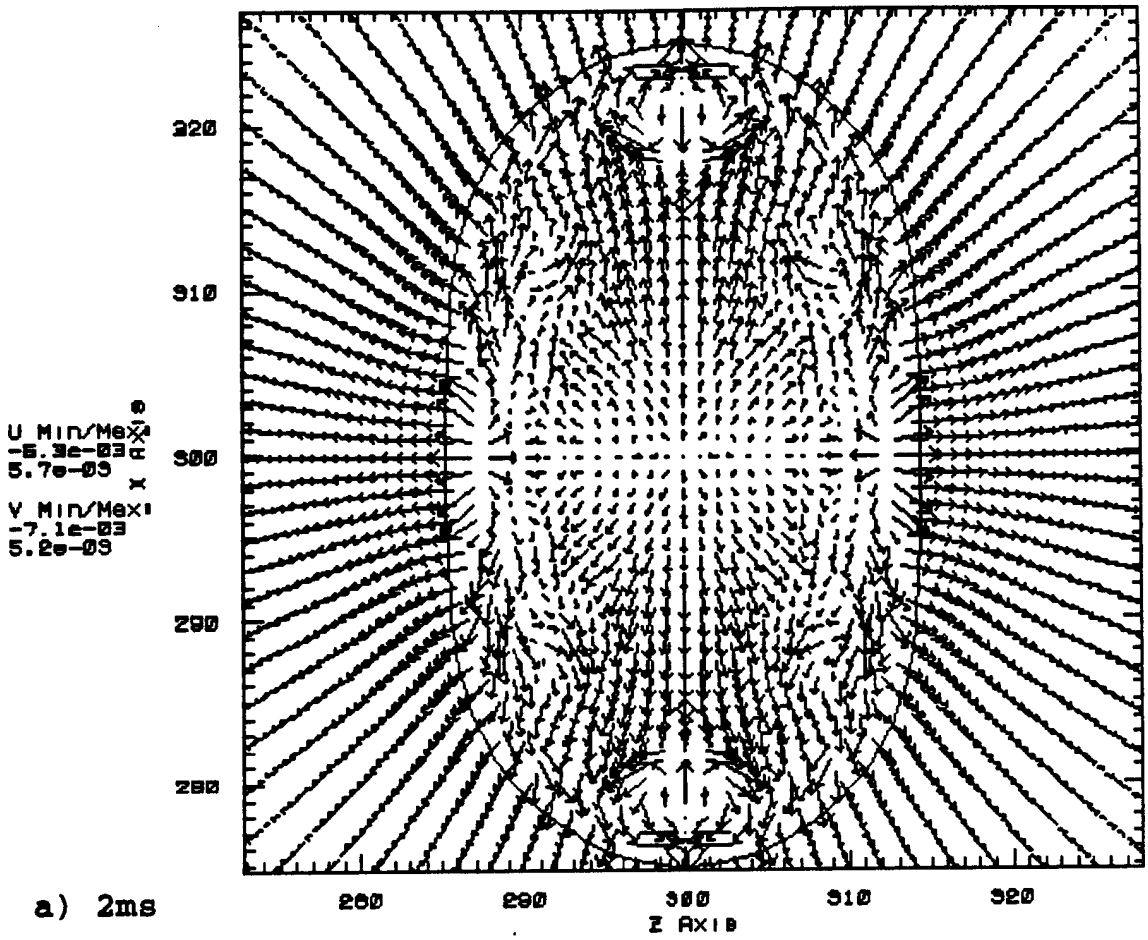
U Min/Max
-5.3e-03
5.7e-03
V Min/Max
-7.1e-03
5.2e-03
320
310
300
290
280
260
290
300
310
320
Z Axis

a) 2ms

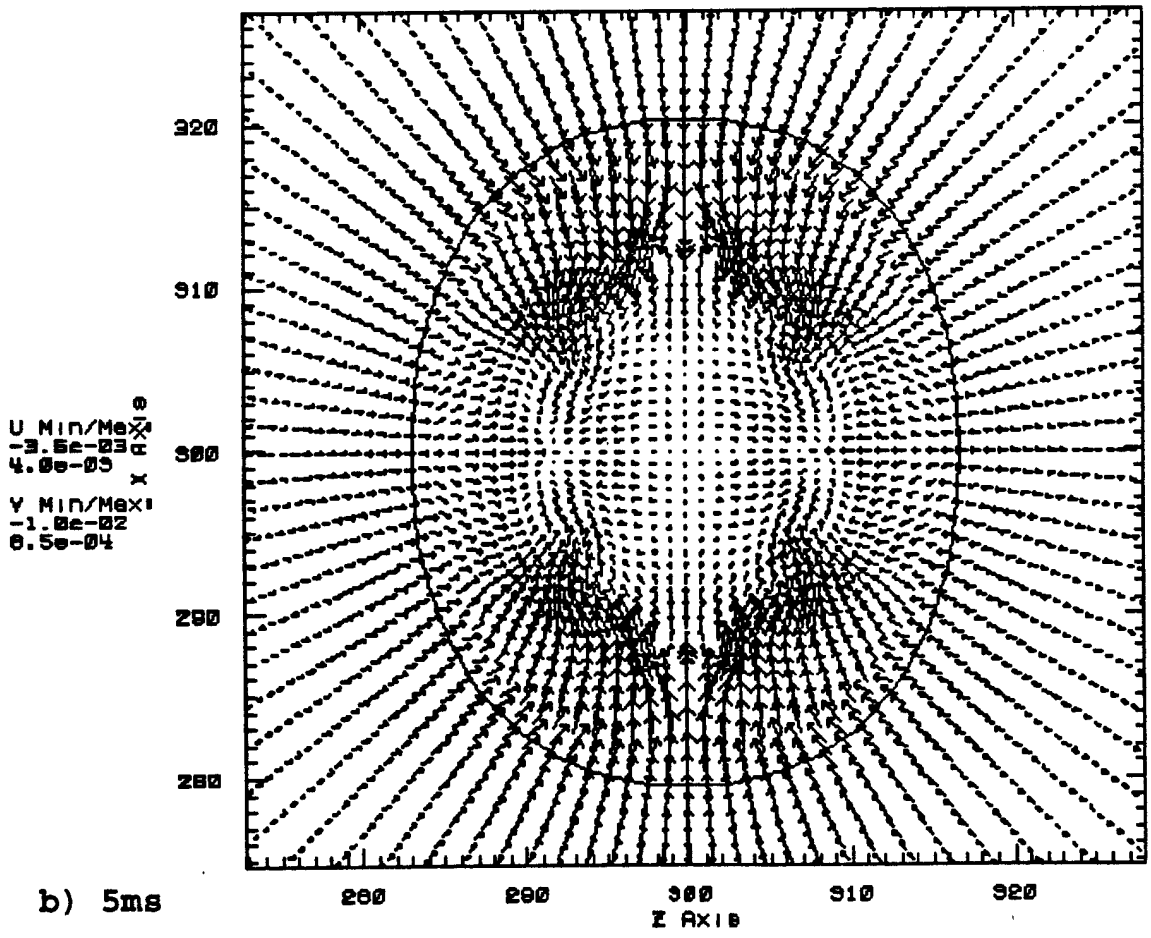
U Min/Max
-3.6e-03
4.0e-03
V Min/Max
-1.0e-02
6.5e-04
320
310
300
290
280
260
290
300
310
320
Z Axis

b) 5ms

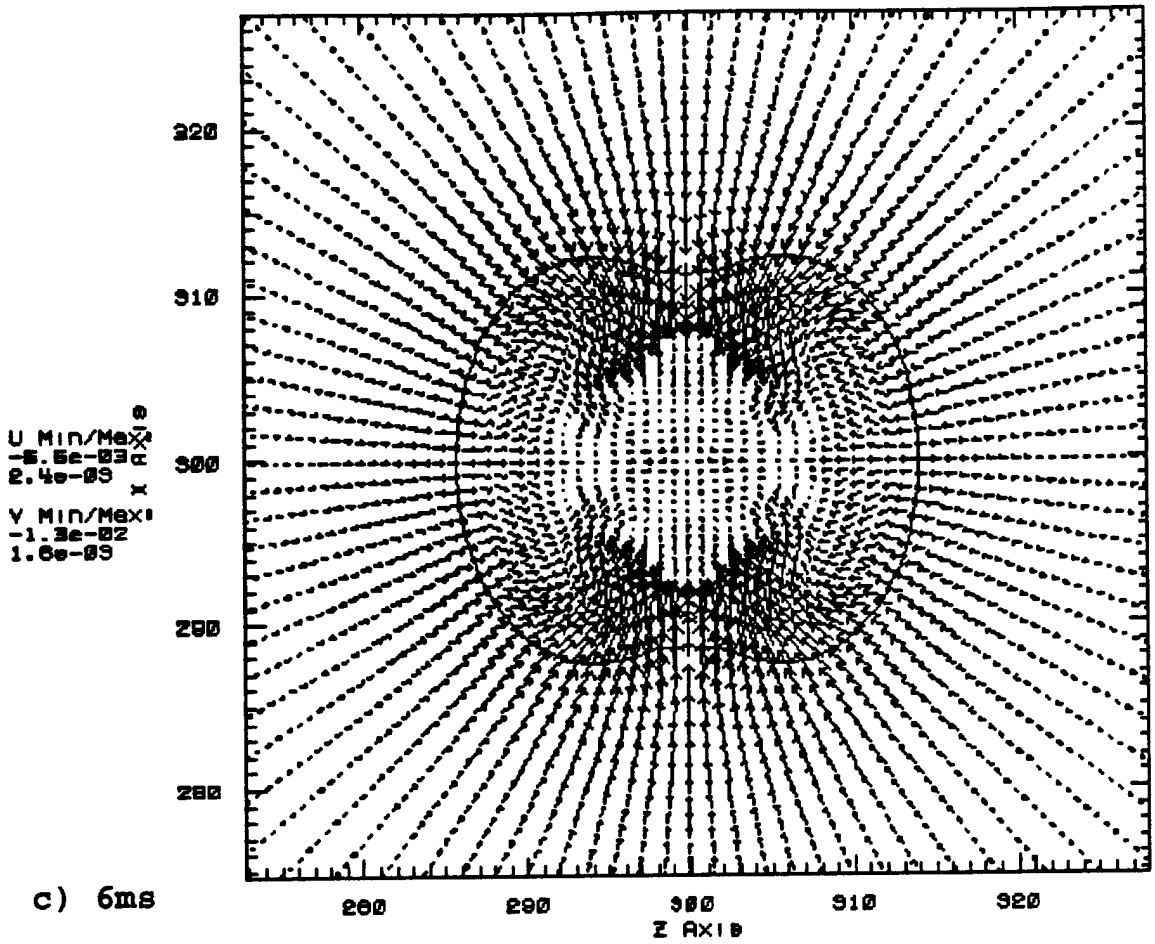
U Min/Max
-5.5e-03
2.4e-03
V Min/Max
-1.3e-02
1.6e-03
320
310
300
290
280
290
300
310
320
Z Axis

c) 6ms

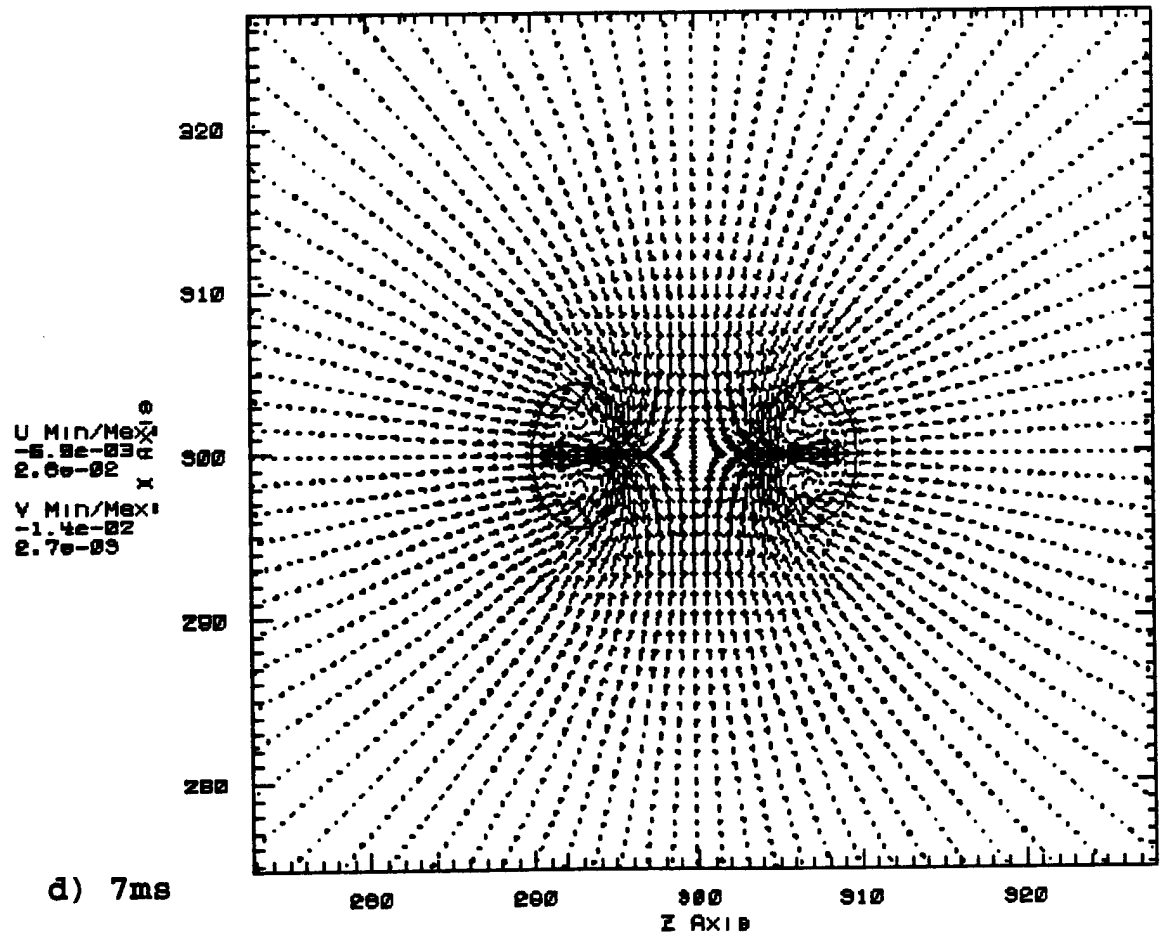
U Min/Max
-5.3e-03
2.6e-02
V Min/Max
-1.4e-02
2.7e-03
320
310
300
290
280
290
300
310
320
Z Axis

d) 7ms

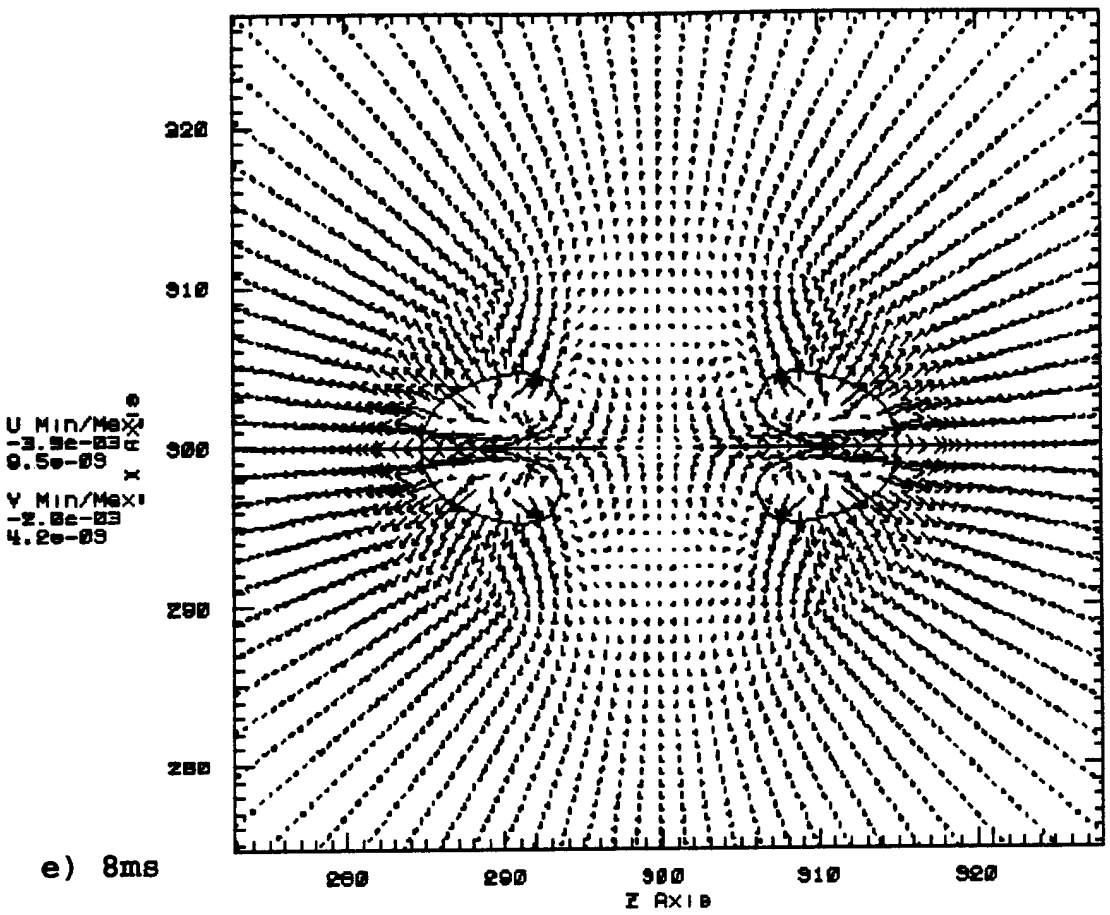


e) 8ms

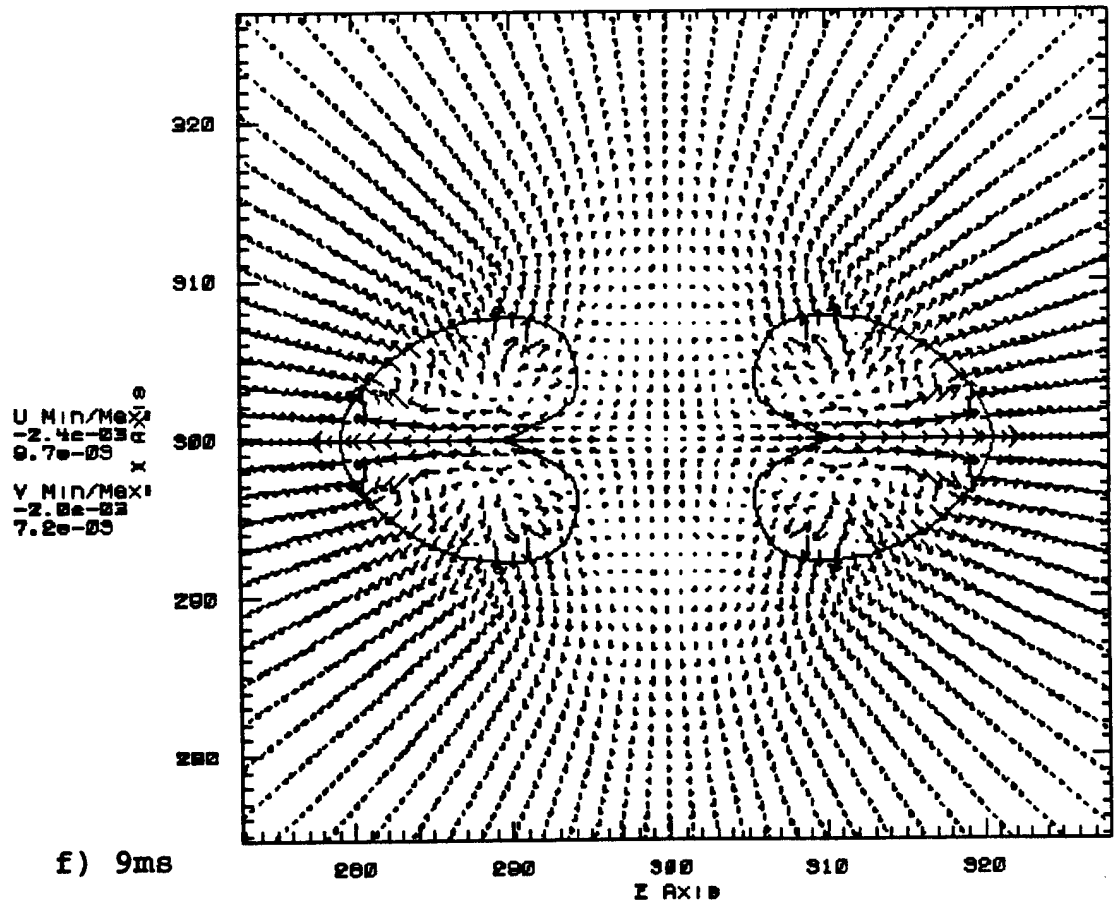


f) 9ms

Fig.3 Velocity vector field around a freely oscillating bubble formed by a cord explosive( with slice parallel to the axis of the cylinder.

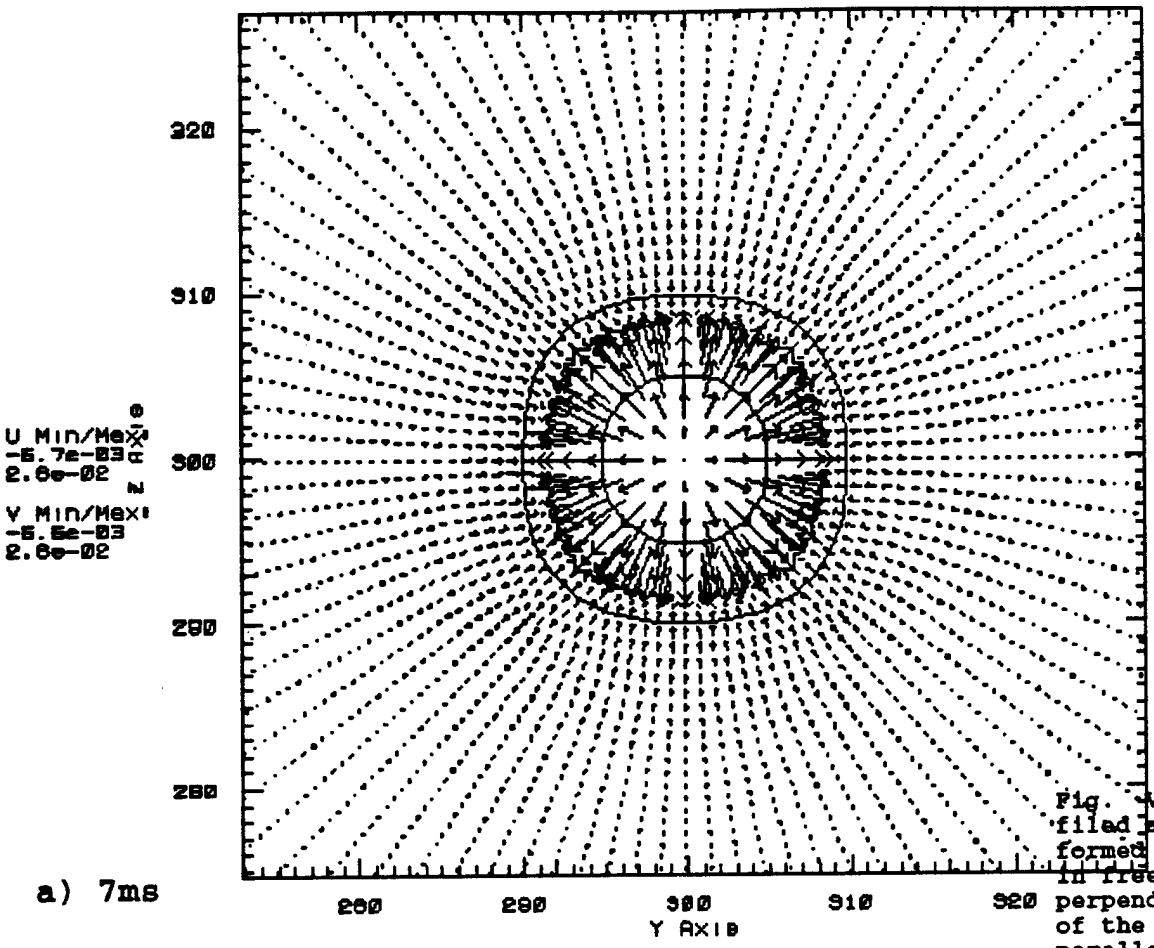


a) 7ms

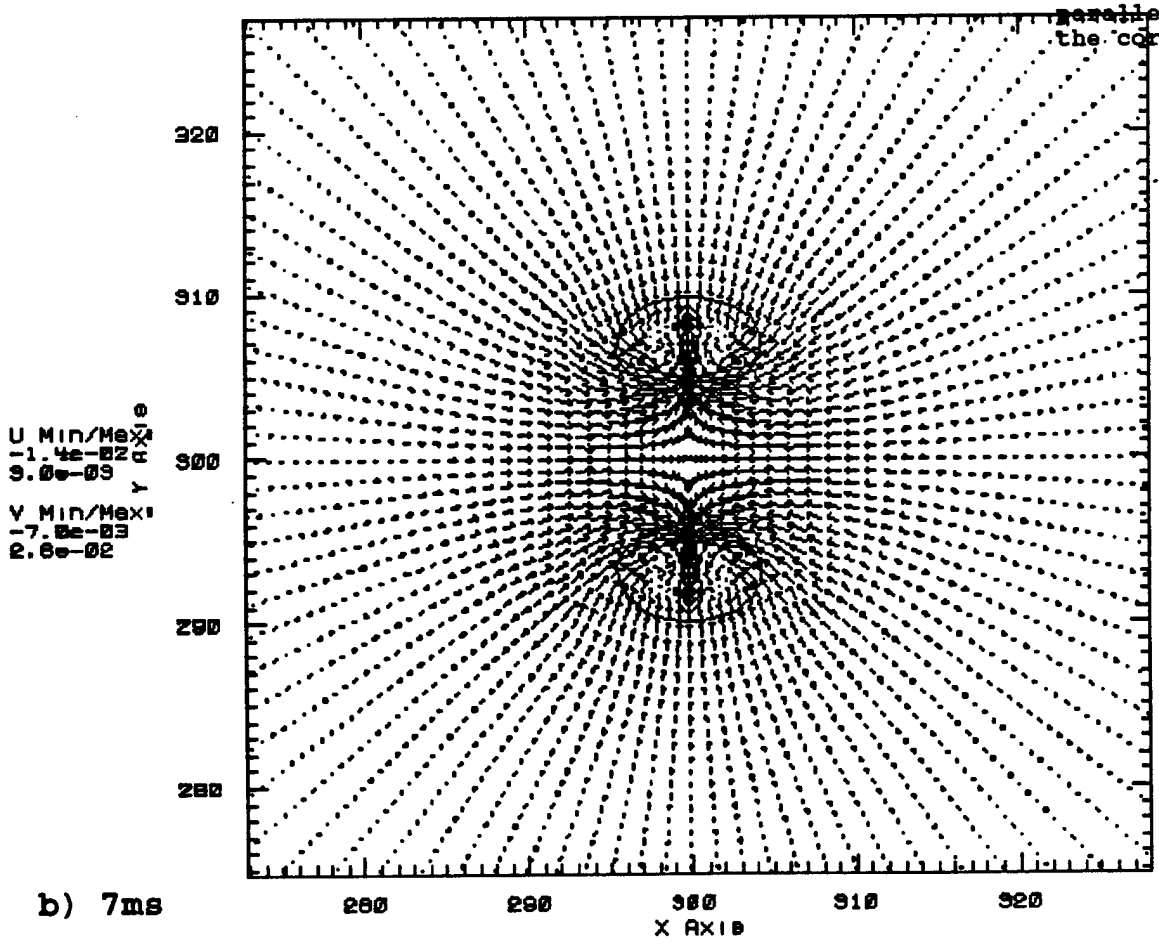


b) 7ms

Figure 32

Fig. Velocity vector filed around the bubble formed by a cord explosive in free field.a) Slice perpendicular to the axis of the cord and b) Slice parallel to the axis of the cord.

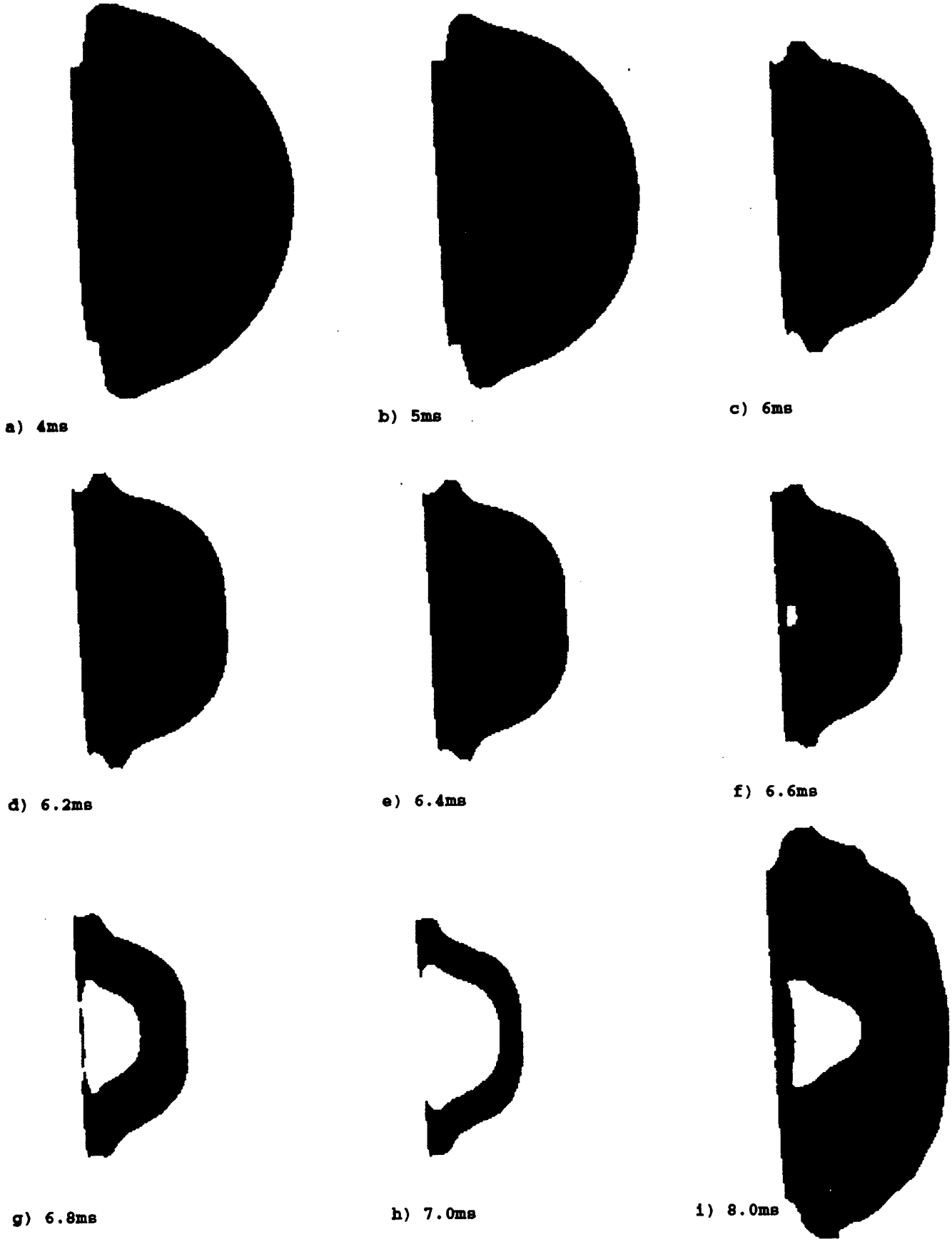


Fig.33 Time sequence of the bubble generated by a cord exploding near a rigid wall. a)-f) During Collapse, g) Jet formation and h)&i) During Rebound.

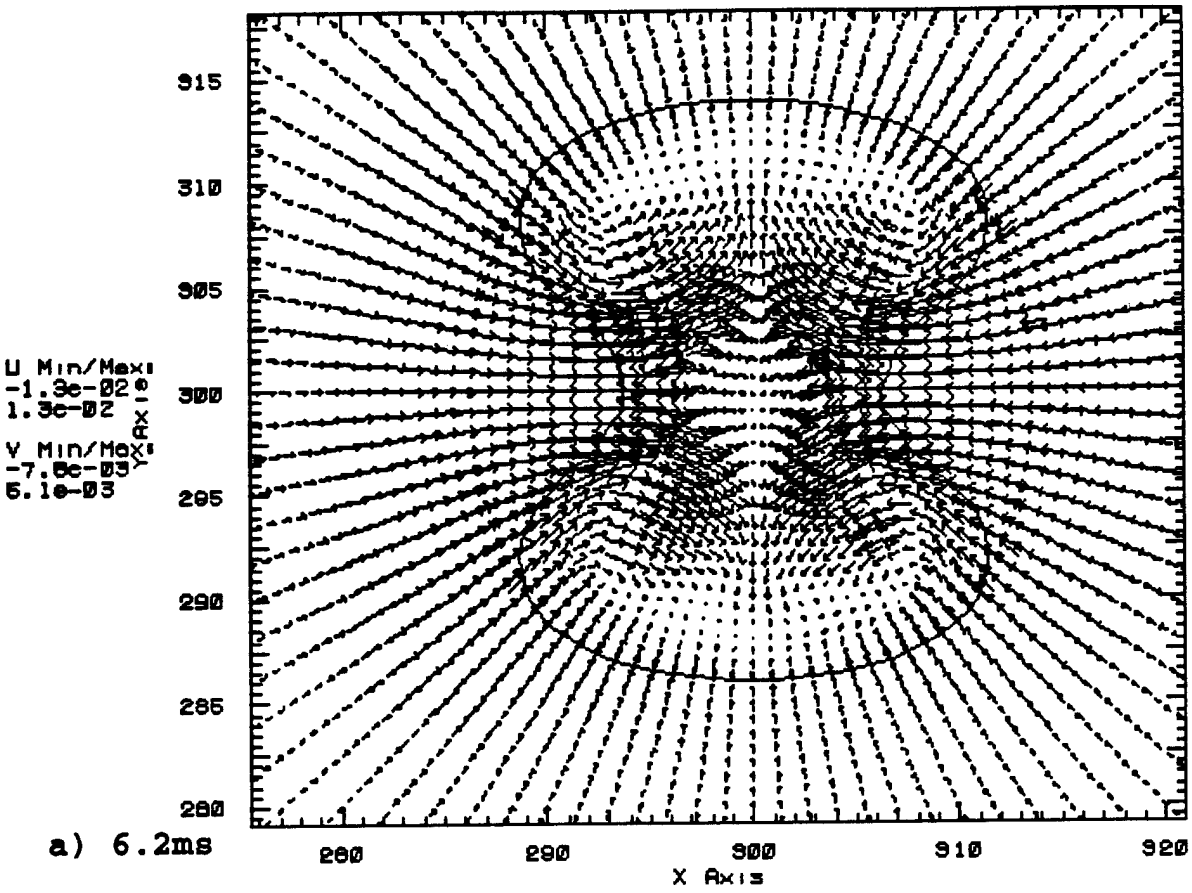
U Min/Max:
-1.3e-02
1.3e-02
V Min/Max:
-7.6e-03
6.1e-03
Y Axis
915
310
905
300
295
290
285
280
280
290
900
910
920
X Axis

a) 6.2ms

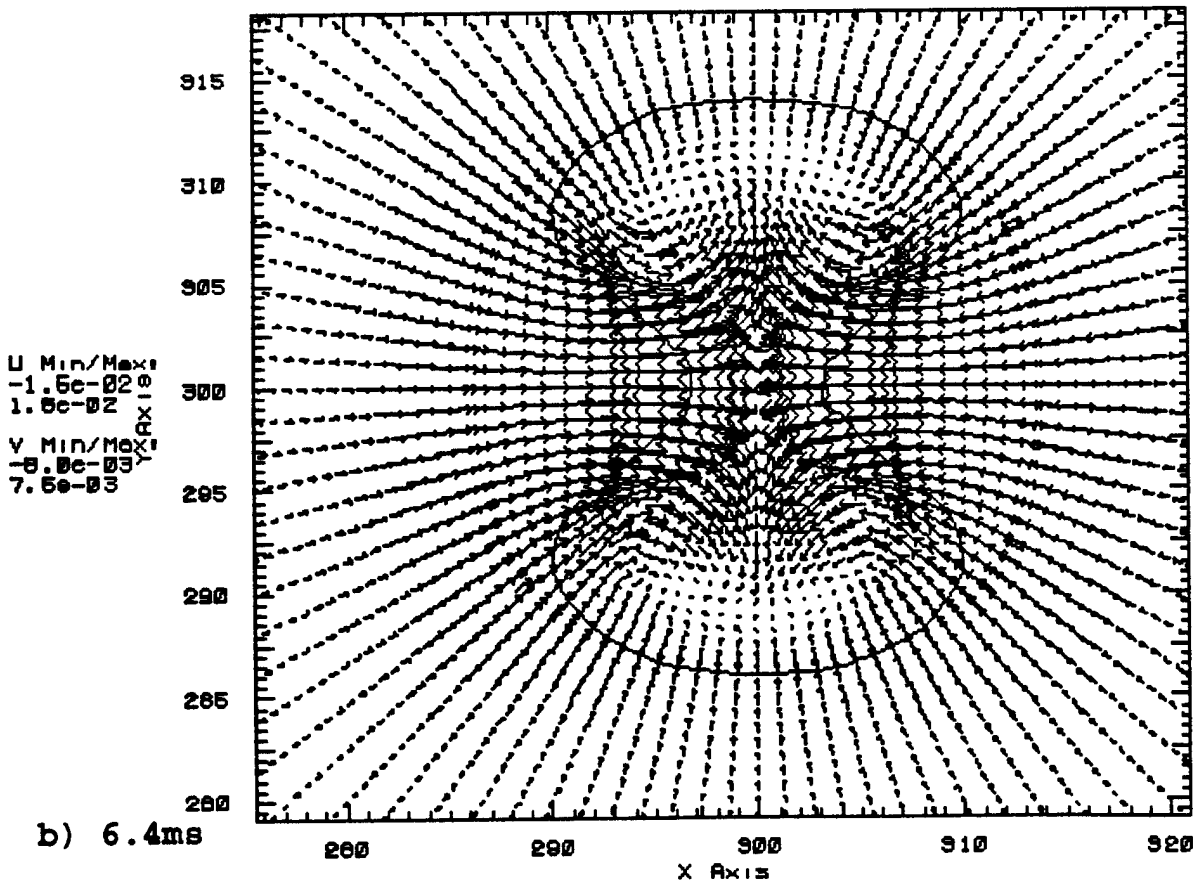
U Min/Max:
-1.5e-02
1.5e-02
V Min/Max:
-8.0e-03
7.6e-03
Y Axis
915
310
905
300
295
290
285
280
280
290
900
910
920
X Axis

b) 6.4ms

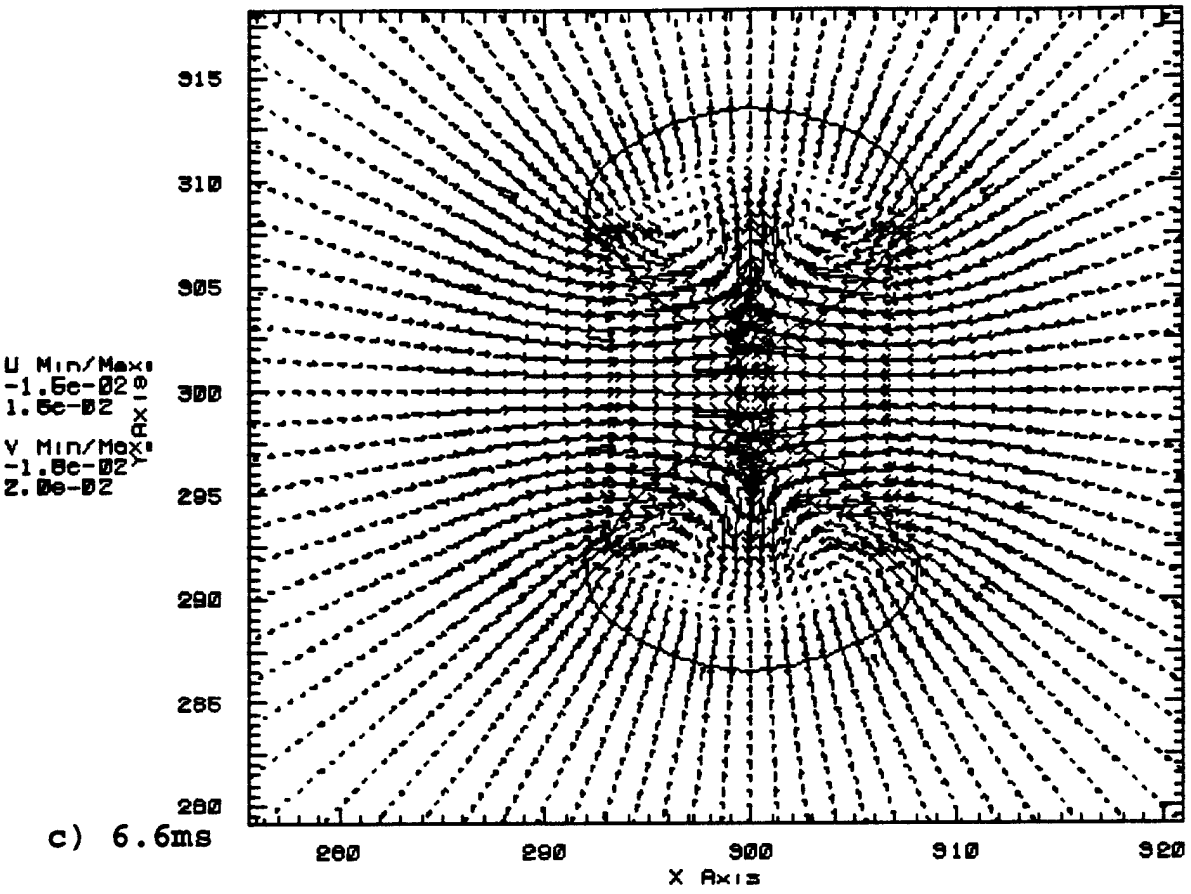
U Min/Max:
-1.5e-02
1.5e-02
V Min/Max:
-1.8e-02
2.0e-02
Y Axis
315
310
305
300
295
290
285
280
280
290
300
310
320
X Axis

c) 6.6ms

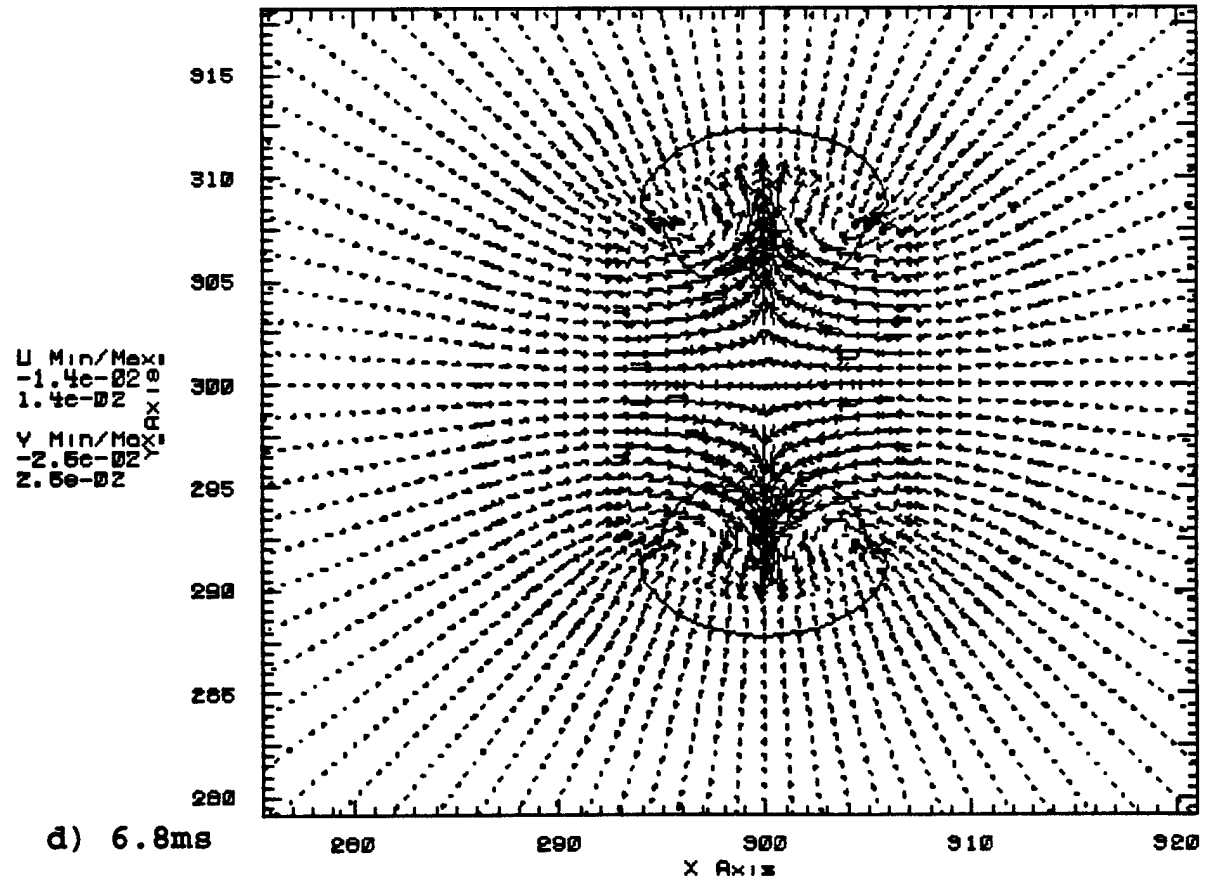
U Min/Max:
-1.4e-02
1.4e-02
V Min/Max:
-2.6e-02
2.6e-02
Y Axis
315
310
305
300
295
290
285
280
280
290
300
310
320
X Axis

d) 6.8ms

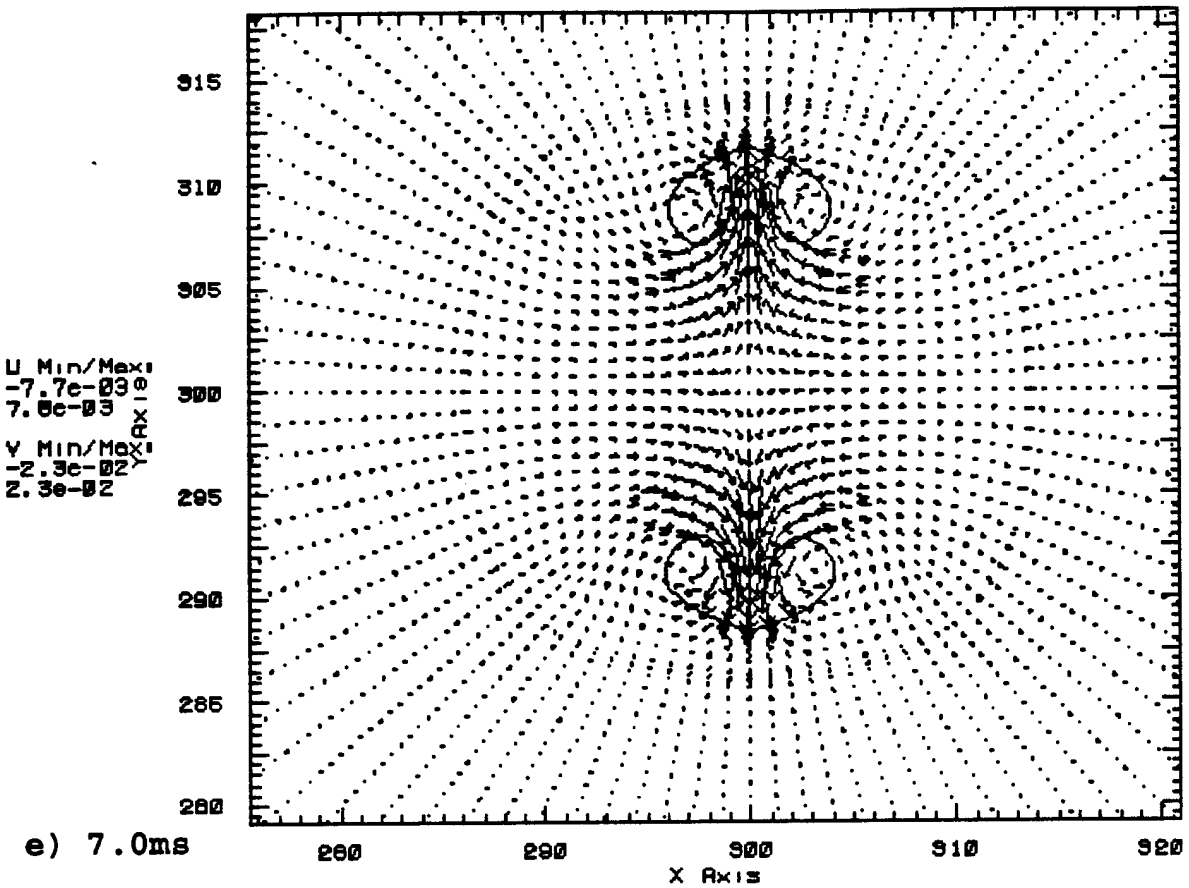


e) 7.0ms

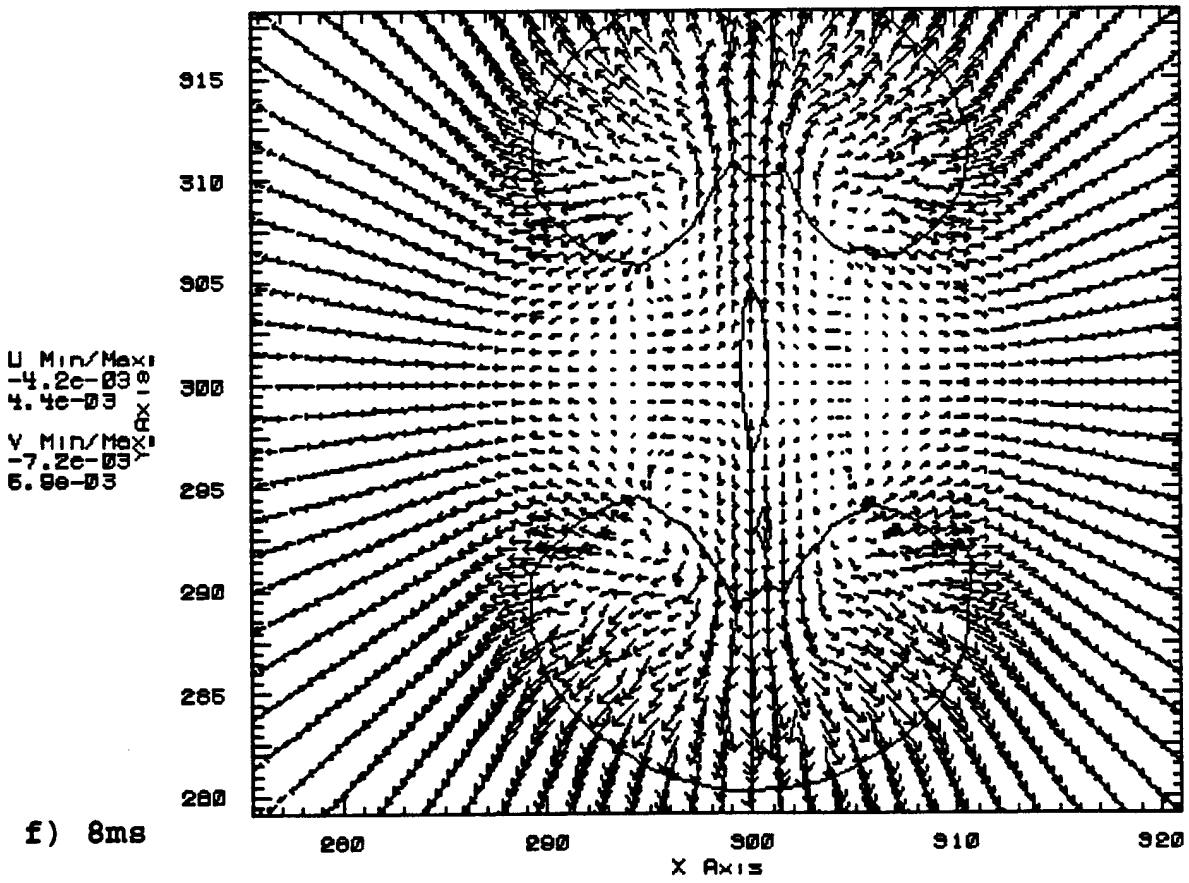


f) 8ms

Fig.34 Velocity vector field around the cord collpsing near the wall.a),&b) During collapse, c) Just before the jet formation, d) After jet formation and e)&f) During Rebound.(Plan View with wall at the bottom and in the plane of paper.)

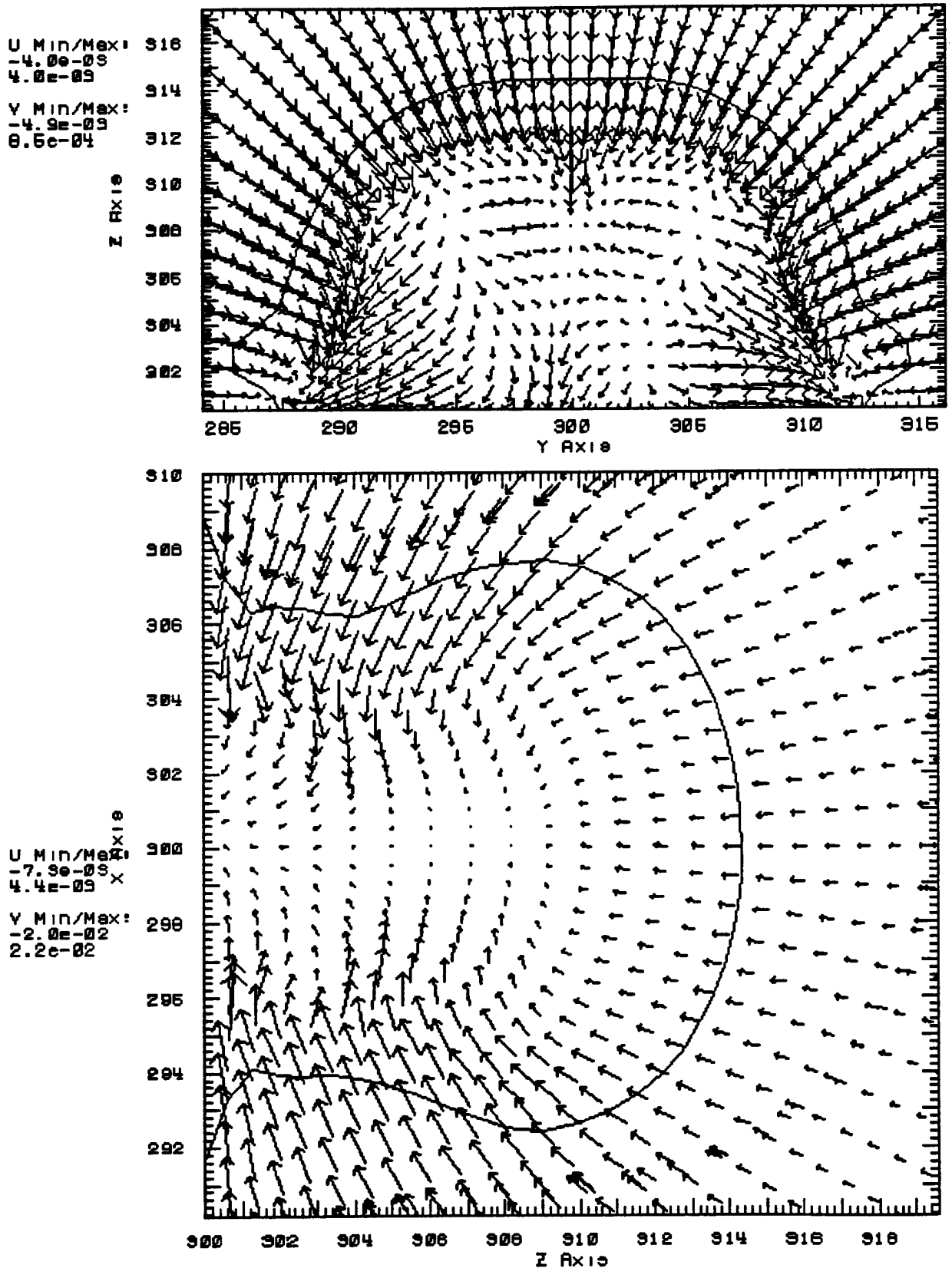


Fig.35 Different side views corresponding to Fig.34a. a) Slice along the cord with wall at the bottom and perpendicular to the plane of the paper and b) Slice along the axis of the cord with the wall towards the left and perpendicular to the plane of the paper.

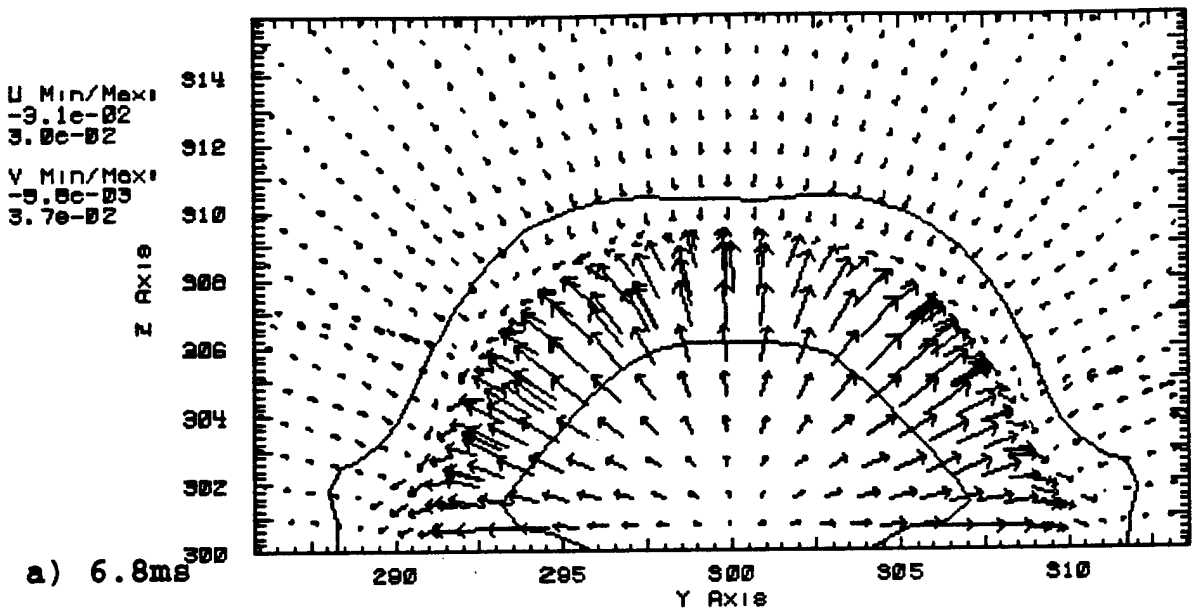


a) 6.8ms

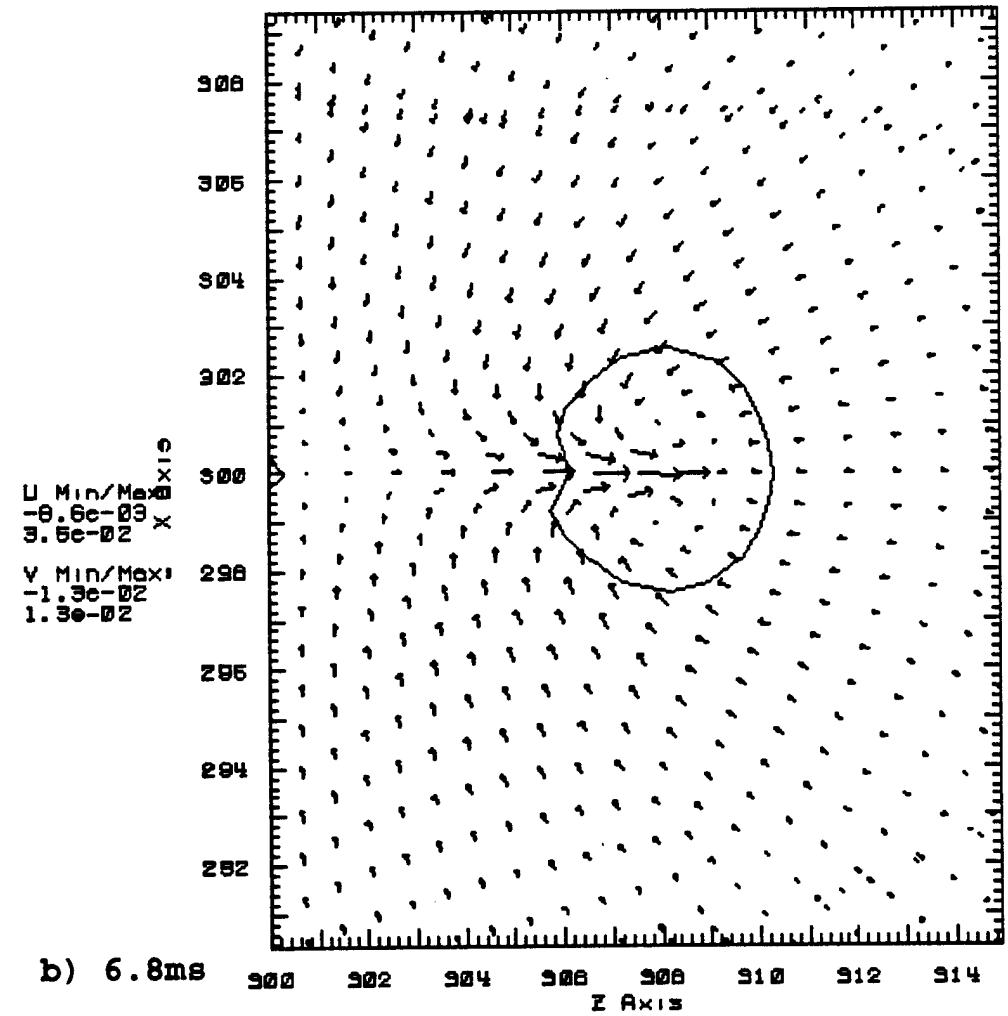


b) 6.8ms

Fig.35 Different side views corresponding to Fig.34d. a) Slice along the cord with wall at the bottom and perpendicular to the plane of the paper and b) Slice along the axis of the cord with the wall towards the left and perpendicular to the plane of the paper.

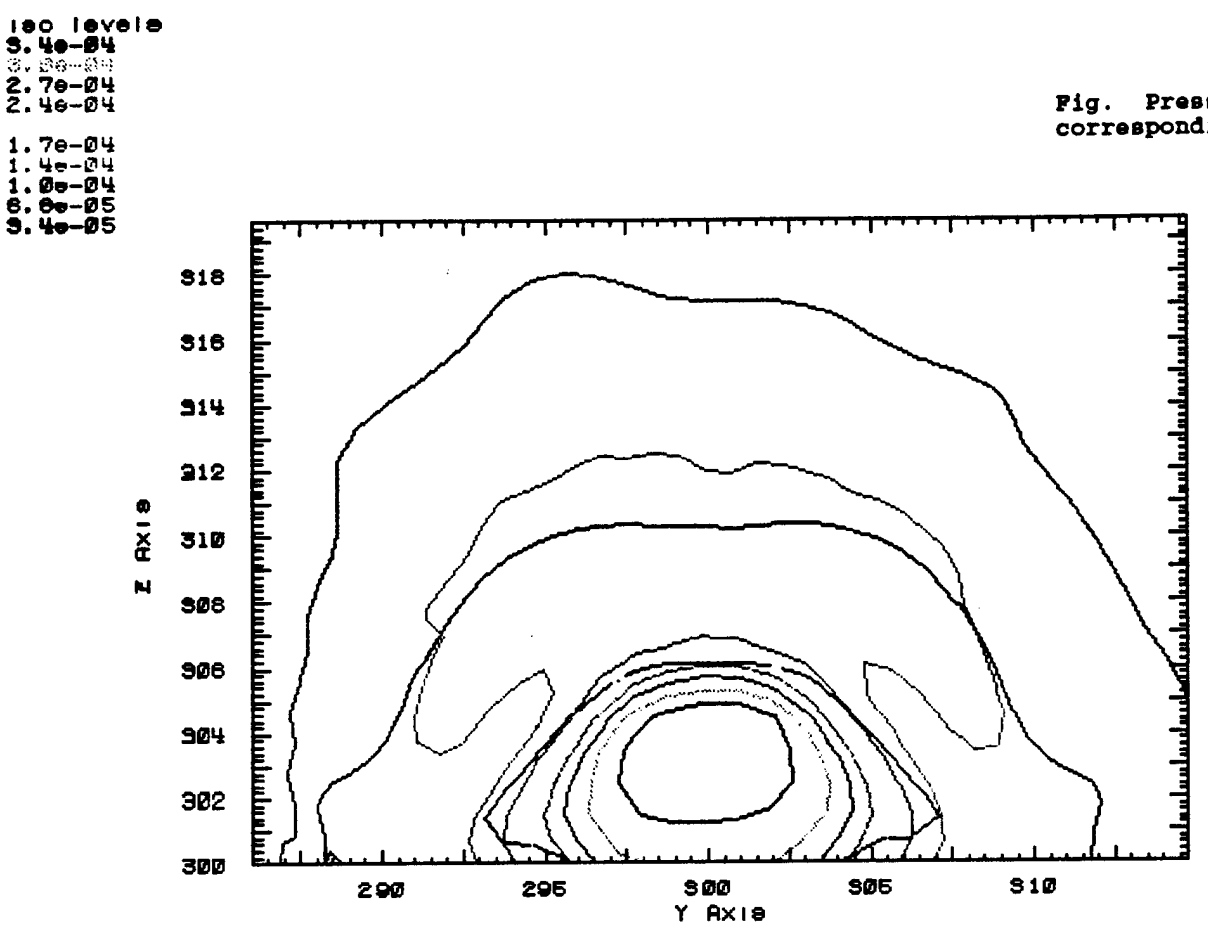


Fig. Pressure contours corresponding to Fig. 36a.

(a)

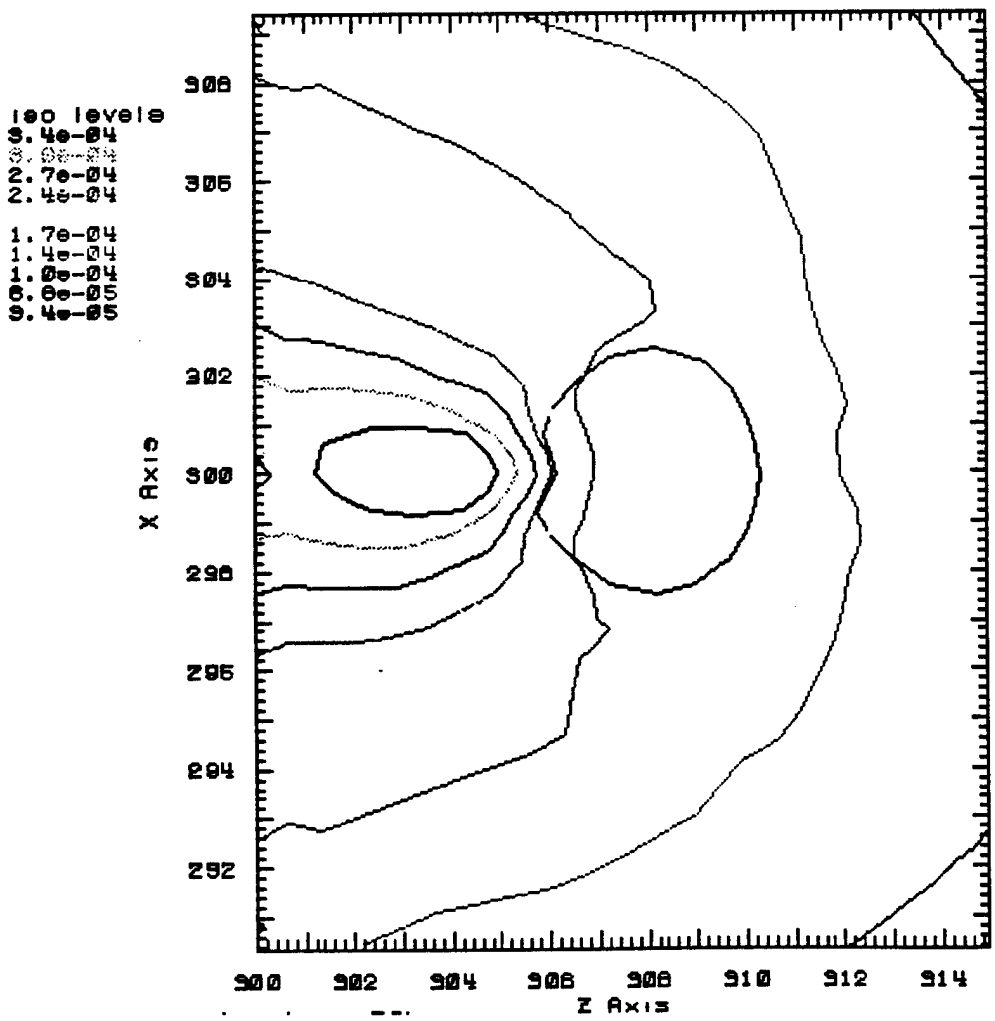


(b)

Figures 37

Fig. Pressure contours corresponding to Fig. 36b

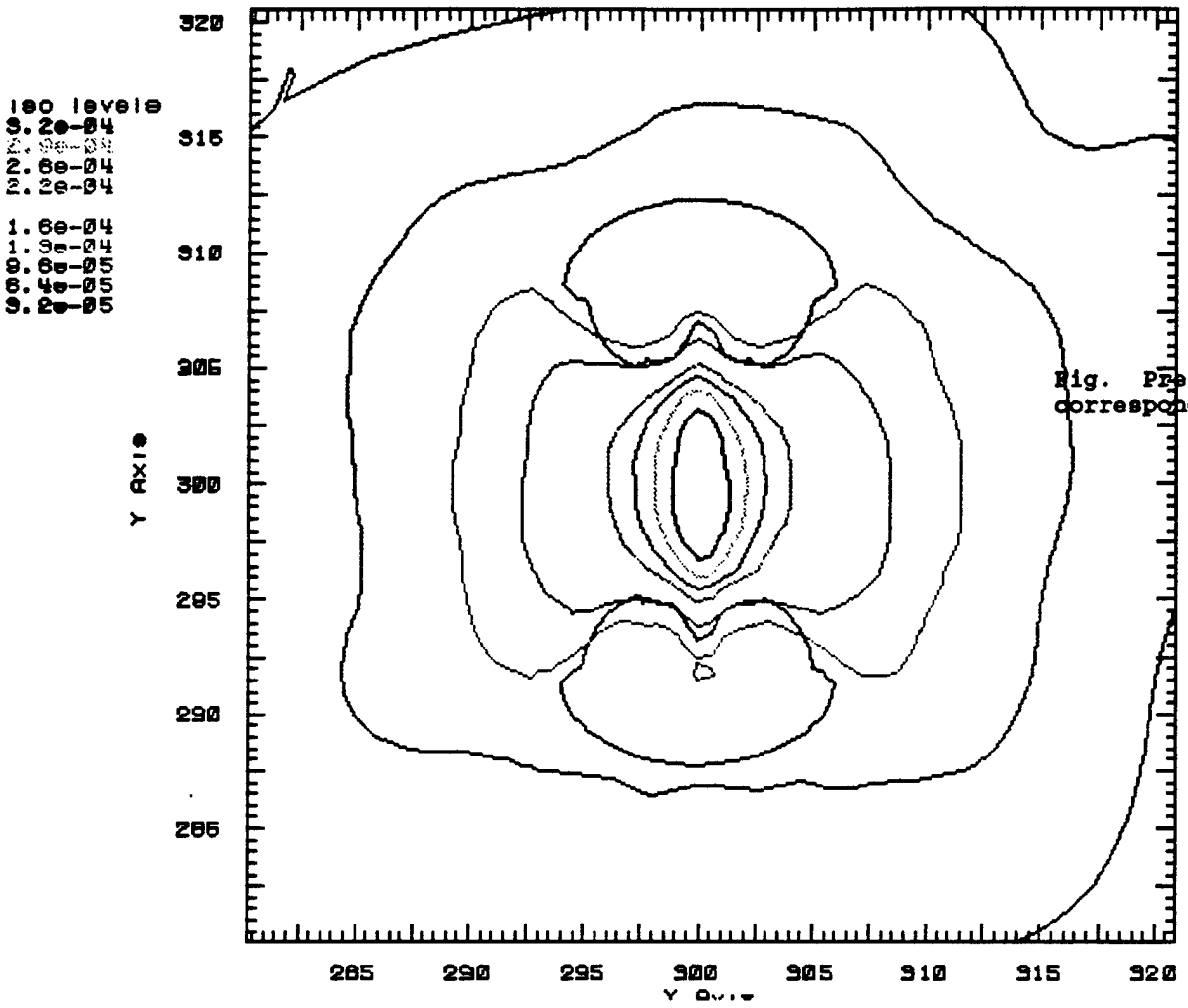


Figure 37 (c)

Fig. Pressure contours corresponding to Fig.34d

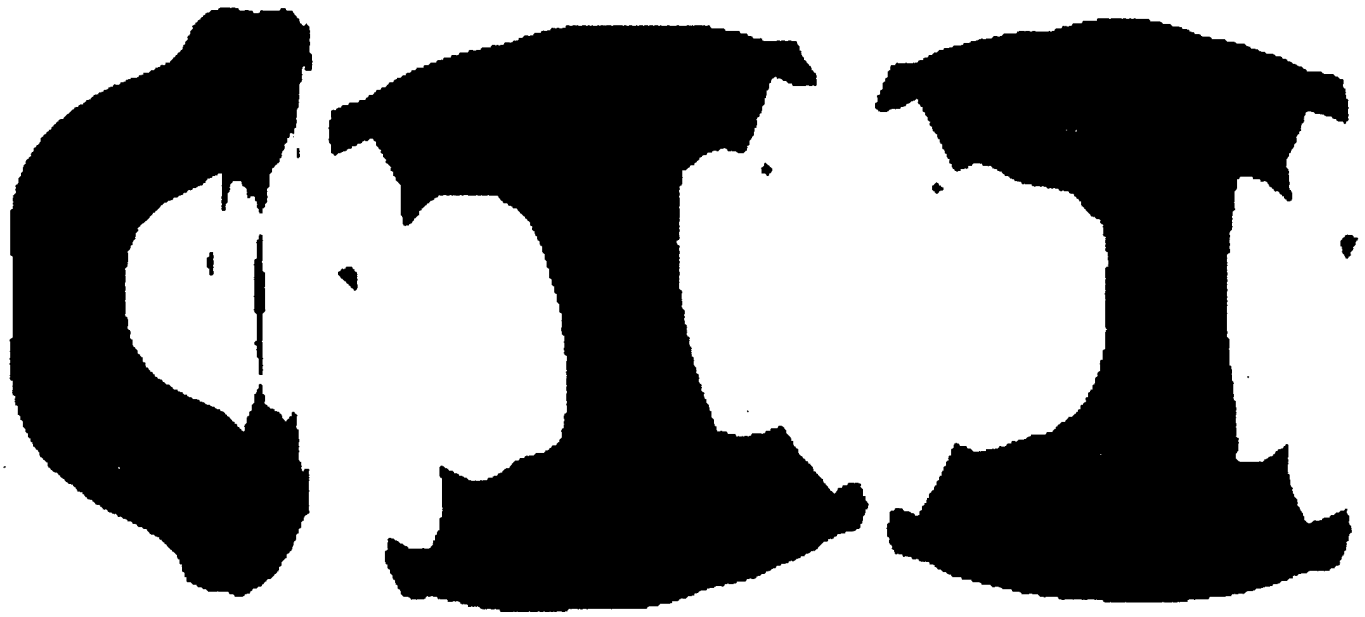

Fig.38 Different views of the bubble formed the explosive cord collapsing near a wall at the instant before the jet formation at 6.8ms after the explosion.

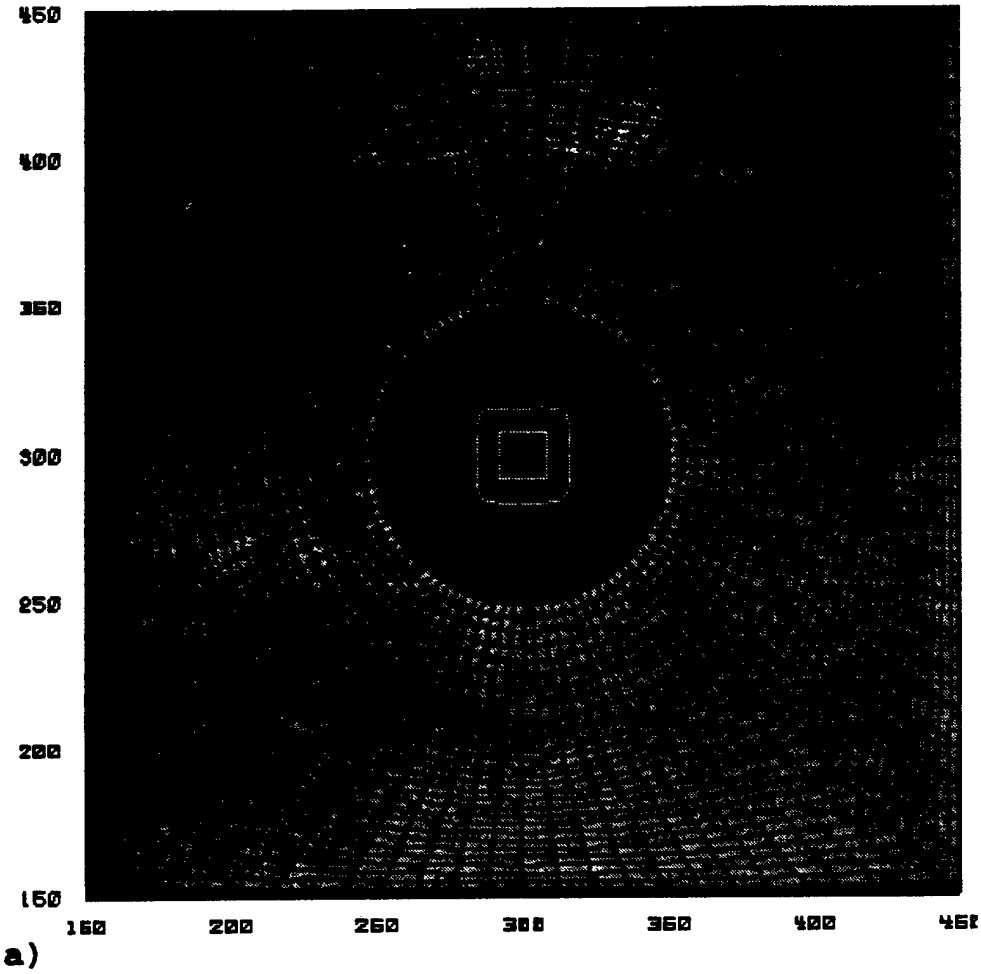


a)

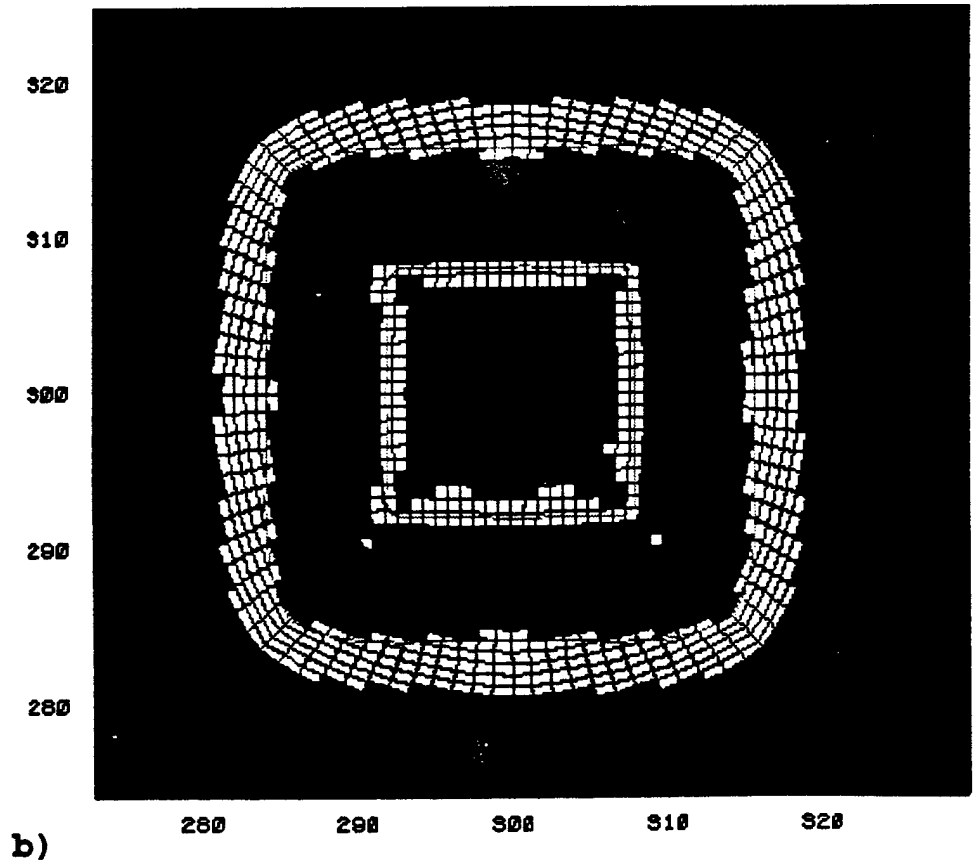


b)

Fig. 39: Figure showing the grid used in ALE3D square grid expl. runs. a) The View of the whole domain & b) View of the domain in the proximity of the explosive.

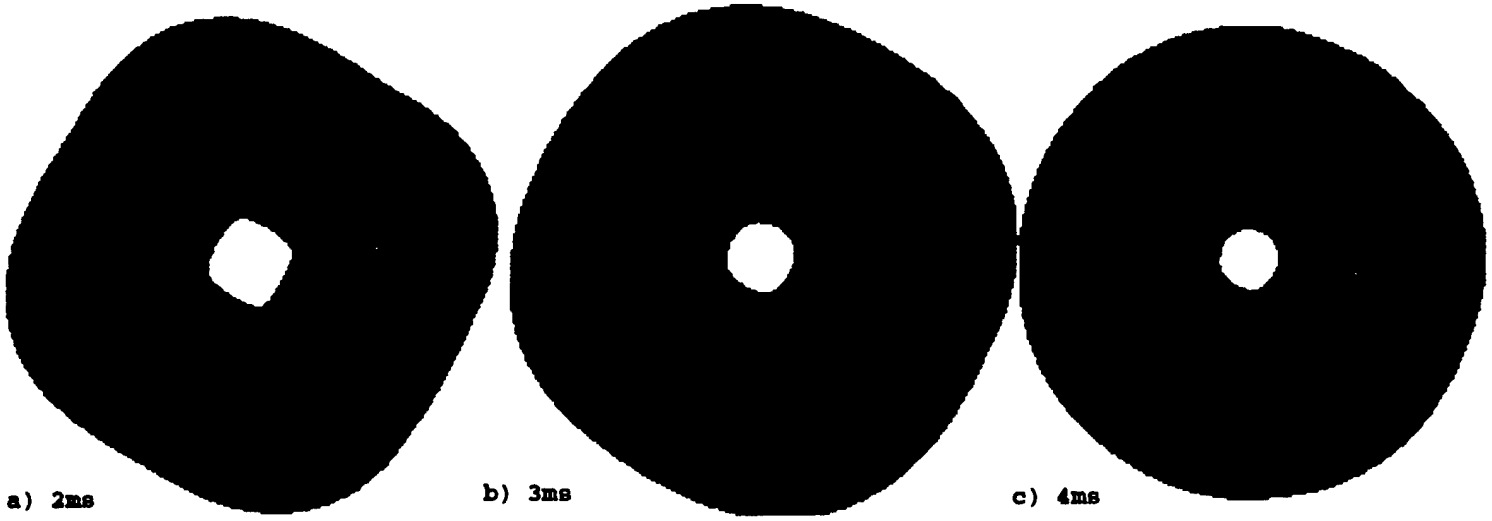


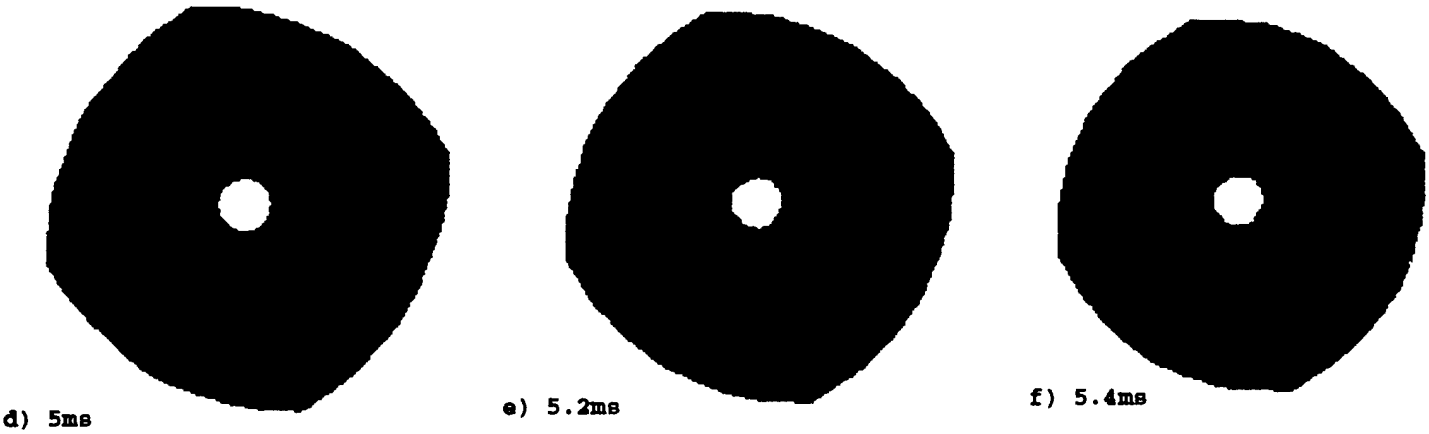


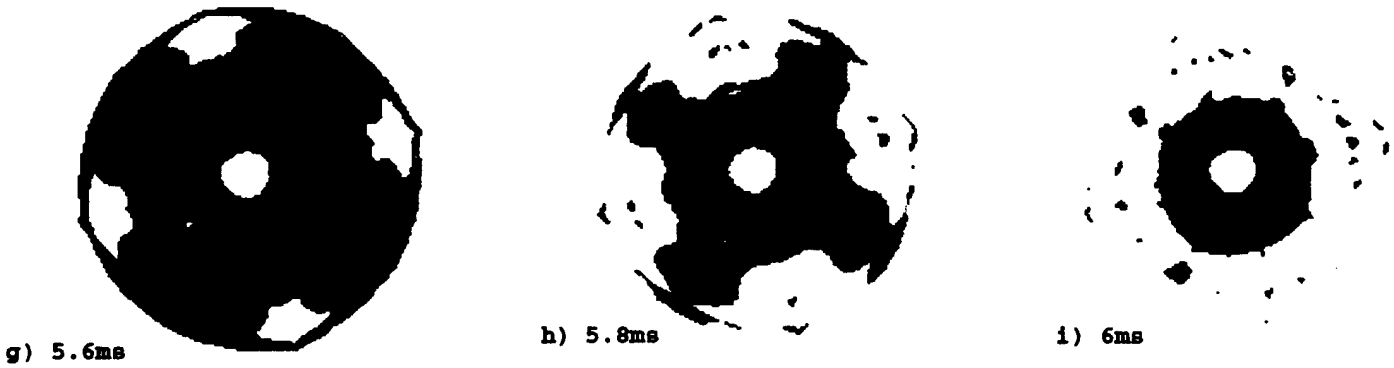


Fig.4D Time sequence of the bubble generated by a square explosive grid near a rigid wall.a) Before max., b) At max., c),d),e) & f) During collapse, g)&h) during the jet formation and i) after the jet formation.

a) Top view

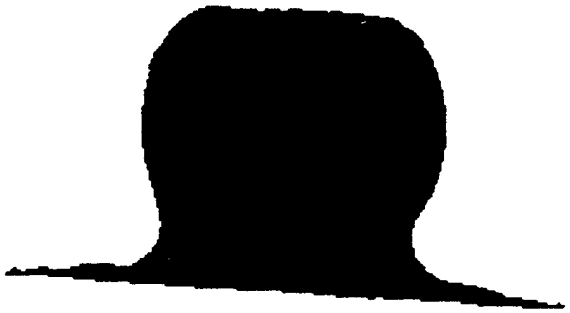

b) Side View

c) Isometric View

d) View from the wall

Fig.41 Different views of the Square grid generated bubble at time 5.8ms

a) Top view

b) Side View

c) Isometric View

d) View from the wall

Fig 42 Different views of the Square grid generated bubble at time 6ms

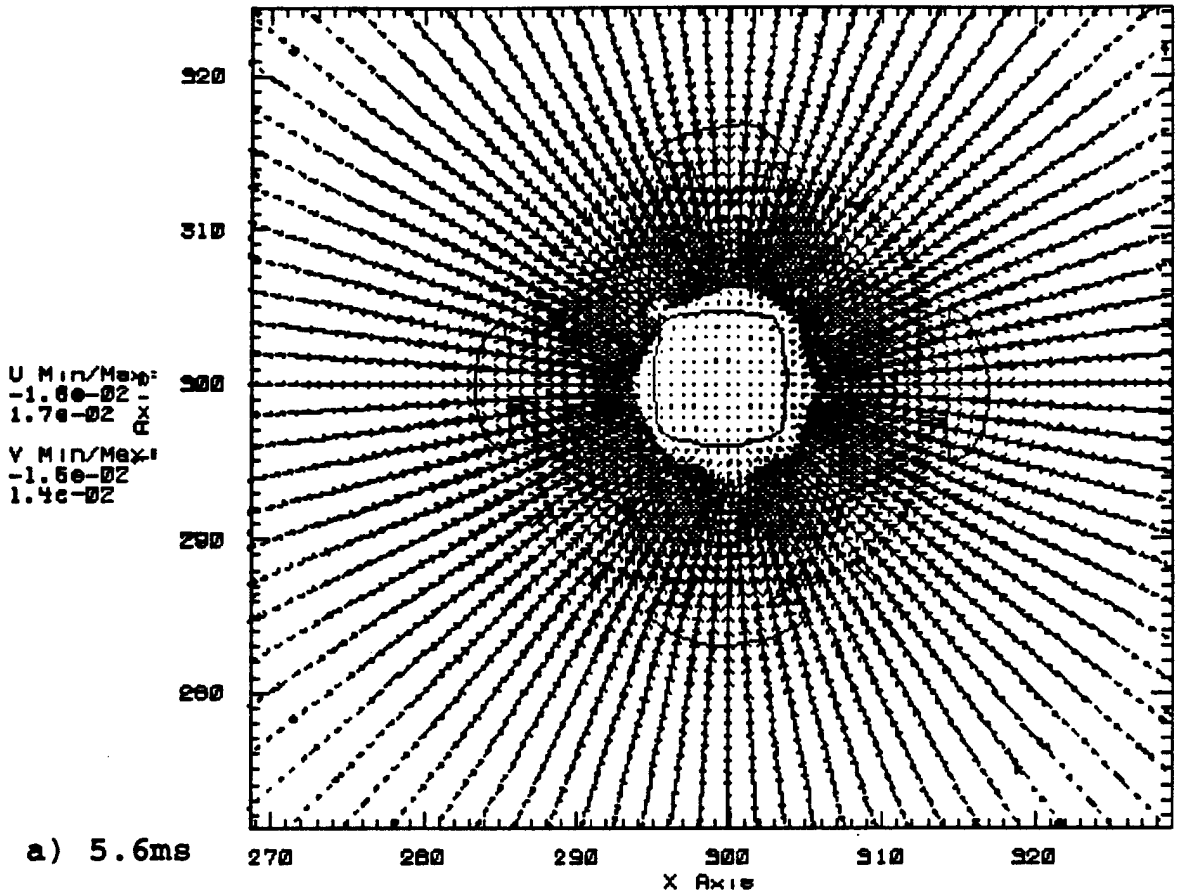
320
310
300
290
280
U Min/Max:
-1.6e-02
1.7e-02
V Min/Max:
-1.6e-02
1.4e-02
270
280
290
300
310
320
X Axis

a) 5.6ms

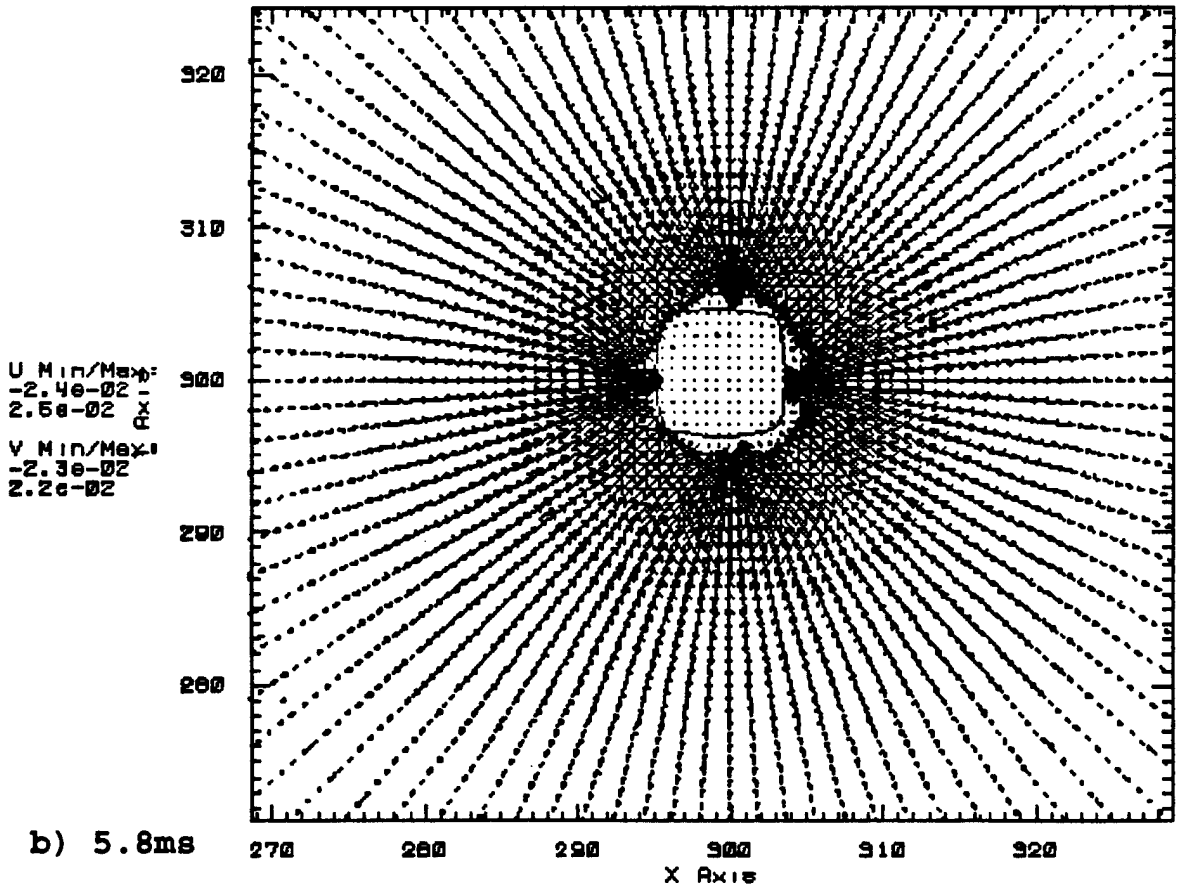
320
310
300
290
280
U Min/Max:
-2.4e-02
2.5e-02
V Min/Max:
-2.3e-02
2.2e-02
270
280
290
300
310
320
X Axis

b) 5.8ms

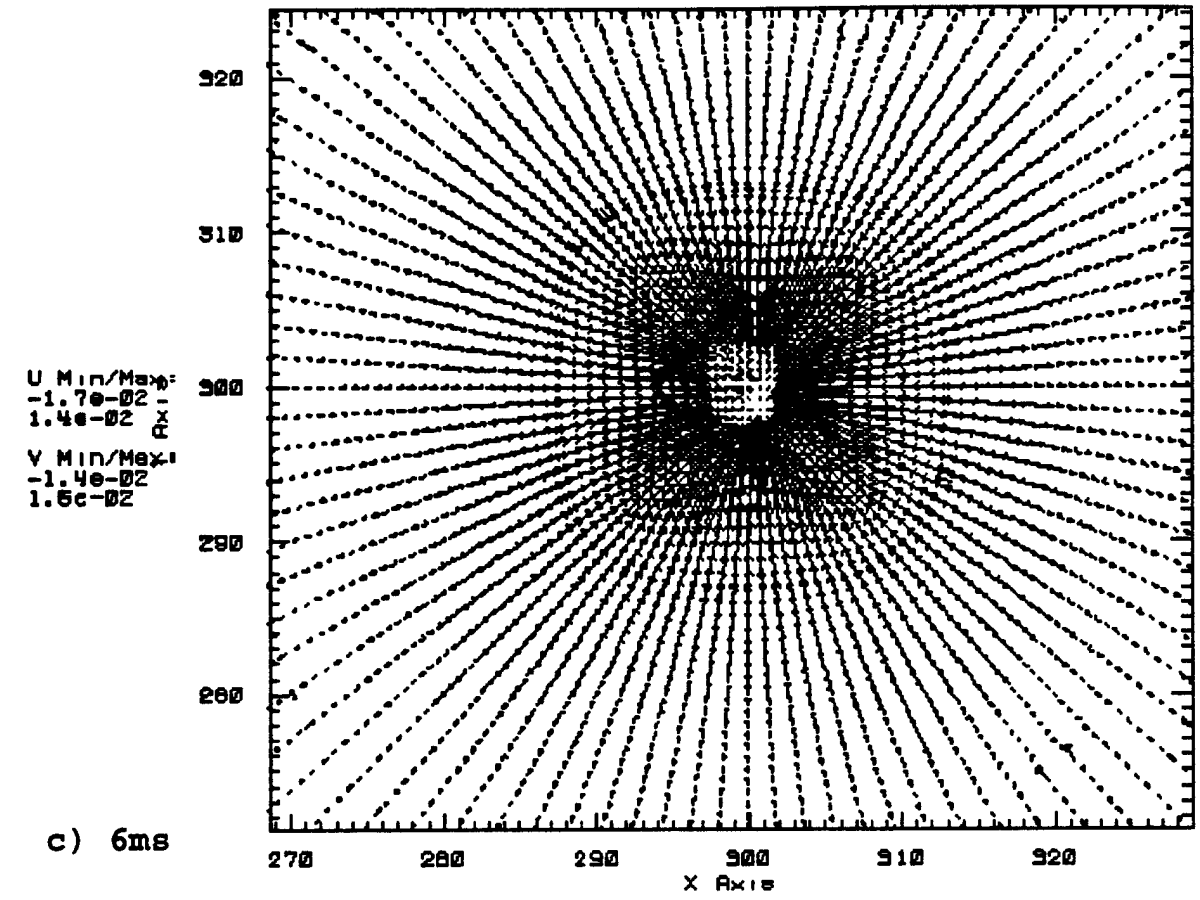
U Min/Max:
-1.7e-02
1.4e-02
V Min/Max:
-1.4e-02
1.6e-02
320
310
300
290
280
270
280
290
300
310
320
X Axis

c) 6ms

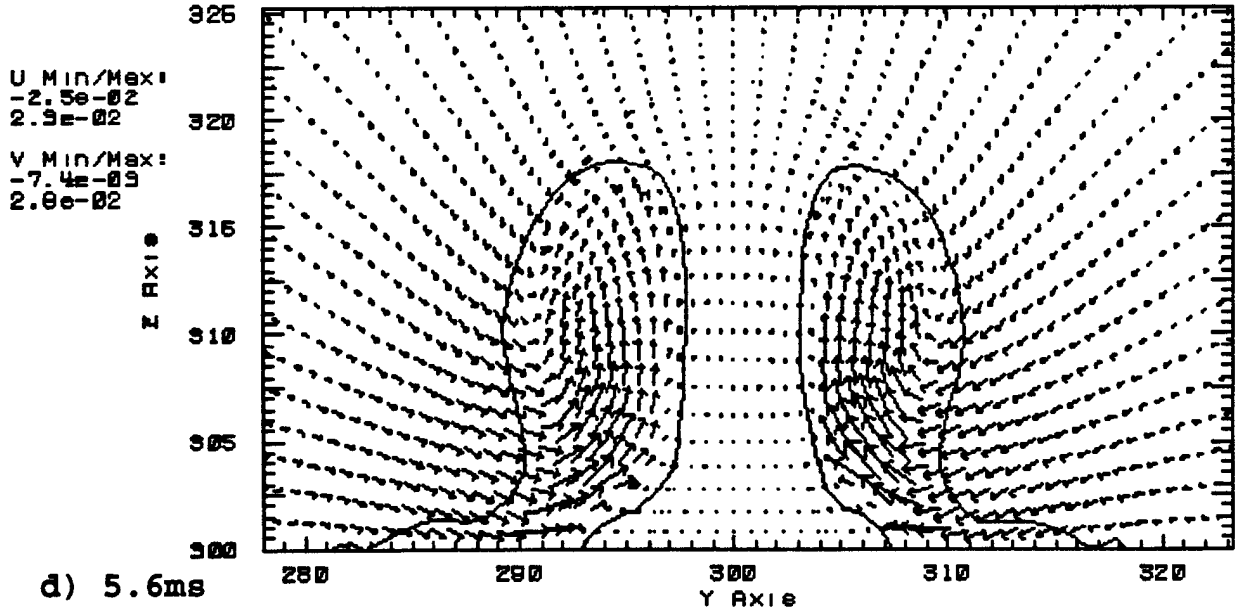
U Min/Max:
-2.5e-02
2.9e-02
V Min/Max:
-7.4e-03
2.8e-02
325
320
315
310
305
300
280
290
300
310
320
Y Axis
Z Axis

d) 5.6ms

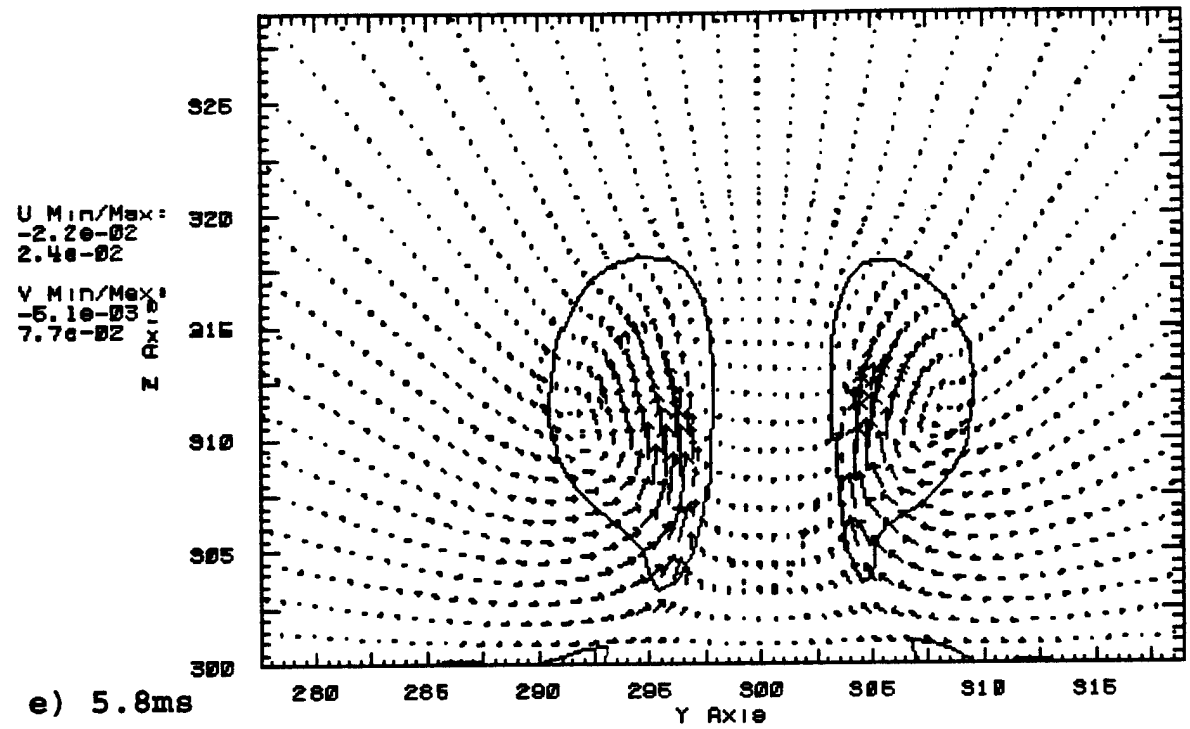


e) 5.8ms

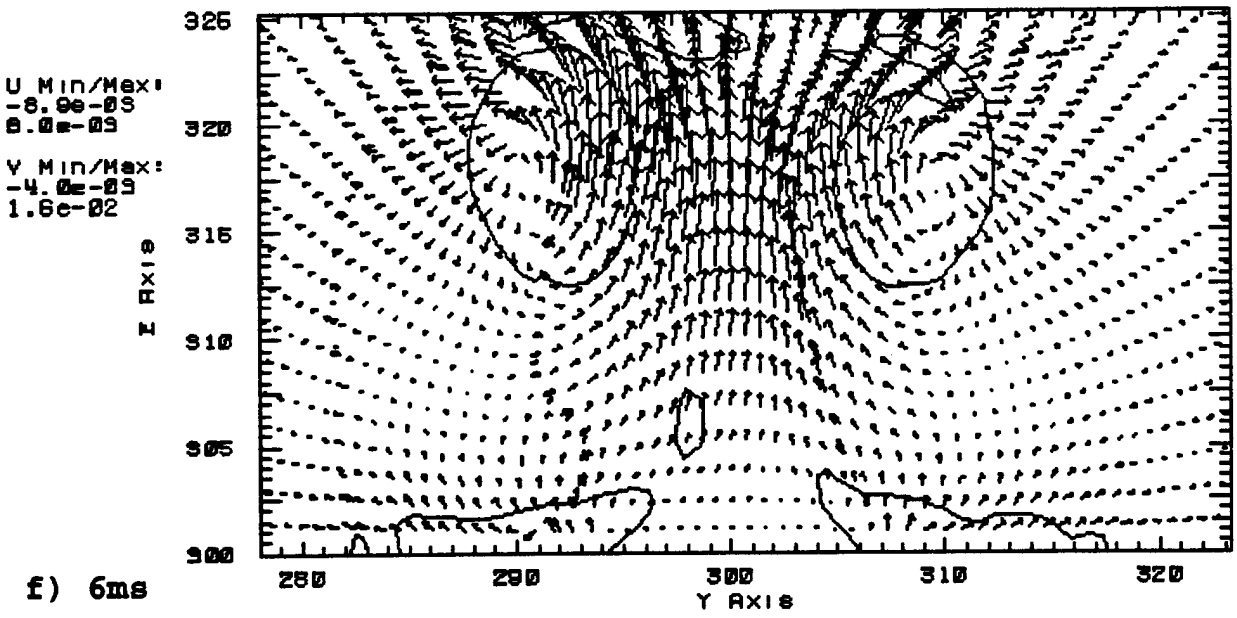


f) 6ms

Fig. 45 Velocity Vectors around a square grid explosive bubble collapsing near a rigid wall. a),b) and c) are top views at different instances and d),e) and f) are the corresponding side views.

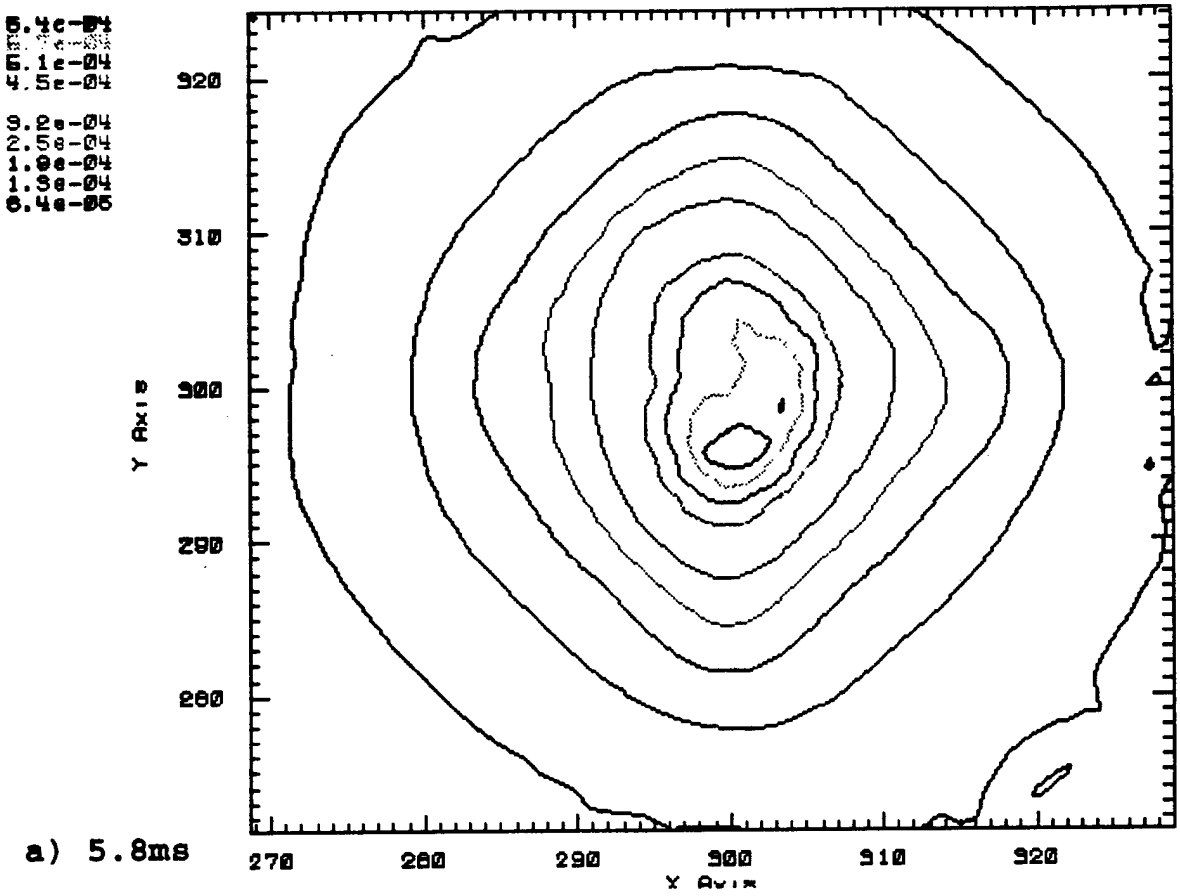


a) 5.8ms

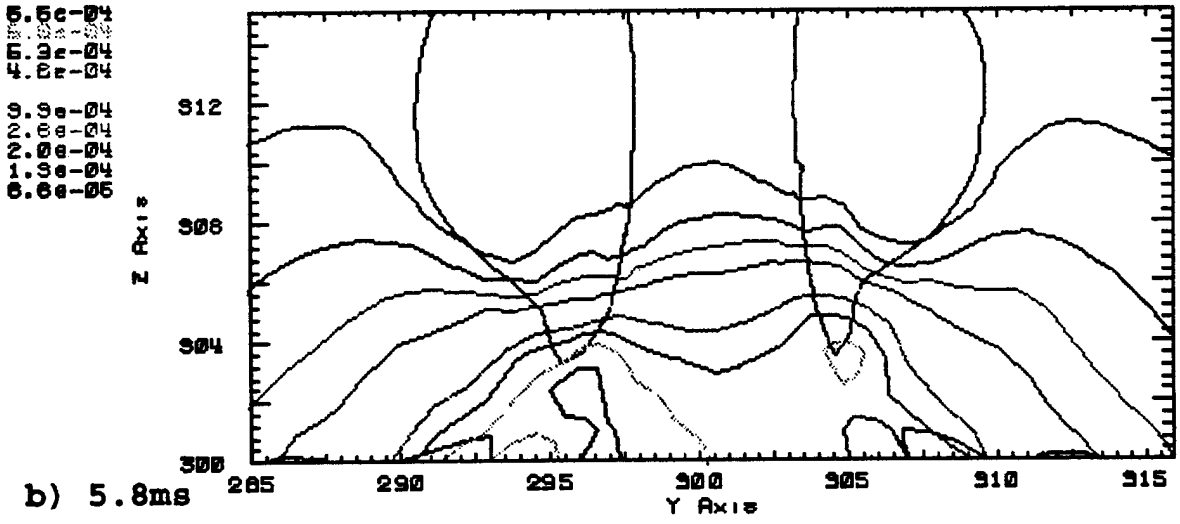


b) 5.8ms

Fig.44 Pressure contours corresponding to the a) Fig.43b & b) Fig.43c

# APPENDIX A

## Underwater Explosions Near Exposed And Buried Rigid Surfaces

# Underwater Explosions near Exposed and Buried Rigid Surface

**S. Menon and M. Lal**
**School of Aerospace Engineering**
**Georgia Institute of Technology**
**Atlanta, Georgia 30332-0150**

## Introduction

Vapor and gas bubble dynamics are of great practical interest in the prediction and prevention of cavitation erosion of marine propeller and turbine blades. It is well known that when an explosion bubble collapses near a rigid surface, a strong re-entrant water jet is directed towards the wall. The impact of this jet on the plate results in impact pressure that can be much larger than the explosion pressure. This impact on the surface can cause structural damage especially when the explosion energy (and hence the bubble size) is large. Both experimental and numerical studies have been carried out in the past to study the complex flow fields associated with such explosions. Detailed reviews have summarized many of the pertinent results obtained in past studies. Experimental studies are too numerous to list completely; however, most studies in the past focused on cavitation (small) bubbles. Many studies have focused on explosions near structures. See references cited and the discussion in the main text (and therefore, not included here). However, in most of these studies, the primary focus has been on small bubbles.

Recently, a series of experiments were carried out to investigate underwater explosions in shallow water (1 atmosphere ambient pressure) to understand the dynamics of bubble-wall interaction in such flows and to investigate feasibility of targeting and destroying mines buried in beaches. In this configuration (shown in Fig. 1), the free water surface is close enough to the bubble-wall interaction region to play a role in modifying the dynamics of the bubble collapse. The free surface provides a constant pressure boundary in close proximity to the wall. It is known that the bubble moves away from the free surface and a reentrant jet is formed which pierces the bubble in the direction of its migration . Therefore, the presence of the free surface above the bubble collapse region is likely to increase the net impact pressure on the wall.

Another issue that was investigated is the behavior of the impact process when the rigid surface is buried below a layer of sand as would be the case for buried mines. This study was motivated by some earlier observations that when the rigid flat plate was buried below a layer of clay, the impact pressure felt on the plate was still significant. On the

other hand, when a thick layer of sand was used (without the presence of the rigid plate), no significant impact process was observed. To resolve these issues, experiments were carried out to investigate what parameters control the impact process. Obviously, the distance of the bubble from the plate and the sand layer thickness are two important parameters for given explosion. Scaling analysis of this data could shed light on the interaction process when the upper layer is made up of loosely packed material that has a tendency to deform under pressure. Some interesting results have been obtained and summarized in this communication.

**Results and Discussion**

Underwater explosion experiments near a solid boundary were conducted by exploding fuel (Carbon Monoxide) and oxidizer (Oxygen) mixture contained in a glass globe of average volume of 90 ml (6.35 cm diameter) over a steel plate (shown in Fig. 1). The premixed fuel-air stoichiometric mixture is ignited by an electric spark and the explosion takes place at a constant volume until the globe bursts. A pressure transducer is placed in the bubble holder to record the explosion pressure and the pressure in the bubble during expansion/collapse process. Since the experiments were conducted in a laboratory shallow water setup using a gaseous explosive mixture, the bubbles are relatively smaller (although much larger than cavitation bubbles) than those observed in deep sea explosions. To determine the impact pressure, eight KISTLER pressure transducers were mounted on the plate, as shown in Fig. 2, to obtain a surface distribution of the impact pressure field. Optical record of the bubble wall interaction was also obtained using a CCD enhanced digital video camera. Since the viewable picture size is inversely proportional to the recording speed of the camera, the maximum speed was limited to 2000 frames per second in order to obtain a full screen image.

Parameteric studies of the impact process was carried out by systematically varying the distance between the globe and the plate to investigate the effect of solid wall location relative to the explosion. The layer thickness of the sand above the instrumented plate was also varied to determine how the impact pressure is effected by the porous material above the plate. All the experimental data have not been fully analyzed as yet. However, the results obtained so far do suggest some interesting trends and also provide an estimate of the effect of the sand layer on the impact pressure. For all studies discussed here, the

explosion strength and the initial bubble size were held constant. Only characteristic results of this study are summarized here.

Bubble-Wall Interactions

The collapse process near the wall (with and without the sand layer) was dynamically similar. The bubble expands subsequent to the explosion, however, the extent of the expansion (for a free field explosion, these bubbles were found to expand up to three times the initial diameter) depends on the relative position of the free surface and the rigid plate. Figure 3 shows a time sequence of the bubble expansion and collapse for a given set of parameters. For this case the bubble does not fully expand as in the free field case due to the presence of the wall. By the time the bubble has expanded, it already is interacting with the plate. The collapse of the bubble, the formation and the impingement of the water jet on the plate can be seen in these figures. The time period for the expansion/collapse process is found to be 19 ms (for this configuration), while it is around 15 ms in free field configuration. Therefore, as the bubble is brought close to the surface, an increase in the time period of oscillation is observed. If the bubble is brought further close to the surface beyond the optimum distance (defined below), the time period reduces slightly to 18 ms.

The pressure data recorded on the plate was found to be a strong function of the initial location of the bubble relative to the plate. The impact pressure recorded by the eight pressure transducers were not the same suggesting that the impact jet is highly coherent and focused. Figures 4a-d show the pressure data from the plug transducer (Fig. 4a) and three of the eight transducers (4b-d; see Fig. 2 for their locations). It can be seen that the transducer no. 8 (which is located right below the bubble center) records the highest impact pressure while the transducers away from this location records much lower pressures. This behavior was seen for all cases studied so far and suggests that the impinging water jet is highly focused in a narrow jet.

The impact pressure recorded on the plate for all the test cases are summarized in Figs. 5a and 5b. Figure 5a shows that impact pressure (normalized by the explosion pressure) measured by the transducer No. 8 as a function of the initial distance of the bulb above the plate (normalized by the initial bulb size). Figure 5b shows the impact pressure data from the other two transducers (shown in Fig. 4c, d). As the bulb is brought closer to the plate, up to a certain distance, an increase in the impact pressure is recorded by all

transducers. If the distance between the bulb and the plate is further reduced beyond the certain distance, a reduction in the impact pressure is noted. The optimum distance determined from the current data set appears to be $d/R_o = 2$; where d is the distance between the bulb and plate, and $R_o$ is the initial globe radius. The impact pressure ratio for this configuration was $P_{Imp}/P_o = 4.19$. Here, $P_{Imp}$ is the impact pressure on the plate at the center and $P_o$ is the explosion pressure inside the bubble.

It is worthwhile noting here that the recent numerical studies described in the main text also reproduced the impact process (see Figs. 29). It was determined that there is an optimum location for peak impact as seen in the experiments; however, the optimum location was found to be smaller than that seen in these experiments. There are many artifacts in the experiment such as, the presence of the pressure transducer and the igniter in the bulb holder, the presence of the glass bulb and the formation of glass fragments after the explosion. These features were not included in the numerical studies. However, the relative agreement between the experimental and numerical data do suggest that the present experiments are dynamically correct.

Additional data are still being analyzed. Numerical studies for these cases and also for realistic deep sea explosions near rigid surfaces are planned to determine how the impact pressure scales with the parameters of this problem. These results will be reported later.

Bubble-Sand-Wall Interactions

Experiments were also conducted to simulate underwater explosion over a buried surface near a beach by covering the plate with varying depths of sand on the top. The typical parameters are identified in Fig. 1. The bubble collapse process optically obtained for this case is shown in Fig. 6. The bubble is once again attracted towards the plate and a reentrant jet is formed in the bubble in the direction of its migration. It can be seen from this figure that the bulb is almost touching the sand. The effect of covering the plate with sand is to reduce the impact pressure on the plate. Figure 7 shows the impact pressure at the center of the plate for various sand depths. When the plate is covered with the sand while maintaining the same distance between the plate and the bulb, a reduction in the impact pressure at the center of the plate is observed. When the sand depth is further increased so as to bring the bulb closer to the sand, a partial recovery of the impact pressure occurs as shown in Fig. 7.

In order to simulate the explosion near a beach and to investigate the effect of the proximity of the free surface, the water depth, $d_w$, was lowered. Since water free surface is known to repel the bubble, the free surface should aid in the impact process. This was confirmed in the experiments. Figure 8 shows the impact pressure on the plate for cases with sand covering as a function of varying water depth. A lower water depth increases the impact pressure and decreases the time period of oscillation. The time period of oscillation of the bubble shown in Fig. 6 is about 16 ms. When the water depth is decreased for this experiment such that the bulb center is only about 10 cm below the free surface, the period of oscillation reduces to 14 ms.

Other studies for varying sand depths showed qualitatively similar results. In some cases, when the bulb was placed much above the plate, the impact process is completely inhibited and in some cases, the bubble collapse occurred after multiple oscillations. Further analysis of this data will be carried out and reported in the near future.

## Conclusions

The results obtained so far suggest that the impact pressure resulting from the impinging water jet can be more than 4 times the explosion pressure for the laboratory test cases. Furthermore, the analyses of the pressure distribution on the plate show that the peak impact is felt only in a narrow region right below the center of the bubble. Further away from the central region the peak pressure felt on the plate is smaller by an order of magnitude. This clearly shows that the impinging jet is highly focused and does not spread at all. The region where peak impact is felt appears to be smaller than the radius of the initial bubble size.

Studies using a layer of sand above the plate showed that both the locations of the initial bubble and the sand layer thickness control the pressure impact process. In general, the peak impact pressure recorded on the buried plate is lower than the exposed plate case. However, the reduction of the impact pressure by the damping effect of the sand can be alleviated by bringing the bubble closer to the surface. The effect of free surface above the interaction zone was to increase the impact pressure consistent with the notion that the free surface repels the bubble.

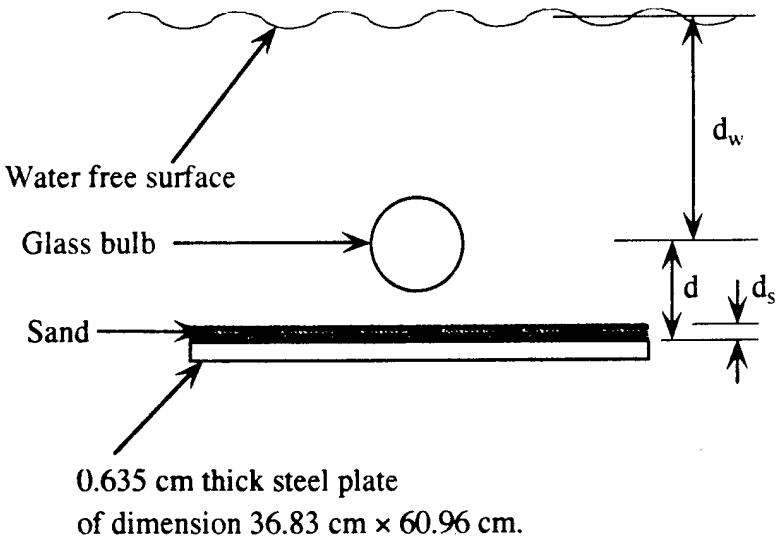


**Fig. 1. Experimental setup for simulating explosion near an exposed or buried object. For exposed object, $d_s = 0$.**

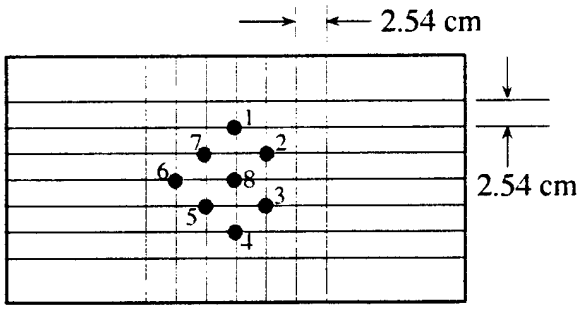


**Fig. 2. Layout of pressure transducers on the plate**

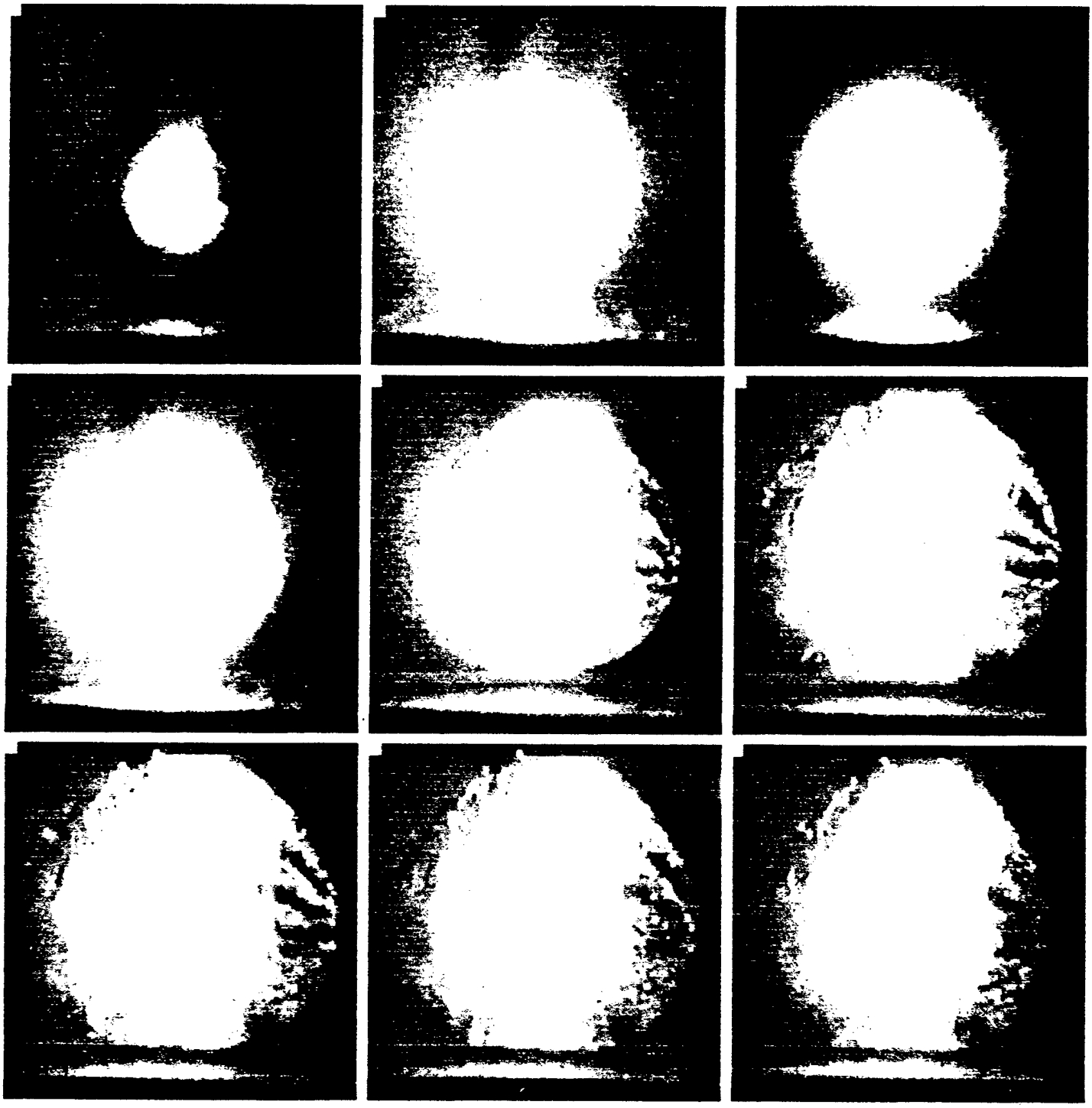

**Fig. 3. Time sequence of bubble collapse near an exposed plate for $d/R_0 = 2$.**

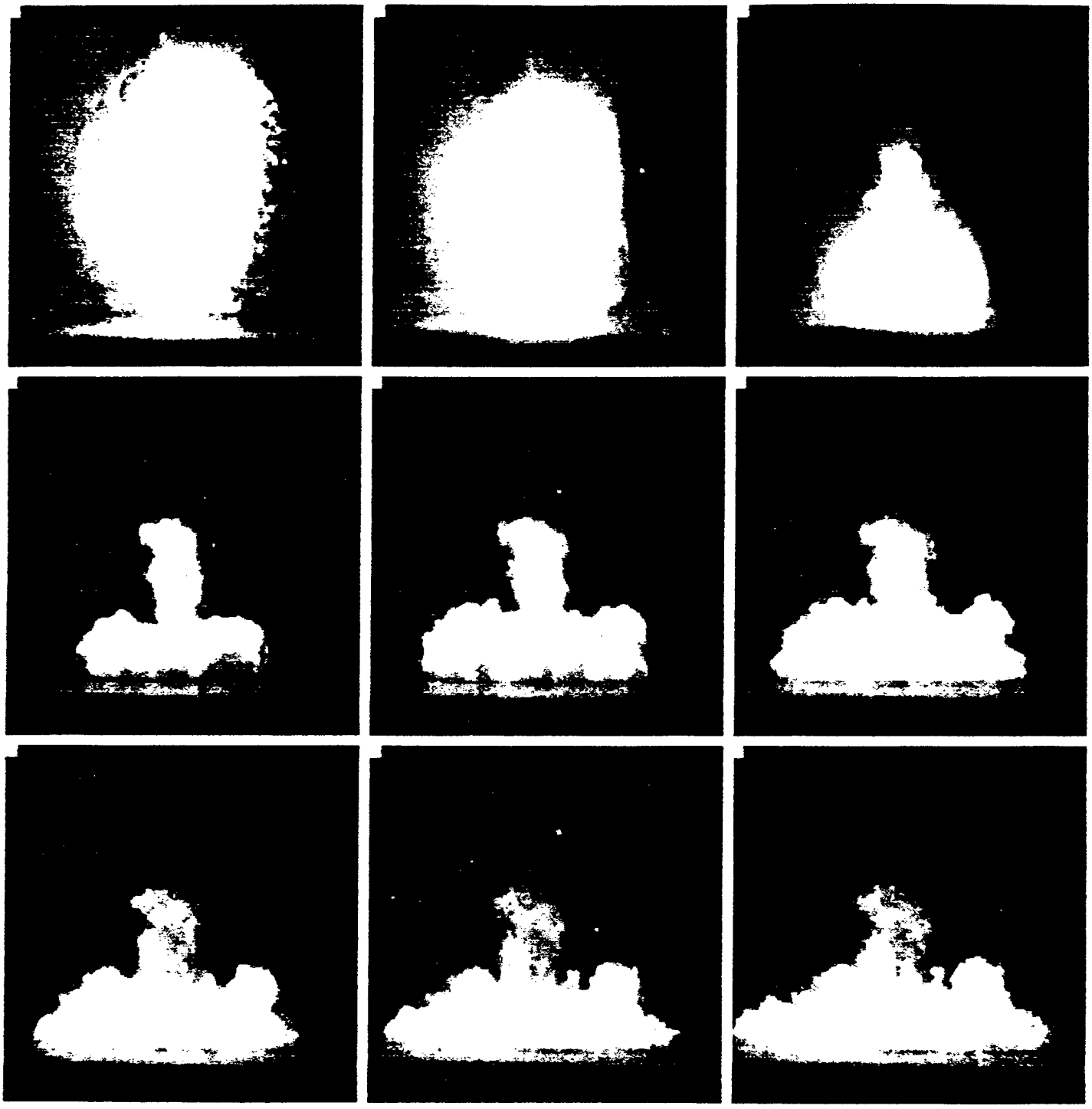

Fig. 3. (Continued)

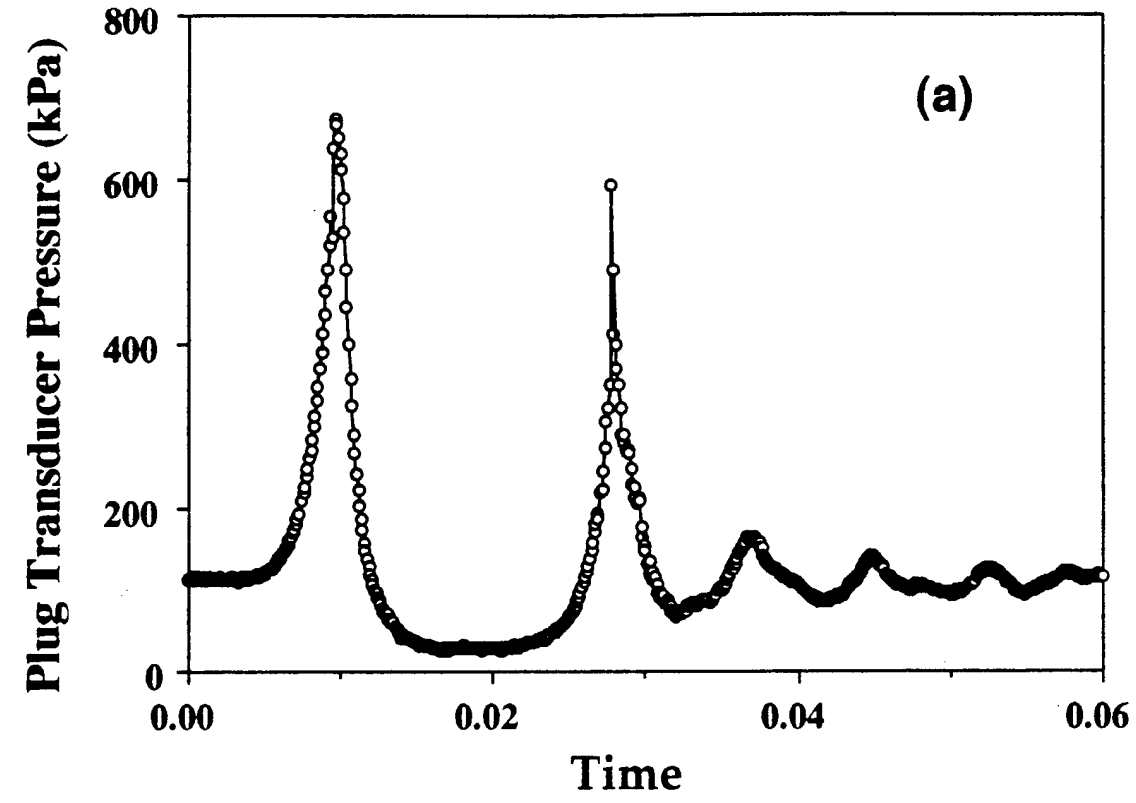


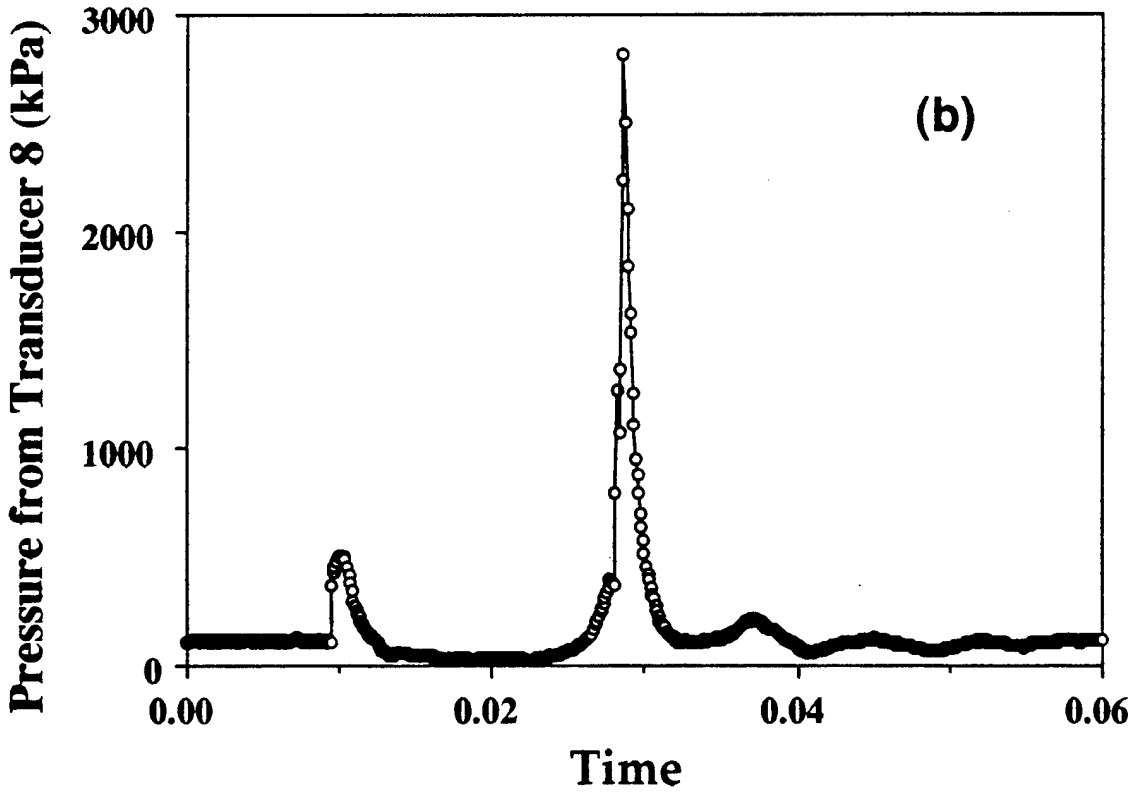


**Fig. 4. Pressure time trace recorded by (a) the plug transducer; and (b-d) the plate transducers for the exposed plate case with $d/R_o = 2$.**

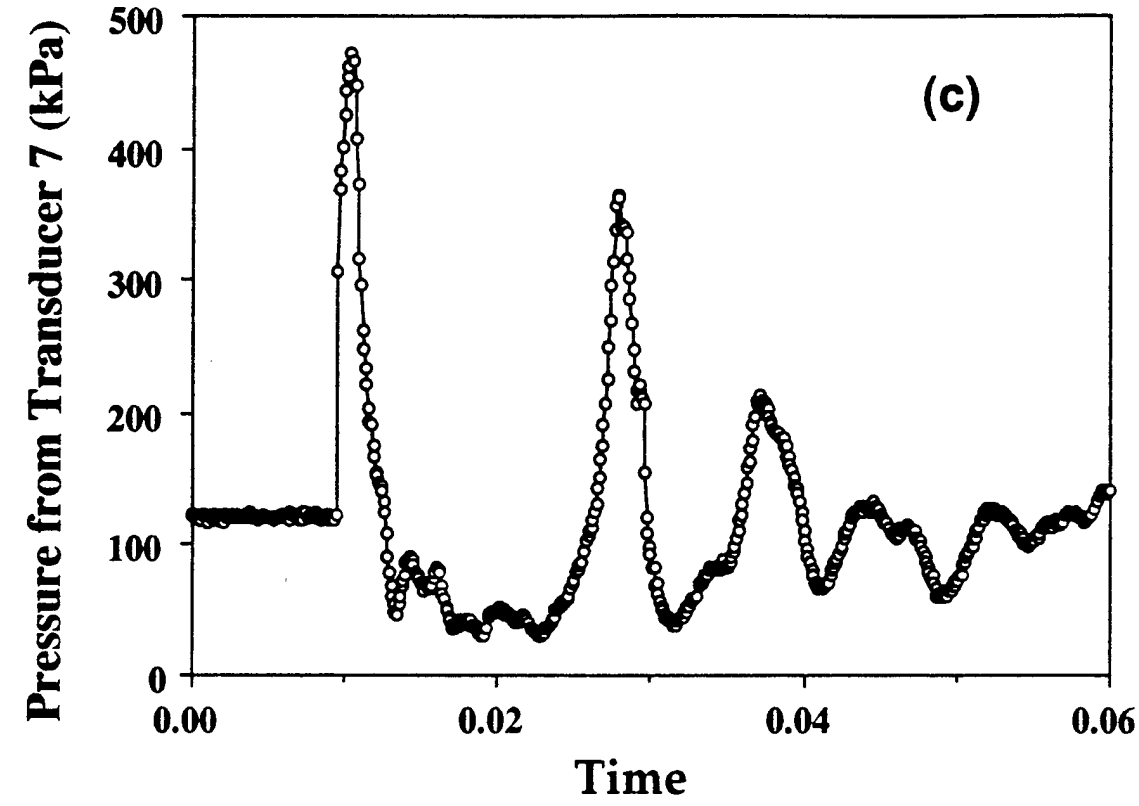


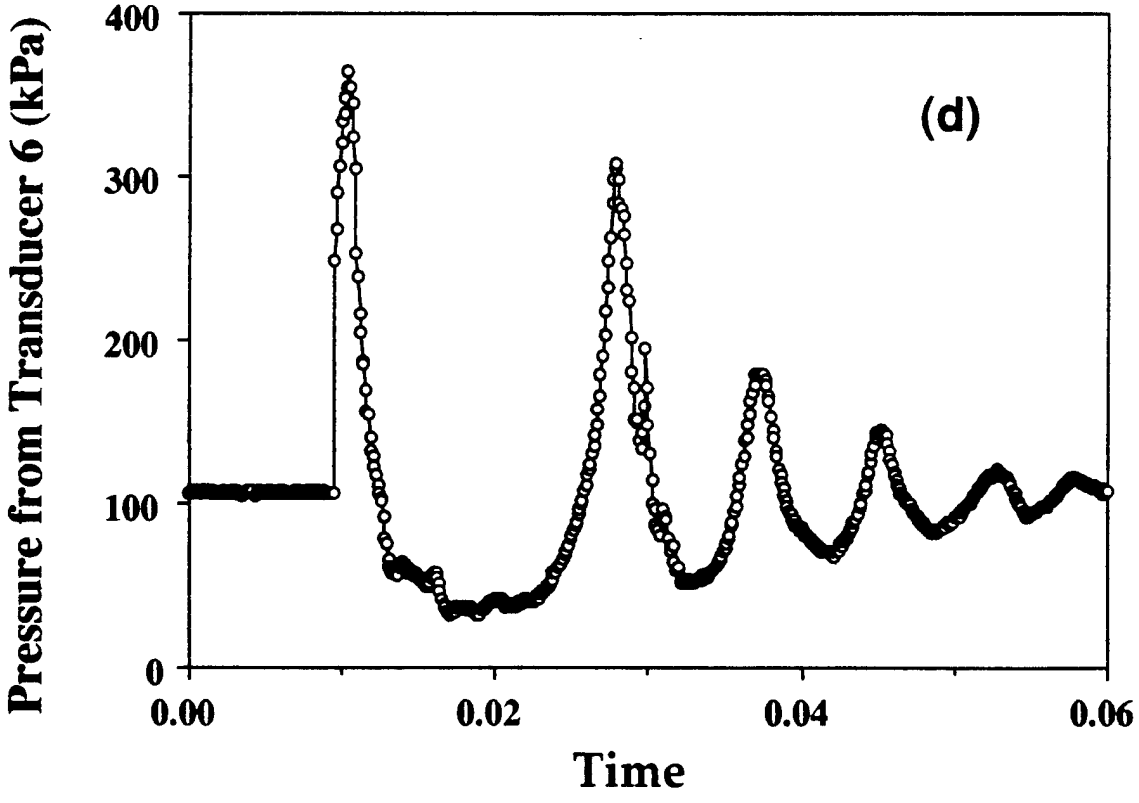


Fig. 4. (Continued)

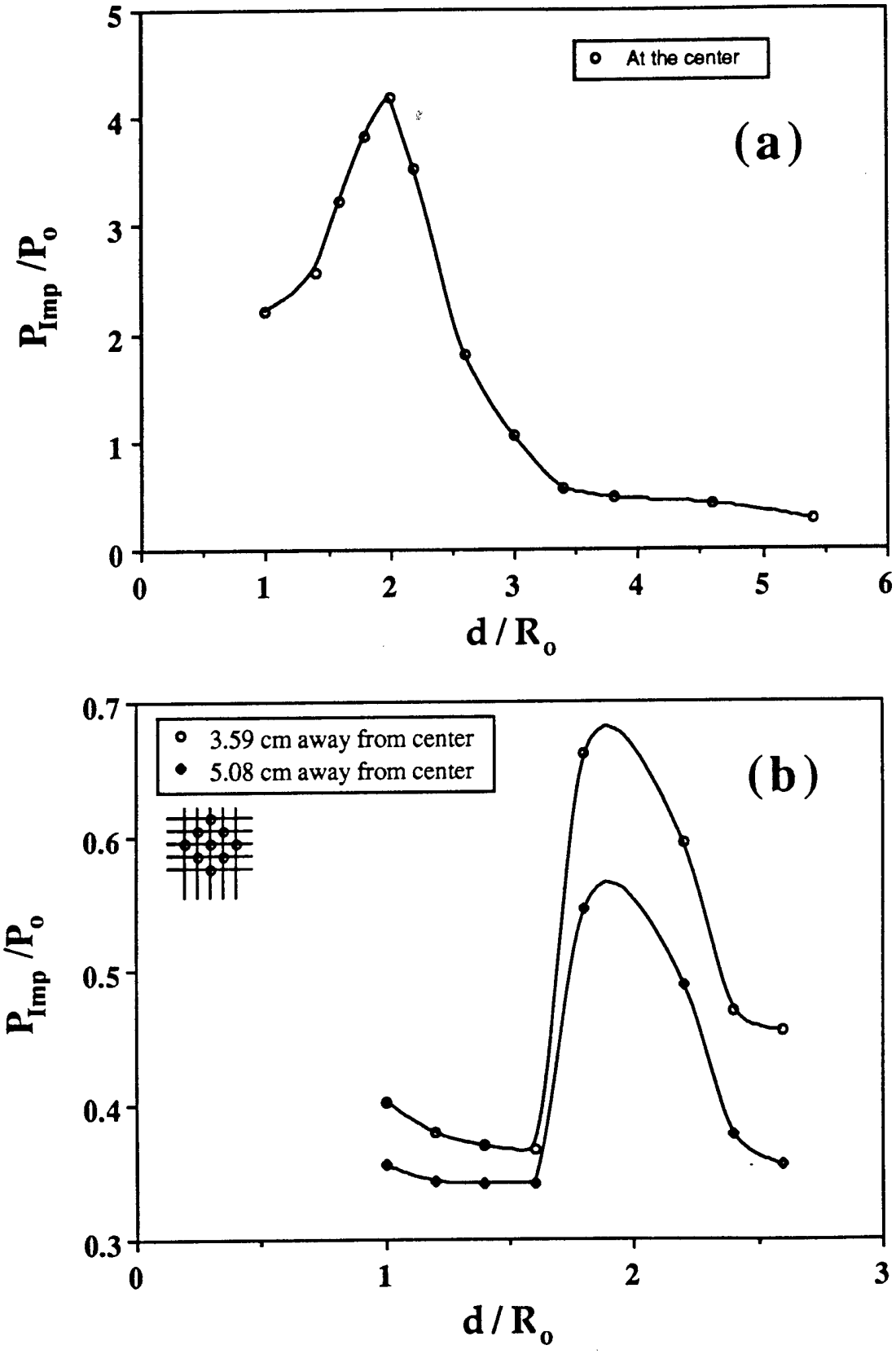


Fig. 5. Normalized impact pressure measured by (a) transducer no. 8; and (b) transducer no. 6 and 7 (away from the center) as a function of distance of the initial bulb from the plate.

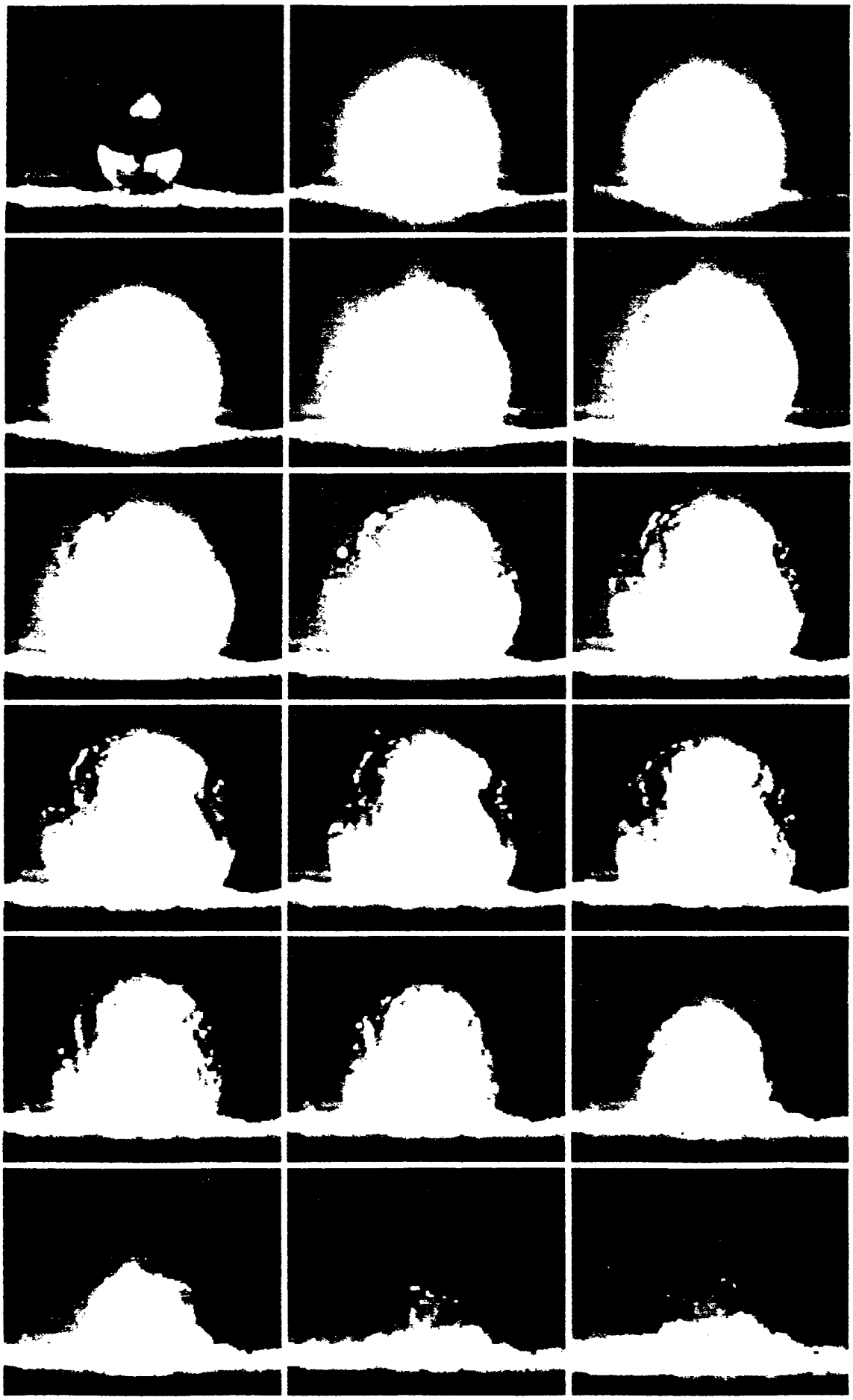

Fig. 6. Bubble collapse near a buried object. $d/R_0 = 2.4$, $d_s/R_0 = 1.1$ and $d_w/R_0 = 24$.

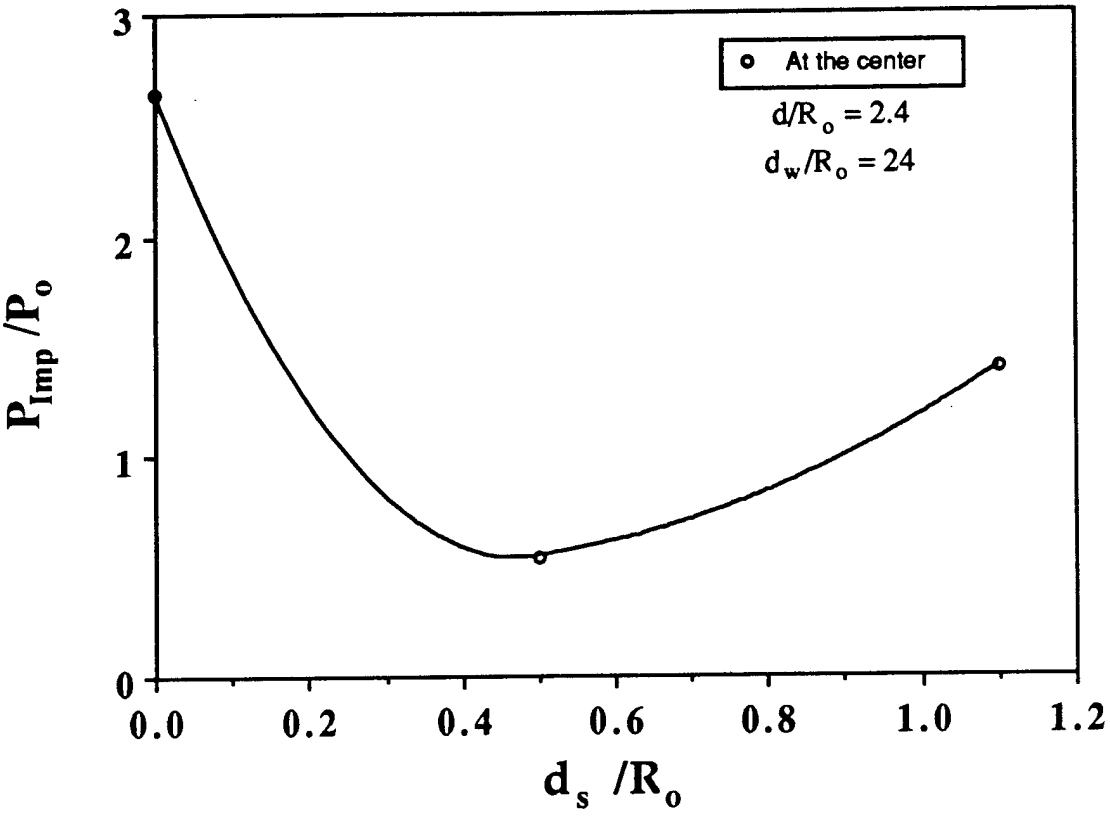


Fig. 7. Normalized impact pressure at the center as a function of sand layer thickness.

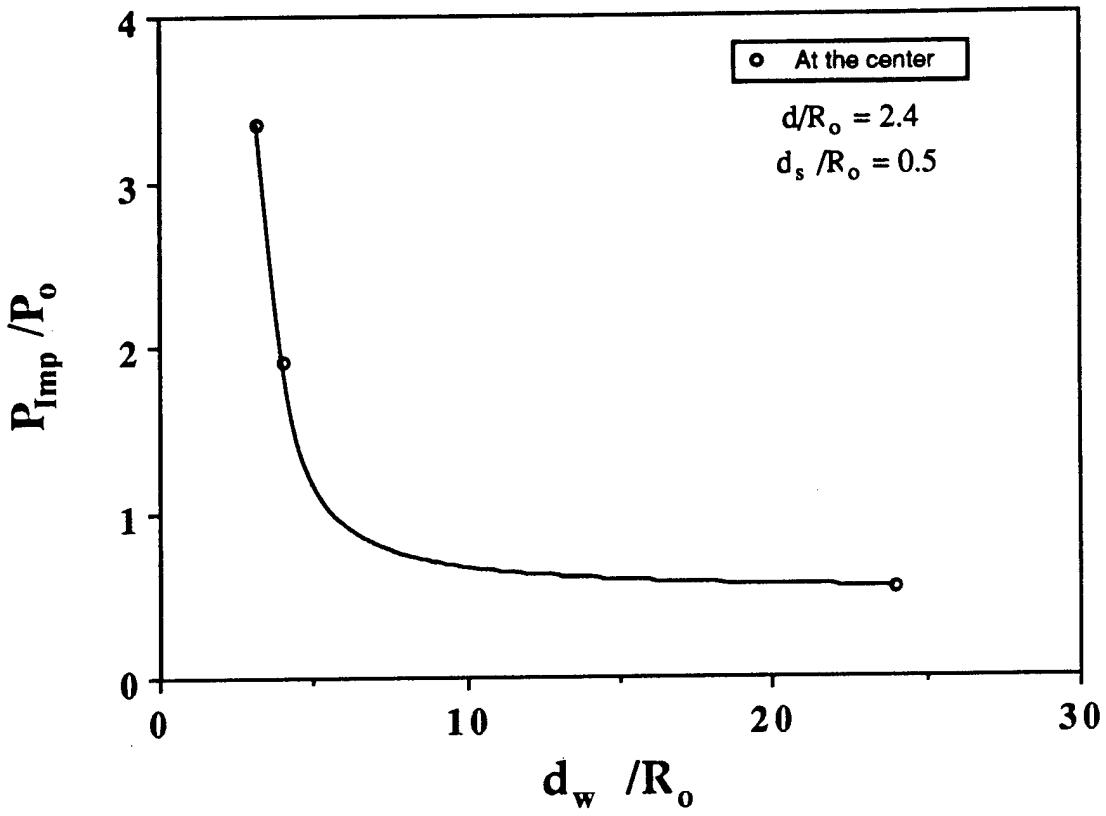


**Fig. 8. Normalized impact pressure at the center as a function of the location of free water surface above the bubble.**

# APPENDIX B

## Dynamics of Interaction between Two Underwater Explosion Bubbles

# DYNAMICS OF INTERACTION BETWEEN TWO UNDERWATER EXPLOSION BUBBLES

**Mihir Lal and Suresh Menon***
**School of Aerospace Engineering**
**Georgia Institute of Technology**
**Atlanta, Georgia 30332-0150**

**Submitted to**

**ASME Journal of Fluids Engineering**
**October 1996**

* Corresponding Author, (404) 894-9126, Fax (404) 894-2760
email: menon@falcon.ae.gatech.edu

# Dynamics of Interaction between Two Underwater Explosion Bubbles

**Mihir Lal**
Post-Doctoral Fellow

**Suresh Menon**
Associate Professor

School of Aerospace Engineering
Georgia Institute of Technology
Atlanta, GA 30332-0150

ABSTRACT

Underwater explosion bubbles are created by detonating a mixture of oxygen and Carbon Monoxide or Hydrogen in glass globes submerged in a water tank. A cinematographic technique is employed to capture entire interaction process in both horizontal and vertical configurations. Instrumented tubes and plugs measure pressure inside and outside the bubbles. Depending on the delay between two explosions and inter-bubble distance, the bubbles may either attract each other to form a single coalesced bubble, or they may violently repel each other. A violent interaction between the bubbles leads to an increased instability of the bubbles. When a coalesced bubble is formed by merging the energies of two bubbles, the resulting bubble has more residual energy and is more stable for successive oscillations. An out-of-phase oscillation generates a reentrant water jet which pierces the bubble. Experiments were also conducted to qualitatively and quantitatively study the interaction of a free surface with the explosion bubble(s).

## Introduction

Much of the research activities in the area of underwater bubble dynamics has been focused on the behavior of cavitation bubbles. Cavitation bubble dynamics play very important role in underwater acoustics and in predicting and preventing propeller and turbine blade damage. These bubbles, however, seldom occur singly. Actual cavitation fields contain several thousands of

oscillating and translating microbubbles. Study of the behavior of a cloud of bubbles thus becomes inevitable and experimental (e.g., Chahine and Sirian, 1985; Tomita et al., 1984), numerical (e.g., Chahine and Liu, 1985; Chahine, 1991; Chahine and Duraiswami, 1992; Wang and Brennen, 1994) and analytical (e.g., Van Wijngaarden, 1972) techniques have all been developed. The simplest model that has been studied by the researchers is the interaction between two bubbles. Theoretical and numerical studies of the interaction of two spherical or nonspherical bubbles of same or different sizes (e.g., Fujikawa et al., 1985; Fujikawa and Takahira, 1986; Fujikawa and Takahira, 1988; Morioka, 1974; Serebryakov, 1992; Shima, 1971; Takahira, 1988) have also been carried out. Interesting experimental observations of the interaction of a gas bubble with a pressure wave (Shima and Tomita, 1988) or with a vapor bubble (Smith and Mesler, 1972) have also been made. However, most of these observations are for microbubbles and find applications in cavitation, erosion and related topics.

Large bubbles, such as those created by underwater explosion, owing to their tremendous inherent destructive capabilities upon collapse near a rigid boundary, find practical applications in underwater weaponry. Detailed measurements and imaging of pulsating bubbles formed during deep sea explosions are very difficult due to a variety of obvious reasons (e.g., Arons et al., 1948) and therefore, there is insufficient data available to analyze the dynamics of interaction of bubbles. Controlled experiments described here, are required to investigate the physical processes that contribute to the interaction of bubbles. These experiments were conducted in a laboratory shallow water setup using a gaseous explosive mixture. The observations reported here are of practical significance for buried mines detection in shallow water beaches, where the interaction of an explosion bubble with a solid boundary and water free surface is anticipated.

The interaction of two underwater explosion bubbles is a very interesting and complex phenomenon, because of the fact that one bubble is influenced by the time-delayed pressure or shock wave radiated from the adjacent bubble. Radial motion of the bubble may be greatly excited

or subdued due to the interaction depending on their temporal and spatial separations. Though some experimental work has been done on the interaction of gas bubbles with two adjacent underwater explosion bubbles, and it has been shown that strong and complicated interactions ensue, it appears that no detailed results on the interaction of two underwater explosion bubbles have been published in the public domain literature.

This paper reports the results of the experiments carried out in a laboratory water tank to study the interaction between two adjacent bubbles created by underwater explosion of flammable gas contained in glass globes. The globes were placed side-by-side either in a horizontal or a vertical plane. The distance between the two globes and their sizes were both varied. This paper also discusses the interaction of single and double explosion bubble(s) with the water free surface.

## Experimental Procedures

Underwater explosion experiments were conducted in a wooden tank of dimension 2 m × 1.5 m × 1.5 m, coated with fiberglass resin from inside. The tank, as shown in Fig. 1, has three windows on three sides for optical imaging. The underwater explosion bubble is generated by centrally igniting a mixture of an explosive gas (either Hydrogen or Carbon Monoxide) and oxygen contained in a hand-blown glass globe. Three different sizes of glass globes were used for present experiments with average radii of 2.9 cm, 3.2 cm, and 3.8 cm. The glass globe, as shown in Fig. 2, has an electric spark ignition system connected to a 3000V DC power supply. The explosion takes place at a constant volume until the globe bursts. Since the experiments were conducted in a laboratory shallow water setup and using a gaseous explosive mixture, the bubbles are relatively smaller (although much larger than cavitation bubbles) than those observed in deep sea explosions. Using both geometric and dynamic (based on Froude number) scaling analysis (e.g., Shepherd, 1988), it is shown that the present experiments approximately simulate deep sea bubble dynamics. The explosion bubble thus formed is a reasonable subscale approximation of the deep sea underwater explosion bubble.

The pressure response in the water around the bubbles were recorded during the experiments by means of 4 KISTLER dynamic piezoelectric pressure transducers fitted at the ends of 4 stainless steel (1.27 cm diameter) tubes bent at right angle, as shown in Fig. 1. A hydrophone is also mounted in the tank and is used for measuring acoustic pressure. Pressure inside the bubble during its oscillation is measured by another KISTLER transducer which is mounted inside the plug, as shown in Fig. 2. Signals from these six pressure transducers and the hydrophone were digitized using National Instrument's AT-MIO-16X analog-to-digital convertion board, and were recorded into a microcomputer. Eight channel data recording was performed with a sustained sampling rate of 10,000 samples per second per channel.

The tank was illuminated by either direct overhead flood lights or an argon-ion laser sheet which lies in a vertical plane perpendicular to the camera axis. The optical recording of the bubble motion was performed by a CCD enhanced digital video camera with a maximum speed of 6000 frames per second. Since the viewable picture size is inversely proportional to the recording speed of the camera, the maximum speed was limited to 2000 frames per second as the image size reduces to half at this speed. Many of the experiments, however, were performed at a lower speed of 1000 frames per second in order to obtain a full screen image.

The two glass globes were supported inside the tank by means of a modified sting which made the pressure transducers mounted inside the two globes to face each other (Fig. 1). This facilitated direct measurement of the fluctuation in the pressure inside one bubble due to its interaction with the other. Six holes were drilled in the supporting copper pipe (1.6 cm diameter) of Fig. 1 at equal spatial separation from either ends in order to provide a means for altering the distance between the two bubbles. Experiments were conducted in primarily two configurations; a horizontal configuration, when the supporting pipe was horizontal, and a vertical configuration,

when it was vertical. The former configuration prohibited the use of laser light sheet and only the flood lights were used for imaging, while the latter allowed the use of laser light sheet.

Experiments were also conducted to study the interaction of water free surface with the explosion bubble(s). The motivation for these experiments has obvious reasons. The free surface provides a constant pressure boundary in close proximity of the oscillating bubble. It is known that the bubble moves away from the free surface and a reentrant jet is formed which pierces the bubble in the direction of its migration (e.g., Birkhoff, 1957; Blake and Gibson, 1981; Chahine, 1977; Chahine, 1982; Wilkerson, 1989). Wilkerson (1989) developed a boundary integral technique for the analysis of expansion and collapse of an explosion bubble in free field, near a rigid surface, or near a free surface. To verify the accuracy of his method for predicting reentrant water jet tip velocities for a bubble near a free surface, he compared his results with a PISCES code calculation and expressed his inability to predict an accurate estimation of the error involved in his method because of the unavailability of any such experimental data. This observed lack of data motivated the current experiments to study the interaction of a free surface with an explosion bubble.

## Results and Discussion

The interaction process is highly dependent on the time delay between the two explosions. This time delay is related to a variety of hardware and bubble response characteristics. The two globes have independent power supplies and there is always a time delay between the occurrence of the spark and when the bubble(s) starts expanding. The bubble expansion occurs immediately after the glass globe bursts. The time delay depends primarily on the gas volume (globe size) and the nature of gas mixture inside the globe. A bigger globe size will create a larger time delay. Similarly, fuel-rich or fuel-lean mixtures will also create larger delays as compared to the one associated with a stoichiometric mixture. In addition to this delay, there is another time delay which is associated with the spark system itself. This delay is between the instant when the power

is turned on and when the spark actually fires. This delay primarily depends on the actual gap between the two spark wires since a bigger gap creates a larger delay. The actual delay (temporal separation) between two explosions is therefore measured from the recorded video images as the time elapsed between the instant when the individual globe bursts. It was therefore deemed necessary to conduct several experiments to collect statistical information about the range of bubble behavior with respect to the delay between two explosions.

The entire spectrum of delay can be classified into two broad regions: in-phase oscillation and out-of-phase oscillation (e.g., Morioka, 1974; Shima, 1971; Smith and Mesler, 1972). In most of the past analytical, numerical or even experimental work on the interaction of two cavitation bubbles, interest has been focused primarily on the contraction phase of the bubble oscillation. This yields an in-phase oscillation of identical bubbles as they both start collapsing at the same time following a sudden change in the ambient pressure. In-phase oscillation is obtained when there is strictly no delay between the explosions; both the bubbles start their oscillation cycle at the same time, both have identical time period of oscillation and are in phase at any instant throughout their oscillation cycle. This is the simplest scenario and has been analyzed comprehensively.

Another interesting scenario is a 180° out-of-phase oscillation and it can be best understood in the interaction of two identical explosion bubbles as a case where one bubble starts its oscillation cycle when the other has already reached its maximum radius. In fact, this is one of the two scenarios predicted by Morioka's (1974) theoretical analysis of natural frequencies of two pulsating bubbles which predicts the existence of two natural frequencies corresponding to in-phase and 180° out-of-phase oscillations, respectively. Of course, in an experimental setup one can have any amount of delay between zero to 180°, or even beyond 180°. Two bubbles oscillating in-phase behave in a nearly identical manner as a single bubble near a rigid boundary and therefore, are of considerable practical interest since it has been shown that the collapse of a

bubble near a wall can cause significant damage. The bubbles have an increasing repulsive effect as the delay between two explosions increases, up to the point when they oscillate 180° out-of-phase (Smith and Mesler, 1972).

Figure 3 shows an example for two underwater explosion bubbles oscillating in-phase. The initial volume of the right glass globe is 94 ml and that of the left glass globe is 90.5 ml. They are in a horizontal configuration and are initially separated by a distance d, where $d/R_o = 2.32$. Both of them are filled with stoichiometric mixture of Carbon Monoxide and Oxygen. There is virtually no delay between two explosions (determined from the image data) and since the two globes have almost same volume, they burst also at the same time (time, t = 0 ms). Since the initial spatial separation between the globes was intentionally kept to a very small value so that a violent interaction can ensue, the bubbles soon come in contact with each other. They deviate more and more from sphericity as they expand with time. The bubbles merge together to form a single coalesced bubble.

The surface where the two bubbles come in contact in Fig. 3 grows in size as the bubbles grow and is initially curved. The contact surface slowly becomes a plane surface and remains so thereafter until the bubbles collapse on to each other. This plane surface of contact may be considered as a rigid surface in an equivalent single bubble analogy. Figure 4 shows the relative position of this surface with respect to the initial globes' centers. Notice that this surface is almost perpendicular to the line joining the initial globes' centers and is located almost midway. The time period of oscillation of the bubbles shown in Fig. 3 is about 21 ms, while that of an identical bubble in free-field is less than 15 ms. Therefore, for two identical bubbles oscillating in-phase, an increase in the bubble period is observed. A similar observation was made by Chahine (1991).

The pressure traces measured around the bubbles show that the bubble behavior is symmetrical. A pressure fluctuation of about 700 kPa exhibited by the plug transducers near

bubble minimum demonstrates the severity of collapse of the jets formed in two bubbles on to each other. The pressure drops exponentially as one moves away from the bubble (Cole, 1948). A pressure drop of 70% (from 1000 kPa to 300 kPa) over a distance of 14 cm, and that of 80% (from 1000 kPa to 200 kPa) over a distance of 34 cm from the bubble center have been recorded by tank transducers.

The coalesced bubble quickly breaks into cloud of smaller bubbles which migrate upward due to buoyancy effect. The bubble contour is traced and 360 bubble radii are obtained at equal azimuth locations. A mean radius is obtained from this data, which is used to normalize the radii data. These data are then Fourier analyzed and the results are shown in Fig. 5, which shows the power spectral density of the coalesced bubble's interface at three instants: just after it is formed and 1 and 5 ms after it collapses. Here c is the bubble circumference and $\lambda$ is the wavelength. It can be seen that the coalesced bubble starts exhibiting pronounced and distributed peaks in power spectral density soon after collapse. A peak is actually the square root of the sum of the squares of mode amplitude coefficients and occurs at integral fractions of bubble circumference because a periodic trace is being analyzed. The coalesced bubble is therefore very unstable.

A single coalesced bubble does not form only in an in-phase oscillation. Another situation where the formation of a single coalesced bubble has been observed repeatedly and most surprisingly, is associated with a nonzero time delay and a very short inter-bubble distance. This case is shown in Fig. 6. The initial volume of the right glass globe is 125 ml and that of the left glass globe is 127 ml. They are almost touching each other such that the initial separation distance between them, d, is given by $d/R_o = 2.1$. Both of them are filled with stoichiometric mixture of Carbon Monoxide and Oxygen. The right globe explodes first (at time t = 0 ms) and tries to encompass the left globe as the bubble grows. When the left globe explodes (at time t = 8 ms), the shock wave emitted by this bubble travels through the right bubble as is evident by its protruding pieces. The right bubble, however, maintains its coherence and sphericity. It seems that the

energy of the left bubble is substantially transferred to the right bubble, and it does not even get a chance to expand to its maximum radius. A force field is generated such that when the right bubble starts to collapse, the left bubble just merges into its predecessor to form a single coalesced bubble, which continues the oscillation cycle as a single explosion bubble. Since no jets are formed and the coalesced bubble is formed by merging the energies of two bubbles, it has more residual energy than that of the previous example and does not disintegrate into smaller bubbles so quickly. In fact, it is even more stable than a single explosion bubble in free field and can, therefore, be used for focusing bubble energy for enhancement of its destructive capabilities.

The available energy for successive pulsations of the coalesced bubble can be calculated using Vokurka's (1986 and 1987) energy balance analysis. The various formulae for this analysis are given in the cited references and are, therefore, avoided here for the sake of brevity. The energy, $E_0 = 4\pi R_0^3 P_l/3$, where $R_0$ is the initial globe radius and $P_l$ is the ambient hydrostatic pressure at the explosion depth, is used to nondimensionalize energy and the heat release of stoichiometric carbon monoxide is taken to be 284 KJ/mole (Strahle 1994). The total nondimensional energy available for oscillation of the right bubble at time t = 0 can be given by $\bar{E}_0 = 78.439$ for an explosion depth of 0.65 m. The nondimensional internal and the potential energies of the right bubble at its maximum radius for an expansion ratio of $R_{max} / R_0 = 2.738$, are estimated to be 38.043 and 19.528, respectively. The energy dissipated into the surrounding water by a shock wave thus equals $20.868E_0$. Therefore, the energy available for successive oscillation of the right bubble at its maximum radius equals $57.571E_0$. A similar analysis for the left bubble for a smaller explosion pressure and expansion ratio of only 1.095 yields the value of the available energy at its maximum radius to be $11.916E_0$. The coalesced bubble should apparently have available energy of $69.487E_0$ for its successive oscillation, which is roughly 20.7% more than what a single explosion bubble should have in a free field condition. The coalesced bubble is, in fact, observed to oscillate for an extended period of time.

The effect of the shock wave generated during the formation of the right bulb is reflected by a 150 kPa peak in the left plug transducer pressure trace (not shown). On the other hand, the plug transducer inside the expanding right bubble records only a tiny fluctuation of 10 kPa when the left bulb explodes. It is interesting to note that the explosion pressure for the left bubble (200 kPa) is only about 20% of what it would have been in a free field case. Thus, an expanding bubble appears to inhibit the formation of another explosion bubble in its close proximity by reducing its explosion pressure. This may be the reason why the left bubble does not have sufficient energy to expand to its maximum radius. But, it certainly aids its predecessor to form a coalesced bubble with a greater energy to collapse violently and this fact is captured by all the transducers and hydrophone in the form of elevated collapse peaks. This time, the right plug transducer lies inside the coalesced bubble as it collapses. The collapse pressure recorded by this transducer is very high (2500 kPa). In addition to a large peak near bubble collapse, the hydrophone pressure also shows a larger acoustic pressure oscillation following the collapse. Except for the plug transducers, the pressure traces recorded by the right and left transducers are once again almost identical, indicating a symmetrical bubble behavior.

Similar dynamic behavior is exhibited by the interaction of bubbles of initially different sizes. It is not possible, however, to obtain an in-phase oscillation because the two bubbles have different time period of oscillation. On the other hand, the formation of a coalesced bubble by mergence of two bubbles, have also been exhibited by bubbles of different sizes when the smaller bubble has been absorbed into the larger bubble. This kind of bubble dynamics is not feasible for large inter-bubble distance.

When the initial separation distance is sufficiently large, the bubbles start repelling each other for a nonzero time delay. The repulsion force increases with the delay between explosions, up to the point when they are oscillating 180° out-of-phase. In this case, when the predecessor bubble collapses, the successor bubble reaches its maximum radius. At this point, the pressure

field is abruptly reversed and this causes the formation of a strong reentrant water jet in the successor bubble. Figure 7 shows how this reentrant jet travels with time for a case of identical bubbles oscillating 180° out-of-phase with each other. Here, x denotes the location of the jet tip relative to the inertial frame (the tank) and x = 0 corresponds to the instant when the jet tip becomes visible for the first time. The formation of a strong reentrant water jet has also been observed for two bubbles of different sizes.

As the phase delay between two explosions increases beyond 180°, the repulsion force as well as the water jet velocity decrease in magnitude. If the phase delay between two explosions increases beyond 360° (i.e., if one bubble has already completed one oscillation cycle when the other bubble forms), the resulting interaction is very weak. In this case, even though the predecessor bubble manages to create a depression in successor bubble at its maximum radius, formation of a jet is not observed.

The horizontal configuration is very important from a practical standpoint, as it can set a catastrophic bending vibration to a nearby rigid body if tuned properly. The vertical configuration is also equally important, as it can dramatically enhance the impact pressure of a single bubble when collapsed near a rigid body. If two bubbles are placed close to each other along an axis perpendicular to a nearby rigid body, and if these two bubbles are tuned to oscillate 180° out-of-phase with each other, a water jet will be formed directed towards the rigid surface with a velocity which will be higher than that formed by the collapse of a single bubble under similar circumstances. The bubble dynamics in vertical configuration in the present study (in the absence of any nearby rigid body), however, do not show a remarkable difference from that of horizontal counterpart. This is because of the fact that only the orientation of the gravitational force changes between two configurations. In practical high explosive cases, the force field generated by the interaction between bubbles is much more stronger to be affected negligibly by the gravitational force.

Experiments were also carried out to study the interaction of a free surface with explosion bubble(s). A simple sting mount was used to support a glass globe and the depth of water in the tank was decreased in an increment of 2.54 cm. It was found that the bubble migration velocity smoothly changes its direction as well as its magnitude. The transition point determines the maximum inter-bubble distance for which the two identical bubbles will start interacting while oscillating 180° out-of-phase with each other. Figure 8 shows the transition of bubble migration velocity with water depth. The maximum center-to-center distance between two identical interacting bubbles (of approximate volume of 230 ml) oscillating 180° out-of-phase with each other was found to be $6.8R_0$, $R_0$ being the initial radius.

Both out-of-phase and in-phase oscillations of two explosion bubbles in a horizontal configuration near a free surface were also studied. The bubbles oscillating out-of-phase with each other repel each other and the effects of the free surface become apparent only after they have been repelled by each other. This once again indicates that the force field generated by the interaction between two bubbles is much stronger than that of a free surface and there have been instances where one of the bubbles actually migrates upward. Experiments were also conducted with two globes in a vertical configuration near a free surface. Out-of-phase oscillation was obtained and the consequences are not hard to imagine. Since the force field generated by the interaction between two bubbles is much stronger than that of a free surface, one bubble rapidly migrated downward and the other undoubtedly broke through the free surface venting its high pressure gases to the atmosphere.

## Conclusions

Underwater explosion experiments were conducted in a water tank using flammable gases in glass globes to study the dynamics of interaction of two explosion bubbles in both horizontal and vertical configurations. The former configuration can excite a nearby submerged structure in

bending vibration mode, while the latter can easily be tailored for the directionality and enhancement of the impact pressure resulting from the collapse of an underwater explosion bubble near a solid boundary. Depending on the delay between two explosions and inter-bubble distance, the bubbles may either attract each other to form a single coalesced bubble, or they may violently repel each other. A violent interaction between the bubbles leads to an increased instability of the bubbles. If a coalesced bubble is formed by merging the energies of two bubbles, the resulting bubble has more residual energy and is more stable for successive oscillations. An out-of-phase oscillation generates a reentrant water jet which pierces the bubble in the direction of its migration. Water free surface repels the bubble and the transition point of bubble migration velocity determines the maximum inter-bubble distance required for the initiation of interaction between two identical out-of-phase pulsating bubbles. These observations are of considerable practical significance for buried mines detection in shallow water beaches, where the interaction of an explosion bubble with a solid boundary and water free surface is anticipated.

## Acknowledgment

This work is supported by the Office of Naval Research under Grant No. N00014-91-J-1963 and monitored by Drs. Richard Miller and Judah Goldwasser.

## References

Arons, A. B., Slifko, J. P., and Carter, A., 1948, "Secondary Pressure Pulses Due to Gas Globe Oscillation in Underwater Explosions: I. Experimental Data," *The Journal of the Acoustical Society of America*, Vol. 20, pp. 271-276.

Birkhoff, G., and Zarantonello, E. H., 1957, *Jets, Wakes, and Cavities*, Academic Press Inc, New York, pp. 241-243.

Blake, J. R., and Gibson, D. C., 1981, "Growth and Collapse of a Vapor Cavity near a Free Surface," *Journal of Fluid Mechanics*, Vol. 111, pp. 123-140.

Chahine, G. L., 1977, "Interaction Between an Oscillating Bubble and a Free Surface," *Journal of Fluids Engineering*, Vol. 38, pp. 709-716.

Chahine, G. L., 1982, "Experimental and Asymptotic Study of Nonspherical Bubble Collapse," *Applied Scientific Research*, Vol. 38, pp. 187-197.

Chahine, G. L., and Liu, H. L., 1985, "A Singular Perturbation Theory of the Growth of a Bubble Cluster in a Superheated Liquid," *Journal of Fluid Mechanics*, Vol. 156, pp. 257-279.

Chahine, G. L., and Sirian, C. R., 1985, "Collapse of a Simulated Multibubble System," *ASME, Cavitation and Multiphase Flow Forum*, Albuquerque, New Mexico, pp. 78-81.

Chahine, G. L., 1991, "Dynamics of the Interaction of Non-Spherical Cavities," *Mathematical approaches in Hydrodynamics*, ed., T. Miloh, Society for Industrial Applications of Mathematics, Philadelphia, pp. 51-67.

Chahine, G. L., and Duraiswami, R., 1992, "Dynamical Interactions in a Multi-Bubble Cloud," *Transactions of the ASME*, Vol. 114, pp. 680-686.

Cole, R. H., 1948, *Underwater Explosions*, Princeton University Press, Princeton.

Fujikawa, S., Takahira, H., and Akamatsu, T., 1985, "Underwater Explosion of Two Spherical or Nonspherical Bubbles and Their Interaction With Radiated Pressure Waves," *Shock Waves and Shock Tubes*, Proceedings of the Fifteenth International Symposium, Berkeley, CA, pp. 737-744.

Fujikawa, S., and Takahira, H., 1986, "A Theoretical Study on the Interaction between Two Spherical Bubbles and Radiated Pressure Waves in a Liquid," *Acustica*, Vol. 61, pp. 188-199.

Fujikawa, S., and Takahira, H., 1988, "Dynamics of Two Nonspherical Cavitation Bubbles in Liquids," *Fluid Dynamics Research*, Vol. 4, pp. 179-194.

Moroika, M., 1974, "Theory of Natural Frequencies of Two Pulsating Bubbles in Infinite Liquid," *Journal of Nuclear Science and Technology*, Vol. 11, pp. 554.

Serebryakov, V. V., 1992, "Expansion of Axisymmetric and Spherical Cavities, and Their Interactions," *Fluid Mechanics Research*, Vol. 21, No. 2, pp. 67-79.

Shepherd, J. E., 1988, "Interface Effects in Underwater Explosions," *Conventional Weapons Underwater Explosions*, ONR Workshop Report, pp. 43-83.

Shima, A., 1971, "The Natural Frequencies of Two Spherical Bubbles Oscillating in Water," *ASME Journal of Basic Engineering*, Vol. 93, pp. 426-432.

Shima, A., and Tomita, Y., 1988, "Impulsive Pressure Generation by Bubble/Pressure-Wave Interaction," *AIAA Journal*, Vol. 26, No. 4, pp. 434-437.

Smith, R. H., and Mesler, R. B., 1972, "A Photographic Study of the Effect of an Air Bubble on the Growth and Collapse of a Vapor Bubble near a Surface," *Journal of Basic Engineering*, pp. 933-942.

Strahle, W., and Liou, S. G., 1994, "Physical and Chemical Observations in Underwater Explosion Bubbles," *Symposium (International) on Combustion*, Vol. 25, pp. xx-xx, .<<< **********

Takahira, H., 1988, "Nonlinear Oscillation of Two Spherical Gas Bubbles in a Sound Field," *ASME Cavitation and Multiphase Flow Forum*, pp. 1-4.

Tomita, Y., Shima, A., and Ohno, T., 1984, "Collapse of Multiple Gas Bubbles by a Shock Wave and Induced Impulsive Pressure," *Journal of Applied Physics*, Vol. 56, No. 1, pp. 125-131.

Van Wijngaarden, L., 1972, "On the Collective Collapse of a Large Number of Gas Bubbles in Water," *Proceedings of the 11th International Congress of Applied Mechanics*, Springer, Berlin, pp. 854-865.

Vokurka, K., 1986, "A Method for Evaluating Experimental Data in Bubble Dynamics Studies," *Czech. Journal of Physics*, B, Vol. 36, pp. 600-615.

Vokurka, K., 1987, "Oscillations of Gas Bubbles Generated by Underwater Explosions," *Acta Technica Csav*, Vol. 2, pp. 162-172.

Wang, Y. C., and Brennen, C. E., 1994, "Shock Wave Development in the Collapse of a Cloud of Bubbles," *Cavitation and Multiphase Flow Forum*, Vol. 194, pp. 15-19.

Wilkerson, S. A., 1989, "Boundary Integral Technique for Explosion Bubble Collapse Analysis," *Energy-Sources Technology Conference and Exhibition*, 89-OCN-2, Houston, Texas, pp. 1-12.

## List of Figures

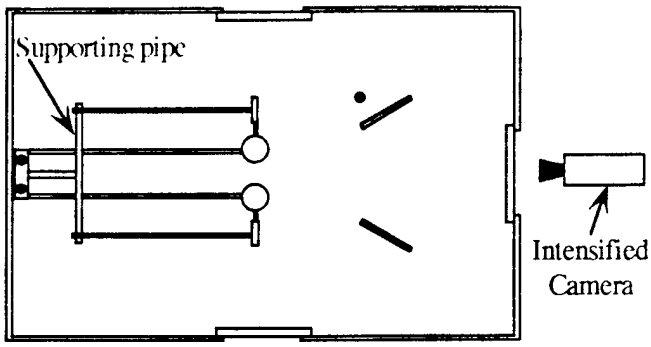


**Top View**

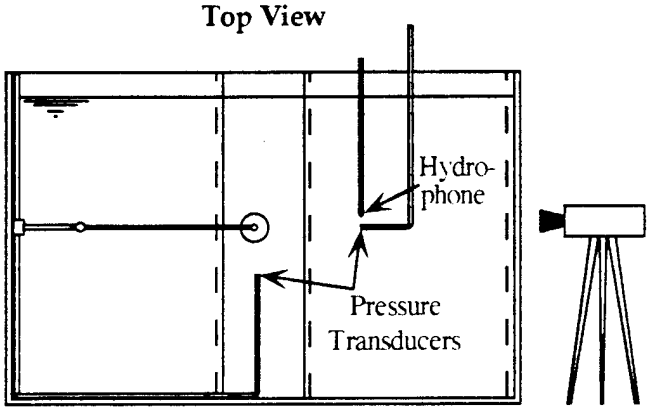


**SideView**

Fig 1.

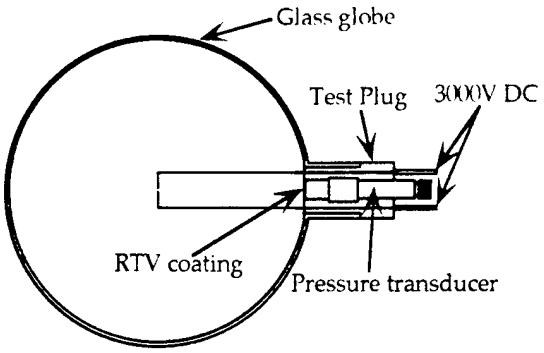


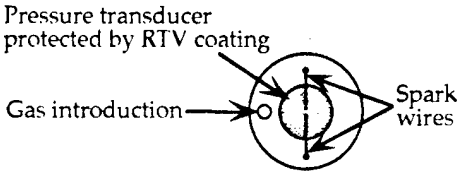


**Top view of the test plug**

Fig 2

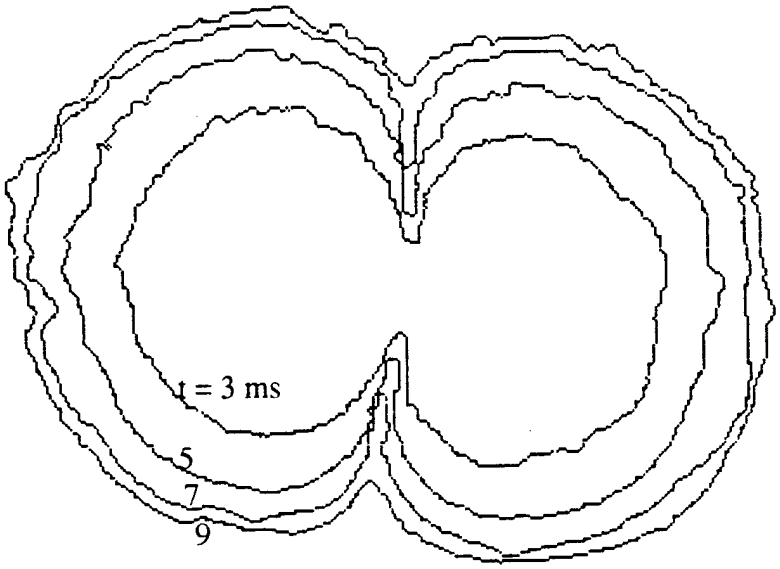


Fig 3.1

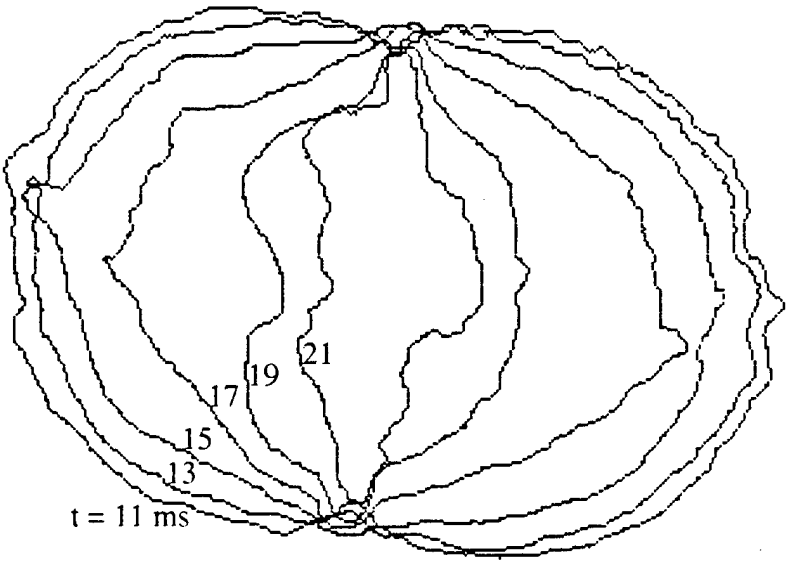


Fig 3.2

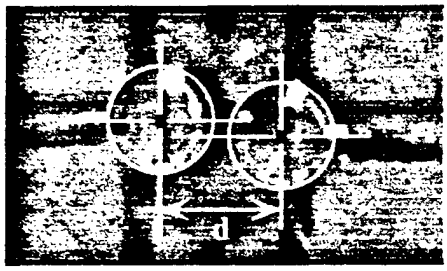

$d/R_o = 2.32$

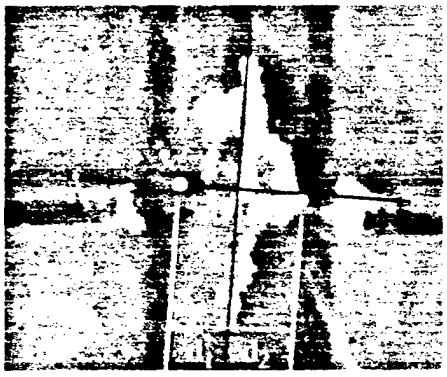

$d_1/R_o = 1.1$; $d_2/R_o = 1.22$

Fig 4

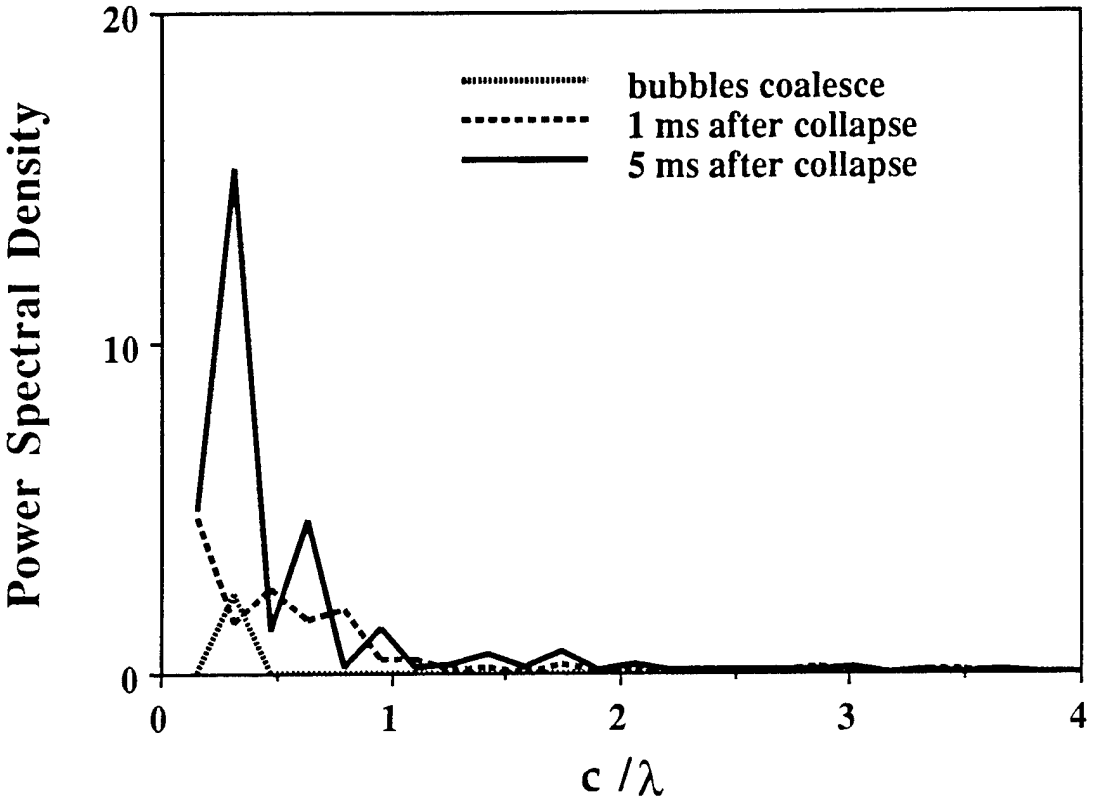
20
10
0
0
1
2
3
4
Power Spectral Density
c /λ
bubbles coalesce
1 ms after collapse
5 ms after collapse

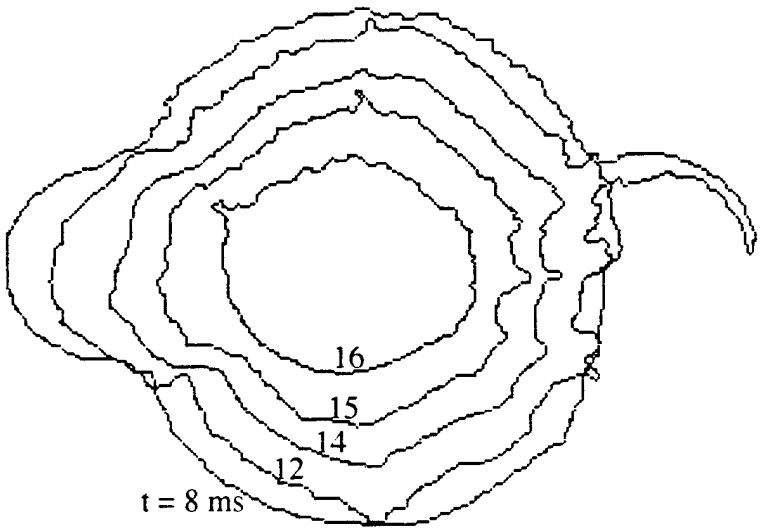


Fig 6

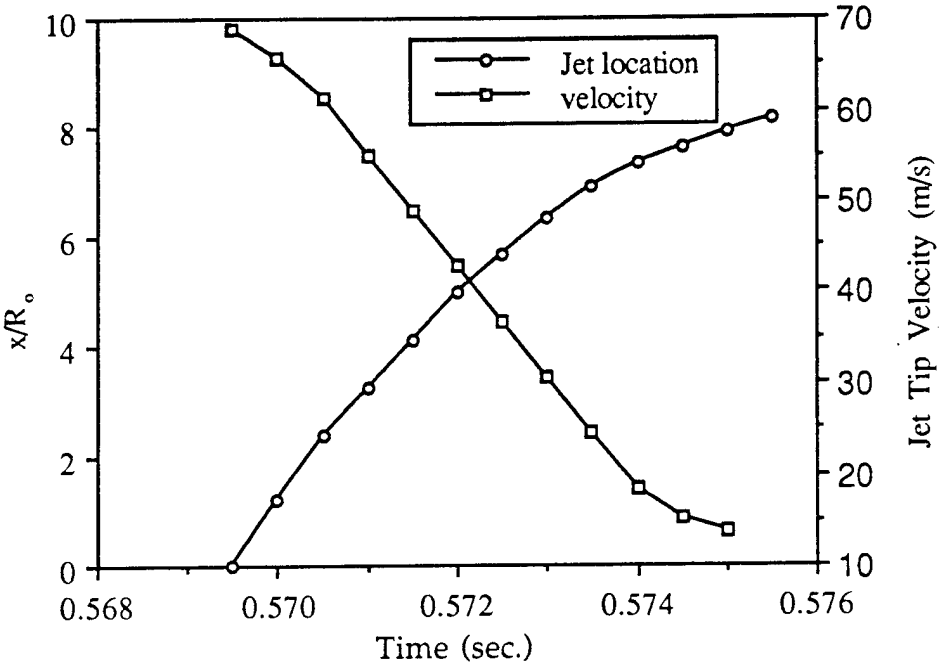
Jet location
velocity
x/R$_o$
Jet Tip Velocity (m/s)
Time (sec.)
0
2
4
6
8
10
10
20
30
40
50
60
70
0.568
0.570
0.572
0.574
0.576

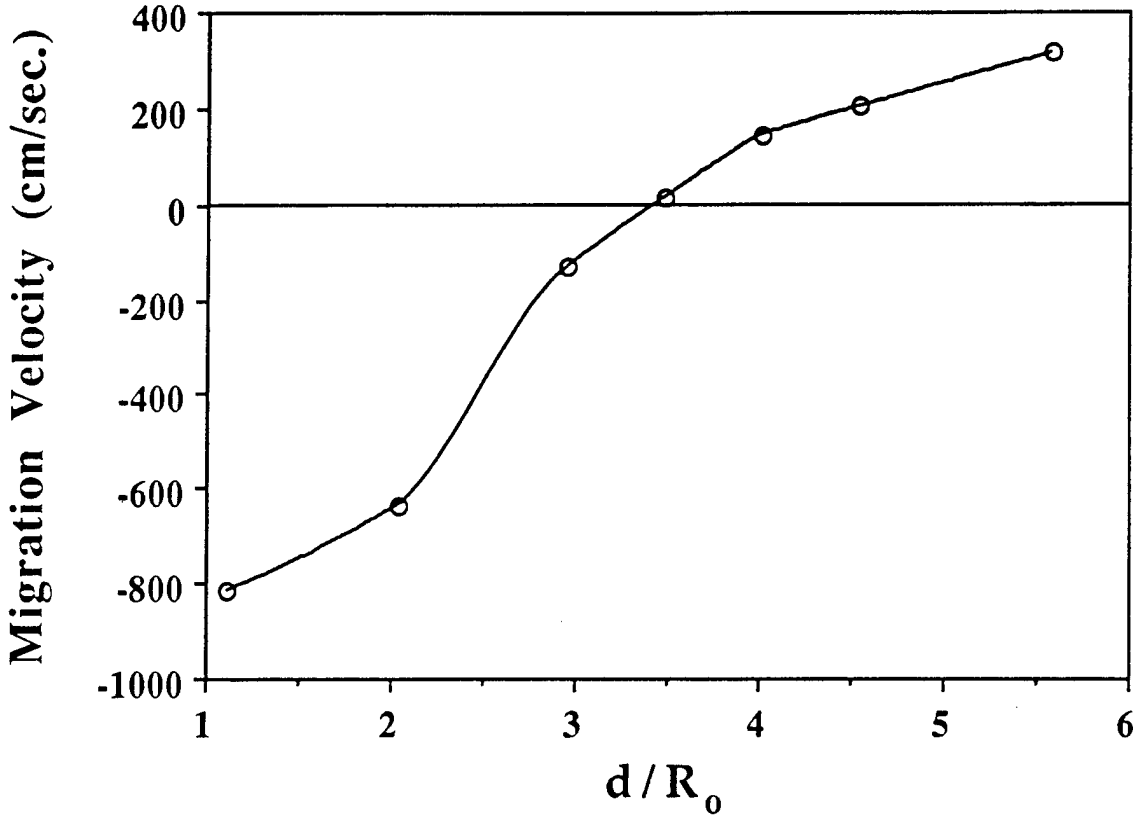
Migration Velocity (cm/sec.)
400
200
0
-200
-400
-600
-800
-1000
1
2
3
4
5
6
d / R0

Fig. 5

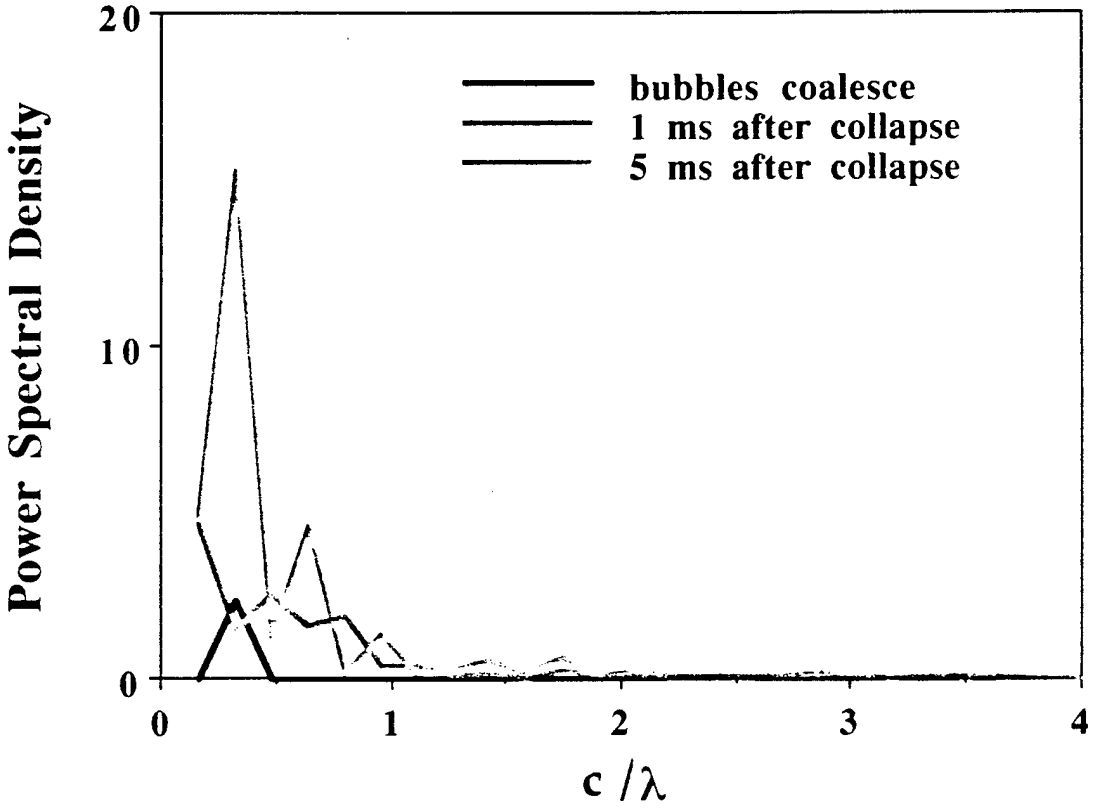
20
10
0
Power Spectral Density
bubbles coalesce
1 ms after collapse
5 ms after collapse
0
1
2
3
4
c /λ

Fig 5

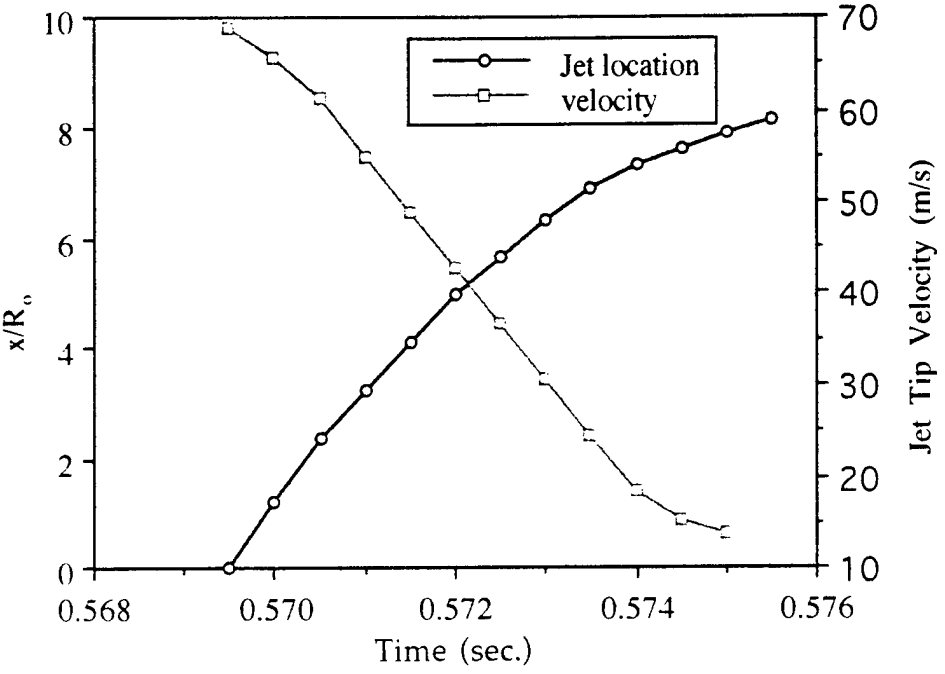
Jet location
velocity
x/R$_o$
Jet Tip Velocity (m/s)
Time (sec.)
0
2
4
6
8
10
10
20
30
40
50
60
70
0.568
0.570
0.572
0.574
0.576

Fig 7

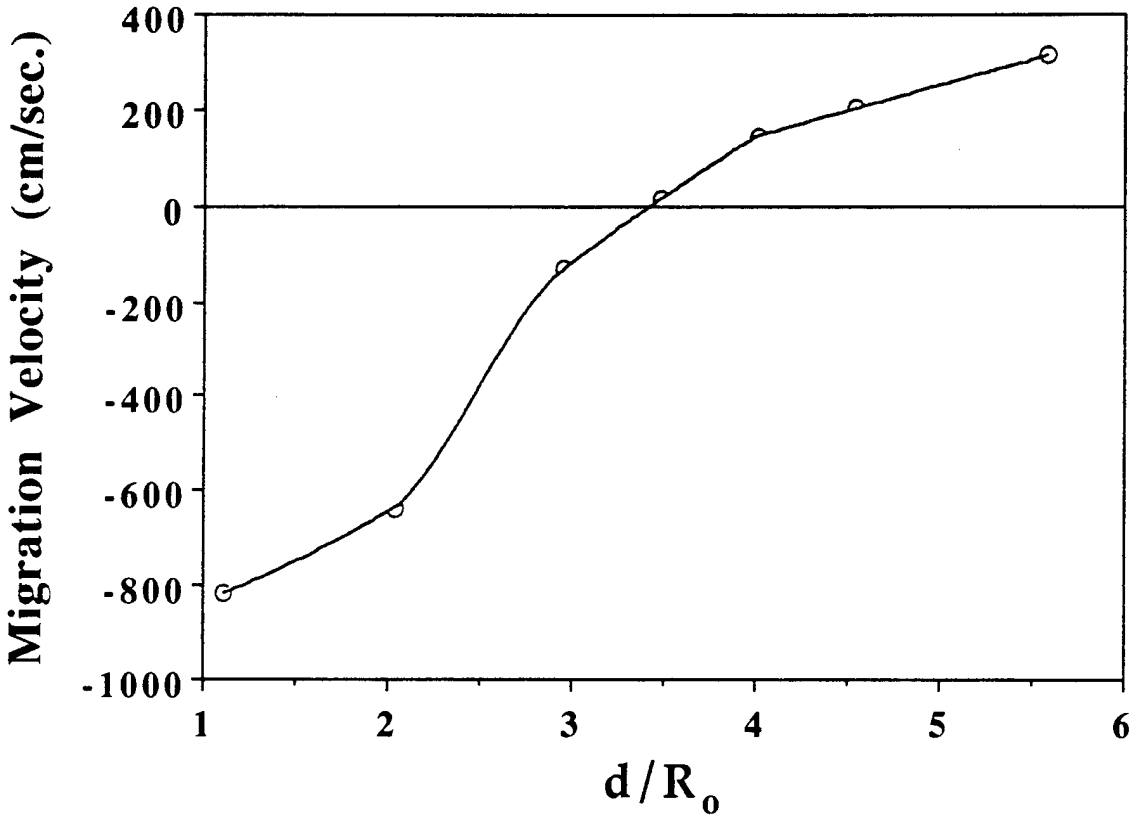
Migration Velocity (cm/sec.)
400
200
0
-200
-400
-600
-800
-1000
1
2
3
4
5
6
d/R0

Fig 8

# APPENDIX C

## Interaction of Two Underwater Explosion Bubbles

Proceedings of the 1996 ASME Fluids Engineering Division Summer Meeting
San Diego, California; July 7-11, 1996, FED Vol. II, pp. 595-600

# INTERACTION OF TWO UNDERWATER EXPLOSION BUBBLES

**Mihir K. Lal**

**Suresh Menon**

School of Aerospace Engineering
Georgia Institute of Technology
Atlanta, Georgia 30332
Phone: (404) 894-9126
Fax: (404) 894-2760
E-mail: menon@falcon.ae.gatech.edu

## ABSTRACT

Underwater explosion bubbles are created by detonating a mixture of oxygen and Carbon Monoxide or Hydrogen in glass globes submerged in a water tank. A cinematographic technique is employed to capture entire interaction process in both horizontal and vertical configurations. Depending on the delay between two explosions and inter-bubble distance, the bubbles may either attract each other to form a single coalesced bubble, or they may violently repel each other. A violent interaction leads to an increased instability of the bubbles. When a coalesced bubble is formed by merging the energies of two bubbles, the resulting bubble has more residual energy and is more stable for successive oscillations. An out-of-phase oscillation generates a reentrant water jet which pierces the bubble. Water free surface repels the bubble and the bubble migration speed and direction change smoothly as the explosion depth is continuously decreased.

## INTRODUCTION

Much of the research activities in the area of underwater bubble dynamics has been focused on the behavior of cavitation bubbles. Cavitation bubble dynamics play a very important role in underwater acoustics and in predicting and preventing propeller and turbine blade damage. These bubbles, however, seldom occur singly. Actual cavitation fields contain several thousands of oscillating and translating microbubbles. Study of the behavior of a cloud of bubbles thus becomes inevitable and experimental (Chahine and Sirian 1985), numerical (Chahine and Liu, 1985; Chahine, 1991; Chahine and Duraiswami, 1992) and analytical (Van Wijngaarden, 1972) techniques have all been developed. The simplest model that has been studied by the researchers is the interaction between two bubbles. Theoretical and numerical studies of the interaction of two spherical or nonspherical bubbles of same or different sizes (Fujikawa et al., 1985; Fujikawa and Takahira, 1986; Fujikawa and Takahira, 1988; Morioka, 1974; Shima, 1971) have been carried out. Interesting experimental observations of the interaction of a gas bubble with a pressure wave (Shima and Tomita, 1988) or with a vapor bubble (Smith and Mesler, 1972) have also been made.

Large bubbles, such as those formed during underwater explosion, owing to their tremendous inherent destructive capabilities upon collapse near a rigid boundary, find practical applications in underwater weaponry. These bubbles were recently simulated experimentally on a laboratory scale in a free field configuration (Menon and Lal, 1996).

The interaction of two underwater explosion bubbles is a very interesting and complex phenomenon, because of the fact that one bubble is influenced by time-delayed pressure or shock wave radiated from the adjacent bubble. Radial motion of the bubble may be greatly excited or subdued due to the interaction depending on their spatial and temporal separations. Though some experimental work have been done on the interaction of gas bubbles with two adjacent underwater explosion bubbles, and it has been shown that strong and complicated interactions ensue, it appears that no detailed results on the interaction of two underwater explosion bubbles have been published in the public domain literature.

This paper reports the results of the experiments carried out in a laboratory water tank to study the interaction between two adjacent bubbles created by underwater explosion of flammable gas contained in glass globes. The globes were placed side-by-side either in a horizontal or a vertical plane. The distance between the two globes and their sizes were both varied. This paper will also deal with the interaction of single and double explosion bubble(s) with the water free surface.

## EXPERIMENTAL PROCEDURES

Underwater explosion experiments were conducted in a wooden tank of dimension 2 m×1.5 m×1.5 m, coated with fiberglass resin from inside. The tank, as shown in Fig. 1, has three windows on three sides. The underwater explosion bubble is generated by centrally igniting a mixture of an explosive gas (either Hydrogen or Carbon Monoxide) and oxygen contained in a hand-blown glass globe. Three different sizes of glass globes have been used for present experiments with average radii of 2.9 cm, 3.2 cm, and 3.8

cm. The glass globe, as shown in Fig. 2, has an electric spark ignition system connected to a 3000V DC power supply. The explosion takes place at a constant volume until the globe bursts. It has been shown (Menon and Lal, 1996) with the help of geometric and dynamic scaling rules that the explosion bubble thus formed is a reasonable subscale approximation of the deep sea underwater explosion bubble.

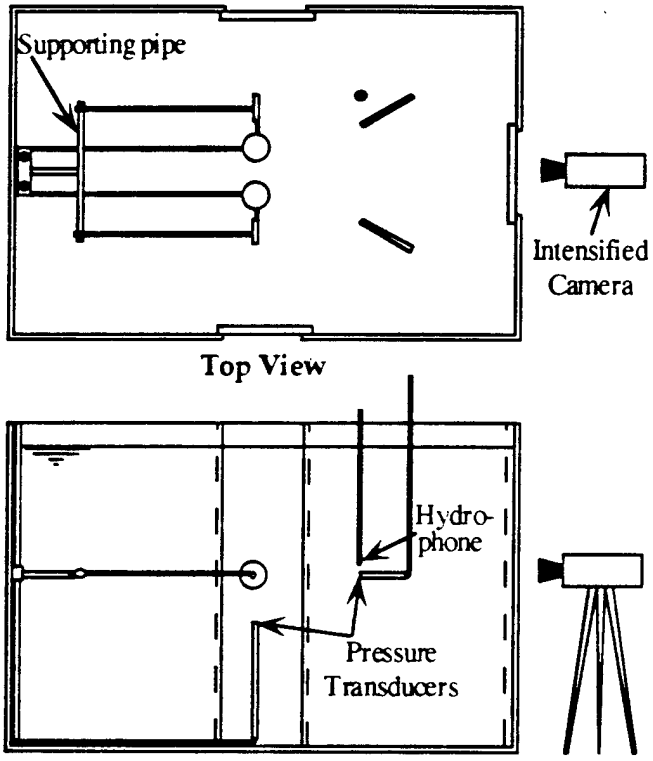


**Fig. 1. Experimental setup**

The pressure responses in the water around the bubbles are recorded during the experiments by means of 4 KISTLER dynamic piezoelectric pressure transducers fitted at the ends of 4 stainless steel (1.27 cm diameter) tubes bent at right angle, as shown in Fig. 1. A hydrophone is also mounted in the tank and is used for measuring acoustic pressure. Pressure inside the bubble during its oscillation is measured by another KISTLER transducer which is mounted inside the plug, as shown in Fig. 2. Signals from these six pressure transducers and the hydrophone are digitized using National Instrument's AT-MIO-16X analog-to-digital converter board, and are recorded into a microcomputer. Eight channel data recording are performed with a sustained sampling rate of 10,000 samples per second per channel.

The tank is illuminated by either direct overhead flood lights or an argon-ion laser sheet which lies in a vertical plane perpendicular to the camera axis. The optical recording of the bubble motion is performed by a CCD enhanced digital video camera with a maximum speed of 6000 frames per second. Since the viewable picture size is inversely proportional to the recording speed, the maximum speed was limited to 2000 frames per second as the image size reduces to half at this speed. Most of the experiments, however, were performed at the speed of 1000 frames per second (full screen image).

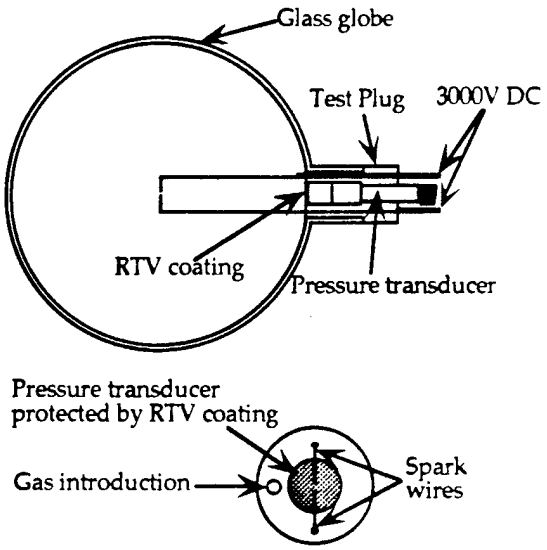


**Fig. 2. Glass bulb and test plug instrumentation**

The two glass globes are supported inside the tank by means of a modified sting which makes the pressure transducers mounted inside the two globes to face each other. This facilitates the direct measurement of the fluctuation in the pressure inside one bubble due to its interaction with the other. In order to provide a means for altering the distance between the two bubbles, six holes were drilled in the supporting copper pipe (1.6 cm diameter) of Fig. 1 at equal spatial separation from either ends. Experiments were conducted in primarily two configurations; a horizontal configuration, when the supporting pipe was horizontal, and a vertical configuration, when it was vertical. The former configuration prohibited the use of laser light sheet and only the flood lights were used for imaging, while the latter allowed the use of laser light sheet.

Experiments were also conducted to study the interaction of water free surface with the explosion bubble(s). The motivation for this kind of experiments has obvious reasons as detailed in the next section. The free surface provides a constant pressure boundary in close proximity of the oscillating bubble. It is known that the bubble moves away from the free surface and a reentrant jet is formed which pierces the bubble in the direction of its migration (Birkhoff, 1957; Blake and Gibson, 1981; Chahine, 1982; Wilkerson, 1989). Wilkerson (1989) developed a boundary integral technique for the analysis of expansion and collapse of an explosion bubble in free field, near a rigid surface, or near a free surface. To verify the accuracy of his method for predicting reentrant water jet tip velocities for a bubble near a free surface, he compared his results with a PISCES code calculation and expressed his inability to predict an accurate estimation of the error involved in his method because of the unavailability of any such experimental data. This observed lack of data motivated the current experiments to study the interaction of a free surface with an explosion bubble.

## RESULTS AND DISCUSSION

The interaction process is highly dependent on the time delays between the two explosions. These time delays are related to a variety of hardware and bubble response characteristics. The two globes have independent power supplies and there is always a time delay between the occurrence of the spark and when the bubble starts expanding. The bubble expansion occurs immediately after the glass globe bursts. The time delay depends primarily on the gas volume (globe size) and the nature of gas mixture inside the globe. A bigger globe size will create a larger time delay. Similarly, fuel-rich or fuel-lean mixtures will also create larger delays as compared to the one associated with a stoichiometric mixture. In addition to this delay, there is another time delay which is associated with the spark system itself. This delay is between the instant when the power is turned on and when the spark actually fires. This delay primarily depends on the actual gap between the two spark wires since a bigger gap creates a larger delay. The actual delay (temporal separation) between two explosions is therefore measured from the recorded video images as the time elapsed between the instant when the individual globe bursts. It was therefore deemed necessary to conduct several experiments to collect statistical information about the range of bubble behavior with respect to the delay between two explosions.

The entire spectrum of delay can be classified into two broad regions and they are called in-phase oscillation and out-of-phase oscillation (Morioka, 1974; Shima, 1971; Smith and Mesler, 1972). In most of the past analytical, numerical or even experimental work on the interaction of two cavitation bubbles, interest has been focused primarily on the contraction phase of the bubble oscillation. This yields an in-phase oscillation of the bubbles as they both start collapsing at the same time following a sudden change in the ambient pressure. In-phase oscillation is obtained when there is strictly no delay between the explosions and both the bubbles start their oscillation cycle at the same time. Of course, it is assumed that the two bubbles have identical time period of oscillation and they are in identical phase at any instant throughout their oscillation cycle. This is the simplest scenario and has been analyzed comprehensively.

Another interesting scenario is 180° out-of-phase oscillation and it can be best understood in the interaction of two identical explosion bubbles as a case where one bubble starts its oscillation cycle when the other has already reached its maximum radius. In fact, these are the two scenarios predicted by the analytical theories (Morioka, 1974). Morioka's (1974) theoretical analysis of natural frequencies of two pulsating bubbles predicts the existence of two natural frequencies corresponding to in-phase and 180° out-of-phase oscillations, respectively. Of course, in an experimental setup one can have any amount of delay between zero to 180°, or beyond.

The behavior of explosion bubbles under these two scenarios have long been predicted (Birkhoff, 1957; Bjerknes, 1906; Cole, 1948; Young, 1989) and it is called the laws of Bjerknes. Bjerknes showed in 1868 that two spheres pulsating in-phase attract each other, and those pulsating 180° out-of-phase repel each other. Two spheres collapsing in-phase are equivalent to a single sphere collapsing near a rigid surface at a distance which is exactly equal to the half of the distance between two spheres. Similarly, two spheres oscillating 180° out-of-phase are equivalent to a single sphere pulsating near a free surface at a distance equal to half of the distance between two spheres. It has been shown (Birkhoff, 1957) that the migration speed of the bubble towards a rigid surface or away from a free surface is inversely proportional to $r^3$, where r is the instantaneous bubble radius. Therefore, most of the migration would take place when the bubble radius is small (i.e., when the bubble is collapsing and approaching its minimum radius). Also, Bjerknes (Bjerknes, 1906; Young, 1989) showed as an analogy with gravitational and electromagnetic forces that the attractive force, $F$, between two bubbles of volumes $V_1$ and $V_2$ a distance $d$ apart in a pressure field is given by $F \propto V_1 V_2 / d^2$. Since the bubble migration velocity is directly proportional to the attractive force, its magnitude is expected to increase for bigger bubbles pulsating out-of-phase at a shorter inter-bubble distance, and decrease for smaller bubbles at a larger distance.

Fig. 3 shows a perfect example for two underwater explosion bubbles oscillating in-phase. The numbers in the parentheses denote the frame numbers, with frame number 1 corresponding to the instant when the sparks are visible for the first time. The initial volume of the right glass globe is 94 ml and that of the left glass globe is 90.5 ml. They are in a horizontal configuration and are initially separated by a distance $d$, where $d/R_o = 2.32$. Here $R_o$ is the initial bubble radius, which is taken to be the radius of the glass globe. Both are filled with stoichiometric mixture of Carbon Monoxide and Oxygen. It can be seen in Fig. 3 that there is virtually no delay between two explosions. Since the initial spatial separation between the globes was intentionally kept to a very small value so that a violent interaction can ensue, the bubbles soon come in contact with each other. They deviate more and more from sphericity as they expand with time. Fig. 4(a) shows how different radii of the left bubble change with time. A similar behavior is exhibited by the right bubble. The deviation from sphericity is more clearly demonstrated in Fig. 4(b), where the time history of the ratio of major and minor radii is plotted. As is evident from this figure, the bubbles quickly deviate from sphericity and the maximum deviation is attained at around frame no. 11. This deviation slowly diminishes and the bubbles become nearly spherical at around frame no. 21. When the bubbles merge together to form a single coalesced bubble, it becomes difficult to isolate them individually.

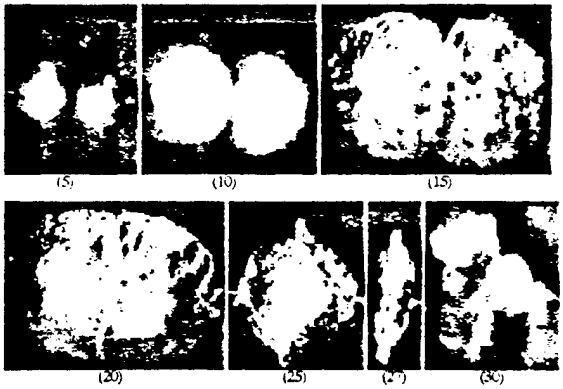


**Fig. 3. In-phase oscillation**

The surface where the two bubbles come in contact in Fig. 3 grows in size as the bubbles grow and is initially curved. The bubbles reach their maximum radii at around frame no. 18 and start collapsing thereafter. The surface of contact slowly becomes a plane surface around frame no. 21 and remains so thereafter until the bubbles collapse near frame no. 28. This plane surface of contact may be considered as a rigid surface in an equivalent single bubble

analogy. This surface is almost perpendicular to the line joining the initial globes' centers and is located almost midway.

The frames shown in Fig. 3 have been recorded at a speed of 1000 frames per second. The time period of oscillation of the bubbles is found to be about 21 ms, while that of an identical bubble in free-field is less than 15 ms (Menon and Lal, 1996). Therefore, for two identical bubbles oscillating in-phase, an increase in the bubble period is observed (Chahine, 1991).

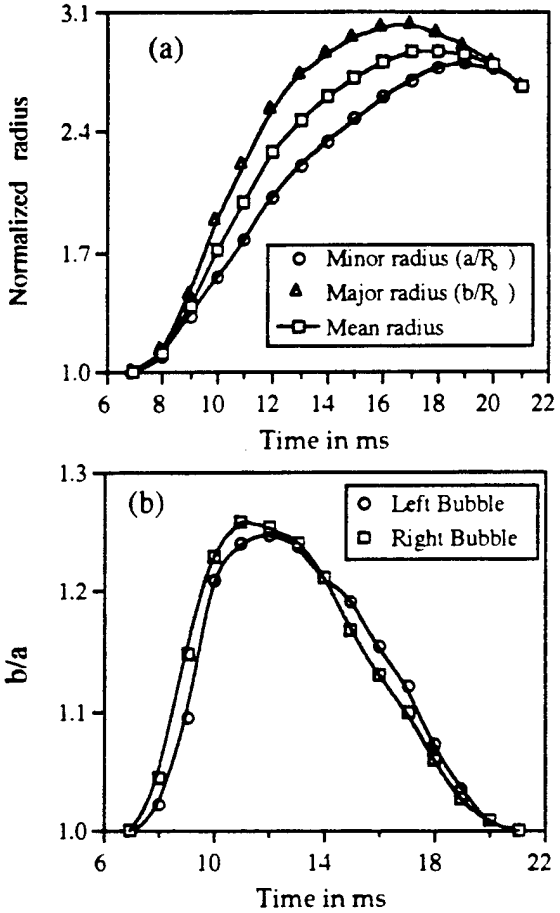


**Fig. 4. (a) Different radii of the left bubble. (b) Ratio of major and minor radii.**

The collapse is very violent (as recorded by two plug transducers) and the coalesced bubble quickly disintegrates into a cloud of bubbles. The bubble contour is traced and 360 bubble radii are obtained at equal azimuth locations. A mean radius is obtained from this data, which is used to normalize the radii data. These data are then Fourier analyzed and the results are shown in Fig. 5, which shows the power spectral density of the coalesced bubble's interface at three instants: just after it is formed and 1 and 5 ms after it collapses. Here c is the bubble circumference and $\lambda$ is the wavelength. The coalesced bubble is therefore very unstable.

The pressure traces measured around the bubbles show that the bubble behavior is symmetrical. A pressure fluctuation of about 700 kPa exhibited by the plug transducers near bubble minimum demonstrates the severity of the collapse of the jets formed in the two bubbles onto each other. The pressure drops exponentially as one moves away from the bubble (Cole, 1948). A pressure drop of 70% (from 1000 kPa to 300 kPa) over a distance of 14 cm, and that of 80% (from 1000 kPa to 200 kPa) over a distance of 34 cm from the bubble center have been recorded by tank transducers.

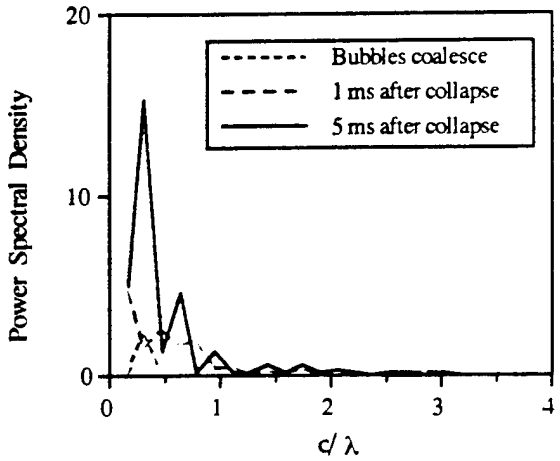


**Fig. 5. Power spectral density of the bubble.**

A single coalesced bubble does not form only in an in-phase oscillation. Another situation where the formation of a single coalesced bubble has been observed repeatedly and most surprisingly, is associated with a nonzero time delay and a very short inter-bubble distance. This case is shown in Fig. 6. The initial volume of the right glass globe is 125 ml and that of the left glass globe is 127 ml. They are almost touching each other such that the initial separation distance between them, $d$, is given by $d/R_o = 2.1$. Both of them are filled with stoichiometric mixture of Carbon Monoxide and Oxygen. The right globe explodes first (around frame no. 11) and tries to encompass the left globe as the bubble grows. The left globe explodes near frame no. 19 and the shock wave emitted by this bubble travels through the right bubble as is evident by its protruding pieces (frames 21,24). The right bubble, however, maintains its coherence and sphericity. It seems that the energy of the left bubble is substantially transferred to the right bubble. A force field is generated such that when the right bubble starts to collapse, the left bubble just merges into its predecessor to form a single coalesced bubble, which continues the oscillation cycle as a single explosion bubble. Since no jets are formed and the coalesced bubble is formed by merging the energies of two bubbles, it has more residual energy than that of the previous example and does not disintegrate into smaller bubbles so quickly. In fact, it is even more stable than a single explosion bubble in free field.

The effect of the shock wave generated during the formation of the right bulb is reflected by a 150 kPa peak in the left plug transducer pressure trace. On the other hand, the expanding right bubble acts as a screen for the propagation of the shock wave generated during the formation of the left bubble, and this is reflected by a tiny fluctuation of 10 kPa in the right plug transducer pressure trace. It is very interesting to note that the explosion pressure for the left bubble (200 kPa) is only about 20% of what it would have been in a free field case. Thus, an expanding bubble inhibits the formation of another explosion bubble in its close proximity by reducing its explosion pressure. This is the reason

why the left bubble does not have sufficient energy to expand to its maximum radius. But, it certainly aids its predecessor to form a coalesced bubble with a greater energy to collapse violently and this fact is captured by all the transducers and hydrophone in the form of elevated collapse peaks. This time, the right plug transducer lies inside the coalesced bubble as it collapses (see Fig. 6, frame no. 27). The collapse pressure recorded by this transducer is very high (2500 kPa). The pressure traces recorded by this right and left transducers are once again almost identical, indicating a symmetrical bubble behavior.

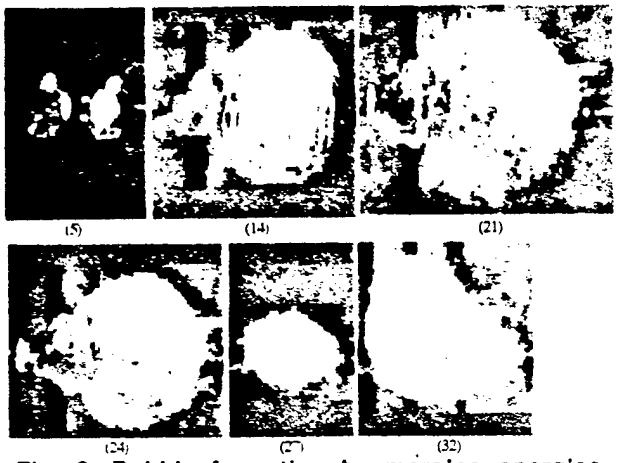


**Fig. 6. Bubble formation by merging energies.**

Similar dynamic behavior is exhibited by the interaction of bubbles formed by glass globes of initially different sizes. It is not possible, however, to obtain an in-phase oscillation because of a simple reason that the two bubbles have different time periods of oscillation. On the other hand, the bubble dynamics observed where the coalesced bubble is formed by merging the energies of two bubbles have been exhibited by the bubbles of different sizes where the small bubble has been gobbled up by its predecessor large bubble. This kind of bubble dynamics is not feasible for large inter-bubble distance.

When the inter-globe distance is sufficiently large, the bubbles start repelling each other for a nonzero time delay. The repulsion force increases with the delay between the explosions, up to the point when they are oscillating 180° out-of-phase. In such cases, the formation of a strong reentrant water jet in the successor bubble is observed with increasing magnitude. Figure 7 shows how this reentrant jet travels with time for a case of 180° out-of-phase oscillation. Here x denotes the location of the jet tip relative to the inertial frame (the tank) and x = 0 corresponds to the instant when the jet tip becomes visible for the first time. As the phase delay between two explosions increase beyond 180°, the repulsion force as well as the water jet velocity decrease in magnitude. If the phase delay between two explosions increase beyond 360° (i.e., if one bubble has already completed one oscillation cycle when the other bubble forms), the resulting interaction is very weak. In this case, though the predecessor bubble manages to create a depression in successor bubble at its maximum radius, neither a jet nor a repulsion force is formed.

The horizontal configuration is very important from a practical standpoint, as it can set a catastrophic bending vibration to a nearby rigid body if tuned properly. The research effort is being pursued in this direction. The vertical configuration is also equally important, as it can dramatically enhance the impact pressure of a single bubble when collapsed near a rigid body. If two bubbles are placed close to each other along an axis perpendicular to a nearby rigid body, and if these two bubbles are tuned to oscillate 180° out-of-phase with each other, a water jet will be formed and directed towards the rigid surface with a velocity which will be higher than that formed by the collapse of a single bubble under similar circumstances. This is also being studied.

The bubble dynamics in vertical configuration in the present study (in the absence of any nearby rigid body), however, does not show a remarkable difference from that of horizontal counterpart. This is because of the fact that only the orientation of the gravitational force changes between two configurations. In practical cases, the force field generated by the bubbles is much more stronger to be affected negligibly by the gravitational force.

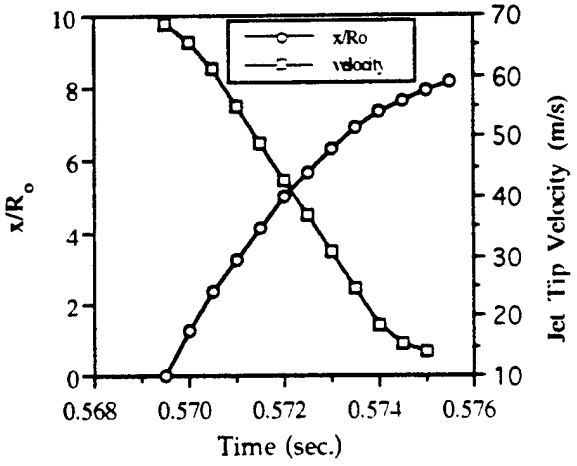


**Fig. 7. Water jet tip location and velocity**

## Bubble(s)-Free Surface Interaction

Since it was shown earlier that two bubbles oscillating 180 ° out-of-phase are equivalent to a single bubble oscillating near a free surface, experiments were carried out to study the interaction of a free surface with explosion bubble(s). Figure 8 shows the transition of bubble migration velocity with water depth.

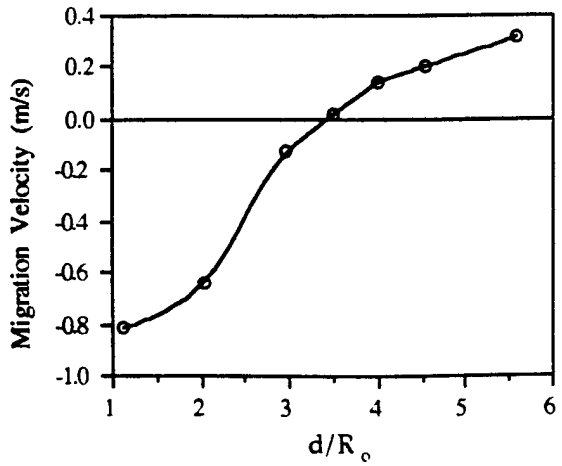


**Fig. 8. Bubble migration velocity with water depth.**

A simple sting mount was used to support a glass globe and the depth of water in the tank was decreased in a step of 2.54 cm. It was found that the bubble migration velocity smoothly changes its direction as well as its magnitude. The transition point determines the maximum inter-bubble distance *(2d)* for which two identical bubbles will start interacting while oscillating 180° out-of-phase with each other. It is found that $d = 3.4R_o$.

Both out-of-phase and in-phase oscillation of two explosion bubbles in a horizontal configuration near a free surface were also studied. The bubbles oscillating out-of-phase with each other repel each other and the effect of the free surface becomes apparent only after they have been repelled by each other. This once again indicates that the force field generated by the interaction between two bubbles is much stronger than that of a free surface and there have been instances where one of the bubbles actually migrates upward.

## CONCLUSIONS

This paper discusses results obtained in an experimental investigation of the dynamical interaction of two underwater explosion bubbles in both horizontal and vertical configurations. The former configuration can excite a nearby submerged structure in bending vibration mode, while the latter can easily be tailored for the directionality and enhancement of the impact pressure resulting from the collapse of an underwater explosion bubble near a solid boundary. Depending on the delay between two explosions and inter-bubble distance, the bubbles may either attract each other to form a single coalesced bubble, or they may violently repel each other. A violent interaction between the bubbles leads to an increased instability of the bubbles. If a coalesced bubble is formed by merging the energies of two bubbles, the resulting bubble has more residual energy and is more stable for successive oscillations. An out-of-phase oscillation generates a reentrant water jet which pierces the bubble. Water free surface repels the bubble and the transition point of bubble migration velocity determines the maximum inter-bubble distance required for the initiation of interaction between two out-of-phase pulsating bubbles.

## ACKNOWLEDGMENT

This work is supported by the Office of Naval Research under Grant No. N00014-91-J-1963 and monitored by Drs. Richard Miller and Judah Goldwasser.

## REFERENCES

Birkhoff, G., and Zarantonello, E. H., 1957, "Jets, Wakes, and Cavities," Academic Press Inc, New York, pp. 241-243.

Bjerknes, V. F. J., 1906, "Fields of Force," Columbia University Press, New York.

Blake, J. R., and Gibson, D. C., 1981, "Growth and Collapse of a Vapor Cavity near a Free Surface," Journal of Fluid Mechanics, Vol. 111, pp. 123-140.

Chahine, G. L., 1977, "Interaction Between an Oscillating Bubble and a Free Surface," Journal of Fluids Engineering, Vol. 38, pp. 709-716.

Chahine, G. L., 1982, "Experimental and Asymptotic Study of Nonspherical Bubble Collapse," Applied Scientific Research, Vol. 38, pp. 187-197.

Chahine, G. L., and Liu, H. L., 1985, "A Singular Perturbation Theory of the Growth of a Bubble Cluster in a Superheated Liquid," Journal of Fluid Mechanics, Vol. 156, pp. 257-279.

Chahine, G. L., and Sirian, C. R., 1985, "Collapse of a Simulated Multibubble System," ASME, Cavitation and Multiphase Flow Forum, Albuquerque, New Mexico, pp. 78-81.

Chahine, G. L., 1991, "Dynamics of the Interaction of Non-Spherical Cavities," Mathematical approaches in Hydrodynamics, T. Miloh, ed., Society for Industrial Applications of Mathematics, Philadelphia, pp. 51-67.

Chahine, G. L., and Duraiswami, R., 1992, "Dynamical Interactions in a Multi-Bubble Cloud," Transactions of the ASME, Vol. 114, pp. 680-686.

Cole, R. H., 1948, "Underwater Explosions," Princeton University Press, Princeton.

Fujikawa, S., Takahira, H., and Akamatsu, T., 1985, "Underwater Explosion of Two Spherical or Nonspherical Bubbles and Their Interaction With Radiated Pressure Waves," Shock Waves and Shock Tubes, Proceedings of the Fifteenth International Symposium, Berkeley, CA, pp. 737-744.

Fujikawa, S., and Takahira, H., 1986, "A Theoretical Study on the Interaction between Two Spherical Bubbles and Radiated Pressure Waves in a Liquid," Acustica, Vol. 61, pp. 188-199.

Fujikawa, S., and Takahira, H., 1988, "Dynamics of Two Nonspherical Cavitation Bubbles in Liquids," Fluid Dynamics Research, Vol. 4, pp. 179-194.

Menon, S., and Lal, M. K., 1996, "On the Dynamics and Instability of Bubbles Formed During Underwater Explosions," Submitted to International Journal of Engineering Fluid Mechanics.

Moroika, M., 1974, "Theory of Natural Frequencies of Two Pulsating Bubbles in Infinite Liquid," Journal of Nuclear Science and Technology, Vol. 11, pp. 554.

Shima, A., 1971, "The Natural Frequencies of Two Spherical Bubbles Oscillating in Water," Journal of Basic Engineering, Vol. 93, pp. 426-432.

Shima, A., and Tomita, Y., 1988, "Impulsive Pressure Generation by Bubble/Pressure-Wave Interaction," AIAA Journal, Vol. 26, No. 4, pp. 434-437.

Smith, R. H., and Mesler, R. B., 1972, "A Photographic Study of the Effect of an Air Bubble on the Growth and Collapse of a Vapor Bubble near a Surface," Journal of Basic Engineering, pp. 933-942.

Van Wijngaarden, L., 1972, "On the Collective Collapse of a Large Number of Gas Bubbles in Water," Proceedings of the 11th International Congress of Applied Mechanics, Springer, Berlin, pp. 854-865.

Wilkerson, S. A., 1989, "Boundary Integral Technique for Explosion Bubble Collapse Analysis," Energy-Sources Technology Conference and Exhibition, 89-OCN-2, Houston, Texas, pp. 1-12.

Young, F. R., 1989, "Cavitation," McGraw-Hill Book Company (UK), The Alden Press, Oxford.

# APPENDIX D

## Simulations of Underwater Explosion Bubble Dynamics using an Arbitrarily Lagrangian-Eulerian Formulation

*Paper presented for review for(Symposium) presentation at the 1997 ASME Fluids Engineering Summer Meeting, Vancouver, BC, Canada, June 22-26,1997*

# SIMULATIONS OF UNDERWATER EXPLOSION BUBBLE DYNAMICS USING AN ARBITRARY LAGRANGIAN-EULERIAN FORMULATION

**Suresh Menon**
**Sreekanth Pannala**

Georgia Institute of Technology
Atlanta, Georgia 30332-0150
(404)-894-9126
(404)-894-2760(FAX)
menon@falcon.ae.gatech.edu

## ABSTRACT

The dynamics of bubbles formed during underwater explosions are numerically investigated using an Arbitrary Lagrangian-Eulerian three-dimensional finite-element code and compared with experimental data. Both experimental and numerical results show good qualitative and quantitative agreement and suggests that the excitation of Rayleigh-Taylor instability is a major cause of interface instability. Simulations have also been carried out to investigate bubble-bubble interactions. Results show the formation of a water jet as one bubble collapses into the other, in agreement with recent experimental observation. Finally, the collapse of a bubble near a rigid wall and the formation of high velocity re-entrant jet onto the wall have been successfully simulated. The well known vortex ring bubble during the collapse process has been numerically captured.

## 1. INTRODUCTION

Vapor and gas bubble dynamics are of great practical interest in the prediction and prevention of cavitation erosion of marine propeller and turbine blades. The destructive nature of strong underwater explosions near walls is well known. Detailed reviews (e.g., Blake and Gibson, 1987; Prosperetti, 1982) have summarized past experimental and numerical results. Experimental studies are too many to list completely; however, most past studies focused on cavitation (small) bubbles. Among the studies that focused on large scale explosions are the studies reported in Cole (1948) for freely oscillating, deep sea explosion bubbles and the studies of bubble collapse near walls (e.g., Tomita and Shima, 1986). Bubble-bubble interactions have also been studied in the past (e.g., Warren and Rice, 1964). However, in most cases, due to difficulties in acquiring detailed data, only limited information has been obtained. Recently, experiments were carried out to investigate large-scale bubble explosions (Menon and Lal, 1996; Lal and Menon, 1996a, b). These experiments were conducted in shallow water due to an interest in understanding the dynamics of bubble-wall interaction in such flows and to investigate the feasibility of targeting buried mines for destruction in beaches. The data obtained from these experiments have been used to validate the numerical model discussed in this paper.

Numerical studies in the past range from simple 1-D analytic solutions (e.g., Lauterborn, 1976; Plesset, 1971; Prosperetti, 1982) to more complex 2D/3D studies. Many studies employed the Boundary Element Method (BEM) or its variants (e.g., Chahine and Perdue, 1988; Duncan and Zhang, 1991; Blake et al., 1986, Plesset and Chapman, 1970). This method has some inherent limitations. For example, compressibility in the gas cannot be included and in the study of bubble collapse near a surface, BEM can be used only up to the point of jet formation. To model the flow beyond the point of bubble collapse, BEM has been modified by introducing vortex elements (e.g., Zhang and Duncan, 1994; Zhang et al., 1993; Best and Kucera, 1992; Best, 1993). Furthermore, to set up this problem, recourse to experimental observation is required to obtain characteristic parameters. Such an approach is not general and cannot be used when the details of the explosion dynamics is unknown.

There are other assumptions used in past studies that are known to be in error. For example, significant compressible effects are known to occur in the collapse phase especially in deep sea strong explosions. Bubble shape is also known to quickly deviate from sphericity at bubble maximum, thereby, violating axisymmetric assumptions used in the past (e.g., Szymczak et al., 1993; Zhang and Duncan, 1994) and requiring full 3D treatment. Thus, simple 1-D or 2-D/axisymmetric analysis or incompressible methods cannot completely resolve the bubble and the flow dynamics. Furthermore, such simplified treatments also do not to provide details of the flow field inside and outside the bubble and cannot account for the interaction between the vapor and the liquid phases. Conventional numerical treatments (even using full 3D) such as Lagrangian or Eulerian techniques are also not practical, since the expansion and collapse of bubbles create severe fluid motion so that a Lagrangian approach (in which the grid points move with the fluid resulting in severe grid distortion) becomes inappropriate, while in an Eulerian approach, adequate resolution in the regions of interest is very difficult to achieve since the bubble's shape changes very rapidly.

A numerical method that includes both compressibility and an ability to capture the entire bubble collapse in complex configuration

is used in this study. This numerical code(ALE3D) combines lagrangian and eulerian features and is based on the Arbitrary Lagrangian-Eulerian (ALE) scheme and is developed at the Lawrence Livermore Lab. Past applications of this method include the 2D (e.g., Tipton, et al., 1992) and the full 3D (Milligan et al., 1995) studies of bubble collapse. However, it appears that so far, the full capabilities of the ALE3D have not yet been exploited to simulate and investigate the dynamics of underwater explosions. This paper reports some recent results of both single and double bubble explosions both in free field and in the vicinity of a rigid wall.

## 2. THE NUMERICAL METHOD

ALE3D (Anderson et al., 1994) is an explicit, 3D finite element code that simulates the fluid motion and elastic-plastic response on an unstructured grid. The grid may consist of arbitrarily connected hexahedral shell and beam elements. The ALE algorithm is implemented by carrying out a complete Lagrangian calculation followed by an advection step. After each lagrangian step, a new mesh is created using a finite element based equipotential method to relax the distorted grid. In the eulerian advection step, the fluid variables such as mass, density, energy, momentum and pressure are reevaluated on the new mesh by allowing fluid motion. The details of the constitutive models are described elsewhere (e.g., Steinberg, 1991) and, therefore, are not described here for brevity.

The advection step uses a second order, monotonic advection algorithm. This can create mixed material elements (i.e., liquid and vapor). Material interfaces are not explicitly tracked but for the purpose of carrying out mixed element advection, they are inferred from volume fractions. Separate state variables are kept for each component of a mixed element.

## 3. RESULTS AND DISCUSSION

In this section, the results obtained for the various test cases are summarized and discussed. These studies serve to identify the capabilities and limitations of the ALE3D code and to identify areas for further study.

### 3.1 Free Field Single Bubble Oscillation

This simulation employed test conditions similar to the experimental set-up of Menon and Lal (1996) and is modeled as a freely oscillating bubble placed in the center of a 1.5 m x 1.5 m x 1.5 m tank filled with water. The initial bubble diameter is 6.34 cm and the initial explosion pressure is 9.34 atmospheres. The water pressure is 1 atmosphere. The ALE mesh treatment is applied to all the elements in the bubble and in the vicinity of the bubble. But away from the bubble where the bubble explosion does not cause much grid distortion, lagrangian mesh treatment is used. The number of elements used to resolve the bubble and the surrounding water was varied to confirm that the results are grid independent. For a typical 3D simulation, 64512 elements were used to discretize the domain., but as many as 150000 elements were used for carrying out the grid independence tests for this test case. Although various cases have been simulated, only characteristic results are discussed below.

The bubble grows after the explosion due to the high vapor pressure inside the bubble. Because of inertia, this results in an over expansion and the pressure inside the bubble falls below the ambient (water) pressure. As a result, the bubble collapses and reaches a bubble minimum at which time the internal pressure again exceeds the external pressure. Thus, a bubble oscillation process is set up and continues as long as there is sufficient energy available. However, energy is continuously lost during the oscillation due to irreversible mechanical work done on water and vapor and due to the onset of various instabilities. Detailed analyses of the losses and the instability mechanisms were performed earlier (Menon and Lal, 1996) and results suggest that during the collapse process the Rayleigh-Taylor (R-T) instability occurs at the interface. This results in a distortion of the vapor-water interface. This phenomenon has been captured in the numerical study. For example, Figs. 1a and 1b shows snapshots of bubble at the first maximum and the first minimum. As can be seen, near the bubble minimum, wave-like distortion appears along the bubble interface. Figures 2a-b show the corresponding velocity vector field inside and outside the bubble. Figure 2a shows the outward motion of the bubble just before the bubble maximum and Fig. 2b shows the outward motion of the bubble just after the first bubble minimum. The magnitude of the velocity vectors also indicate that the acceleration of the fluid is minimum at the beginning and end of compression or expansion phases.

The deviation from sphericity and the formation of waves on the bubble interface are characteristics of Rayleigh-Taylor instability. To ensure that this interface distortion is not due to acoustic reflections from the wall, calculations were carried out by moving the wall further and by replacing the rectangular domain by a spherical domain. Results showed that, although there are changes in the bubble oscillation period, the interface distortion appears near the bubble minimum in all cases. The R-T instability can also be inferred by analyzing the variation of the radius with time. For example, Fig. 3 shows the region (near bubble minimum) where $d^2R/dt^2 > 0$ (which is a necessary condition for R-T instability).

Figure 4 compares the pressure history during the first oscillation in the bubble with experimental data (Menon and Lal, 1996). It can be seen that the computed first period of oscillation (around 15 ms), the peak pressure (at first bubble maximum) and the maximum radius (at bubble maximum) agrees well with data. The differences during the contraction phase may be due to differences between the two setups. For example, the experimental set-up employed a glass globe (which contained the stoichiometric fuel-air mixture) with a metal insert that contained the pressure transducer and the spark generator while these features were ignored in the numerical model. In addition, the effect of glass fragments (during the explosion) have not been included in the numerical model.

Figure 5a shows the time trace of pressure in the tank away from the bubble and close to a wall. It is very similar to the high frequency pressure oscillations as recorded by the tank transducer in the experiments (Menon and Lal, 1996) and is shown in Fig. 5b. The slight differences in the two plots may be attributed to the idealization of the tank as a cube with walls all around( whereas, for the experiment, the top surface was a free surface; see below).

As mentioned earlier, simulations were carried out to ensure grid independence, and to confirm that the presence of walls do not effect the overall dynamics. It has been determined that the presence of walls does effect (decrease) the oscillation period; however, the bubble dynamics are captured relatively accurately. To simulate true free field explosion requires using outflow boundary conditions on the far wall or by moving the walls far enough to minimize the impact of the acoustic reflection. However, at present, the ALE3D code requires that the far field boundary be modeled as a solid reflecting wall. This limitation of the code can be removed only by modifying the source code. This is will be investigated in the future.

To extend the applicability of ALE3D to real underwater explosions is quite trivial. To demonstrate this capability a deep sea underwater explosion was simulated using pentolite as the explosive.

The time period (not shown) scales as approximately two times the non dimensional time based on the maximum radius of the bubble, the ambient(water) pressure and the water density $\left(R_{max}/\sqrt{\frac{P_\infty}{\rho_w}}\right)$, as found in the above simulations and earlier studies (eg. Chahine and Perdue,1988 ).

### 3.2 Bubble-Bubble Interactions

To investigate bubble-bubble interactions, a series of studies were carried out using bubbles of various sizes. A limitation of the current ALE3D code is that it does not allow phase difference between the two explosions to be incorporated into the model. However, by using different bubble sizes (or using different explosive strength) the net effective energy release from each bubble can be varied. The effect of inter-bubble distance on the interaction process was also studied. Due to space limitation only characteristic results are discussed below.

When two identical bubbles (of initial radii 3.17 cm and placed 8 cm apart) are exploded the bubbles expand and then collapse onto each other and a reentrant water jet with a high speed (30 m/s) is formed in both vertical and horizontal directions. Figures 6a-c show snapshots of the bubble-bubble interaction and the corresponding velocity fields are shown in Figs. 7a-c, respectively. Fig. 8a-c show photographs from the experiments (Lal and Menon, 1996a) for the present case with two bubbles of same size exploding in phase with each other. Although not clearly seen in the experimental Fig. 8c, studies have show the presence of vortex ring bubble. The jet directed towards the adjacent bubble impinges on its counterpart as in a stagnation point flow. As the bubble-bubble process continues, two counter vortex rings are formed with the velocity between the bubble increasing to as high as 50 m/s. There is reasonable agreement between the experimental observations and the present computations.

When same size bubbles were exploded at the same distance as before, but with one bubble containing four time more energy than the other, a similar result was obtained except that in this case, the weaker bubble is sucked into the other bubble with a velocity reaching a maximum of around 85 m/s (not shown). The reentrant waterjet is first formed in the weaker bubble during the first oscillation and the vortex ring thus formed merges into the (still coherent) stronger bubble. The jet formation in the stronger bubble is delayed until the second oscillation, at which time the second bubble also collapses.

When two bubbles of different size (e.g., of radii 3.17 cm and 2.17 cm (and thus, with different total explosion energy) are exploded, the results are quite similar to the case discussed above. During the expansion phase, the greater inertia and explosion strength of the bigger bubble inhibits the smaller bubble. During the collapse, the pressure drop in-between the bubbles is more than on the other sides and this pressure differential causes the smaller bubble to be engulfed into the larger bubble. The center of motion of the water jet directed towards the bubbles does not immediately adjust to the motion of the bubbles and, thus, the water motion is directed off center of the bubble. This creates a very high pressure on the side of the smaller bubble away from the larger bubble. This high pressure and the low pressure in-between the bubbles creates enough momentum to form a water jet through the bubbles which penetrates to the other side of the bubble. Final stage of the jet formation is shown in Figs. 9a and 9c.

The velocity vector field shows the formation of the water jet in agreement with experimental study (Lal and Menon, 1996a). A water jet was also observed in the experiments when two identical bubbles were exploded out-of-phase, as shown in Fig. 9b. Out-of-phase explosion essentially changes the relative strength of the bubble explosion during interaction and is, therefore, similar to the present case with two unequal bubbles exploding simultaneously and the similarities can be seen in Figs. 9a-c. However, as mentioned earlier, the current ALE3D code cannot simulate phase difference between the adjacent explosions. This feature will be included in the code at a later date.

Finally, Fig. 10 compares the pressure between the two bubbles for the various test cases. All cases have the same period of oscillation. However, the case with increased energy content shows the strongest water jet formation (around 85 m/s) and the largest impact pressure at the first bubble minimum.

### 3.3 Bubble-Wall Interactions

Bubble collapse near a rigid wall is of significant interest due to a variety of reasons related to its ability to cause serious damage to the structure. This is because when the bubble collapses near a rigid surface, a strong reentrant water jet is formed that is directed towards the wall. The peak impact pressure on the wall due to this water jet can be substantially higher that the explosion pressure especially when the initial explosion energy is very large. Various simulations were performed by varying the explosion strength and distance of the bubble from the rigid plate. However, only characteristic results are discussed here to highlight the pertinent observations.

Two cases are discussed here with bubble placed 5 cm above (buoyancy inhibiting jet formation) and 5 cm below (buoyancy aiding the jet formation) the wall. Figures 11a-d show the velocity field at various stages of the collapse for the first case. Initially, the bubble is almost spherical but begins to distort as it collapses. The physics of the jet formation is quite similar to the bubble-bubble case. Since there is less volume of water between the wall and the bubble during the collapse, the pressure drop is quite large relative to the pressure on other sides of the bubble. This pressure differential further forces the bubble towards the wall. Since steam is lighter, the bubble tends to move further away from the wall (due to buoyancy) for the case where the gravitational force is inhibiting the jet formation, while for the second case, the bubble is further accelerated towards the wall (Fig. 12). The water surrounding the bubble is directed off-center relative to the bubble geometric center, thereby, creating a higher pressure on the side of the bubble away from the wall. The combination of these effects causes the water to penetrate the bubble from the high pressure side and to form a high-speed water jet that impacts the rigid surface. As this jet impacts on the rigid plate, a ring bubble vortex is formed as shown in the figures. The maximum jet velocity obtained is around 40m/s. It scales as approximately 11 times the non-dimensional velocity scale based on the ambient(water) pressure and water density $\left(\sqrt{\frac{P_\infty}{\rho_w}}\right)$ and this scaling is in excellent agreement with earlier results (eg. Chahine and Perdue,1988).

The effect of buoyancy in the formation of jet is very evident in fig. 13 where the impact pressure on the wall is plotted versus time. The buoyancy aided case almost doubles the impact pressure than for the buoyancy inhibited case and is as much as two-and-half time that of the peak explosion pressure. For the buoyancy inhibited case (as in the experiments, Lal and Menon, 1996b)

The present study was able to capture the vortex ring bubble as shown above. This vortex ring bubbles after the jet impact has been also observed both in experiments ( e.g., Tomita and Shima,1986; Vogel, et al., 1989) and in numerical studies (Best,1993; Szymczak, et al., 1993; Zhang and Duncan 1994).

## 4. CONCLUSIONS

These studies show that the ALE3D code can be used for bubble explosions. The basic code has been validated using shallow water explosion data. In addition to isolated bubbles, bubble-bubble and bubble-wall interaction studies were also performed. It has been shown that all the features observed in past experiments have been captured in these studies. The formation of reentrant waterjet as the bubble collapses near a rigid surface and the formation of ring vortex bubble have been captured in the simulation. These features are in good agreement with experimental data.

Some limitations of the current ALE3D code have also been identified in these studies. For example, the current code is unable to simulate bubble-bubble interaction with a phase difference between the explosions. However, these features can be incorporated by proper modifications to the code. These issues are still under investigation.

## ACKNOWLEDGMENTS

This work is supported by the Office of Naval Research under grant No. N00014-91-J-1993. ALE3D, a product of Lawrence Livermore National Laboratories was used for the simulations in this paper.

## REFERENCES

Anderson, S., Dube, E., Futral, S., Otero , I., and Sharp, R. (1994) " Users Manual For ALE3D," Lawrence Livermore National Lab., CA.

Best, J. (1993) "The Formation of Toroidal Bubbles upon the Collapse of Transient Cavities", J. Fluid Mech., 251, pp. 79-107.

Best, J. P., and Kucera, A. (1992) "A numerical investigation of non-spherical rebounding bubbles", J. Fluid Mech., 245, pp. 137-154.

Blake, J. R., Taib, B. B., and Doherty, G. (1986) "Transient Cavities Near Boundaries. Part I. Rigid Boundary," J. Fluid Mech., 170, pp. 479-497.

Chahine, G. L., and Perdue, T. O. (1988) "Simulation of the Three-Dimensional Behavior of an Unsteady Large Bubble near a Structure," 3rd International Colloquium on Bubbles and Drops, Monterey, CA.

Cole, R. H. (1948) "Underwater Explosions," Princeton University Press, Princeton.

Duncan, J. H., and Zhang, S. (1991) " On the Interaction of a Collapsing Cavity and a Compliant Wall," J. of Fluid Mech., 226, pp. 401-423.

Lal, M. K., and Menon, S. (1996a) "Interaction of Two Underwater Explosion Bubbles", ASME, Fluids Engg. Div. Conf., Vol. 1, pp. 595-600.

Lal, M. K. and Menon, S., (1996b) "Experiments in Underwater Explosions near rigid surface", under preparation.

Lauterborn, W., (1976) "Numerical Investigation of Nonlinear Oscillations of Gas Bubbles in Liquids," J. Acoust. Soc. Am., 59, pp. 283-293.

Menon, S., and Lal, M. K., (1996) "On the Dynamics and Instability of Bubbles Formed During Underwater Explosions," submitted to Experimental Thermal and Fluid Science Journal.

Milligan, C. D., Duncan, J. H, and Stillman, D. J. (1995) "A Numerical Study of Underwater Explosion Bubble Phenomena," preprint.

Plesset, M. S. (1971) "The Dynamics of Cavitation Bubbles," Trans. ASME, J. Appl. Mech., 16, pp. 277-282.

Plesset, M. S. and Chapman, R. B. (1971) " Collapse of an initially spherical cavity in the neighbourhood of a solid boundary," J. of Fluid Mech., 47(2), pp. 283-290.

Prosperetti, A. (1982)"A Generalization of the Rayleigh-Plesset Equation of Bubble Dynamics. Phys. Fluids, 25, pp. 409-410.

Steinberg, D. (1991) "Equation of State and Strength Properties of Selected Materials," Lawrence Livermore Nam. Lab., Livermore, CA, UCRL-MA-106439.

Szymczak, W. G., Rogers, J. C. W., Solomon, J. M. and Berger A. E. (1993) "A numerical algorithm for hydrodynamic free boundary problems," J. Comput. Phys., 106, pp. 319-336.

Tomita. Y., and Shima. A. (1986) "Mechanisms of Impulsive Pressure Generation and Damage Pit Formation by Bubble Collapse," J. Fluid Mech., 169, pp. 535-564.

Tipton, R. E., Steinberg, D. J., and Tomita, Y. (1992) "Bubble Expansion and Collapse Near a Rigid Wall," JSME , 35, pp. 67-75.

Vogel, A., Lauterborn, W. and Timm, R., 1989, "Optical and acoustic investigations of the dynamics of the dynamics of laser-produced cavitation bubbles near a solid boundary", J. Fluid Mech., 206, pp. 299-338.

Warren, G. R. and Rice, T. W (1964) "The Interaction of the Gas Bubbles from Two Adjacent Underwater Explosions," Foulness Division Note 9-64, Atomic Weapons Research Establishment, United Kingdom Atomic Energy Authority.

Zhang, S., Duncan, J. H. and Chahine, G. L. (1993) "The final stage of the collapse of a cavitation bubble near a rigid wall," J. Fluid Mech., 257, pp. 147-181.

Zhang, S. and Duncan, J. H., (1994) "On the non spherical collapse and rebound of a cavitation bubble," Phys. Fluids, 6, pp. 2352-2362.

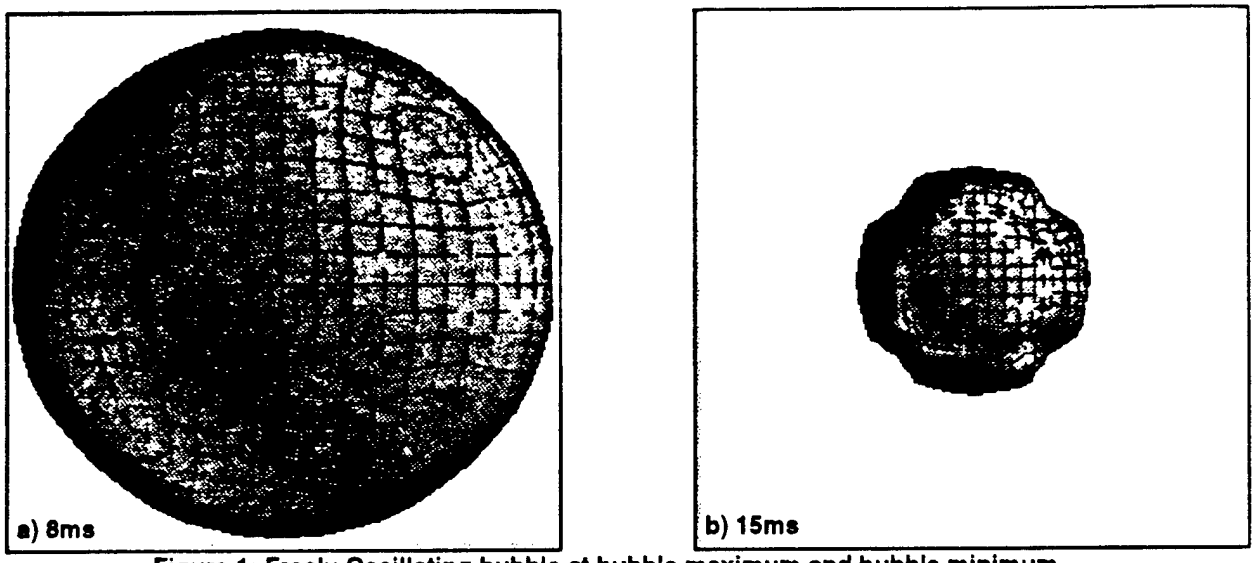


Figure 1: Freely Oscillating bubble at bubble maximum and bubble minimum.

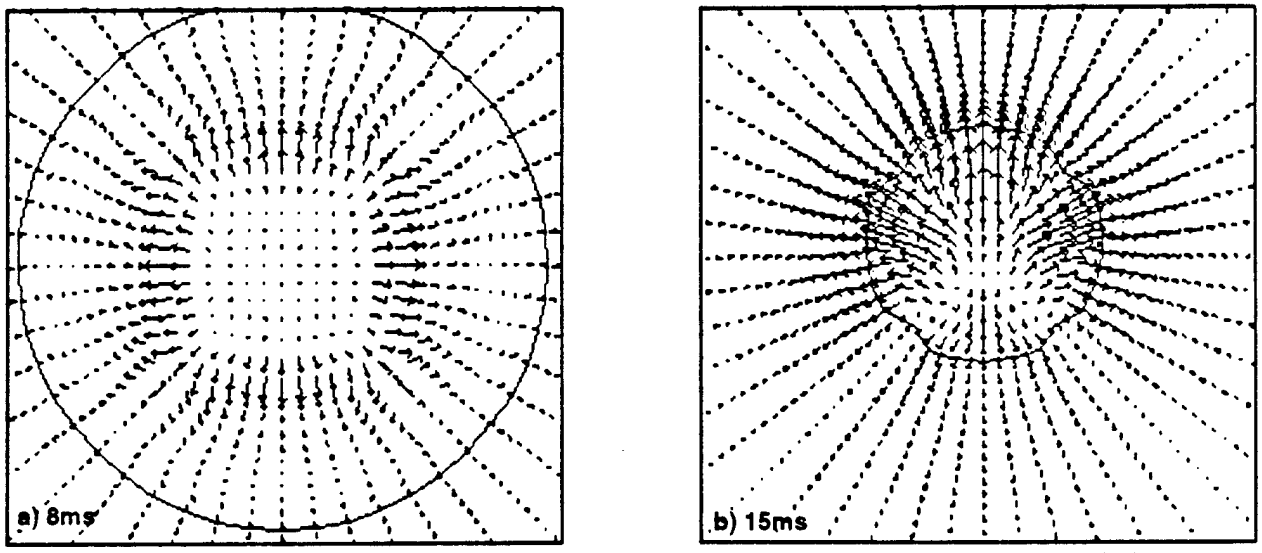


Figure 2: Vector fields around the maximum and minimum of a freely oscillating bubble.

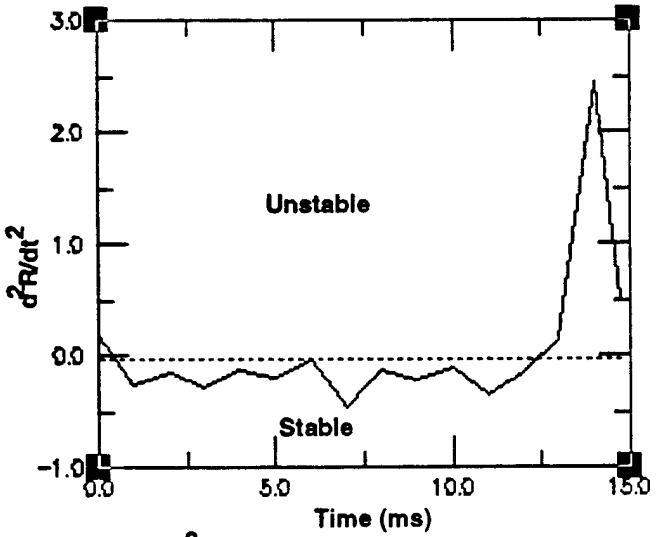


Figure 3: $d^2 R/ dt^2$ versus time plot to identify the regions of R-T stable and unstable regions.

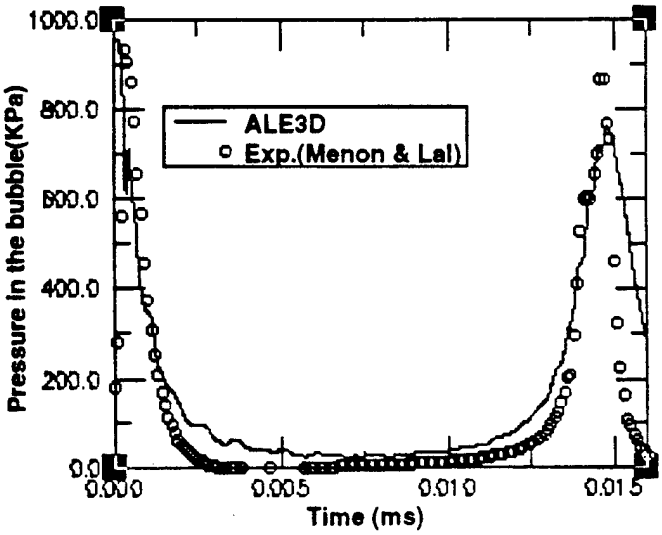


Figure 4. Time trace of pressure in the freely oscillating bubble compared with the experiments.

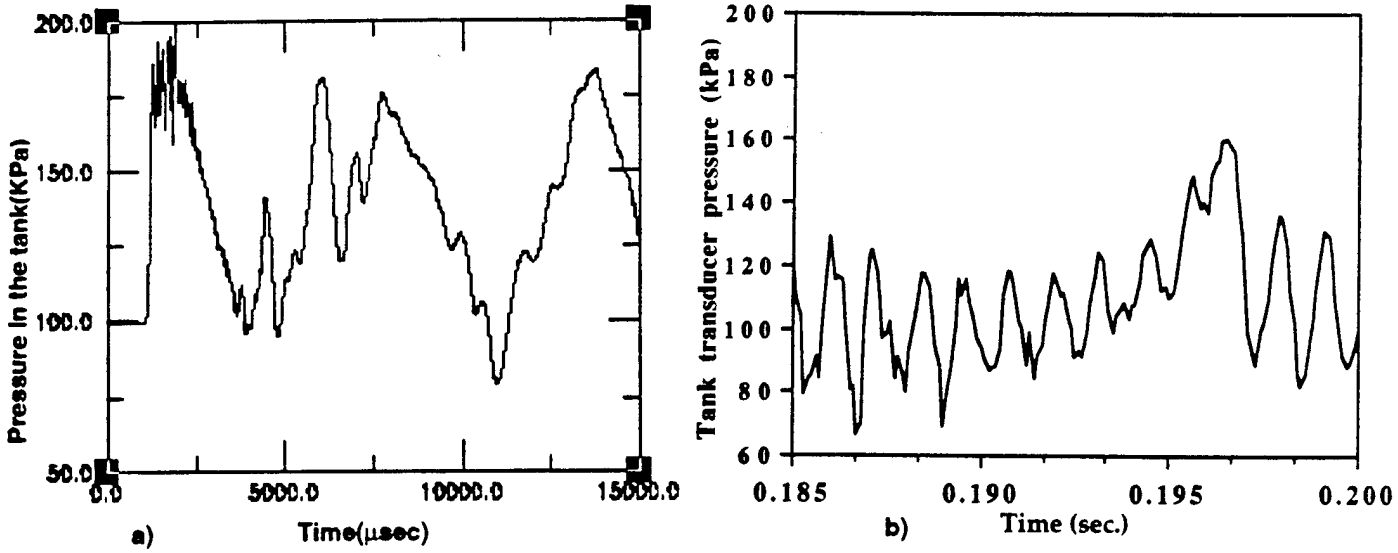


Figure 4: The acoustic pressure signature in the tank awy from the bubble and near the walls. a) Numerical Simulation and b) Experiments(Menon and Lal,1996).

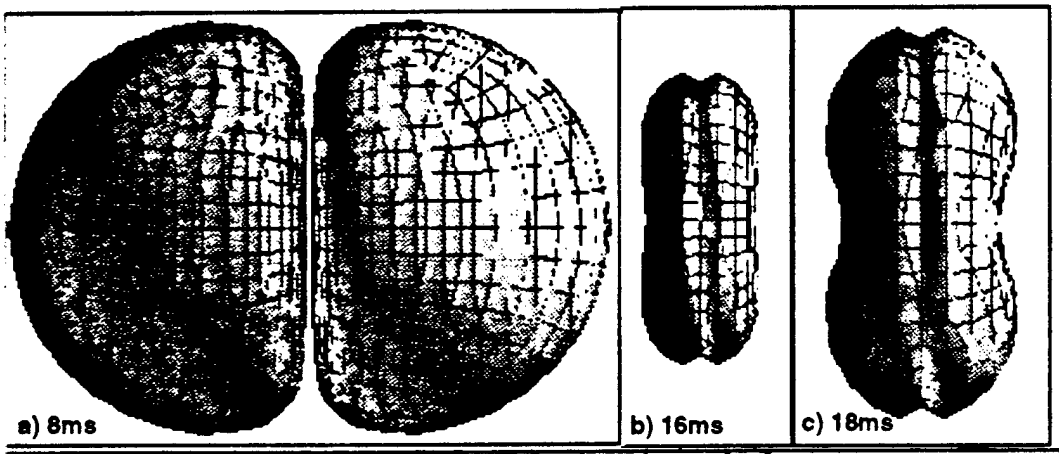


Figure 6: Time sequence of two bubbles of same size interacting. a) At bubble maximum, b) Just before the jet formation and c) Formation of toroidal double ring bubble.

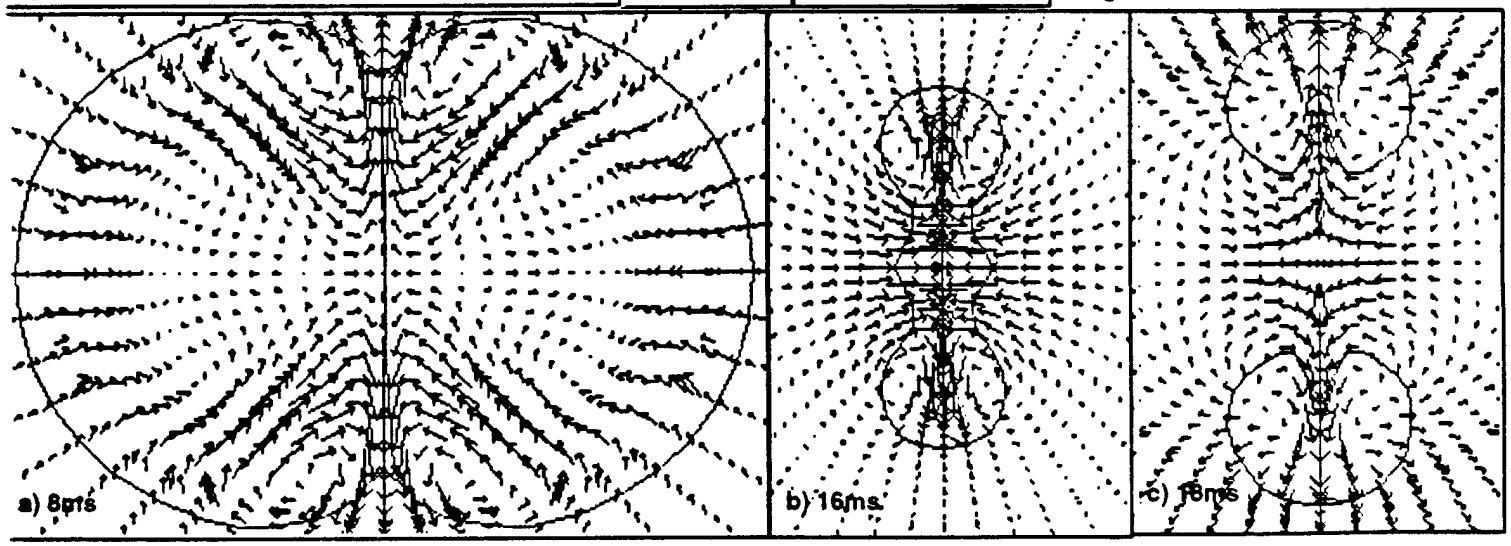


Figure 7: Velocity vectors for the cases discussed in fig. 6.

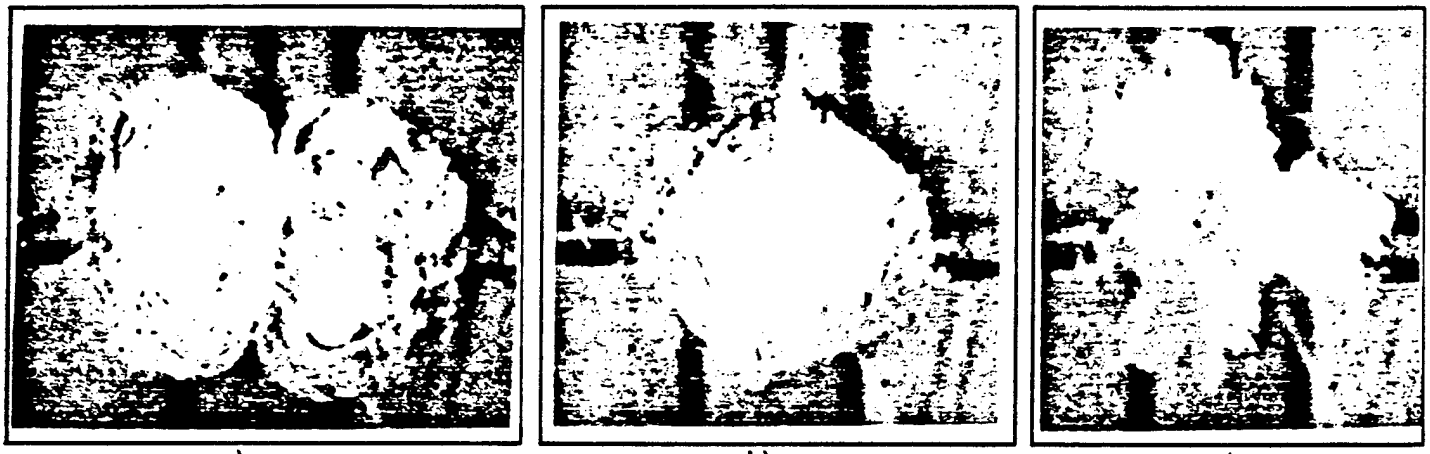


**Figure 8: Snapshots of the bubbles in the expt.(Lal and Menon,1996) for in-phase explosions of same size. a) Corresponds to bubble maximum, b) During Collapse & c) During rebound.**

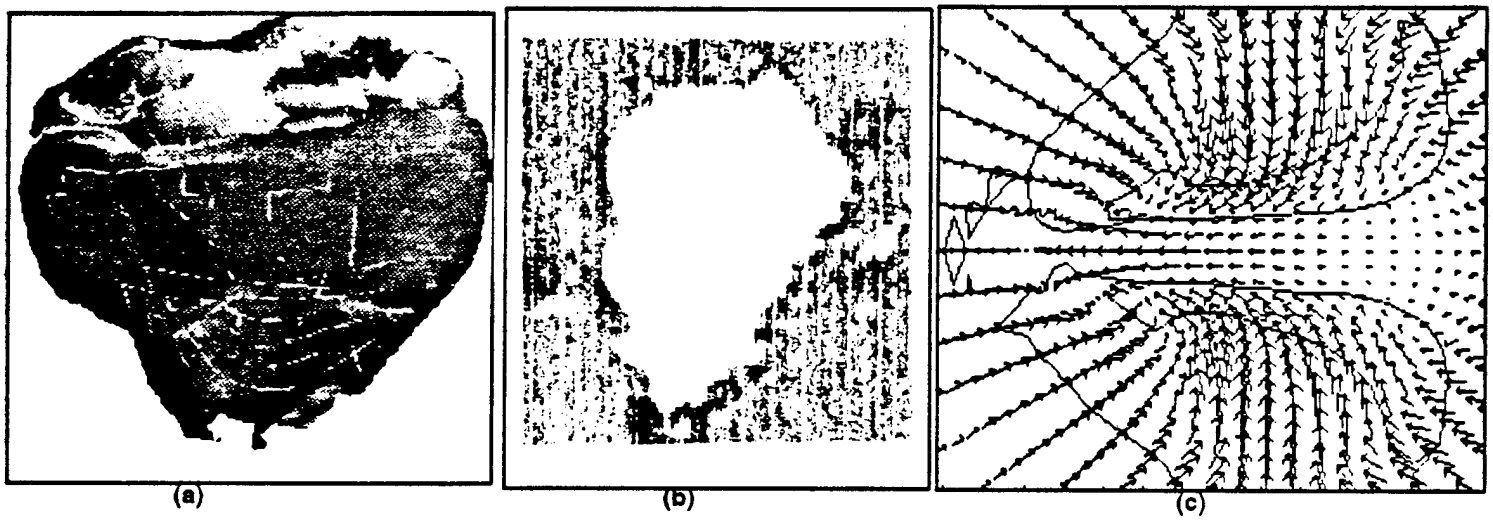


**Figure 9: ALE3D Bubble Shape(a), corresponding expt.(Lal and Menon) snapshot for out of phase explosion(b) and corresponding velocity field(c) at the time of jet formation for the bubbles of different sizes interacting.**

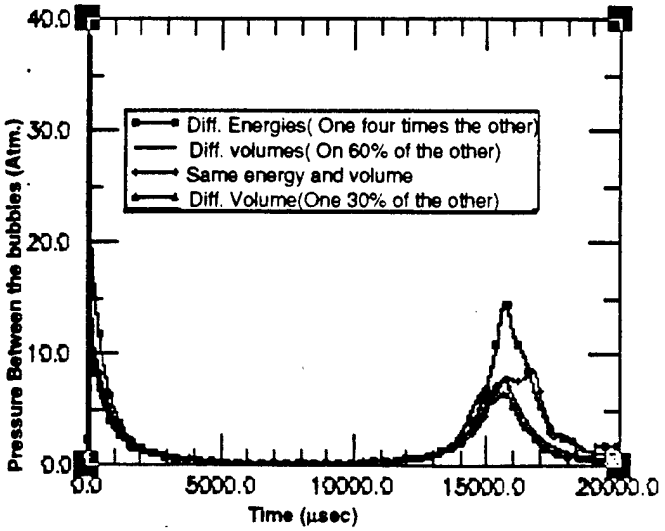


**Figure 10: Time trace of the pressure in between the bubbles for the different cases of double bubble interactions.**

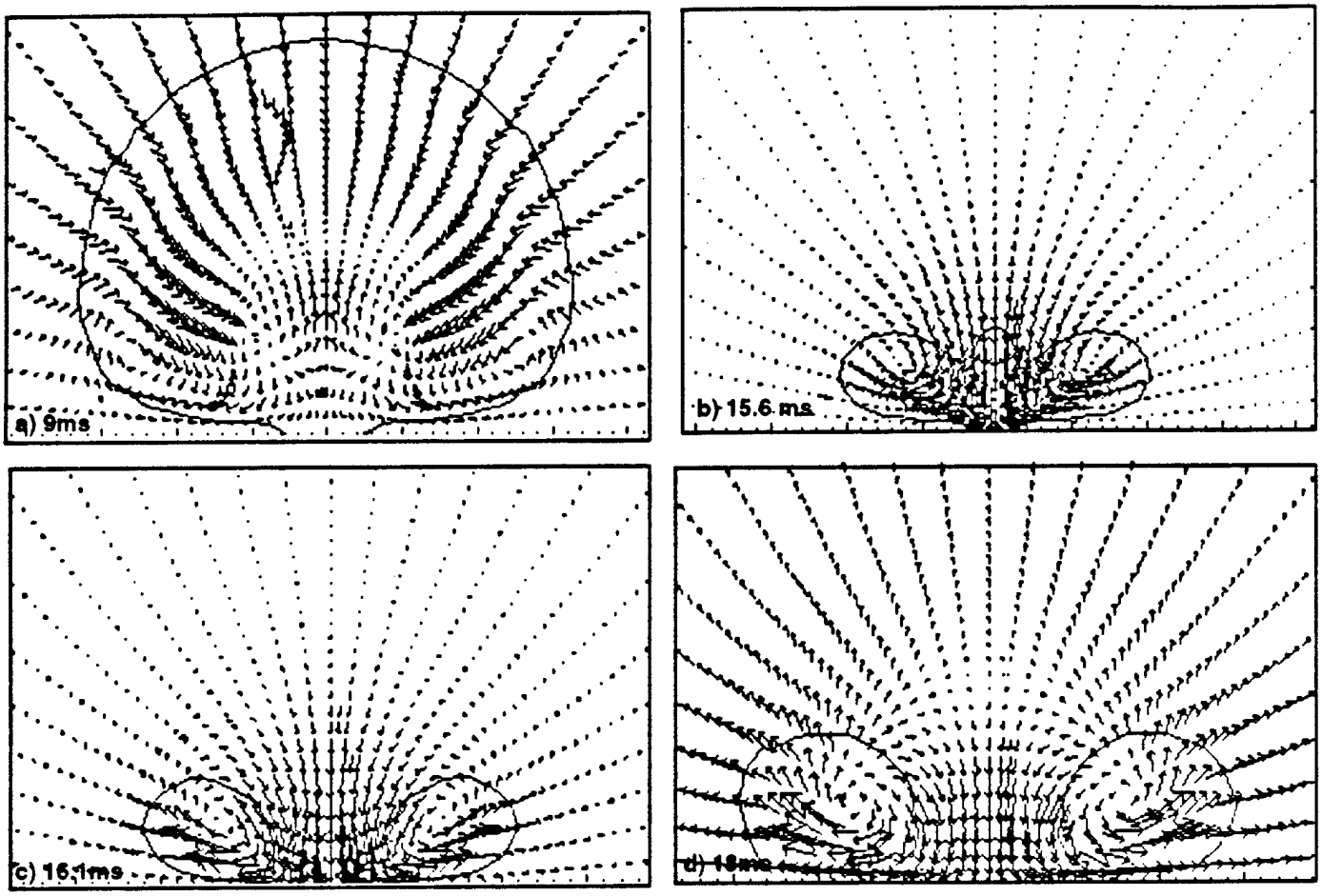


**Figure 11: Velocity field around a bubble collapsing near a wall (Buoyancy Inhibiting). a) At bubble maximum, b) & c) Just before the jet formation and d) After the toroidal bubble is formed during rebound.**

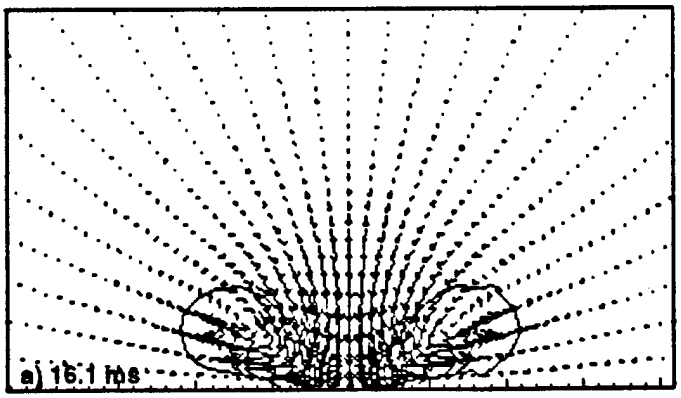


**Figure 12: Velcity field around the bubble collapsing near a rigid wall with buoyancy aiding the collapse.**

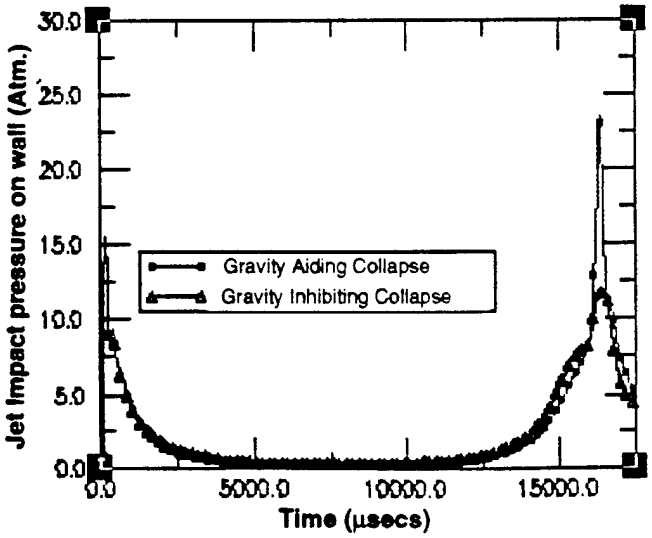


**Figure 13. Impact pressure on the wall for both the bouyancy aiding and inhibiting cases.**